Durham University

Durham E-Theses

The Geochemistry of podiform chromite deposits from two ophiolite complexes, Chalkidiki peninsula, Northern Greece

C. Christodoulou

How to cite:

Christodoulou, C. (1980) The Geochemistry of podiform chromite deposits from two ophiolite complexes, Chalkidiki peninsula, Northern Greece. Masters thesis, Durham University.

Use policy

The full-text may be used and/or reproduced, and given to third parties in any format or medium, without prior permission or charge, for personal research or study, educational, or not-for-profit purposes provided that:

- a full bibliographic reference is made to the original source
- a https://etheses.durham.ac.uk/id/eprint/8087/ is made to the metadata record in Durham E-Theses
- the full-text is not changed in any way

The full-text must not be sold in any format or medium without the formal permission of the copyright holders.

Please consult the full Durham E-Theses policy for further details.

Academic Support Office, The Palatine Centre, Durham University, Stockton Road, Durham, DH1 3LE
e-mail: e-theses.admin@durham.ac.uk Tel: +44 0191 334 6107
https://etheses.durham.ac.uk

The Geochemistry of Podiform Chromite Deposits from Two Ophiolite Complexes, Chalkidiki Peninsula, Northern Greece.

C. Christodoulou, B.Sc.

A thesis submitted for the degree of Master of Science in the University of Durham.

Department of Geological Sciences

October 1980.

The copyright of this thesis rests with the author. No quotation from it should be published without his prior written consent and information derived from it should be acknowledged.

DURHAM UNIVERSITY
16 FEB 19[illegible]
SCIENCE LIBRARY

Dedicated to my Mother and

my Sister

ABSTRACT

The geochemistry of various petrological units from two mafic-ultramafic complexes, from the Chalkidiki peninsula have been studied. These complexes have been tectonically incorporated into the metamorphic country rocks, forming allochtonous bodies bounded by thrust zones. Chromite deposits occur in both complexes. They are highly sheared in the Gomati complex but grade to host dunite in the Vavdos complex.

Major oxide contents and trace element abundances have been determined by X-ray fluorescence spectrometry. Mineral analyses have been made by electron microprobe.

Data on chromite from both complexes reveal that the chromite ores are of metallurgical type in the Vavdos complex and of refractory type at Gomati. The genetic model proposed relates to extraction of basaltic melt from depleted upper mantle material and its subsequent fractional crystallization. Podiform chromites are an early product of the crystallization of such a basaltic melt. They are intimately associated with a dunite host rock.

The structures of the petrologically different rock units, suggest formation through processes involving an original magmatic environment. This is reinforced by trends for particular minerals in the Vavdos complex. In the Gomati complex, the rocks are extensively serpentinized although various rock types can still be recognized. Amphibolites, at the contacts to the country rocks, show similarities to ocean floor basaltic extrusives.

The two mafic-ultramafic complexes have been interpreted as ophiolitic complexes, generated in small ocean basins or marginal seas, and emplaced into the crust during the Mesozoic.

ACKNOWLEDGEMENTS

I would like to thank my supervisor, Dr.D.M.Hirst, for supervising this project. His advice, encouragement and interest have contributed the most for the completion of this work.

I would also like to thank Professor M.H.P.Bott for providing the facilities in the Department of Geological Sciences. I am indebted to Dr,A. Peckett for instruction and assistance in the electron microprobe. In addition, I am indebted to Dr. J.G.Holland for instruction in X-Ray fluorescence analysis.

I am grateful to Mr.R.Phillips and Dr.C.H.Emeleus for many useful discussions. I would like to extend my thanks to the members of the technical staff, and in particular to Mr. R.G.Hardy for assisting in the X-Ray diffraction, Mr. L.MacGregor and Mr. G.Randall for the preparation of thin and polished sections respectively. Mr. R.Lambert carried out the wet chemical determinations.

I wish to thank my colleagues, A.P.Jones, G.R.Moore, and M.Ozcelik, and the former research student of this department, Dr.R.M.Forster, for many useful discussions and their creative criticism.

Finally, I wish to thank Mrs.S.Mellanby for typing the manuscript quickly and with such efficiency.

CONTENTS

LIST OF FIGURES

LIST OF TABLES

CHAPTER 1

INTRODUCTION AND GENERAL GEOLOGY

1.1 LOCATION

The two areas considered, Vavdos and Gomati, are located in Chalkidiki Peninsula, in Northern Greece, Fig 1.1. The Vavdos area lies in the western sector of the peninsula, extending between latitudes 23^{o} 21'- 23^{o} 17' and longitudes 40^{o} 23' - 40^{o} 26' ; the Gomati area lies in the eastern sector of the Chalkidiki Peninsula, and extends between latitudes 23^{o} 45' and longitudes 40^{o} 22' - 40^{o} 25'.

The Vavdos ultramafic-mafic complex is an elongated, lobe-like body, with its long axis having a NW-SE orientation. Vavdos complex occupies a roughly central position in a series of small ultramafic and gabbroic bodies, extending NW-SE, from Panorama (to the east of Thessaloniki) in the northwest, to Ormilia in the southeast, Fig 1.1. The relief of the area occupied by ultramafic rocks is smooth, with no steep slopes or peaks, the highest altitude being 763 m. Most streams flow to the south-southwest. They drain the greater part of the surface area except for the very northern part, where the whole body slopes very steeply to the northeast. The vegetation is restricted, mainly to low bushes.

The central parts of the Vavdos area are now a huge open-pit for the exploitation of magnesite deposits. The exploitation, which started almost 20 years ago, is entirely opencast, and is being carried on by Magnomin Co.

Chromite deposits occur at more than ten different localities. Mining for chromite ores took place during the

16 FEB
SCIENCE LIBRARY

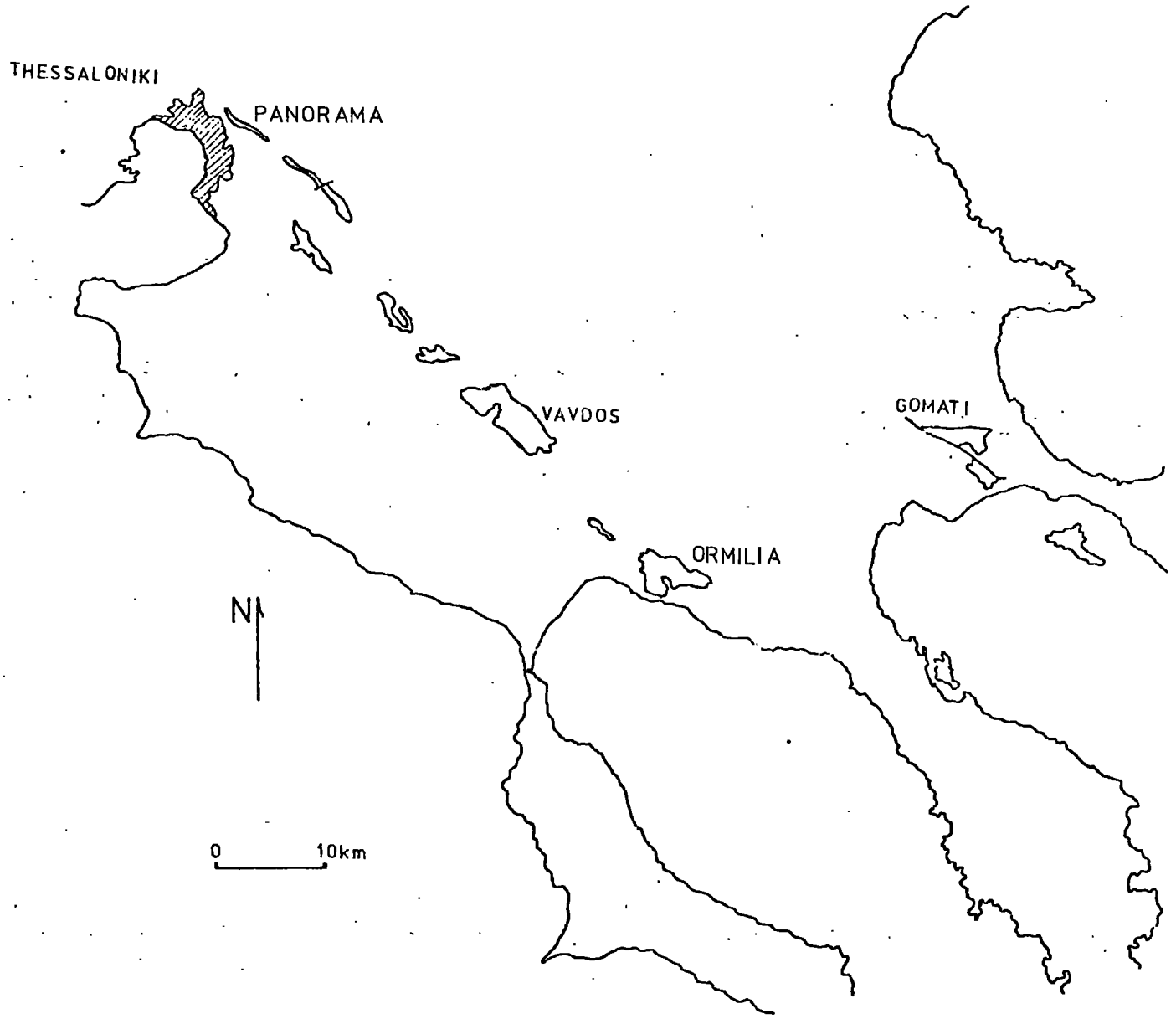

Figure 1.1 The ultramafic-mafic complexes of Chalkidiki peninsula, N.Greece, extending from Thessaloniki to Ormilia. Gomati forms an isolated outcrop in response to the series of other complexes.

second world war by occupying German forces. The extent of these mining operations is unknown, but judging from remaining workings it had to be limited. No recent prospecting for new chromite deposits has been carried out.

The Gomati ultramafic complex consists of two fault-bounded units, with a major thrust direction from SE to NW. Unit ($_1$),the northern part of the complex, rises steeply over Gomati village, with the highest peak, at Paivouni, being 520 m. Unit (2), the southern part, is at lower altitudes extending down almost to sea-level. The vegetation covering Unit ($_1$) comprises thick and high bushes. These impede field work. The whole of Unit (2) is covered by pine trees.

Chromite deposits occur at many different localities in the complex. Local villagers report that the history of mining for chromite ores in the area, goes back to the beginning of the century. Later, however, during the German occupation, extensive mining took place. The tonnage of chromite ore extracted, however, remains unknown. To date, no further exploration for new chromite deposits has been made, most surface excavations remaining as they were left by the Germans. At some locations the surface excavations have a lobe shape, with easily distinguishable disseminated ore in the walls in a serpentinite host-rock, whereas in the bottom of the pits massive chromite occurs.

1.2 REGIONAL GEOLOGICAL SETTING

The Vavdos complex lies in the Vardar zone, and represents one of the several ultramafic-gabbroic bodies extending from NW to SE along the Chalkidiki peninsula. The

Gomati complex lies in the Serbo-macedonian massif. The ultramafic outcrops and the associated chromite mineralization of Greece are shown in Figure 1.2.

The Vardar zone extends from north-northwest to south-southeast and lies between the Pelagonian zone and the Serbo-macedonian massif, Figure 1.3. The basement of the zone is represented by crystalline rocks which have been tectonically incorporated into the zone (Zimmerman and Ross, 1976). The regional metamorphism that characterizes the zone is of greenschist facies, and is considered to be of Late Cretaceous age (Mercier, 1973).

The Serbomacedonian massif is comprised of two formations, the Vertiskos formation and Cerdillia formation. Both formations consist of metamorphic rocks, and the Vertiskos formation is the upper series. Borci et al (1965) have determined the age of the upper parts of the crystalline rocks to be 300 million years. The Gomati ophiolite is incorporated to these rocks tectonically, and is thermally metamorphosed by the Tertiary granitic intrusion of Ierissos. Therefore, it is dated between Permian and Tertiary. A Mesozoic age is reasonable, due to the existence of small ocean basins and multiple subduction zones in Northern Greece during Mesozoic times, Hynes et al (1972). The amphibolites of the Vertiskos formation are possibly also related to oceanic volcanism during the same period.

1.3 BRIEF GEOLOGICAL HISTORY

The present disposition of the Vavdos complex suggests that the sequence is inverted. The contact mylonites support cold intrusion with overthrusting towards the southwest.

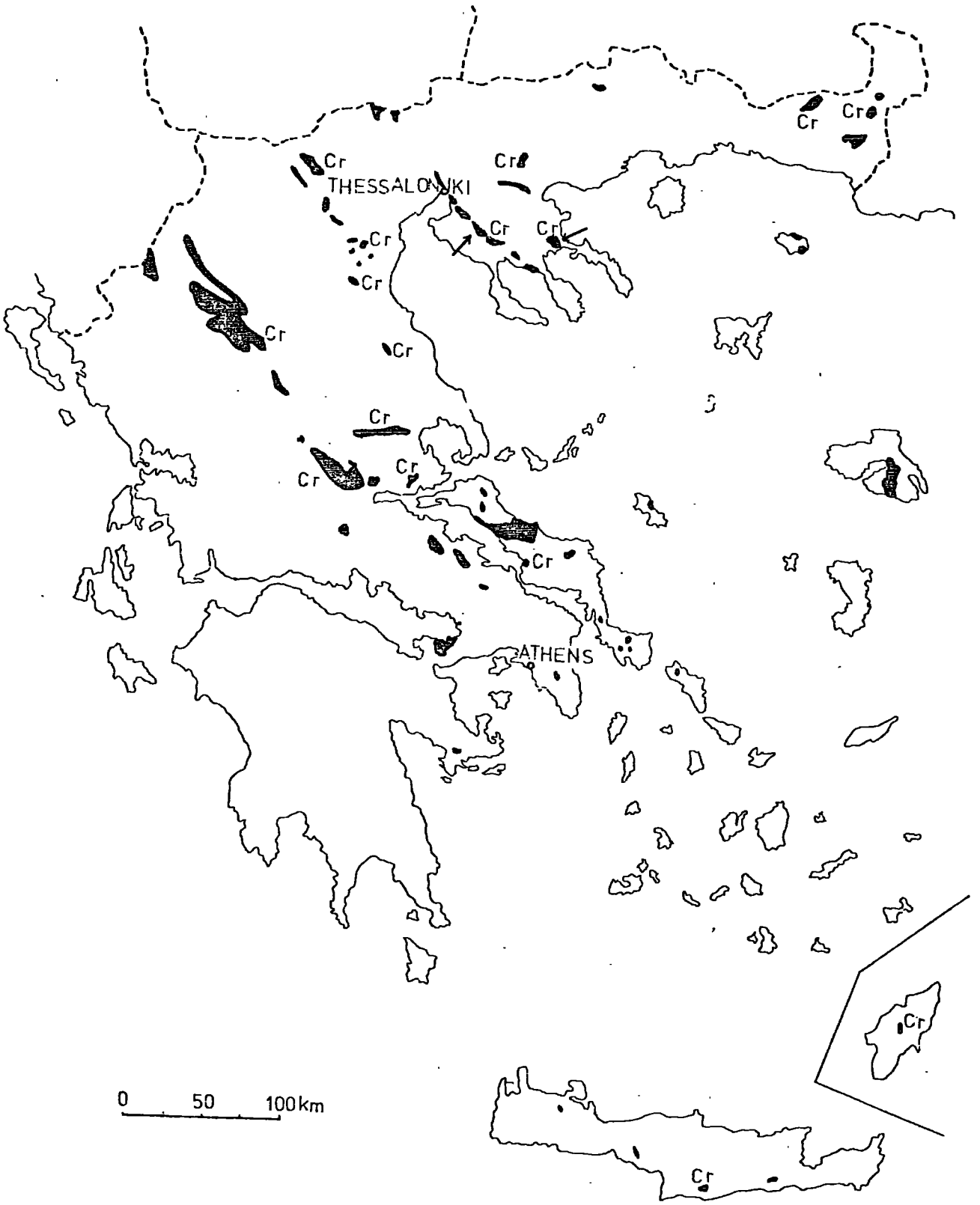

Figure 1.2 The outcrops of ultramafic rocks and associated chromite deposits (Cr) of Greece, according to Zachos (1969). The arrows indicate the two studied areas.

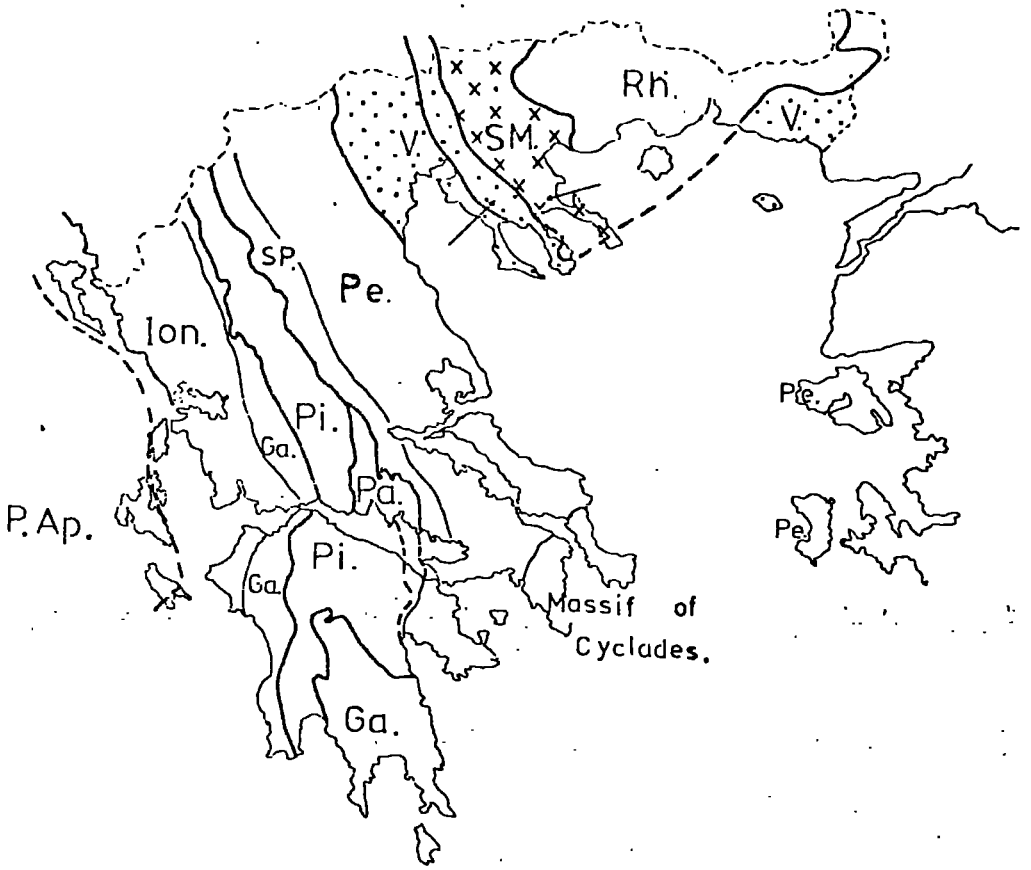

Figure 1.3 Regional tectonic zones of Greece, mainly after Jacobshagen et al (1978). Abbreviations are as follows :

Rh, Rhodope massif
SM, Serbo-Macedonian massif
V, Vardar zone
Pe, Pelagonian zone
SP, Sub-Pelagonian zone
Pi, Pindos nappe
Pa, Parnassus series
Ga, Gavrovo-Tripolitsa series
Ion, Ionian zone and
P.Ap, Preapulian zone

The boundaries between zones are marked as,

——— observed tectonic boundaries
--------- supposed " "
——— gradational boundaries.

The ophiolite complexes of the Vardar and Subpelagonian zones represent detached fragments of oceanic crust and upper mantle, and are related to an oceanic area which existed in Jurassic to Cretaceous times (Bernoulli and Loubscher, 1972). The existence of two, unequal oceanic areas during this period is suggested by Boccaletti et al (1974). They relate the emplacement of ophiolites in the Vardar and Subpelagonian zones to two, subparallel subduction zones dipping north-northeast. This subduction direction is in agreement with the general NW-SE orientation of the series of ultramafic gabbroic bodies (one of them being the Vavdos complex) of the Vardar zone.

Zimmerman and Ross (1976) postulate subduction of the Pelagonian zone beneath the Rhodopian massif at an early stage , the subduction zone dipping eastwards. At a later stage, the subduction direction changes and the Rhodopian massif was subduced beneath the Pelagonian zone. The Vardar zone lies between these two zones and consequently has a complicated tectonic history. Reversal of the direction of subduction may have incorporated tectonic movements responsible for the inverted sequence of the Vavdos ophiolite.

The Gomati ophiolite has been incorporated into the crystalline rocks of Serbomacedonian massif. Its present position gives little indication of past subduction zones.

CHAPTER 2

GEOLOGY OF THE VAVDOS AND GOMATI OPHIOLITE COMPLEXES

2.1 VAVDOS COMPLEX

2.1.1 Country Rocks

(a) Underlying the complex

The country rocks show an increasing degree of deformation and dynamic metamorphism, as the thrust zone below the southwestern contact is approached. The country rocks are brownish grey ; they are well exposed in the stream section (1), Figure 2.1. Schistosity is clearly defined by the separation of mafic and felsic minerals into distinct bands ; feldspar and/or quartz augen can also be seen. The rocks are intensely foliated on a small scale, plates 2.1 and 2.2. They have been defined as two-mica gneisses and are very similar to country rocks of the Gomati area, according to Kockel and Mollat (1970).

The gneiss strikes northwest and dips at angles of 45^{o} to 80^{o} to the northeast. The axial planes of the microfolds also strike northwest. They are asymmetric, occasionally isoclinal, angular and sheared. Their axial planes suggest that the direction of principal compressive stress coincides with the direction of emplacement of the complex.

Near to the contact the gneiss is greenish due to the development of retrograde metamorphic mineral assemblages. Two zones can thus be distinguished below the southern thrust zone. One extends for about 100m from the contact and shows retrograde metamorphic transformations, resulting from the imposed stress. The second zone, farther away, is composed

Plate 2.1 The underlying country rock of Vavdos complex. Schistosity and banding are clearly defined. Note the intense folding.

Plate 2.2 Another view of the intensely folded two mica gneiss. The white bands are quartz.

of gneisses which do not show retrograde effects, but have been intensely deformed and folded.

(b) Country rocks overlying the complex

The country rock above the northern contact, extending NW-SE, is a green schist which belongs to the Chortiatis metamorphic series.

The schist is a finely banded rock, mainly green in handspecimen, with minute feldspars conforming to the foliation. The rock strikes northwest and dips mainly to the northeast, although locally both strike and dip change, especially near the contact where the dip reaches 90^{o}. Near the contact the greenschists are contorted and show small scale folding. Axial planes strike northwest and shear planes are almost vertical. Away from the contact zone the greenschists dip at angles of about 60^{o} to the northeast.

The greenschists have been derived by regional metamorphism of a range of primary rocks from ultramafics to granites. Metamorphism was during the Mesozoic. The rocks are characterized by greenschist facies mineral assemblages. Near the contact with the ophiolite complex, the schists are highly deformed, and have a mineral assemblage of actinolite-plagioclase. This assemblage is indicative of retrograde metamorphism coincident with the imposition of shearing stress during emplacement of the ophiolite.

(c) Sedimentary rocks

Pleistocene sediments compose the tableland extending to the north of the ophiolite and they contain pebbles and sand of various origins. Talus cones have been formed in the vicinity of the complex, because of the steep slopes.

The south-southwest directed drainage system has

resulted in the formation of gullies and the deposition of transported, fragmented rock materials of variable size. These include a series of red clays which form an elongate zone, widening to the southwest and covering the mafic and ultramafic rocks of the complex. Hipparion has been found in these clays, indicative of an upper Miocene to lower Pliocene age.

Conglomerates form the lower horizons and cover the mafic-ultramafic rocks to the south and southeast. They are mainly red-brown in colour and are composed of red clays with pebbles of magmatic and metamorphic rocks.

2.1.2 Contact Zones

The Vavdos complex is an allochton emplaced in an almost solid state into the metamorphic country rocks. Because of its allochtonous origin it is bounded by thrust zones. Topographic evidence suggests the ophiolite is upthrust to the north with a continuous thrust zone to the northeast, stretching northwest-southeast. A dynamothermal contact forms the base of the complex and also extends northwest-southeast.

The northern thrust zone can be distinctly inferred from physiographic features. Slopes on the ophiolite complex are steep and rise to a height of 500m from the tableland. The ophiolitic rocks have been eroded and a talus has formed at lower altitudes. The abrupt elevation of the easily weathered ultramafic rocks with no continuity in the foreland, strongly suggests a dislocation, interpreted here as a thrust zone.

The northeast contact is deduced by the abrupt change from gabbros to the green schists. The actual contact cannot be seen, because of the cover of erosional materials. The characteristic indicative feature of the close vicinity of the

contact is microfold structures seen in handspecimens. This thrust zone, extending from northwest to southeast, parallels the basal, southwestern contact of the complex.

The basal contact strongly suggests dynamic emplacement of the complex. The actual contact is a tectonic breccia, which has been traced for a distance of about 2 km. The general direction is northwest-southeast although locally it can change to the north or to the south. At Calamoudi, intensely folded serpentinites overlie the tectonic breccia with fold axes parallel to the thrust plane. The tectonic breccia is variable. Within 2m of the serpentinite the rock is cataclastic and cryptocrystalline. Further away from the serpentinite small angular fragments are set in a light brown, calcareous, fine-grained matrix. The fragments are composed of peridotite, the underlying gneiss, quartz autoliths and spongy carbonates. Within a few meters the incorporated blocks rise in size, some being rounded. A characteristic feature of these rocks is their strength and cohesiveness. They are coloured in variations of light brown to red-brown due to oxidation.

At Climatsida the contact serpentinite is a light green material which changes gradually through pale brown to a light red-brown cryptocrystalline cataclastic rock at the contact. This cataclastic rock shows successive stages of mixing with calcareous material from the country rocks.

2.1.3 Mafic and Ultramafic Rocks

(a) Gabbro

Two gabbroic outcrops can be distinguished, one in the north and one near the southern contact, above the serpentine zone, both representing the uppermost parts of this ophiolite complex.

The northern gabbro outcrop forms a zone ranging from 250m to 1 km in width and extending to about 7.5km in length. It has a NW-SE orientation. The gabbro is massive, coloured grey, with no foliation or layering evident. It is in an advanced stage of alteration and weathering.

The change from dunite to gabbro is abrupt with no transitional zone. The exact location of the contact, however, could not be inferred because of deep weathering and extensive vegetative cover. Kockel and Mollat (1970) have defined a fault contact between the dunite and gabbro which is orientated NW-SE.

The northern margin of the ophiolite complex is defined by the fault between the gabbro and the greenschists of the Chortiatis magmatic suite. Near the contact the colour of the massive gabbro changes from grey to green, indicating the replacement of pyroxenes by amphibole. As the contact is approached the gabbro develops a tectonic fabric with plagioclase crystals having a preferred orientation. Microfolding can also be observed.

The gabbroic rocks, between the zone of interlayered pyroxenite and gabbro and the basal serpentinite, are massive and deeply weathered. Near the contact to the basal serpentinite, the gabbro is transformed to amphibolite, which shows microfolding and foliation.

(b) Interlayered pyroxenite-gabbro

A discontinuous zone of alternating pyroxenite and gabbro is located above the lower gabbroic unit. The pyroxenite is black and grades from medium grain-size to rocks with crystals up to 5cm long. The pale-coloured gabbro shows a similar gradation in grain size, all pyroxenes usually being replaced

by amphiboles. Adjacent layers are parallel with sharp contacts (plate 2.3), although small scale variations occur within individual layers. The layers generally dip to the east-northeast at angles less than 45^{o}. They show typical structures, including trough-banding (plate 2.4), indicative of magmatic processes. These features indicate that the sequence is inverted.

(c) Pyroxenite

Several outcrops of black pyroxenite occur as irregular elongate bodies within the dunite, and between the dunitic and gabbroic units when there is a transitional contact. They are coarse grained, usually massive, and show gradational contacts to the adjacent dunite and gabbro.

The big bluish-grey to black clinopyroxene crystals reveal no prominent preferred orientation or lineation, but suggest accumulation due to magmatic processes, slightly affected by later metamorphic events.

(d) Dunite-Serpentinite

Dunite is the predominant rock type of the complex. It is composed of olivine, and up to 5% by volume of accessory chromite. No conspicuous primary layering or banding can be recognized. The dunite is extensively altered to serpentinite, and weathering is in an advanced stage. The most fresh samples, collected from a collapsed adit at Aggitsa, have a bright, light apple-green colour. As serpentinization proceeds the rocks become darker, olive-green. In places, where the rocks are fresh, single olivine crystals up to 2-3cm long are visible.

Near to the contacts of the complex the dunite has been converted to serpentinite. At the base of the complex the serpentinite zone parallels the thrust zone for its entire

Plate 2.3 Pyroxenite-gabbro layers from the interlayered zone of the gabbro-pyroxenite. Note the sharp contacts between gabbro and pyroxenite, and the size gradation from the top to the bottom.

Plate 2.4 An anorthositic band within pyroxenite showing trough-like structures. Note the sharp contact at the base of this band with the pyroxenite.

length. Near the contact the serpentinite is massive, but further away demonstrates strong schistocity normal to the direction of the thrust zone. The serpentinites at Calamoudi are light-green coloured and contain variable amounts of chromite. The weathered serpentinite is brown, occurs near the surface and is accompanied by magnesite mineralization.

2.1.4 Chromite Deposits

Chromite ore occurrences are associated only with dunite and serpentinite at Calamoudi. The chromitiferous rocks are classified as follows, according to their chromite content :

Massive chromitite, more than 90% chromite,

Olivine chromitite, chromite content is between 50 and 90%,

Chromitiferous dunite, 5 to 50% chromite content,

Dunite, accessory chromite less than 5%.

Chromite ore occurrences, shown in Figure 2.1. There is no limitation on their particular position within the dunite, but the biggest deposits lie away from the dunite-pyroxenite contact. The most common structures among the chromitiferous rocks can be seen in the massive and disseminated ore types. In general, they are very similar to those of podiform chromites (Thayer, 1960 and 1964), but magmatic structures may be present.

Massive ores are widespread and typically form pod-like bodies. The pods are generally small in size, individual pods not exceeding.10cm in length and 5 to 7cm in thickness ; they are also lenticular. Dunite lenses are very common in these pods (samples VP21, VG2), their long axes indicating the lineation. The massive chromite ore may, or may not, grade

outwards to disseminated type ore. Usually tabular chromite bodies show gradational relations with the massive pods and more frequently alternate with dunitic bodies in the close vicinity of a single chromite pod.

Disseminated chromite, either in the form of chromitiferous dunite or olivine chromitite, covers the whole spectrum of compositional variation and is ubiquitous in the vicinity of individual deposits. The chromitiferous dunite, shown in plate 2.5, has stratiform-like structures but usually the desseminated ore-types forms schlieren in the dunite. Trough-like structures (plate 2.6) indicate a magmatic origin in an environment similar to that of stratiform complexes, although the host-rock associations for these massive chromitites, as for the Fiskenaesset complex described by Myers (1976), are distinctly different to the typical dunite host of the Vavdos complex.

Schlieren structures are very common as shown in plate 2.7. The schlieren are usually irregular and vary in size from up to 3 cm wide, to 1 m long where they can be traced in adits. Schlieren may be confused with distorted, tabular chromitiferous bands. The tabular bands may commence from a chromite rod, pencil-like structure (plate 2.8) or show no visible connection with any other chromite (plates 2.9 – 2.10) occurrence. Chromite-rich bands in dunite may be completely undeformed (plate 2.11) or highly deformed with irregular shapes (plate 2.12), especially near the thrust contact at the base of the complex.

Magnesite veins, less than 0.2cm in width, cross-cut the chromitiferous rocks. Feldspar veins up to 1-2cm thick

Plate 2.5 Disseminated type ore. Rich in chromite bands alternate with bare dunite. This sequential repetition suggests magmatic origin.

Plate 2.6 Alternations of chromitite-chromitiferous dunite. The trough-like structure is of unequivocal magmatic origin. The structure as a whole of this sample reveals similarities to typical rock-types from layered intrusions.

Plate 2.7 Schlieren of chromitite within dunite. Note the variability in width of the chromite-band and a later fault, that has displaced the schlieren of chromite.

Plate 2.8 Massive chromitite bands commence from a chromite-rich rod. Chromitiferous dunite forms between the massive chromite bands and at the bottom of the sample. Note the dunite formation between the chromititic bands.

Plate 2.9 Chromite band in dunite from Agitsa. Note the sharp boundary to the right and the undeformed shape. To the left, the chromitiferous band shows gradational schlieven with a remarkable linearity and constancy to the main chromite band.

Plate 2.10 A smaller chromite band from the same locality showing similar features to the above band. Note a second band to the left, which is matching the larger chromite band consistentely.

Plate 2.11 Chromite rich band in dunite. Note the straight boundaries of the band and the sharp alternation to bare dunite.

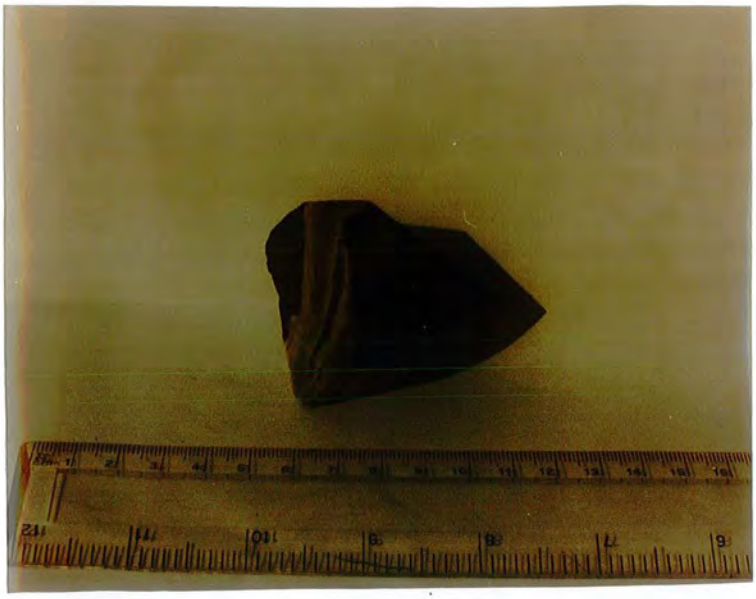

Plate 2.12 Highly deformed chromite bands in dunite from a locality near the basal thrust. Note the irregularity of the bands, and how they squeeze out to dunite.

have also been encountered crosscutting the chromitiferous rocks. Bright green chrometremolite veins sometimes occur, forming elongate, prismatic crystals filling spaces related genetically with small-scale displacements.

2.1.5 Magnesite Deposits

Magnesite ore occurrences are abundant throughout the ultramafic rocks, but are not encountered in the gabbroic rocks. Magnesite veins form intricate networks ranging in width from a few cm to 20 cm. They are very variable in lateral extent. Magnesite mainly occupies the upper parts of the serpentinized ultramafic rocks and shows a close association with brown, weathered serpentinites. It can form a high proportion of these rocks (plate 2.13).

2.1.6 Granitic Rocks

Leucocratic rocks occurring mainly within dunite, extend from NW to SE (plate 2.14). They form narrow elongate bodies up to 100m in length, but not more than one meter in width. More usually single bodies do not exceed 10m in length and 0.5 meters in width.

The bodies have an irregular shape and size overall, but do show a distinct relation to the basal thrust zone to which they are parallel (Figure 2.1).

The vein bodies are formed from three main minerals, quartz, feldspar and black tourmaline or muscovite. The tourmaline forms elongate crystals reaching 15cm in length, but is not always present. Their origin is believed not to be related to the ophiolite, and therefore will not be discussed in detail in this thesis.

A cross-section of the ophiolite sequence is given in Figure 2.2.

Plate 2.13

Thick magnesite mineralization within brown serpentinite from an adit in Photi Rachi.

Figure 2.2

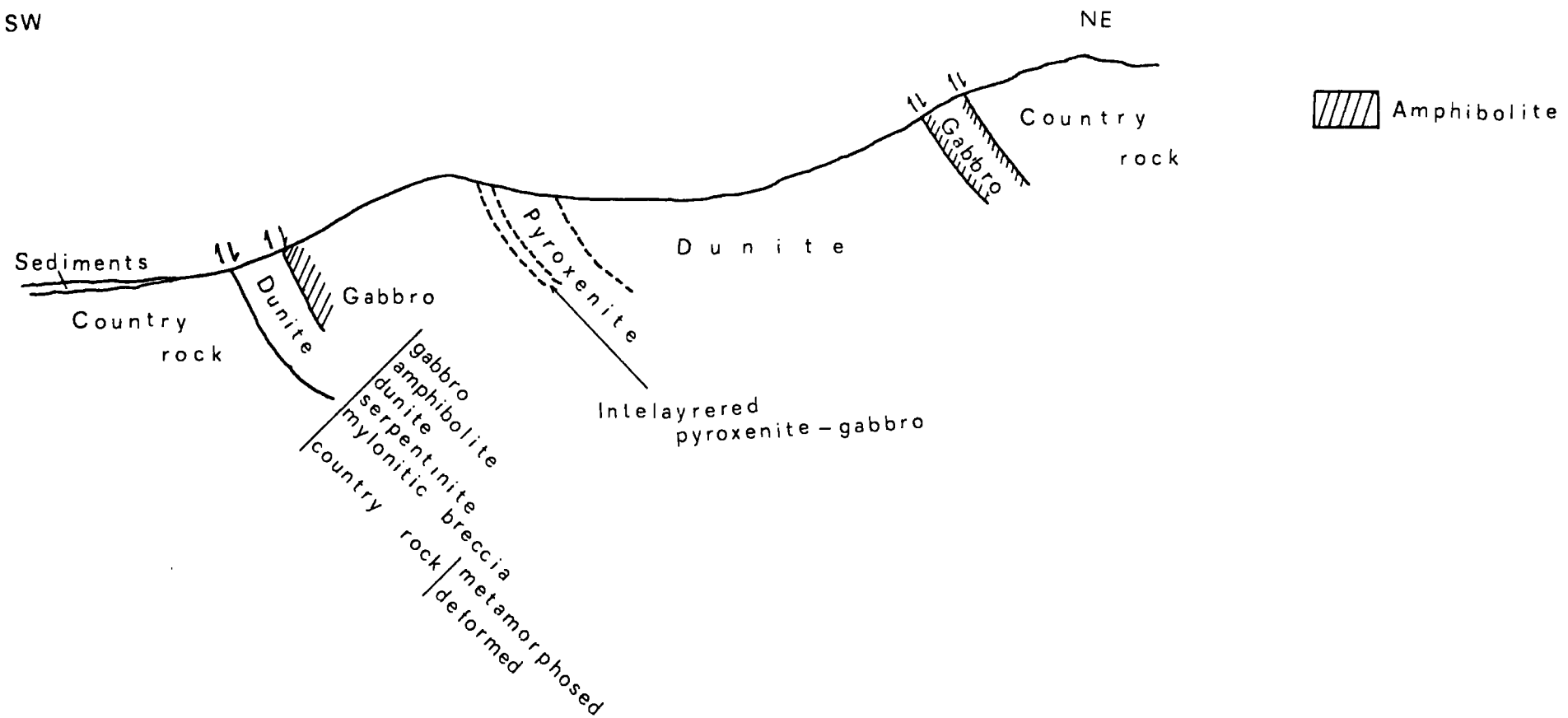

Geological sketch cross-section of the Vavdos complex

Plate 2.14

2.2 GOMATI COMPLEX

2.2.1 Country Rocks

The ultramafic body of Gomati comprises two units, which have been emplaced entirely into metamorphic rocks comprised of schists and gneisses of the Vertiskos formation. These metamorphic rocks belong to the lower sequence of the Vertiskos formation, which forms the upper unit of the Serbomacedonian massif (Kockel et al, 1971). The upper sequences of the Vertiskos formation include metagabbros, metadiabases and amphibolites, derived from basaltic rocks during regional metamorphism. In the southern part of the Vertiskos formation, in the region occupied by the Gomati ultramafic body, the metamorphic rocks are characterized by greenschist facies metamorphism.

The schists and gneisses are dark brown in colour. They are composed of plagioclase, quartz, biotite, muscovite

and accessory minerals. Usually the gneisses are of fine grain-size, foliated, with a NW-SE strike, and vary in dip from 35^{o} to 75^{o} to the S or SW. They occur between the two ultramafic units, and to the north and south of them. The area to the north of the ultramafic body has not been visited. However, Kockel et al (1971) have mentioned contact amphibolites as shown in Figure 2.3, and indicate that neither strike nor dip of the gneisses in the north are uniform.

The schists and gneisses lying between units (1) and (2), as well as those lying to the south, alternate with lens-like bodies of marble. These marbles have a general NW-SE orientation. The gneisses also strike NW-SE, and dip at angles of 35^{o} to 55^{o} to the S and SW below and to the southwest of unit (2). Above and to the east of Unit (2) gneisses again strike NW-SE and dip to the S and SW at angles of 40^{o} to 60^{o}. Near contact zones the gneisses become intensely sheared and their dip angles increase up to 75^{o}, particularly below Unit (1).

To the east of the ultramafic body, the biotite, muscovite granite of Ierissos crops out; this granitic intrusion belongs to the fourth, and last, magmatic phase of the Serbomacedonian massif, and its intrusion is dated between the Eocene and Oligocene.

Sedimentary rocks form the low plains, and are alluvial deposits of recent formation. To the southwest of Unit (1) the unexposed contact of the ultramafics is covered by Quaternary conglomerates of the lowest terrace system. The existence of a thrust-fault has been inferred at this point, as the topography shows sharp elevation above the conglomerate zone, Figure 2.4. The conglomerates slope gradually away to the southwest, where they are overlain by alluvial deposits. The central to western

part of the Gomati ultramafic body is completely covered by alluvial deposits. To the south, towards Develiki, low hills are formed from Tertiary red clays, with irregular intercalcations of calcareous rock. From these hills the relief falls smoothly to the sea, with Tertiary alluvial deposits forming the plain at sea-level.

2.2.2 Contact Zones

The southern contact of Unit (1), at the base of the massif and extending from NW to SE, is extensively covered by a conglomerate, which represents the lower stage of the lowest terrace system. The pebbles of the conglomerate comprise serpentinized dunite and massive chromite at the points where the streams draining from the St.George and Frangokaliva ore occurrences discharge onto the plain. Schlieren of chromite, forming lenses in dunite, are common as pebbles. They are well rounded, and vary in size from coarse sand to blocks half a meter in diameter.

Where this southern contact of Unit (1) is not covered by conglomerates, the contact has a NE-SW trend. Here the serpentinites and country rocks dip to the SE. Normally the strike of both ultramafic and country rocks follows that of the thrust zone, which is NW-SE in orientation. The serpentinites near the contact are strongly sheared and folded. The colour of these serpentinites is bluish-green, but the colour darkens away from the contact. The vegetation changes from low bushes on the metamorphic country rocks, to high and extremely thick bushes and pine trees on the serpentinized ultramafics. This is a characteristic feature and indicative of the exact location of the contact zone. In places, marbles outline the contact between the metamorphic rocks and the ultra-

mafics. The marbles form thin, elongate bodies, incorporated within the metamorphosed country rock as longitudinal lenses, parallel to the major strike direction, NW-SE.

At the eastern contact zone of Unit (1), black amphibolites form lensoid bodies extending into the metamorphic country rocks. The contact is well exposed in stream section (a), where the rocks are fresh. The black amphibolites are veined by irregularly oriented quartz veins of bluish-white colour. In hand specimen pink garnets can be recognised, set in a black, non-foliated matrix of amphibole. Away from the contact the amphibolites become strongly foliated, with distinct compositional banding shown by green and white minerals. The structural and textural features of these green amphibolites suggest strong deformation and regional metamorphism, and is in contrast to the randomly oriented texture exhibited by black amphibolites. The absence of visible plagioclase in black amphibolites, in hand specimen, suggests possible derivation from ultramafic primary material.

The northern contacts of the Unit (1) have not been investigated, but Kockel and Mollat (1970) note the presence of amphibolites.

Unit (2) is a fault bounded, elongate body, conformable to the main strike direction, NW-SE. To the east of the Gomati village and to the north of the ultramafics, a recent E-W normal fault has caused a dislocation of younger formations of Pleistocene or later age. This fault also cuts the ultramafic body as represented in Figure 2.5 and at this point the exposed rock is comprised of ultramafic pebbles set in a fine grained, deeply weathered matrix. The whole appearance of this rock suggests a tectonic breccia, resulting from considerable move-

Figure 2.4

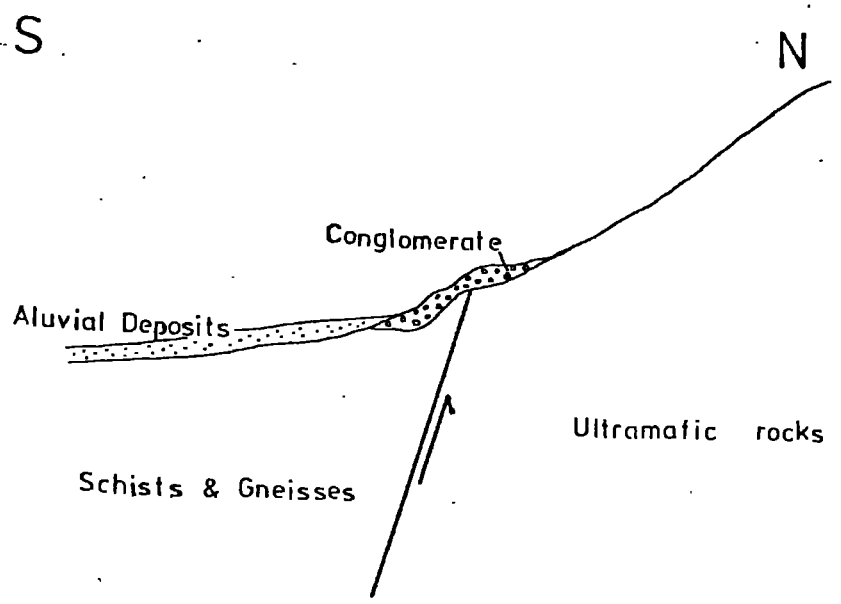

Figure 2.5

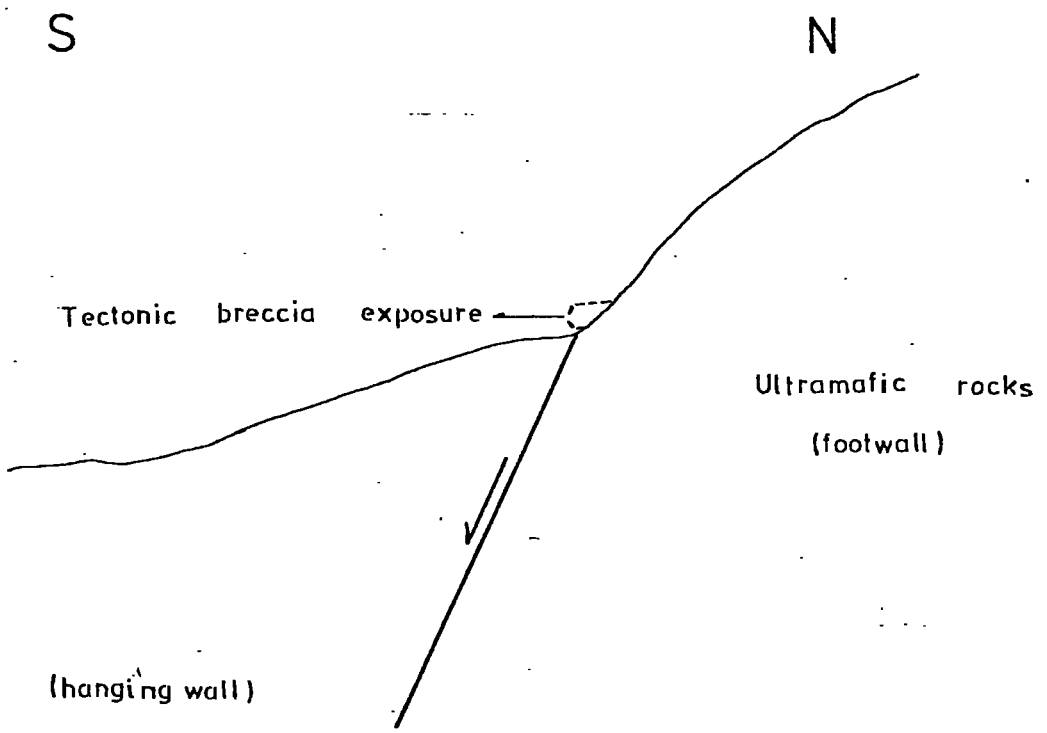

ment on this fault.

In the other parts of Unit (2), the rocks are in an advanced stage of weathering. The only indication of the contact zones is the change of vegetation. All visible contacts with the metamorphic country rocks are thrust faults, striking NW-SE and dipping to the SW.

2.2.3 Ultramafic Rocks

The outcrop of the ultramafic rocks occur in two units, one lying to the north and northwest of Gomati village, and the other, smaller unit, to the southeast.

The northern unit, Unit (1), has wedge-like shape in outcrop, and is 5km long and 0.5-2.5km wide. The unit extends almost due east-west. Paivouni mountain rises steeply, from about 200m to 520m at the peak. In general, the topography is characterized by steep elevations, especially in stream sections. The streams have a general flow pattern from north to south, the biggest being the Verkos river, which flows across the ultramafic outcrop and has its head waters in the metamorphic country rocks to the north.

The peridotites are highly serpentinized and weathered and are strongly sheared near fault contacts. The peridotite is a highly serpentinized dunite, in which primary olivines are not easily recognised. In places, Paivouni-Tripes, bands of amphiboles alternate with serpentine, suggesting a parent rock type other than dunite. Chromite is a constant accessory mineral, scattered throughout all rock types. Relatively fresh rocks, in hand specimen, have been found only close to stream sections. Fresh dunite occurs at Frangokaliva. It is light green in colour, with tabular bands or disseminated to schlieren-type chromite ore. The contact between dunite and

chromite bands, in hand specimen is sharp. At St.George, the serpentinized dunite, which is massive in appearance, strikes to the northwest and dips to the south-southeast at angles between 70^{o}-80^{o}. A characteristic feature at this locality, is the intense, closely-spaced shear fracturing and the resultant jointed appearance of the massive rock.

The most strongly sheared serpentinites have been found near to the southern contact of the ultramafic rocks of Unit (1). The serpentinites strike to the NW and dip at angles of about 80^{o} to the SW. Their colour in hand specimen ranges from blue-green, for the most sheared rocks, to grey to dark grey-green for the less sheared rocks. A common feature of all serpentinites, whether lying close or relatively far away from the southern contact, is their large dip angle, almost always around 80^{o} to the south, but locally following the contact in regard to the direction of dip and strike. Thus, where the contact extends in a NE-SW orientation, the dip is to the SE, whereas when the contact has a NE-SW orientation, the serpentinites dip to the SW.

The serpentinites and serpentinized dunites are weathered, and exhibit reddish colours at the surface. Where weathering is deeply extensive, white and buff colours characterize a thicker mantle enveloping the less weathered rock. In the light green coloured serpentinites, e.g. Paivouni, disseminated spinel crystals can be seen in hand specimen.

At Tripes, the serpentinites form black-green massive bands, alternating with greyish bands composed mainly of amphiboles. The rock as a whole shows compositional banding and accessory chromite is conspicuous in both types of rock.

Stream sections, in this unit, are deeply incised, suggesting elevation of the whole area at a much later time than the emplacement of the ultramafic rocks.

Unit (2) is smaller than the Unit (1), has a NW-SE orientation and an almost rectangular shape. Although the relief on a gross scale is smooth, stream sections are steeply incised, terminating abruptly in alluvial deposits at sea level.

In Unit (2), the rocks are deeply weathered. At Kroupnos, the serpentinites are strongly deformed and folded, because of their proximity to the contact. Adits have been opened at three places, and disseminated and schlieren type chromite ore can be seen in the walls. Nearby, the serpentinite strikes to the NW and dips to the S-SW at angles of approximately 50^{o}-60^{o}. Magnesite veins form intricate networks of massive cryptocrystalline magnesite, exhibiting cauliflower structure. These magnesite veins are usually encountered in weathered buff-brown serpentinite. Because of the intense weathering, no primary structures can be recognized. In places, serpentinite has a brown-yellow appearance which is due to the formation of limonite and other alteration and weathering bi-products.

Chromite deposits have been reported in two other places near Limonadica, but there has been no recent attempt to develop them, as the workings have been covered for several years.

2.2.4 Chromitites

Podiform chromite deposits occur at the localities shown in Fig 2.3 and mentioned above. They have an irregular

distribution in space, and variable relations to the enclosing serpentinized ultramafic rocks.

At Tripes, two ore bodies occur at different altitudes, one almost coincides with the 350m contour, the other with the 300m contour. The mineralogical similarities of the ultramafic rocks, associated with the higher ore body at Tripes and ore bodies at Paivouni, suggest a possible extension of the same rock type, although the ore deposits at Paivouni lie at the higher altitude of 450m.

The chromite ores have been classified as follows :

(1) Massive chromitite, containing 90-100% chromite,

(2) Olivine and/or pyroxene chromitite, containing 50-90% chromite, and

(3) Disseminated and schlieren type chromitite, containing less than 50% chromite. Accessory chromite is considered to be always less than 5% in any rock type.

Most chromite bodies belong to the massive type, with interstitial silicates reduced to less than 5%. At Tripes, the massive ore grades, at the borders of the pod, to schlieren type (plate 2.15) . In massive chromitites, the chromite forms irregular granulated aggregates with an interstitial lilac-coloured silicate, probably kämmererite. The massive ore shows either well defined contacts with the serpentinized ultramafics, or grades into schlieren type ore. The ore bodies have a pod-like shape, as inferred from surface excavations. They may extend for several metres or may be small lensoid bodies tailing out to tabular, disseminated types. They are always sheared.

In detail, chromite pods contain large crystals, up to 2cm in length, set in a medium grain-size matrix of

Plate 2.15

Chromite schlieren in weathered serpentinite. Note the variability of shapes and the lensoid serpentinite pods occuring between sequential schlieren of chromite.

granulated chromite and silicate. In hand specimens from Moutsara, these large chromite crystals can be seen to conform with the foliation of the host rocks and chromitites. They almost always form egg- and torpedo-shaped crystals, with their long axes lying parallel to the foliation. All these chromite crystals show tensional fractures, normal to the foliation, the degree of fracturing increasing with deformation. These pull-apart textures are best developed in the strongly sheared and folded deposits at Moutsara. Here, the appearance of the large chromite crystals resembles augen structures in gneissic rocks. In general appearance, the chromite has a typical gneissic structure, not only in samples from Moutsara, but from other locations as well, particularly from St. George and Frangocaliva, where larger chromites appear to have been squeezed and disrupted into smaller granules. According to Thayer (1969), this feature suggests a solid state, rather than a plastic flow granulation.

In the olivine or pyroxene chromitites, characteristic egg-shaped crystals of chromite can be easily seen. In hand specimen the rocks have distinct foliation, with chromite-silicate banding usually evident. Pull-apart texture is a most common feature of the large egg-shaped chromites. The foliation may or may not coincide with the layering. They can be seen in coincidence in tabular bodies, which have been strongly deformed and appear now as irregular lenses of low-grade ore, inter-banded with silicates, giving rise to deformed schlieren structures.

The disseminated ore-type is most common in the Paivouni ore deposits large anhedral chromite crystals are scattered throughout the disseminated chromite ore, showing fracturing

and pull-apart texture. The lower ore bodies at Tripes also have chromite belonging to the disseminated type. In hand specimen, the disseminated chromite varies in grade from poor to rich to almost massive. Only locally the disseminated ores reveal a primary igneous layering. The foliation can be seen distinctly to be inclined to these layers.

The schlieren plates, frequently seen to surround or accompany more massive ore deposits are randomly oriented, with the foliation lying in the plane of layering. They represent highly sheared tabular bodies. At Frangocaliva, the host serpentinite dips at high angles of approximately 80^{o} to the SW, and the stringers of ore are concordant ; in the serpentinite, tubular disseminated chromite bodies occur, tailing out into schlieren plates of less disseminated chromite. The schlieren plates form lenses terminated at the edges and connected by thin strings of chromite with the next lensoid body. In general all structures are small scale features.

CHAPTER 3

PETROGRAPHY

3.1 VAVDOS COMPLEX

3.1.1 Dunite

The primary mineral assemblage in the dunite is olivine and accessory spinel. The dunite is serpentinized in variable extent, from 10% serpentine minerals in the most fresh sample (VG1) to 90% or more for the most serpentinized dunite (sample VY1). Talc reaches 15% in certain samples, while carbonates are restricted to vein-fillings. Sampling positions are shown in Figure 3.1.

Olivine is almost always anhedral, forming interlocking crystals of different sizes, but mainly ranging from 5mm in length and 2-3mm in breadth, to rounded, small, subhedral crystals not less than 0.5mm in diameter. Localized strain effects accompany olivine throughout the complex. Deformation twins and bands in olivine sometimes occur in the main dunite, but undulatory extinction and deformation lamellae are always present. Deformation lamellae are considered to be the visible expression of slip planes, and Raleigh (1965) has shown that translational gliding takes place in olivine at 5kb and 700°C to 800°C, producing kink-banding. Strain effects are still evident in the very serpentinized dunites, indicating pre-serpentinization imposition of stress. In samples from serpentinized dunite near the basal thrust zone, olivine, although fractured and penetrated by a thick network of serpentine minerals, shows deformation and granulation. Granulation results in thin zones of minute olivine granules, usually set in a carbonate matrix.

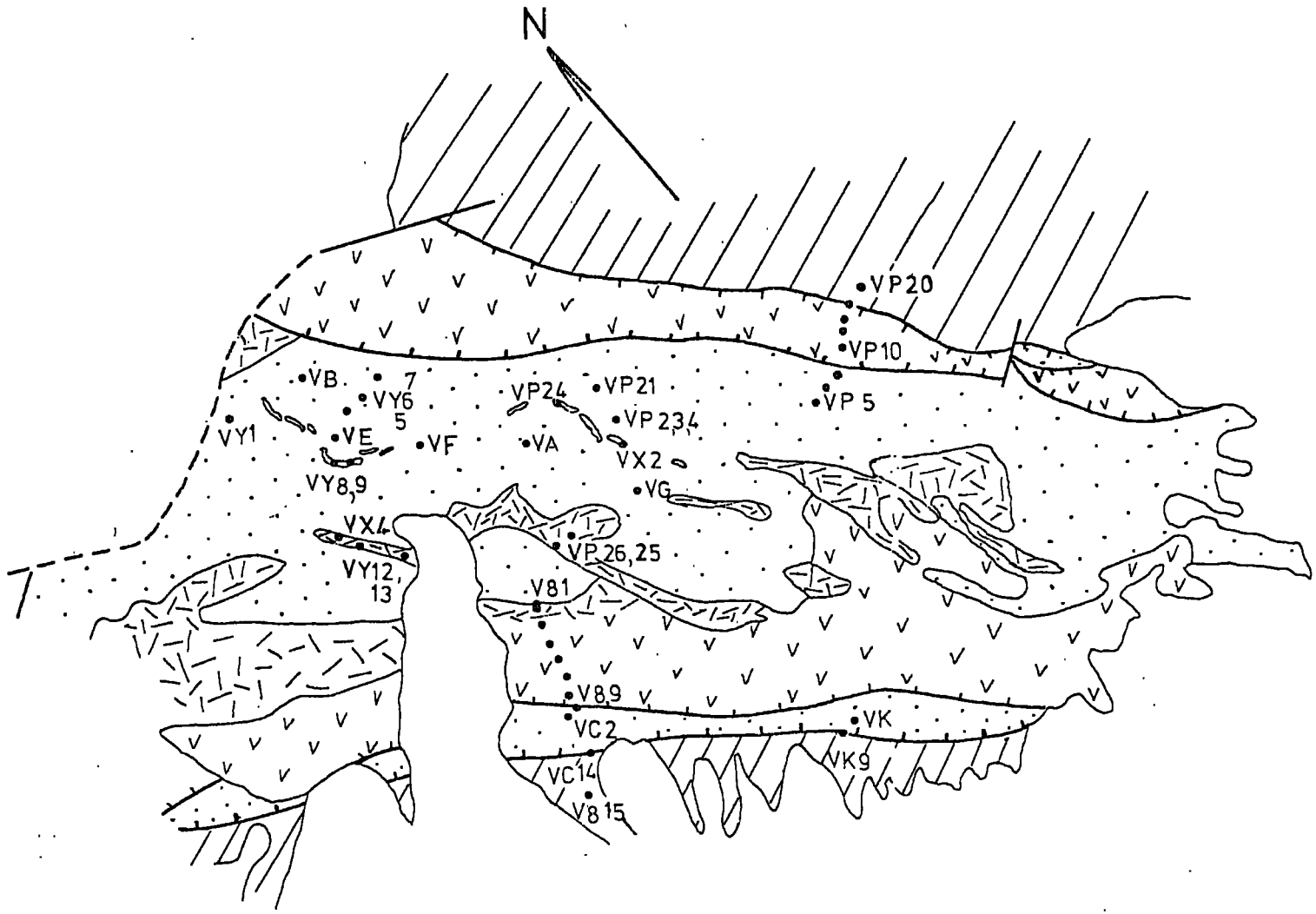
N
VP20
VP10
VB
7
VY6
5
VP24
VP21
VP 5
VP 2,3,4
VY1
VE
VF
VA
VX2
VG
VY8,9
VX4
VP 26,25
VY12,
13
V81
V8,9
VC2
VK
VK9
VC14
V8 15

Figure 3.1

Spinels range in size from 0.5mm to 2mm in length. They are euhedral, particularly in smaller crystals, or subhedral to elongate in certain directions, especially in larger crystals. Some crystals are dark brown with black rims and show pull-apart texture, the cracks often being filled with carbonate. The bigger crystals may be coated by chlorite.

Talc is an important constituent in the serpentinized dunites, reaching 20% in sample VY5. When present, it usually forms fibrous aggregates and sometimes bent strips and shreds. Relict olivine crystals occur within the talc aggregates, although they are sometimes completely replaced, their original boundaries being outlined by powdery magnetite.

Serpentine mainly replaces olivine and varies from about 10% to more than 90% near the basal thrust zone. The serpe ntine minerals show sequential stages of development in response to increasing degrees of serpentinization.

In fresh samples serpentinization follows a major fracture direction, with a less developed secondary fracture set crosscutting the former. These directions represent the initial fractures, which facilitated movement of aqueous fluids responsible for serpentinization, Moody (1976). These primary serpentine "cords" are multiple, penetrating and enclosing the olivine cores, Figure 3.2. Usually the central part of a "cord" is isotropic, followed outwards by fine fibres showing wavy extinction, which are either perpendicular (cross-fibres) or parallel (slip-fibres) to the long direction of the "cord". They are probably γ-serpentine. At some distance from contact zones (samples VC11 and VY1), the γ-serpentine fibres have an oblique orientation to the length of the "cord". Brucite may occur as a dark brown aggregate between serpentine and olivine.

Secondary magnetite, formed during serpentinization, occurs within the "cords" and is more frequent in the highly serpentinized dunites. In sample VY1, multiple serpentine "cords" contain minute and irregular rectangles of magnetite arranged in almost parallel zones. They probably represent deposition of magnetite at sequential stages of serpentinization, Figure 3.2. Antigorite blades occur in samples near thrust zones, as in sample VC11. Chlorite and carbonate patches also occur in this sample.

3.1.2 Chromitiferous Rocks

The chromitiferous rocks consist predominantly of chromite and olivine with the secondary alteration products serpentine and chlorite.

The chromite is red-brown with black rims. Typical cataclastic and pull-apart textures are mainly seen in the chromite concentrations. The chromite is usually anisotropic showing deep red colours under crossed nicols. Massive ore grades to chromitiferous-dunite and dunite within individual thin sections. Nodular chromite was only found in sample VK0, the nodules being less than 2mm in long dimension.

In massive ores no primary textures have been preserved, although sample VG2 gives evidence for an olivine-chromite cumulate (Plate 3.1). The imposed cataclastic textures and/or solid state flow structures obscure any "chain structures" characteristic of most chromite cumulates of layered intrusions. In adjacent dunite-chromitite layers, the olivine grain size reduces from the dunite to the olivine-chromitite, whereas the chromite grain-size changes conversely, being large (about 2mm) in olivine-chromitite but less than 0.2mm in dunite.

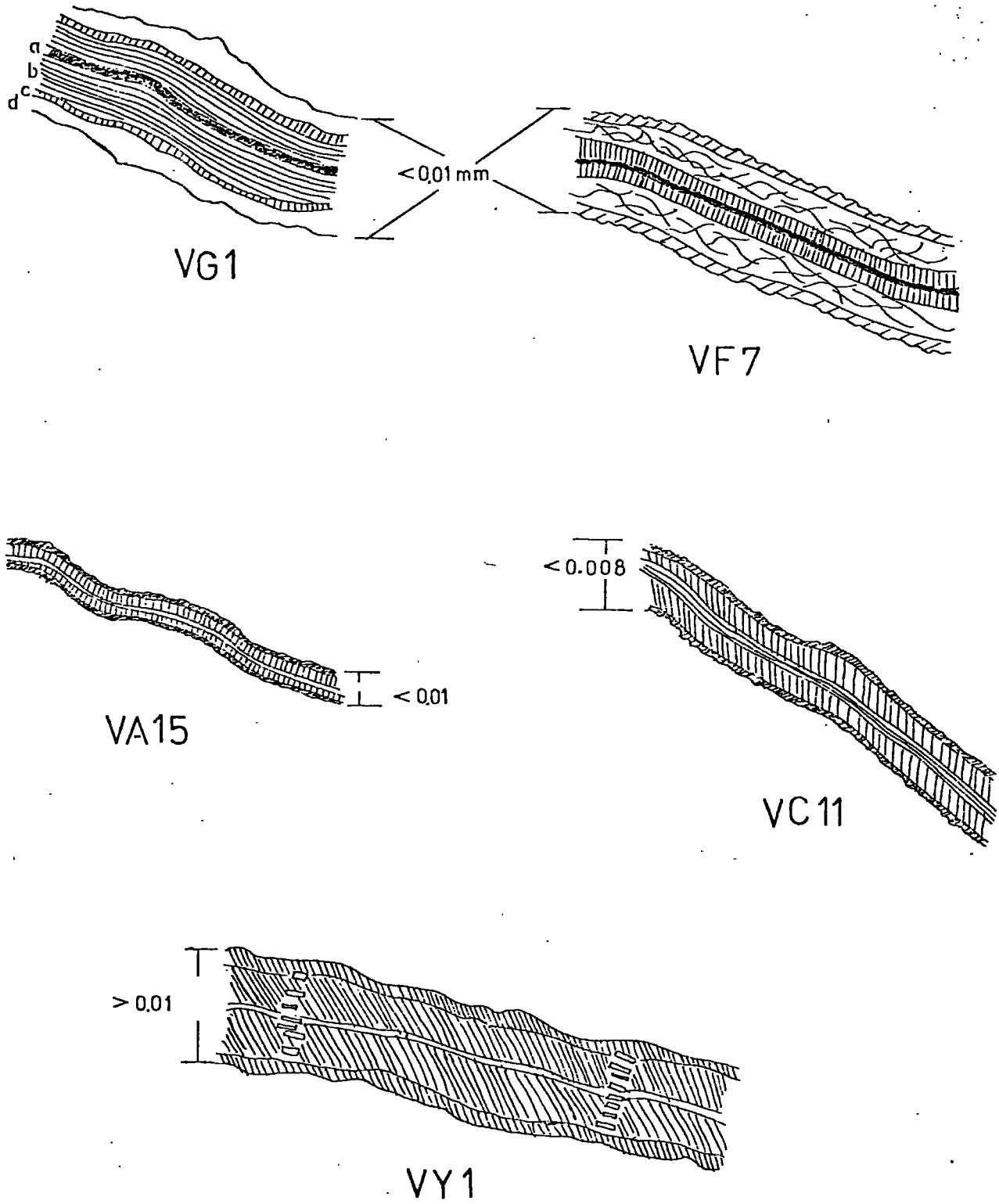

Figure 3.2

In sample VA4, chromitiferous dunite layers, containing about 25% chromite, alternate with dunite layers, a feature of unequivocal magmatic origin. Bands of chromitiferous dunite with sharp boundaries and containing as much as 50% chromite occur in the dunite. The chromite is highly fractured and has a matrix of chlorite.

3.1.3 Pyroxenite

Two varieties of pyroxenite occur. The first variety is an olivine-websterite and the second an amphibole-bearing clino-pyroxenite. Sample positions are shown in Figure 3.1.

The olivine-websterite occurs in the interlayered pyroxenite - gabbro zone. Olivine and orthopyroxene constitute about 15% of the rock. Both occur as inclusions in diopside, while orthopyroxene is also exsolved along the cleavage traces. The diopside forms large crystals ranging from 2mm to more than 5 mm in length ; twinning on (100) is very common. In sample V8.1, small (0.2mm) rhombohedral cross-sections of an amphibole (probably) have been observed. It is pale blue-violet in colour and occurs mainly at diopside grain boundaries, forming up to 1% of the rock.

The amphibole-bearing clino-pyroxenite forms an irregular body within the main dunite. Diopside forms more than 60% of the rock, crystals ranging from 2mm to more than 2cm in size. It shows simple and polysynthetic twinning, probably on (001). Small euhedral amphibole crystals, varying in size from 0.4mm to 1mm for sections parallel to (001), and sometimes reaching 2mm in sections parallel to (010). They have a pale blue-violet colour, with extinction angles for elongate crystals always below 25^{o}. Their boundaries are always sharp. This suggests that the amphiboles were the first crystallized mineral in this

rock unit, as they are usually included in diopside crystals.

3.1.4 Gabbro-Amphibolite

The gabbros are typical magmatic cumulates with cumulus orthopyroxene ; sample VP10 is representative (Figure 3.1). The gabbros from the interlayered pyroxenite-gabbro zone show phase-layering characteristic of sequences in layered complexes.

Although sample VP10 is relatively fresh, the plagioclase is replaced by secondary minerals. It occurs in subhedral or interstitial crystals. The enstatite is slightly pleochroic from pale greenish-pink to pale greenish-grey and varies in size from 0.5mm to 1.5mm. It is usually partially serpentinized along fractures. The diopside usually forms rounded crystals but also has an interstitial habit. It varies from 0.2mm to 1.7mm in length in relatively elongate sections. Pyroxenes represent about 40% of the rock.

In gabbros from the pyroxenite-gabbro zone, pyroxenes are largely replaced by amphibole. In these gabbros, the amphibole and plagioclase form distinct domains. The amphiboles form large, single crystals up to 5mm in length, while the plagioclase is composed of small crystals around 0.4mm in diameter with sutured boundaries indicative of deformation in the solid state. With increasing deformation amphibole grain size is reduced to less than 0.4mm, but there is an increase in the size of the plagioclase crystals. Twinning disappears in the plagioclase and the rocks show development of foliation (sample V8.8).

Within the zone of interlayered pyroxenite-gabbro an anorthositic layer has been encountered. This consists of untwinned plagioclase only, with sutured boundaries indicative

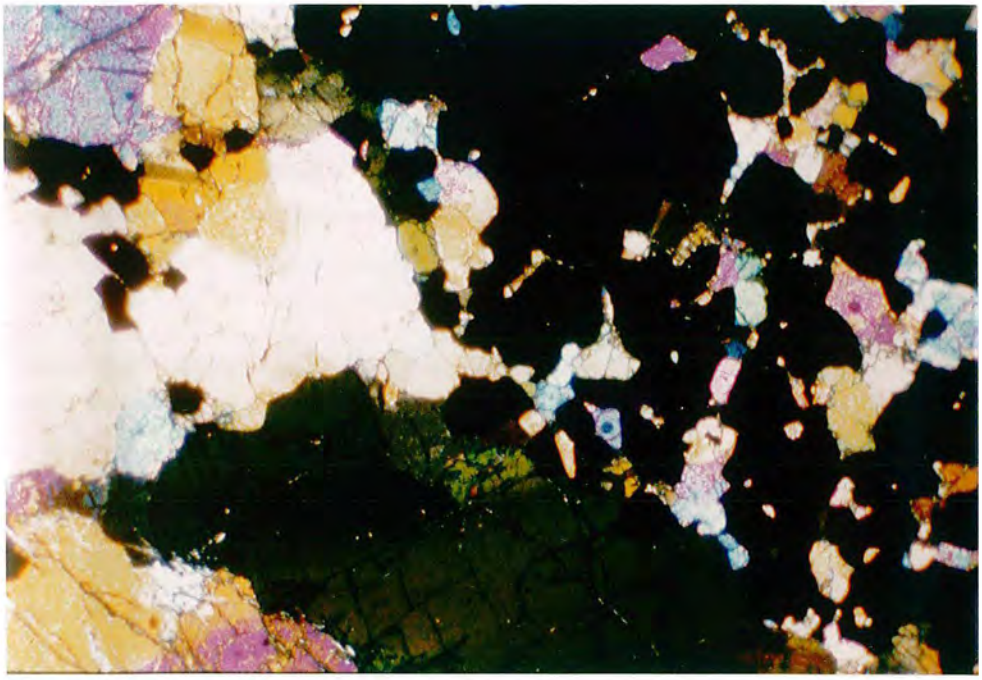

Plate 3.1 Dunite-chromitite contact. The size of chromite crystals reduces from the chromitic layer to the dunitic part. Note the large olivines with localized strain effects in the dunite, in contrast to the small olivines of chromitite. Sample VG2. Crossed polars. X10.

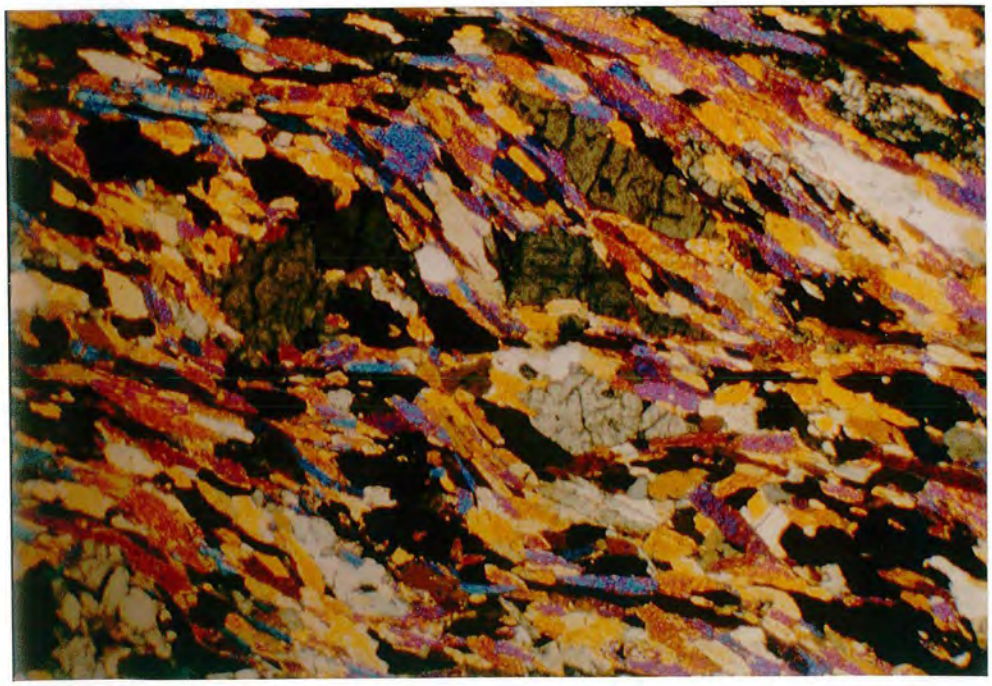

Plate 3.2 Amphibolite from the southern gabbro-dunite contact. Note the strong fabric of the rock, and the plagioclase augens. Sample V8.9 from the Vavdos complex. Crossed polars. X10.

of postcrystallisation deformation.

Sample V8.9 is a strongly deformed amphibolite from close to the southern contact (Plate 3.2). The amphibole is a colourless variety of the tremolite-actinolite series, and forms lensoid crystals up to 0.9mm long. Plagioclase forms elongate augens, usually wrapped-round by the foliation. Microfolding is common in this rock. A plagioclase vein crosscuts this rock normal to the foliation. It is probably of later formation because ofthe very well developed twinning in the plagioclase. Some amphibolites from the contact between the gabbros and the underlying serpentinized dunite show a granular, hornfels texture (sample VC2). The amphibole crystals, less than 0.2mm in length in elongate sections, are slightly pleochroic in pale green colours, and in places have pale brown-yellow cores. Grain boundaries between amphiboles usually show 120^{o} triple junctions. Plagioclase is highly irregular and fractured into small granular domains ; it shows anomalous interference colours.

Cumulate gabbros, dynamically metamorphosed, occur with the serpentinised dunite at the base of the complex. The pyroxenes form the cumulate phase with intercumulus plagioclase in almost equal amount. The pyroxenes are replaced by a mineral of the epidote group. Sphene (2-3%) is a close associate of epidote, both replacing the primary pyroxenes although some diopside remains unaltered. Plagioclase has equilibrated under the new conditions, and shows only deformation twins. Quartz, totalling about 5% of the rock, occurs together with laths of colourless mica, probably muscovite. The quartz has sutured boundaries, undulose extinction and deformation shadows. It is probably of metamorphic origin.

The contact between the gabbros and overlying country rocks is characterized by sequential changes in the primary gabbro with increasing dynamic metamorphism. The slightly metamorphosed gabbro consists of plagioclase and amphibole. Plagioclase is usually concentrated in domains, with crystals varying from 0.8mm to less than 0.1mm in diameter. Primary pyroxene is replaced by amphibole, with a grain size not exceeding 1.5mm. As the contact is approached, the amphibole grain size increases, in places reaching 2.5mm in length in elongate sections. Sample VP16, from the vicinity of the contact, shows intense foliation and microfolding (Plate 3.3). Augen textures are common, with separation of different minerals into distinct bands. The strong fabric suggests dynamic metamorphism, supporting the field interpretation of a thrust contact.

3.1.5 Rocks of Contact Zones

Samples collected from the basal thrust zone are cataclastic with an unfoliated cryptocrystalline matrix.

In sample VC14, antigorite and carbonate compose more than 95% of the rock. The texture is typically cataclastic, the previous mosaic texture being still evident but intensely dismembered. Antigorite mainly forms cryptocrystalline aggregates, although in places, fibrous, flaky, and sometimes radiating aggregates occur. Opaque minerals are euhedral in shape with hexagonal outlines and are surrounded by tabular and bent chlorite crystals. Rare garnet forms idioblastic, dodecahedral crystals, surrounded and outlined by opaques and serpentine. Quartz is a minor constituent and has a typical granoblastic texture.

This rock is an ultracataclasite ; the incipient recrystallization and finely granulated, cryptocrystalline matrix suggest that only dynamic metamorphism was involved, the increase of temperature being mainly due to friction processes.

Some contact rocks are porphyroclastic (sample GK9) with about 50% porphyroclasts and porphyroclastic aggregates in a cryptocrystalline carbonate matrix. Quartz is the most abundant porphyroclast, individuals reaching 5mm in diameter. These porphyroclasts are strained, showing deformation twins, polygonisation and incipient re-crystallization. Mutual grain boundaries are usually sutured and the cracks are filled with carbonate. Garnet forms large crystals in excess of 5mm in diameter. It is fractured and has inclusions of sphene, colourless amphibole, clinozoisite and minute blades of opaques. Egg-shaped aggregates of randomly oriented clinozoisite and chlorite or amphibole also occur within the carbonate groundmass. Clinozoisite is usually anhedral but can also show pseudohexagonal sections, while amphibole is colourless, has parallel extinction, large 2V, and is pleochroic from white to very pale green. Both minerals occur in the carbonate matrix, with prismatic amphibole (0.6mm in length) porphyroclasts forming myrmetitic intergrowths with quartz.

3.1.6 Granitic Rocks

These rocks show a typical metamorphic texture. They consist of quartz and feldspar in almost equal amounts with minor tourmaline, muscovite and garnet.

The potash-feldspar has a perthitic texture and is of coarse grain-size, with crystals up to 6mm in diameter. Single large crystals have an exsolved feldspathic phase at a different

angle to the primary perthitic ribbons. Mortar texture is common, suggesting dynamic metamorphism. Quartz shows typical granoblastic texture with irregular grain boundaries, either lobate or dentate, intense strain effects, and graphic intergrowths with the potash-feldspar. It ranges in grain size from 0.9mm to less than 0.1mm in diameter. Unstrained oligoclase also occurs and microcline is present, up to 8% of the rock ; these two minerals are considered to be of metamorphic origin.

Tourmaline contents are variable, reaching more than 10% in some samples, or forming large isolated crystals in others. It is pleochroic from pale yellow-green to deep green-yellow and shows concentric colour zonation, with the cores usually being yellow and the rims green. The tourmaline is usually poikilitic, enclosing quartz and feldspar. Muscovites are bent and follow the boundaries of large K-feldspars ; they are usually less than 0.4mm in length.

Highly fragmented garnet also occurs. It is not thought to be a primary granitic mineral, but a product of the dynamic metamorphism of these rocks. Fragmented, fine grained olivine also occurs in sample VP4, probably being a xenolith from the dunite.

The origin of these granitic rocks is probably related to the dynamometamorphic episodes, but no precise explanation can be given and their origin will not be discussed further in this thesis.

Plate 3.3 Sheared fabric of a rock sample from the contact between gabbro and overlying country rock in Vavdos. The minerals present, are amphibole and minute, thin-elongated plagioclase. Sample VP16. Crossed polars. X10.

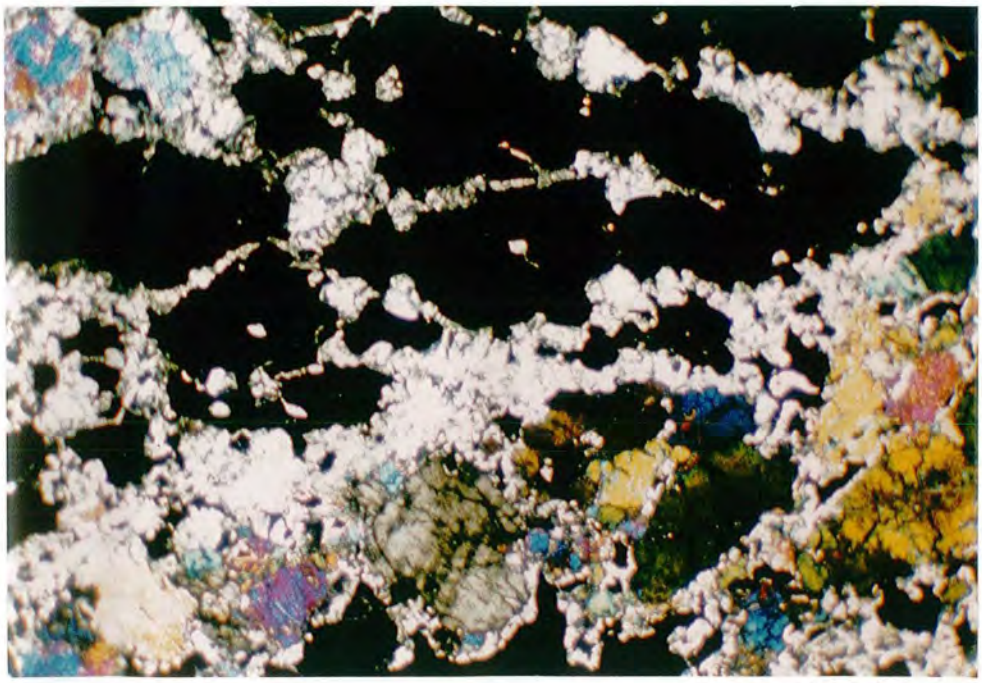

Plate 3.4 Clinopyroxene-bearing chromitite from the Gomati complex. The clinopyroxene is strained and shows twinning. Note the highly sheared chromite crystals and their irregular outlines. Sample GL5. Crossed polars. X10.

3.2 GOMATI COMPLEX

3.2.1 Serpentinites

Serpentinites form the predominant rock type of the peridotite massif. Sample locations are shown in Figure 3.3. The serpentinites exhibit textures which are controlled by the primary mineralogy of the rocks and shearing stress. Among these textures, the predominant are the mesh, bladed-mat, and ribbon-like textures, as well as textures including large bastitic areas.

The opaques belong to three distinct categories. The larger opaque crystals vary from 0.2mm to 1mm in diameter. They show fracturing, are black with metallic lustre and may be surrounded by a reaction rim of chlorite. Opaques interstitial to olivine crystals (sample GM1), have variable grain size, but are usually less than 0.5mm in diameter. They are black and extensively replaced by silicate impurities. Interstitial opaques of very fine grain size delineate pre-existing crystal boundaries ; they are secondary magnetite formed during serpentinization.

The most strongly sheared rocks in Unit 1, occur at the base of the massif near the contact with the metamorphic country rocks ; they show two distinct preferred orientations (sample GN1). One is a foliation of serpentine laminae and granulated opaques of very fine grain size (S1) ; the second a strain foliation (S2) indicated by deformation bands in the serpentine matrix and by the elongation of larger opaques. These reach 1.8mm in length and show tensional fractures perpendicular to the direction of elongation.

Shearing decreases towards the centre of the complex. Sample GN2 still has a strong fabric, with opaques which are

Figure 3.3

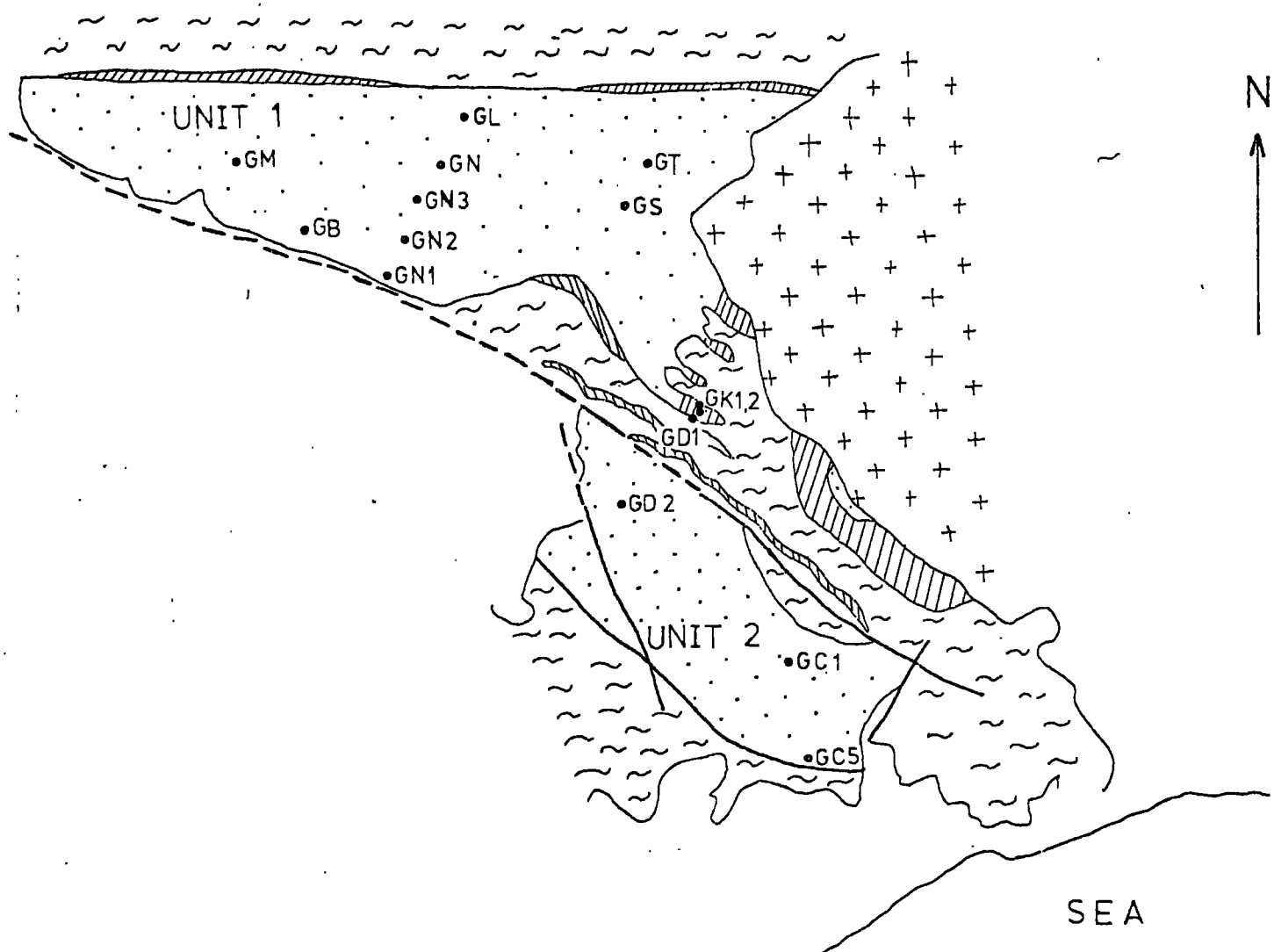
UNIT 1
GL
GM
GN
GT
GN3
GS
GB
GN2
GN1
GK1,2
GD1
GD 2
UNIT 2
GC1
GC5
SEA
N

granulated and streaked out. Relict pretectonic olivines are however present, with irregular mesh-texture serpentinization. They are elongated parallel to the foliation, showing an augen-like structure and tensional cracks. They are wrapped around by the foliation. Later, flaky antigorite forms aggregates replacing both olivine relics and pre-existing serpentine.

In less deformed rocks (sample GN3) preferred orientation is indicated only by granulated opaque minerals. Some opaques show internal S-shaped granulation, interpreted as syn-deformational fracturing.

Olivine is highly serpentinized, and was found only near the base of Unit 1, samples GM1 and GB4 being relatively the most fresh, and probably representing primary dunite. The olivine is highly fractured and replaced by lizardite. Strain effects, like undulatory extinction and deformation lamellae are common. Some olivines show triple junctions characteristic of an annealed fabric.

In the banks of the Verkos stream, several layers of amphibole and chlorite alternate with fine-grained serpentine and chlorite layers. The amphiboles are colourless and reach 0.8mm in length ; they include opaque minerals which outline cleavages. They probably belong to the tremolite-actinolite series and are of metamorphic origin. Occasionally the shape of crystals is indicative of original pyroxenes, now totally replaced by amphibole. Irregular opaques up to 2.5mm in diameter accompany the amphibole bands, but they are always coated by serpentine and chlorite, the latter showing replacement by antigorite. The serpentine bands contain matted antigorite aggregates and opaques which are surrounded by chlorite reaction rims.

Bastite serpentinites, with less than 50% bastitic areas are typical of samples from Moutsara. The bastite is lizardite. It represents primary pyroxene and occasionally shows subhedral shape, with trails of opaques outlining the original crystal boundaries and pre-existing cleavage traces. Antigorite blades are imposed on these bastites, while the non-bastitic areas consist of fine-grained serpentine. The rock is believed to represent serpentinized harzburgite (or olivine-orthopyroxenite).

In Unit 2, the serpentinization is in an advanced stage and is accompanied by weathering. Rocks with typical mesh textures (sample GC1) occur in this unit. Small relict cores of olivine remain, which are now largely replaced by talc. Magnetite dust outlines the primary olivine crystals. Characteristic hour-glass texture has also been observed in sample GD2 of this unit.

3.2.2 Chromitites

In thin section the chromite is red-brown, varying to black along cracks and at the margins of crystals. In some cases entire crystals have been converted to the black variety and contain numerous silicate inclusions (sample GL5). The chromite is slightly anisotropic with deep-red interference colours. It is almost always anhedral and granular, with pull-apart texture normal to the elongation of larger crystals ; the grain-size varies from 0.5mm to 7mm in length. In most specimens fractured chromite crystals show mutual boundaries, suggesting that the fractures are tensional cracks formed during intense shearing. Large egg-shaped chromite crystals are elongated in the foliation plane. They grade into disseminated ore and show great similarity to nodular-type chromite.

Primary inclusions of clinopyroxene occur in the chromites (sample GS4), whereas the interstitial spaces are usually filled with chlorite. The clinopyroxene is a fairly common mineral in samples from the Moutsara locality. The crystals are strained and show kink-banding, deformation lamellae and deformation twins. The chromites of this locality are extremely sheared, with microfolding always present (plate 3.4). A bright green mineral surrounds many chromite crystals or forms pseudomorphs after clinopyroxene ; it is probably pleonaste formed at a late stage.

3.2.3 Amphibolites

The contact amphibolites may exhibit preferred orientation. Samples have been collected only from the southeastern contact of Unit 1.

Pleochroic amphibole about 60%, garnet megacrysts (10%), quartz and plagioclase (20%) with minor amounts of sphene (3%), opaques and carbonate comprise the mineral assemblage of a typical unsheared amphibolite (GK2). The amphibole is a green to straw-yellow pleochroic hornblende, forming subhedral, poikilitic crystals with inclusions of sphene and quartz. The quartz is xenoblastic and interstitial. In places it shows triple junctions and recrystallization textures. At least two varieties of quartz can be distinguished from their impurities, which have aided their nucleation. Pink garnet forms idiomorphic to subidiomorphic crystals. It is cracked and replaced by chlorite and a very pale coloured amphibole. Sphene occurs as wedges, reaching 0.9mm in their long axis, and as small irregular grains replacing opaques. Most minerals show irregular sutured or embayed interphase boundaries, characteristic of non-equilibration. The assemblage is typical of the

almandine-amphibolite facies of Turner and Verhoogen (1960).

The characteristic of a second unsheared garnet-amphibolite is the complete lack of plagioclase (sample GD1). This amphibolite is comprised of hornblende (50%), garnet (30%), epidote (15%) and accessory sphene and apatite. The hornblende is blue-green to pale-green in colour and poikilitic. Garnet porphyroclasts are highly altered and replaced by chlorite. Epidote forms subidioblastic crystals. This rock is extensively altered.

Pleochroic amphibole (40%), plagioclase (30%), carbonate, sphene, accessory opaques, epidote and chlorite form the mineral assemblage of strongly sheared amphibolites (sample GK1). The foliation is produced by parallel alignment of all minerals. The amphibole is a pleochroic hornblende, from green to straw-yellow in cross-sections and from deep-blue green to straw-yellow in longitudinal sections. It is poikilitic, with sphene inclusions, and varies in grain-size from 0.1 to 0.5mm in diameter. Plagioclases are bent, show undulose extinction, deformation shadows and sutured boundaries. Tension cracks normal to the foliation are filled with carbonate. The quartz is interstitial with an irregular shape. Epidote is a retrogressive product of original pyroxene, whose crystals are pretectonic and are also wrapped around by the foliation.

The characteristic feature of all the amphibolites is the development of low grade metamorphic mineral assemblages from higher grade primary minerals. The primary mineral assemblages are characterized by an increase of almandine content at the expense of plagioclase. Green and Ringwood (1967) have shown a gradual increase in garnet and decrease in plagioclase with increasing pressures. The primary assemblages

indicate high temperatures and pressures of formation. Retrogressive metamorphism resulted in the imposition of assemblages characteristic of the upper greenschist facies of Turner and Verhoogen (1960).

3.3 COUNTRY ROCKS

A strongly sheared biotite schist occurs below the Vavdos ophiolite, with elongate biotite indicating the preferred orientation of the rock and also outlining the microfolding. Biotite forms 10% of the rock, garnet is less than 1% and the remainder is quartz and feldspar in almost equal proportions. The plagioclase shows incipient sericitization giving a slight cloudy appearance. It has highly irregular grain boundaries and shape, and a predominant elongation parallel to the strong fabric of the rock. Deformation twins and perthite threads of metamorphic origin also occur, together with myrmekite. The quartz has sutured grain boundaries, deformation shadows and undulatory extinction. Biotite forms bent crystals, usually in sections parallel to (010) and garnet occurs in rounded octahedral sections.

These are typical dynamometamorphic textures, with slight recrystallization. They suggest that the biotite schist has been mainly subjected to shearing stress during the emplacement of the ophiolite stacks.

CHAPTER 4

CHEMISTRY OF SILICATE MINERALS AND ROCKS

4.1 MINERAL CHEMISTRY

4.1.1 Olivine Chemistry

Analyses of olivines from the Vavdos and Gomati complexes have been made by the Geoscan electron microprobe. The results are shown in Appendix II, Tables 3 and 8.

The olivine from the dunite of the Vavdos complex is forsteritic, mainly around Fo_{95} as shown in Figure 4.1, but it ranges from Fo_{92} to Fo_{96}. MgO contents vary from 50.5 to 53.7%, while NiO contents from 0.35 to 0.75% as shown in Figure 4.2a. MnO contents, Figure 4.2b, show a limited range from 0.03% to 0.15%, with the exception of one sample at 0.21%. Olivine from the pyroxenite has a consistent Fo-content of Fo_{82}, Figure 4.1. NiO is below 0.30%, but MnO varies from 0.22 to 0.31%, Figures 4.2a and 4.2b respectively.

Olivines from chromitiferous dunite and dunite of the Gomati complex show no compositional difference, the ratio $Mg \times 100/Mg + Fe^{2+}$ being variable and extending between 88 and 92. The MgO content varies from 47.2 to 49.7%, while NiO ranges from 0.30 to 0.43%. Both values are consistent with those given for other ophiolite complexes, Table 4.2. MnO content is low, varying from 0.09 to 0.17%.

The relations between NiO, MnO and Fo-content for olivines of the Vavdos complex are shown in Figure 4.3. There is an apparent Mg depletion from massive chromite to dunite with concomitant Mn enrichment and Ni impoverishment. However, a more distinct trend is shown in Figure 4.2, with the olivine

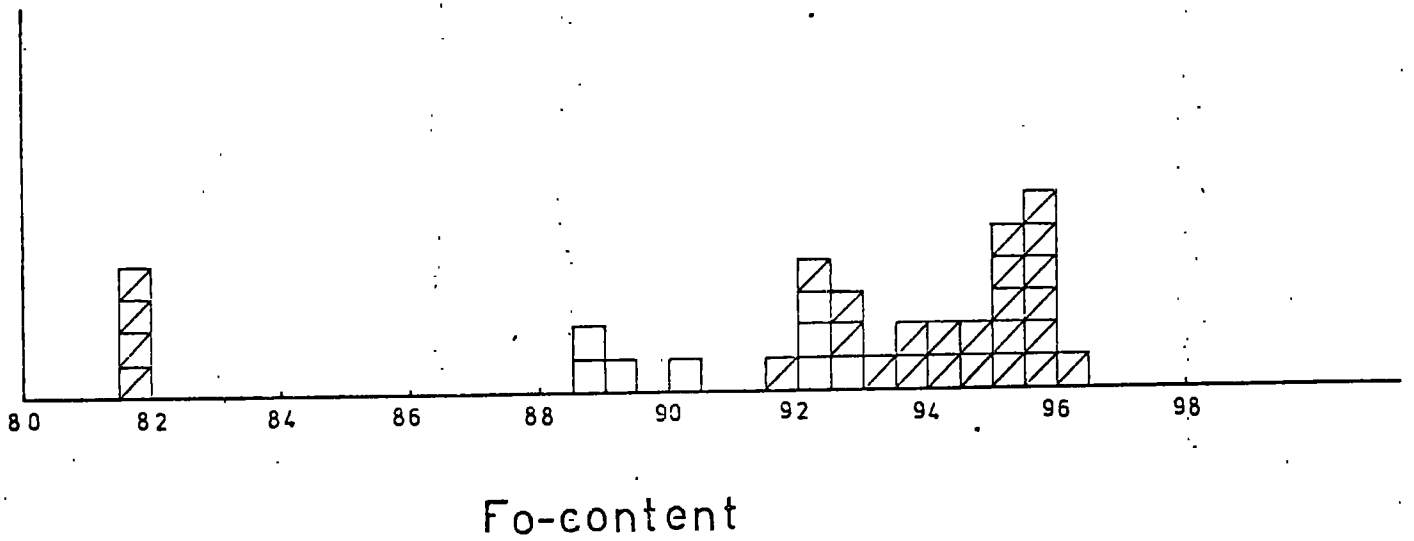

Figure 4.1 Histogram showing the distribution frequency of olivine in both complexes.

Vavdos complex. Gomati complex.

Figure 4.2

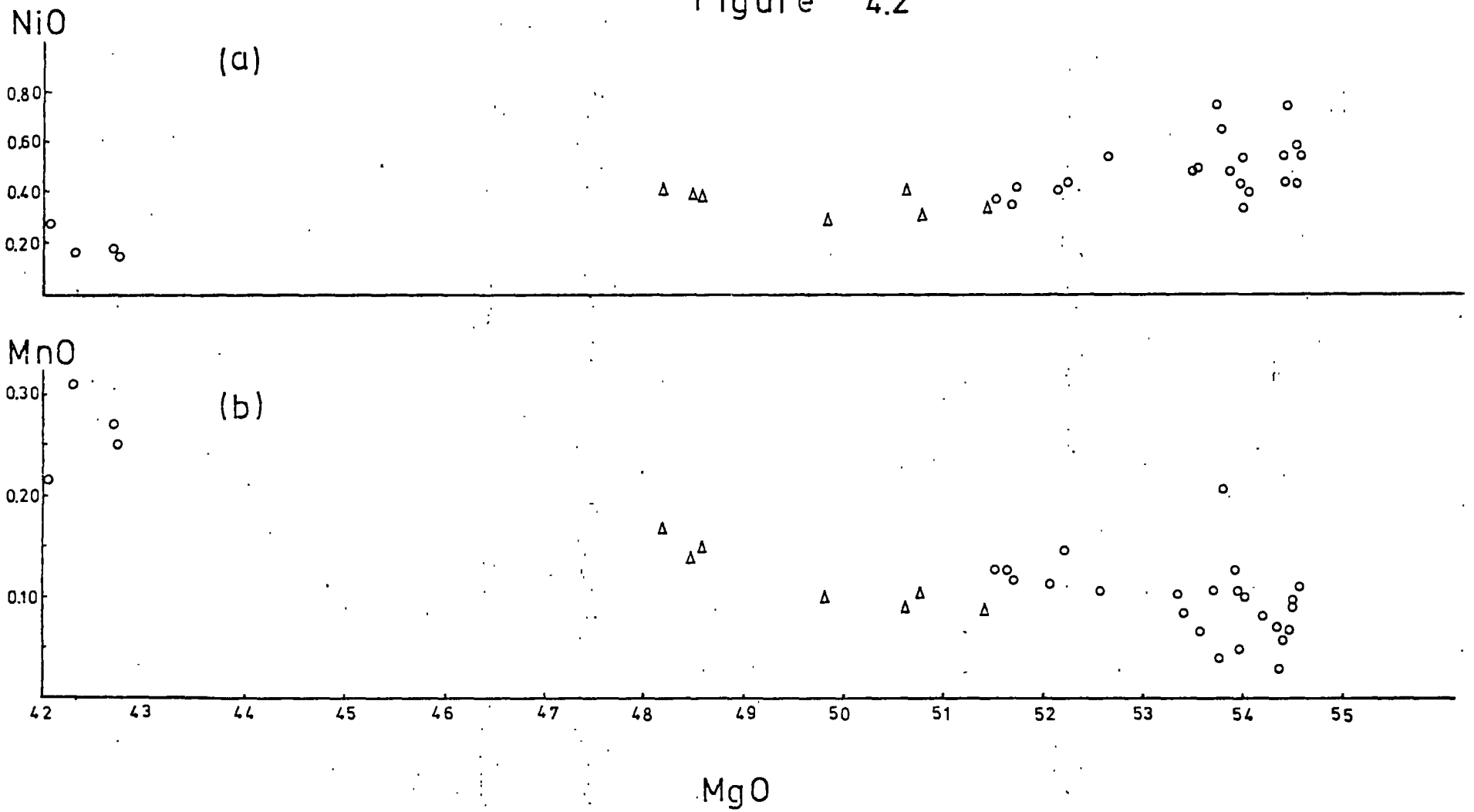
NiO
(a)
0.80
0.60
0.40
0.20
MnO
(b)
0.30
0.20
0.10
42
43
44
45
46
47
48
49
50
51
52
53
54
55
MgO

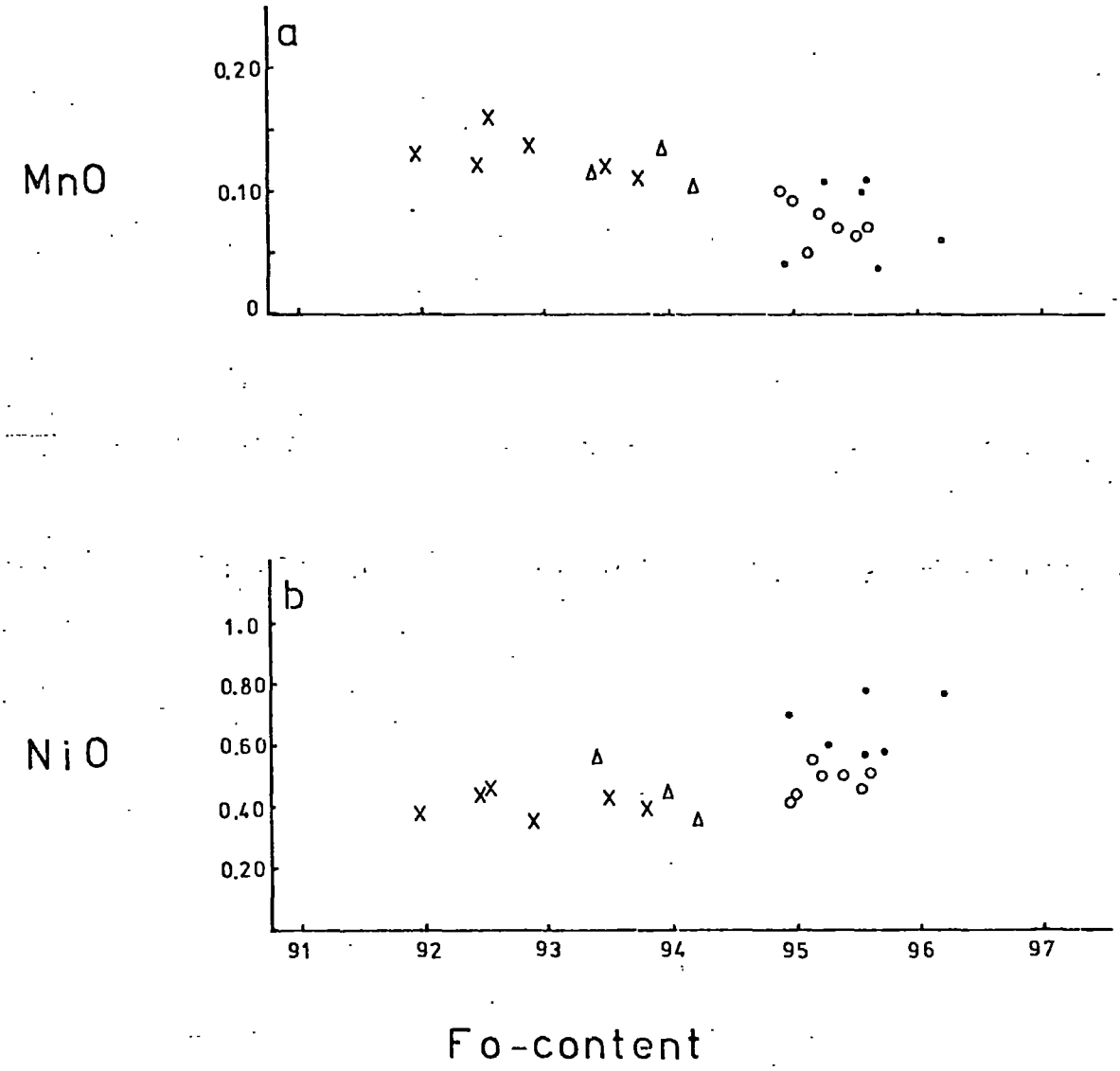

Figure 4.3

Distribution of minor oxides in olivine from the chromitiferous rocks to the main dunite. Olivine from massive chromitites (•), olivine-chromitites (o), chromitiferous dunite (Δ) and dunite (X) is shown. The olivine from massive chromitites is distinctly more Fo-rich and has higher Ni-content than that from the main dunite.

TABLE 4.1 Fo-content of olivine from different alpine type complexes.

	Lherzholite	Harzburgite	Dunite	Chromitite
Vavdos complex	-	-	91.98-93.83	93.36-96.25
Gomati complex	-	-	88.5-92.6	-
Vourinos complex, Greece, Moores, 1969.	-	88.8-91.0%	89.8-91.6%	-
Burro mountain, U.S., Loney et al, 1971.	-	91.1-91.4%	92.4-92.7%	-
Orthris mountains, Greece, Hynes, 1972.	89-90%	91%	-	-
Massif du Sud, S.New Caledonia, Rodgers, 1973.	-	87-92%	87-93%	92-96%
Twin Sisters dunite, U.S, Onyeagocha, 1978.	-	-	90.6-92.2%	92.5-96.2%
Bay of Islands, N.F.,Canada, Malpas and Stevens, 1979.	89.8%	91.4-93%	81.1-89.1%	-
Voyar Massif, Urals, Savelyev and Savelyeva, 1979.	-	89.5-91.6%	90.2-93.2%	-
Josephine peridotite, U.S, Dick, 1977.	-	90.4±0.5%	-	-
Sekinomiya complex, Japan, Arai, 1980.	-	90-91.2%	90.6-93.5%	95-97%
Kempirsai Massif, U.S.S.R, Pavlov and Grigoreva,1977.	-	91.1-92.9%	90.1-94.2%	-

TABLE 4.2 NiO-content of olivine from different alpine type ultramafic bodies.

	Dunite	Chromite pods
Vavdos complex	0.36-0.46%	0.57-0.78%
Gomati complex	0.30-0.43%	-
Blue river ultramafic body, Canada, Pinsent (1974)	0.19-0.47%*	0.52%
Twin sisters dunite, Onyeagocha (1978)	0.32-0.45%	0.39-0.76%

* this range represents NiO-content of olivine from dunite and harzburgite.

from the pyroxenite having distinctly higher Mn and lower Ni contents than that from the dunite. A comparison is made with olivine from other ophiolite complexes in Table 4.1.

4.1.2 Pyroxene Chemistry

Analysed pyroxenes from the Vavdos complex belong to the Ca-rich and Ca-poor series. Representative analyses are given in Appendix II, Table 4.

Compositions of the pyroxenes plot in the pyroxene quadrilateral as shown in Figure 4.4. The orthopyroxenes from the pyroxenite are En_{83}-En_{90}, while those from gabbros are consistent, around En_{81}. Both groups have low Ca-contents, those from the gabbro having the lowest values. Al_2O_3 contents vary from 1.2% to 1.8%, being always higher in pyroxenes from the pyroxenite. Chromium contents are low, particularly in the gabbro where values are below 0.5%, whereas pyroxenes from the pyroxenite are consistent, Cr_2O_3 ranging from 0.22 to 0.23%. The Mn-contents have no consistent distribution but pyroxenes from the pyroxenite have slightly higher Ni-contents.

The Ca-rich pyroxenes are very calcic and overlap in composition with clinopyroxenes from both metamorphic and cumulate parts of other ophiolite complexes, Figure 4.5a. The Ca-rich pyroxenes from gabbro are richer in iron than those from the pyroxenite. The aluminium content of the Ca-rich pyroxenes is higher than that of the orthopyroxenes, reaching 2%, while chromium contents range from 0.28 to 0.59% for pyroxenes from the pyroxenite but are less than 0.07% for those from the gabbro. The Mn and Ni distribution is irregular but sodium is distinctly higher in pyroxenes from the gabbro, reaching 0.33%, whereas it varies between 0.13 and 0.17% in the pyroxenite.

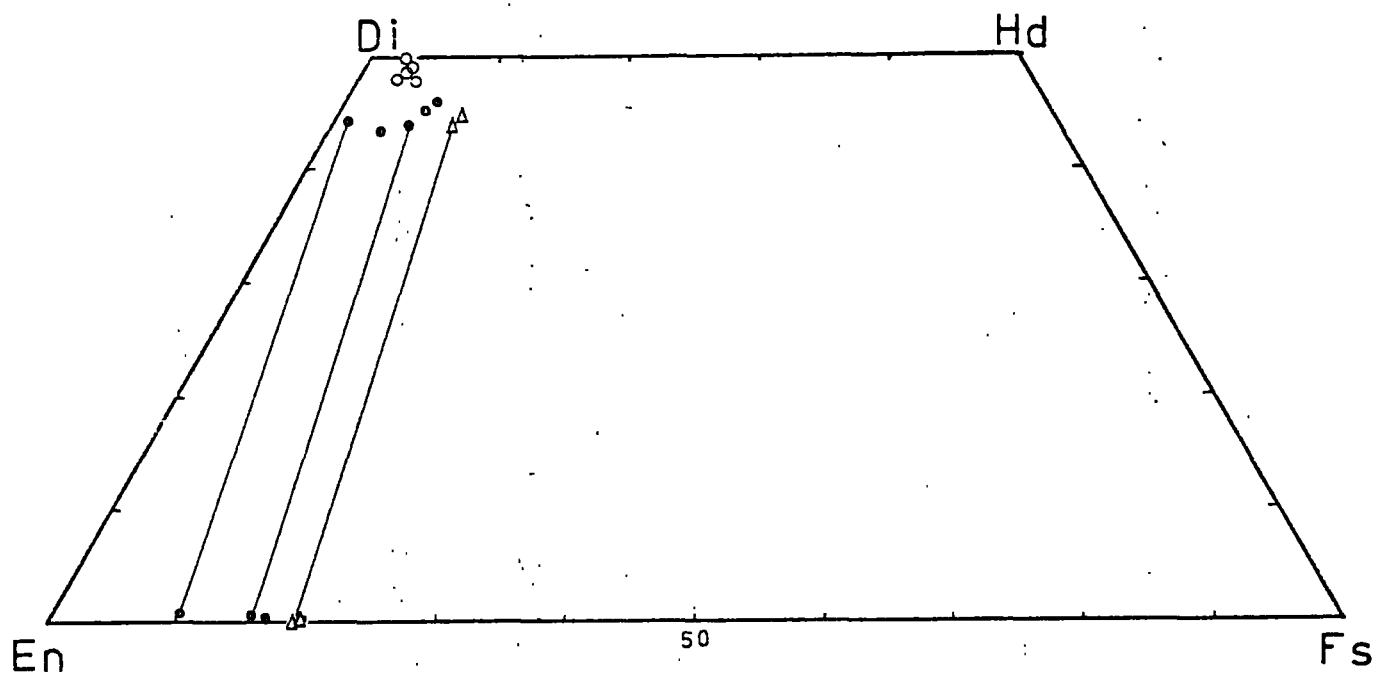

Figure 4.4 Plot Ca-poor and Ca-rich pyroxenes from both complexes in the diopside-hedenbergite-ferrosilite-enstatite diagram. Open circles represent clinopyroxenes from Gomati complex. Solid circles are pyroxenes from the pyroxenite, and triangles are pyroxenes from the gabbro of Vavdos. Tie-lines are between co-existing clino- and orthopyroxenes.

Figure 4.5

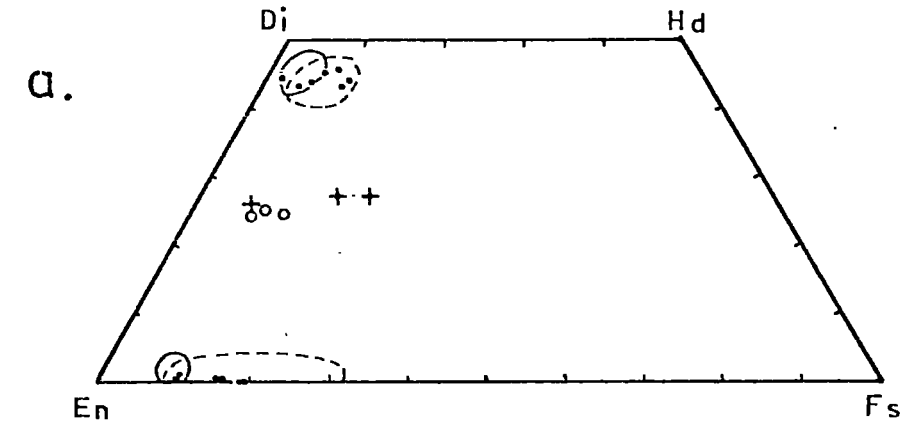

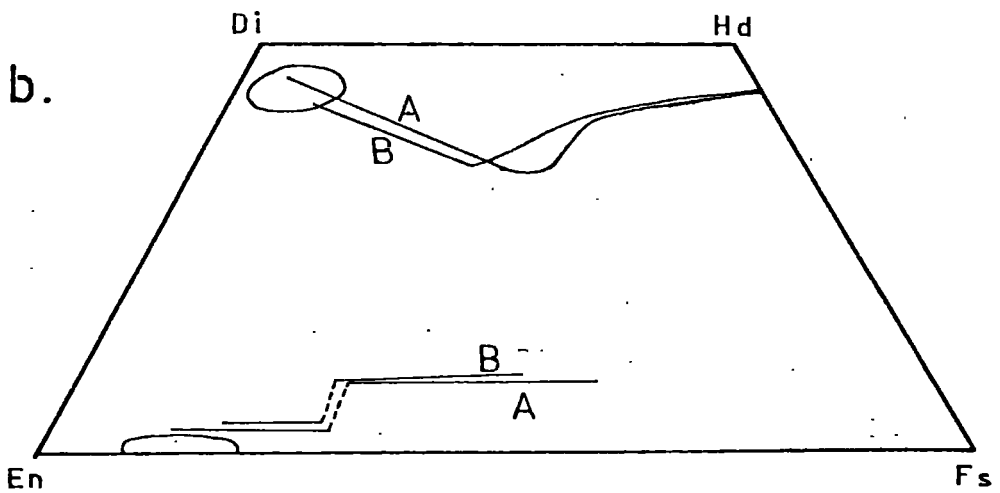

Compositional fields of pyroxenes from Vavdos are shown, with the Bushveld and Skaergaard pyroxene trends for comparison, in Figure 4.5b.

The pyroxenes from the chromitites of Gomati plot very close to diopside, Figure 4.4.

In samples from Moutsara, pyroxene occurs interstitial to chromite crystals. It has a Wo_{48}-Wo_{50} content, and high alumina, chromium and sodium contents in comparison with the pyroxenes from Vavdos. Al_2O_3 varies from 1.43 to 2.48%, Cr_2O_3 from 0.72 to 1.19% and Na_2O from 0.48 to 0.63%. Ti-contents are also much higher than in Vavdos pyroxenes. In general the iron content is much lower than pyroxenes from Vavdos, being always less than 2%.

Two clinopyroxene inclusions in chromite have been analysed from a sample of the Tripes locality. They are Wo_{49}. Their chromium content is higher than those from Moutsara ranging from 1.96 to 2.13% and Al_2O_3 is between 2.13 and 2.56%. They are characterized by high Ti-content, around 0.52% and sodium-content of the range 0.80-0.85% ; both oxides are much higher than those from Moutsara. Pyroxene analyses from Gomati are tabulated in Appendix II, Table 9.

4.1.3 Other Silicate Minerals

Amphiboles from the Vavdos clinopyroxenite, occurring as inclusions in larger diopside crystals, have been analysed and show high total compositions. These analyses are shown in Appendix II, Table 5. They have also been recalculated on the basis of 6 oxygens (pyroxene formula) and plotted in Figure 4.5a; they are very similar to the subcalcic pyroxenes, reported by Menzies (1973) from the Makrirrakhi complex (Greece), which

TABLE 4.3

Garnet VP24		Tourmaline VP24	
Oxides weight percentage			
SI102	38.15		
TI102	0.01	SI102	35.23
AL203	20.30	TI102	1.01
FE101	24.22	AL203	33.50
MN101	11.62	FE101	11.42
MG101	0.55	MN101	0.11
CA101	4.14	MG101	2.16
NA201	0.06	CA101	4.29
K 201	0.02	TOTAL	87.72
NI101	0.03		
TOTAL	99.12		
Atomic proportions on the basis of 24 oxygens		27 oxygens	
Si	6.1987		
Ti	0.0017	SI	6.3969
Al	3.8912	TI	0.1373
Fe	3.2919	AL	7.1741
Mn	1.5999	FE	1.7344
Mg	0.1338	MN	0.0169
Ca	0.7212	MG	0.5847
Na	0.0187	CA	0.8344
K	0.0051		
Ni	0.0037		
Pyrope	2.33		
Spessartine	27.84		
Grossular	12.55		
Almandine	57.28		
Percent	96.59		

TABLE 4.4

Amphibole GT1		Bastite GN10	
Oxide weight percentage			
SI102	57.42	SiO_2	47.95
TI102	0.08	TiO_2	0.34
AL203	1.07	Al_2O_3	5.57
CR203	0.05	Cr_2O_3	0.82
FE101 t	2.76	FeO^t	4.11
MN101	0.11	MnO	0.09
MG101	22.84	MgO	26.02
CA101	12.63	CaO	7.15
NA201	1.13	Na_2O	1.06
K 201	0.15	K_2O	0.34
NI101	0.10	NiO	0.15
TOTAL	98.34	TOTAL	93.59
Atomic proportions on the basis of 23 oxygens			
SI	7.8543		
TI	0.0084		
AL	0.1720		
CR	0.0055		
FE	0.3153		
MN	0.0126		
MG	4.6548		
CA	1.8508		
NA	0.3007		
K	0.0264		
NI	0.0112		

TABLE 4.5

Epidote Analyses GK1 Oxide weight percentage		
SiO_2	38.10	37.16
TiO_2	0.12	0.18
Al_2O_3	25.60	24.60
Cr_2O_3	0.00	0.06
FeO	9.86	11.61
MnO	0.02	0.12
MgO	0.07	0.03
CaO	23.51	23.38
Na_2O	0.07	0.00
K_2O	0.05	0.00
Total	97.40	97.14
Atomic proportion on the basis of 13 oxygens		
Si	3.1887	3.1556
Ti	0.0076	0.0112
Al	2.5269	2.4636
Cr	-	0.0041
Fe	0.6902	0.8247
Mn	0.0014	0.0084
Mg	0.0087	0.0044
Ca	2.1083	2.1275
Na	0.0114	-
K	0.0053	-

TABLE 4.6

Garnet			Apatite	
Oxides weight percentage				
	GK2	GD1		GD1
SiO_2	38.15	38.13		0.03
TiO_2	0.03	n.d.		0.00
Al_2O_3	21.48	21.72		0.02
Cr_2O_3	0.00	0.05		0.00
FeO^t	25.86	23.89		0.13
MnO	4.07	0.87		0.01
MgO	0.31	2.37		0.00
CaO	9.51	12.93		55.50
Na_2O	0.02	0.00		0.00
K_2O	0.02	0.00		0.00
Total	99.45	99.96	P_2O_5	43.77
			Total	99.45
Atomic proportions on the basis of				
24 oxygens			26 oxygens	
Si	6.0993	5.9872		
Ti	0.0040	-		
Al	4.0505	4.0217	SI	0.0051
Cr	-	0.0068	AL	0.0040
Fe	3.4579	3.1368	FE	0.0186
Mn	0.5516	0.1156	MN	0.0014
Mg	0.0744	0.5551	CA	10.1502
Ca	1.6992	2.1755	P	6.3254
Na	0.0060	-		
K	0.0032	-		
End-members				
Pyrope	1.30	9.28		
Spessartine	9.65	1.93		
Grossular	28.52	36.19		
Almandine	60.53	52.43		

TABLE 4.7

Plagioclase Analyses			
	GK1		GK2
Oxides weight percentage			
SiO_2	66.72		65.23
TiO_2	0.03		0.03
Al_2O_3	21.45		22.50
FeO^t	0.05		0.01
MnO	0.02		0.00
CaO	0.86		3.51
Na_2O	11.46		8.38
K_2O	0.10		0.13
Total	100.69		99.80
Atomic proportions on the basis of 32 oxygens			
SI	11.6298	SI	11.4505
TI	0.0037	TI	0.0041
AL	4.4099	AL	4.6588
FE	0.0073	FE	0.0018
MN	0.0028	CA	0.6601
CA	0.1606	NA	2.8516
NA	3.8716	K	0.0295
K	0.0233		

occur as an exsolved phase in Ca-rich pyroxenes. However, Mori (1978) suggested that they probably represent thin amphibole lamellae and not subcalcic pyroxenes.

Garnet and tourmaline analyses from the granitic rocks of Vavdos are presented in Table 4.3. The tourmaline approaches the composition of schorl rather than dravite.

An amphibole from the banded amphibolite-serpentinite (Tripes locality) and a bastite from a bastitic serpentinite (Paivouni locality) from the Gomati complex have been analysed, their analyses given in Table 4.4. The chemistry of both minerals suggests a Ca-rich pyroxene as the original mineral. Chlorite analyses from the serpentinites and chromitites are given in Appendix II, Table 10, while analyzed amphiboles from the contact amphibolites are presented in Appendix II, Table 11. Analysed epidotes from these contact amphibolites, Table 4.5, fall in the clinozoisite-epidote compositional range. Garnet, apatite and plagioclase have also been analysed from these amphibolites, the results are presented in Tables 4.6 and 4.7.

4.2 WHOLE ROCK GEOCHEMISTRY

A number of representative samples from the various petrological units of the two complexes have been analysed for the major constituents SiO_2, Al_2O_3, Fe_2O_3 (total), MgO, CaO, Na_2O, K_2O, TiO_2, MnO, S and P_2O_5 , and the trace elements Ba, Nb, Zr, Y, Sr, Rb, Zn, Cu, Ni, Cr and Ce. FeO, H_2O and CO_2 estimations have been made by wet chemical methods for a limited number of rocks. These analytical results are presented, for completeness, in Appendix III.

Analyses of various rock types from both complexes are plotted in an AFM diagram, Figure 4.6. Three amphibolites from the Gomati complex show typical tholeiitic affinities, while

Figure 4.6

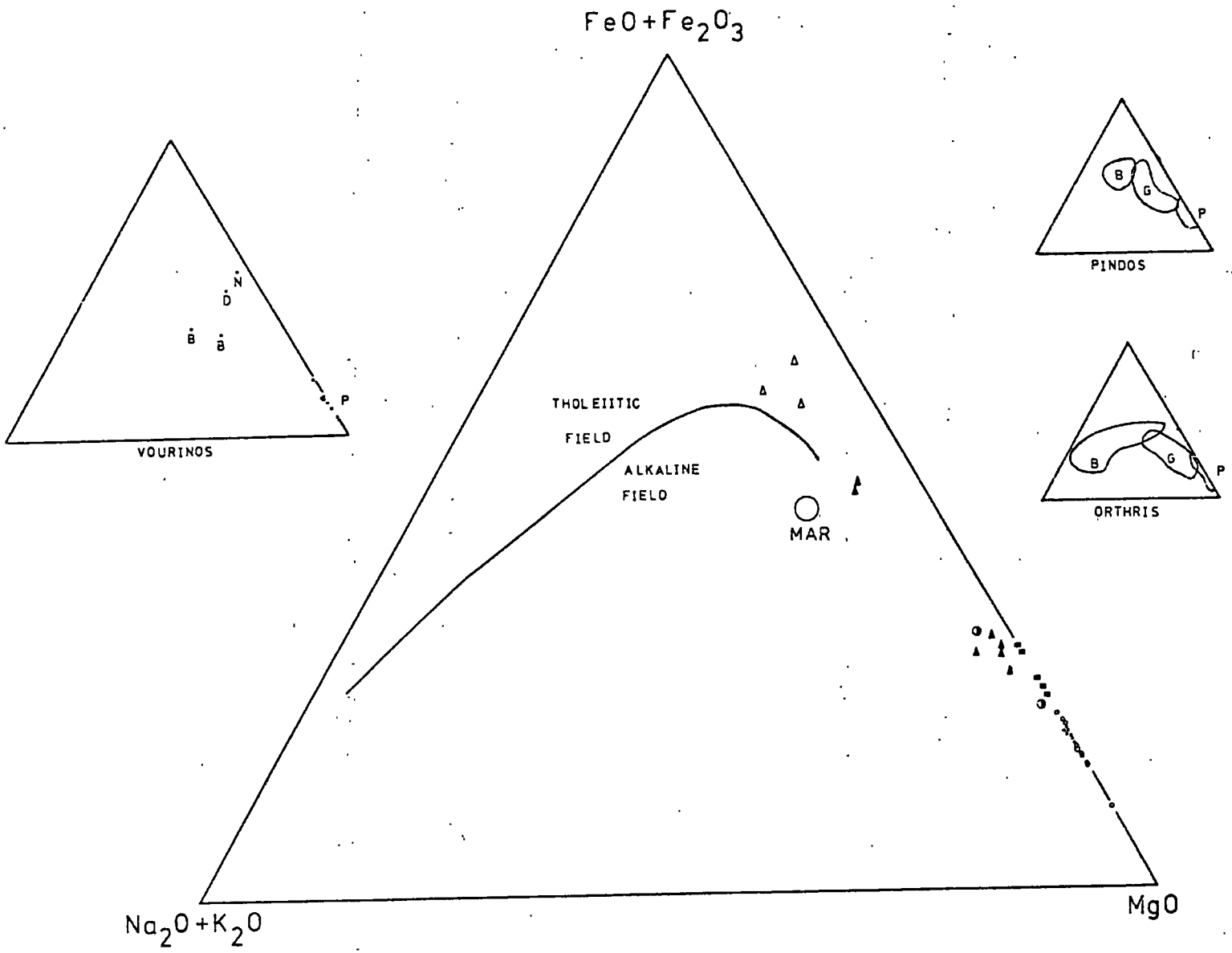
FeO+Fe2O3
Na2O+K2O
MgO
THOLEIITIC
FIELD
ALKALINE
FIELD
MAR
VOURINOS
N
D
B
B
P
PINDOS
B
G
P
ORTHRIS
B
G
P

two from Vavdos plot close to mid-Atlantic ridge basalt (Coleman, 1977). In this figure, plots of different petrological units from three other ophiolite complexes in Greece are shown as well ; data from Vavdos and Gomati show similarities with those from Orthris, but a different trend. Figure 4.7 is a plot of Ni against Cr for amphibolitized gabbro, gabbro, pyroxenite and dunite from the Vavdos complex. There is a clear trend of increasing Cr and Ni from amphibolite and gabbro to pyroxenite. The dunite, however, shows only an increase in Ni relative to the pyroxenite, and plots in the field of alpine type peridotite according to Irvine and Findlay (1972). The gabbros and pyroxenites conform with the gabbro and critical zone of the Muskox cumulate series respectively (Irvine and Findlay, loc.cit.).

The contents of SiO_2, FeO, MgO and TiO_2 of the Gomati amphibolites indicate a tholeiitic affinity for these rocks,as shown in Figure 4.8, conforming with the trends for the abyssal tholeiites and the Skaergaard layered series. These discrimination diagrams, produced by Miyashiro (1973) do not seem to be reliable especially for high silica and low Ti-contents, as can be deduced by the subsequent discussion on the origin of the Troodos ophiolite (Hynes 1975, Moores 1975, Gass et al, 1975) and the replies of Miyashiro (1975). However, the uncertainties of these diagrams seem to reflect mainly the silica metasomatism in the basaltic rocks of ophiolites ; the very low SiO_2 of the three amphibolites from Gomati is a safe criterion for their tholeiitic nature. The high TiO_2 reveals a relation to abyssal tholeiites, conforming with data which suggests that the abyssal tholeiites contain more titanium than that of the island arc tholeiites (Church and Coish, 1976).

Figure 4.7

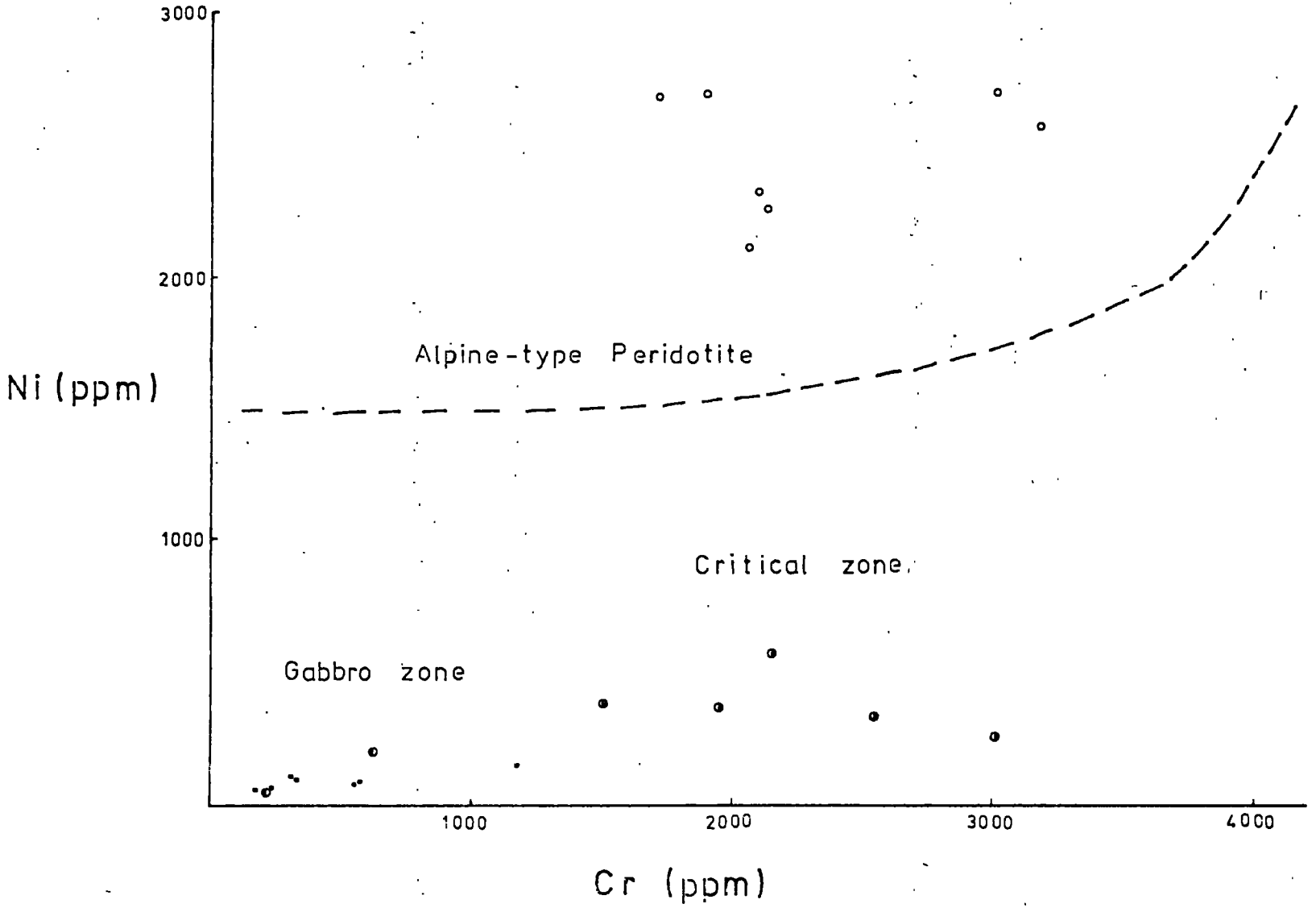
3000
2000
1000
Ni (ppm)
Alpine-type Peridotite
Critical zone
Gabbro zone
1000
2000
3000
4000
Cr (ppm)

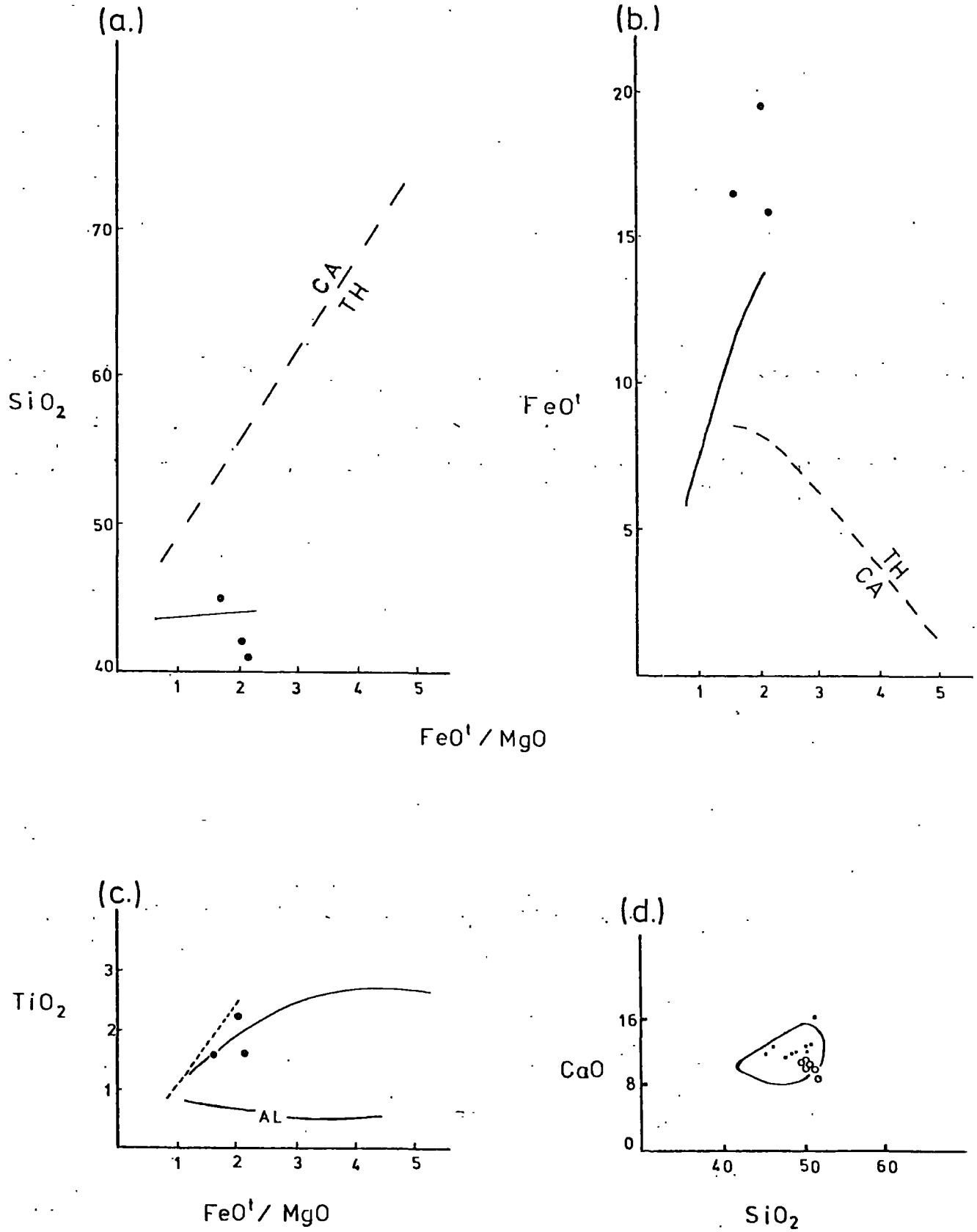
(a.)
SiO2
70
60
50
40
CA
TH
1
2
3
4
5
(b.)
FeO'
20
15
10
5
TH
CA
FeO' / MgO
(c.)
TiO2
3
2
1
AL
FeO' / MgO
(d.)
CaO
16
8
0
40
50
60
SiO2

Figure 4.8

Similar amphibolitized gabbros and metagabbros to those occurring in Vavdos have been described by Bonatti et al (1975) from the mid-Atlantic ridge ; these rocks are dynamically metamorphosed, with banded structures and chemical compositions very close to the gabbros and amphibolites of Vavdos. Analyses from the Vavdos gabbros and amphibolites are compared with gabbros and metagabbros from the mid-Atlantic ridge in Figure 4.8d, and show good positive correlation.

Three amphibolites from Gomati appear to be of basaltic composition, their trace-element contents also supporting this conclusion. Figure 4.9 shows the Ti-Zr distribution and compositional fields for different basaltic rocks. The discrimination between various basaltic rock types is mainly based on discriminant plots produced by Pearce and Cann (1971 and 1973). The Gomati amphibolites fall in the field of ocean floor basalts, although one weathered sample is always displaced. Those amphibolites from Vavdos appear to be metagabbros, being generated by the tectonic processes associated with the emplacement of the complex.

Figure 4.10 shows that the Gomati amphibolites fall in the field of oceanic tholeiitic basalt when plotted in the TiO_2-Y:Nb diagram of Floyd and Winchester (1975), and in the field of mid-ocean ridge basalts in the Zr:Y-Zr plot of Pearce and Norry (1979). The Ti-Zr-Sr plot of Figure 4.11a indicates that, as expected, Sr has been lost during metamorphism, and the analyses thus plot away from the field of ocean-floor basalts. In Figure 4.11b, theY, Nb and Zr contents again indicate a compositional overlap with tholeiitic basalts from the ocean-floor. If Zn contents are considered also, all three amphibolites show positive correlation with tholeiitic volcanic rocks,

Figure 4.9

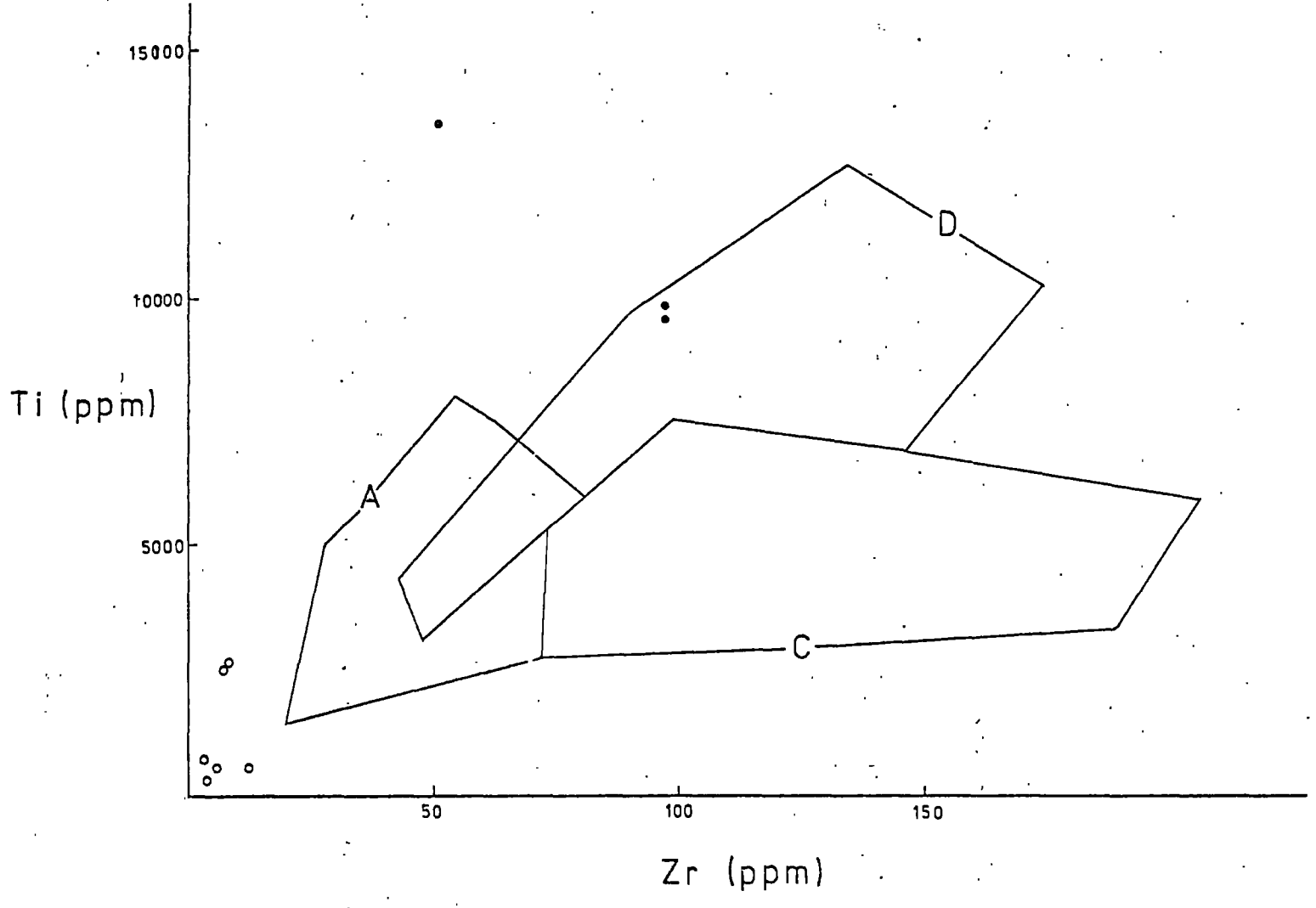

Figure 4.10

a

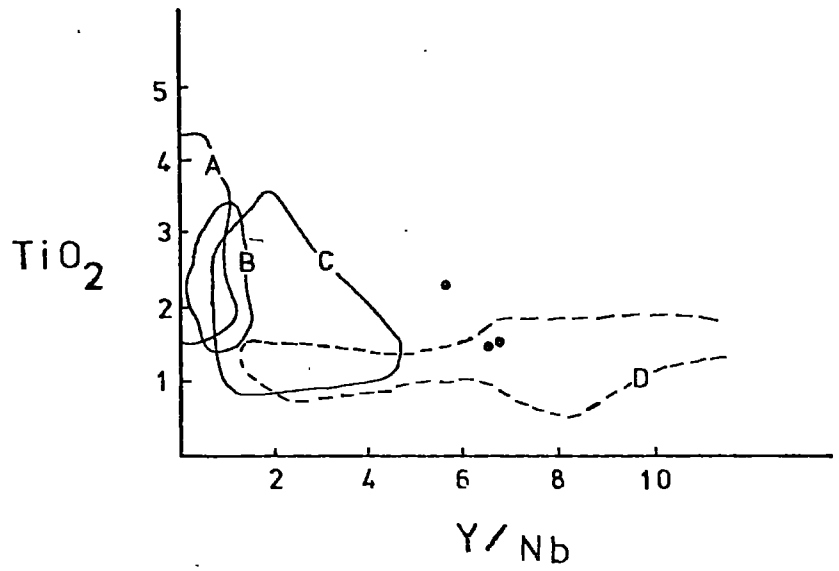

b

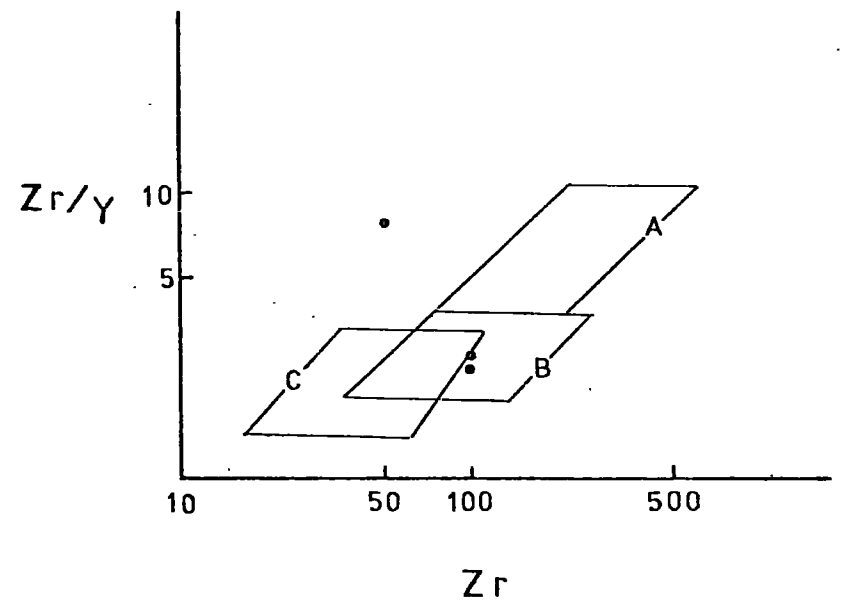

Figure 4.11

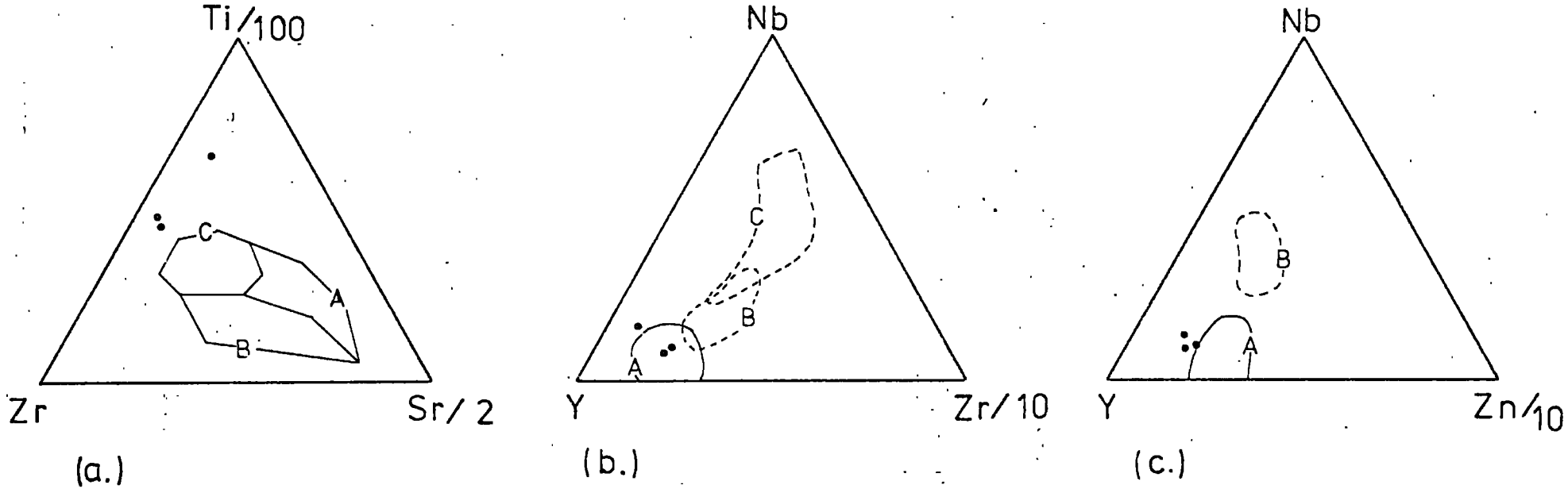

as shown in Figure 4.11c.

The geochemical pattern of trace elements of the three amphibolites from Gomati is in coincidence with the previous conclusions. The trace abundancies are normalized to the mid-ocean ridge basalt, according to the average values given by Pearce (1979), and are plotted in Figure 4.12. The immobile elements (Nb, Ce, Zr, Ti and Y) do not deviate largely from the mid-ocean ridge basalt whereas Sr, K and Rb show the larger deviations. Hart et al (1974) point out that Rb and K increase in basalts during alteration with the sea water and later weathering ; this is in agreement with the high Rb and K values. Sr is probably lost either because of the increase of $Sr^{87}:Sr^{86}$ ratio during weathering (Hart et al, 1974) or because of later metamorphism. However, the deviations in the pattern from Ba to Cr, can be regarded acceptable, because the rocks are metamorphosed ; it is also possible that deviations from the ideal mid-ocean ridge basalt might reflect slow or fast spreading ridges. Alkali basalt and island arc tholeiite are also plotted in Figure 4.12 for comparison ; their patterns are different, especially the immobile elements, and reflect the different tectonic setting and the different type of magma series (alkali basalt).

Three analyses of the granitic rocks from the Vavdos complex are given in Appendix III, Table 4 ; the analysed samples are the VX1, VY8 and VP24. These rocks have high potassium and very high Rb contents, in comparison to the oceanic plagiogranite which is a leucocratic rock type occurring within the mafic rocks of other ophiolites, and being characterised by extremely low K_2O and Rb (Coleman and Peterman, 1975). One analysis from the underlying country

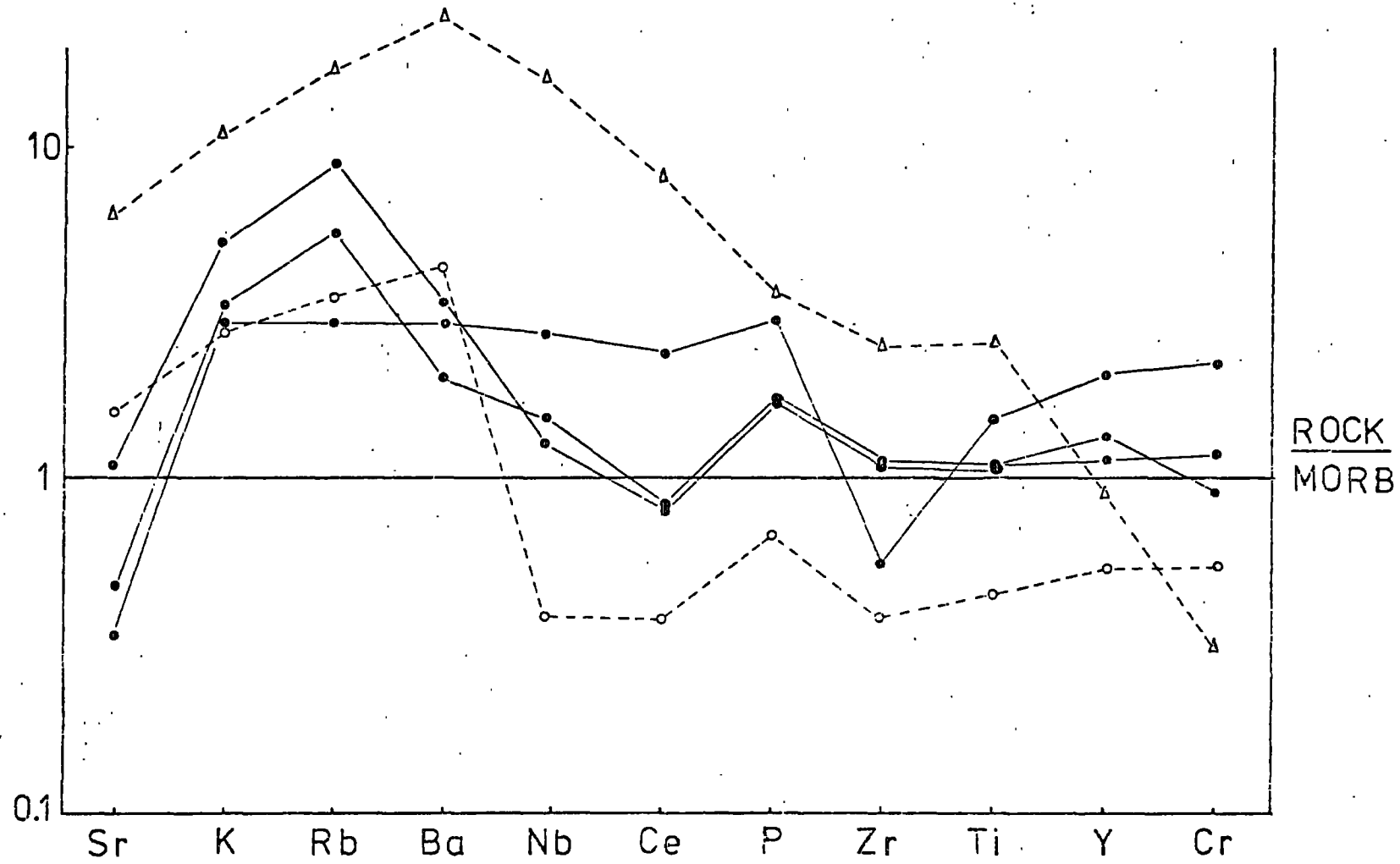

Figure 4.12 Trace element pattern of the Gomati amphibolites (solid circles) normalized to the composition of mid-ocean ridge basalt (MORB). Triangles represent alkali basalt and open circles an island arc tholeiite. Alkali basalt is from a within plate tectonic environment. Data from Pearce(1979).

rock of Vavdos is also presented in Appendix III (Table 4, sample V8-15).

4.3 DISCUSSION

The amphibilites from Gomati show typical tholeiitic affinities, with respect to both major constituents and trace elements. These rocks also contain normative hypersthene, indicative of typical tholeiites, Coombs (1963). This is in agreement with the chemistry and the trend shown by numerous analyses of extrusives from the upper parts of ophiolite sequences, Coleman (1977).

Pyroxenes from pyroxenites of Vavdos have normative hypersthene and plot in the diopside-olivine-quartz-nepheline diagram as shown in Figure 4.13 (plagioclase projection). The Ca-rich pyroxenes have normative hypersthene between 13 and 24% and overlap, in part, with the pyroxene field for tholeiitic rocks given by Coombs (1963) although showing higher normative quartz indicative of silica saturated magmas. The Ca-poor pyroxenes are almost virtually hypersthene. Although this scheme has been applied to pyroxenes from basaltic rocks, it indicates that the gabbro-pyroxenite sequence has been formed from a tholeiitic magma which was more saturated in silica than for typical tholeiitic basalts.

Typical fractionation trends are indicated by Figures 4.14a and 4.14b. Analyses of co-existing orthopyroxene and clinopyroxene from the pyroxenite and gabbro of Vavdos and the Twin sisters dunite (Onyeagocha, 1978) show very good linearity and reveal typical iron enrichment and magnesium impoverishment during the fractionation processes. This is in agreement with the early tholeiitic trend, involving iron enrich-

Figure 4.13

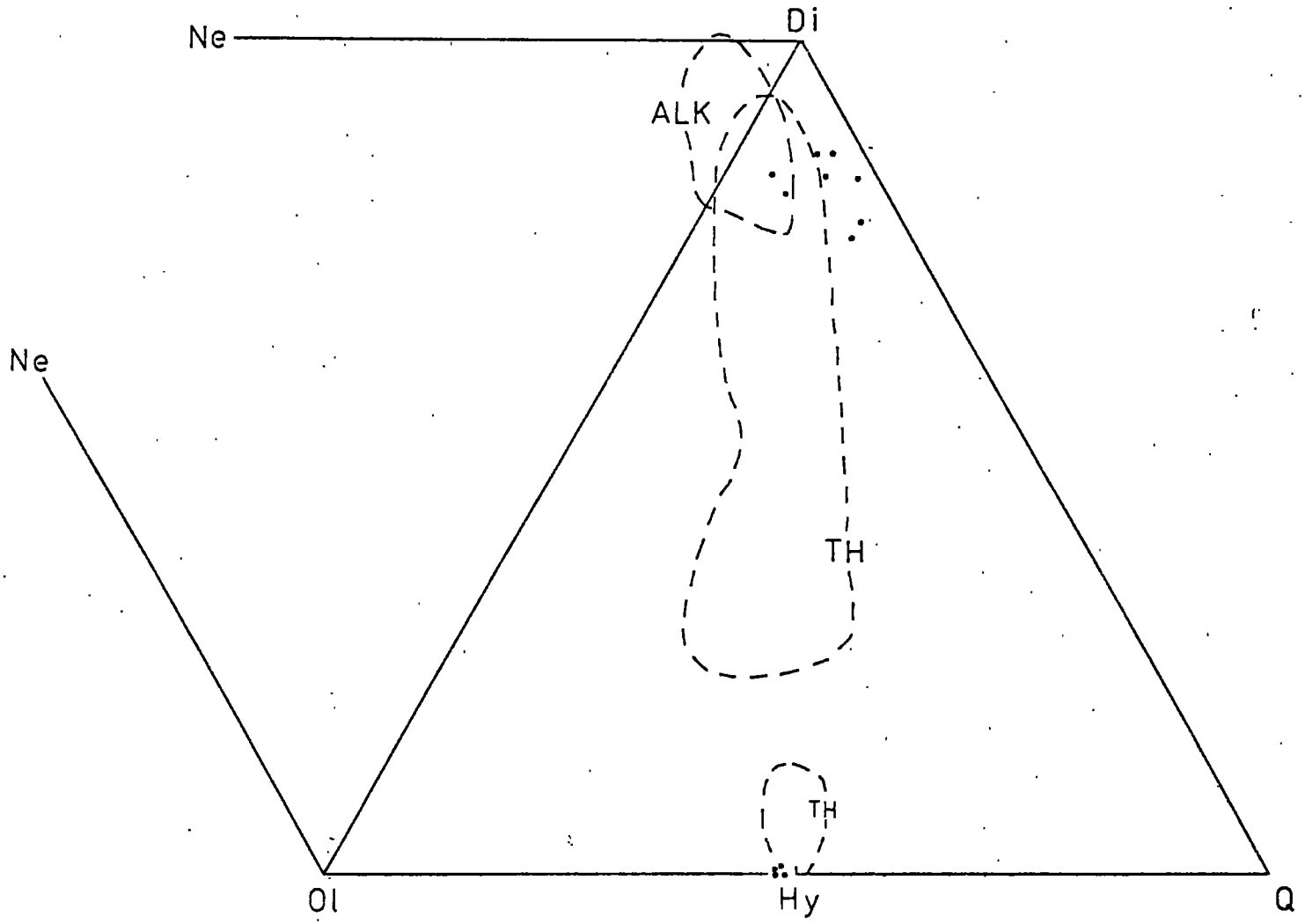

ment and Mg depletion, and results from crystallisation of olivine which forms the main crystalline phase of dunite.

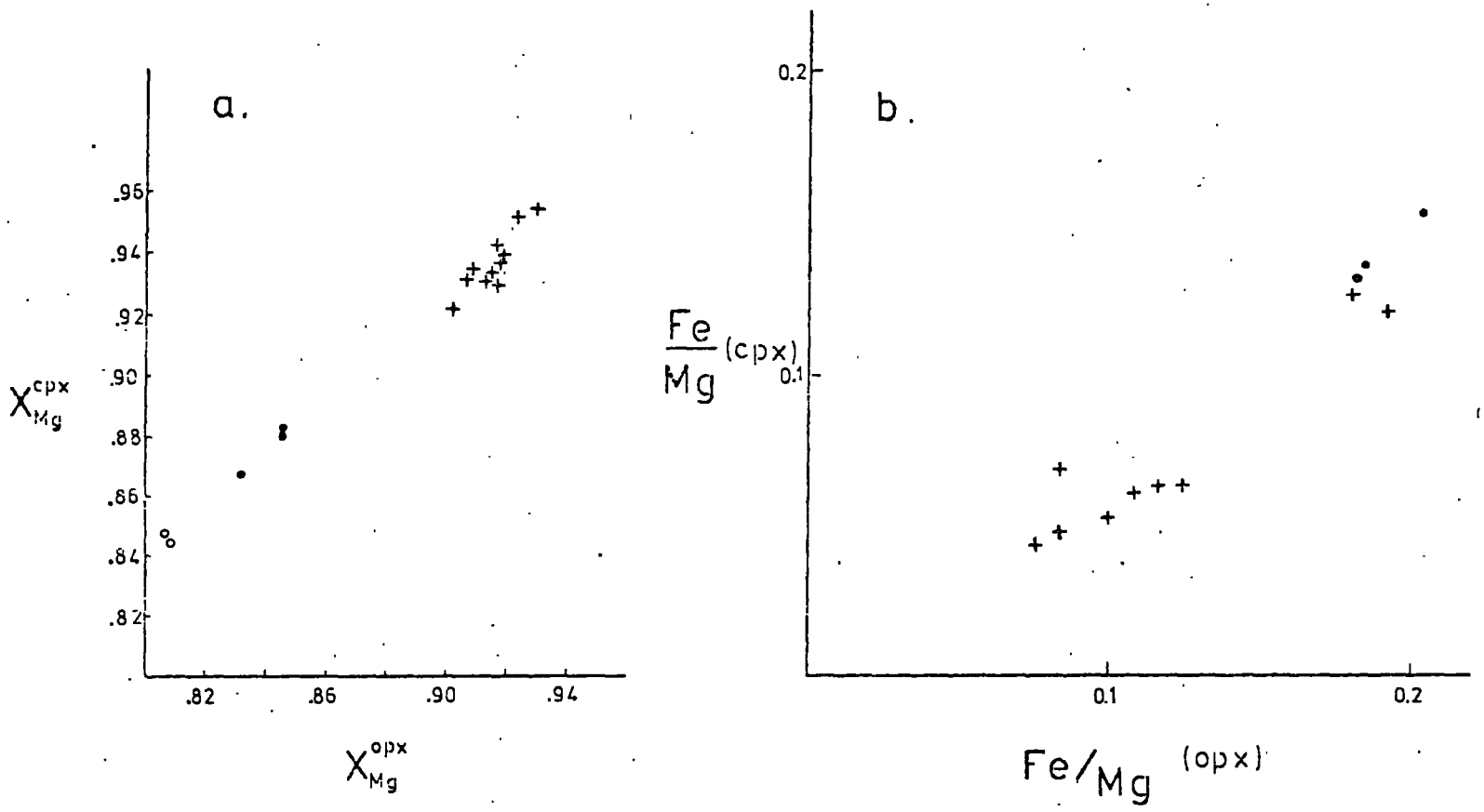

Figure 4.14 (a) Distribution of Mg between co-existing clinopyroxene-orthopyroxene. Symbols : open circles are co-existing pyroxene pairs from gabbro (Vavdos), solid circles from pyroxenite (Vavdos) and crosses from the twin-sisters dunite (Onyeagocha, 1978).
(b) Fe:Mg distribution in co-existing pyroxenes. Symbols are as in (a).

CHAPTER 5

CHROMITE CHEMISTRY

5.1 INTRODUCTION

The analyses of Cr-spinels were carried out on the Geoscan electron microprobe. This technique was preferred, because the Cr-spinels from the Gomati complex were altered and contained silicate impurities that would be retained in any separated chromite concentrates, even if combined separation methods were used.

Perfect spinel stoichiometry has been assumed for the estimation of FeO and Fe_2O_3. Cation proportions have been calculated on the basis of 32 oxygen atoms. The 24 cations have been distributed as follows. For the normal distribution, $8R^{2+}$ in tetrahedral sites (fourfold coordination) and $16R^{3+}$ in octahedral sites (sixfold coordination). The general formula thus does not deviate from the ideal of $R_8^{2+}\ R_{16}^{3+}\ O_{32}$. Taking into account R^{4+} cations, a more generalized equation has $R^{2+} + R^{3+} + R^{4+} = 24$, with R^{2+} equal to $8 + R^{4+}$ and R^{3+} equal to $16-2R^{4+}$. Fe^{2+}, Mg, Mn and Ni have been regarded as R^{2+} cations while Cr, Al and Fe^{3+} are the R^{3+}cations. Ti^{4+} is the only R^{4+} cation.

The inverse spinel distribution refers to the presence of $8R^{2+}$ and $8R^{3+}$ cations in octahedral sites and $8R^{3+}$ in tetrahedral sites. This distribution refers particularly to magnetite.

Spinel analyses have been plotted onto three projections of the spinel compositional prism of Stevens (1944), shown in Figure 5.1.

Figure 5.1

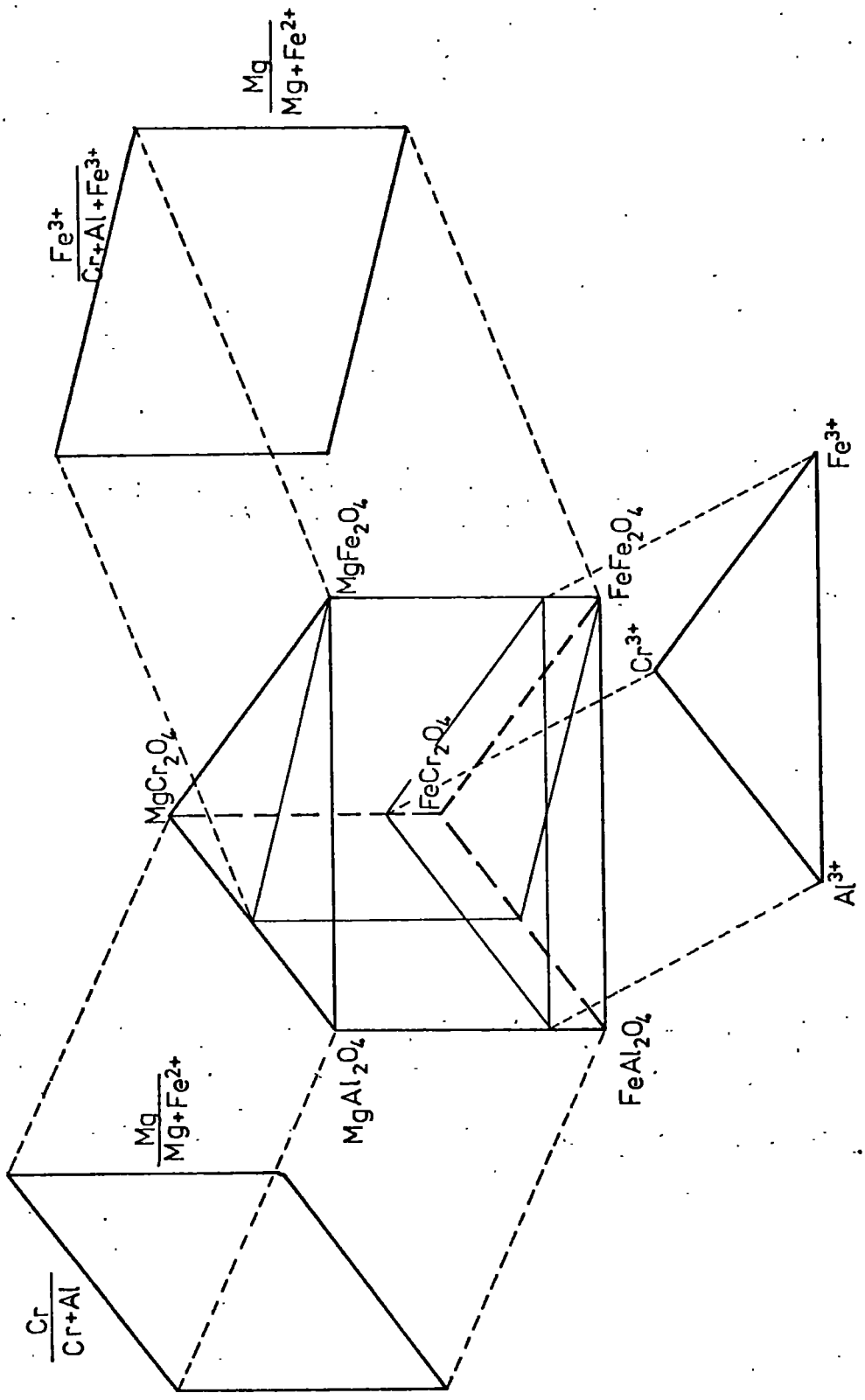
$\frac{Mg}{Mg+Fe^{2+}}$
$\frac{Fe^{3+}}{Cr+Al+Fe^{3+}}$
$MgFe_2O_4$
$FeFe_2O_4$
Fe^{3+}
Cr^{3+}
$MgCr_2O_4$
$FeCr_2O_4$
Al^{3+}
$MgAl_2O_4$
$FeAl_2O_4$
$\frac{Mg}{Mg+Fe^{2+}}$
$\frac{Cr}{Cr+Al}$

5.2 CHROMITES OF THE VAVDOS COMPLEX

5.2.1 Mineral Chemistry

The spinel cations have been plotted in the triangle of trivalent cations Cr^{3+}, Al^{3+} and Fe^{3+}. Considering the stoichiometry on the basis of 32 oxygen atoms, the length of each side of the triangle represents 16 trivalent cations. The distribution of spinels is shown in Figure 5.2a ; they fall in the field of aluminian chromite. The Cr-spinels cannot be distinguished according to their occurrence as the compositional fields from massive chromite concentrations to accessory spinels overlap. The ferric iron content is very low, although some accessory spinels show a relative Fe^{3+} enrichment, indicative of incipient alteration.

The Cr x 100 : Cr + Al ratio of Cr-spinels has been plotted against Mg x 100: Mg + Fe^{2+}, as shown in Figure 5.3a. The Cr-spinels occupy a limited field, having Cr : Cr + Al ratios between 0.68 and 0.85 approximately. All analysed spinels fall in the compositional field for alpine type chromite, as designated by Irvine and Findlay (1972), apart from two accessory spinels, which show iron and chromium enrichment. The Cr-spinels from massive chromitite show a trend towards iron and chromium enrichment, and the Cr-spinels from disseminated ore, are poorer in iron and chromium than the accessory spinels in dunite. No spinel has been found with a Cr x 100 : Cr + Al ratio below the value of 58. Irvine (1967) indicates that all Cr-spinels from stratiform intrusions have values of Cr x 100 : Cr + Al above the value of 58. If the compositional field of these Cr-spinels is compared with fields from other complexes, Figure 5.5, there is overlap only with the fields associated with dunite host

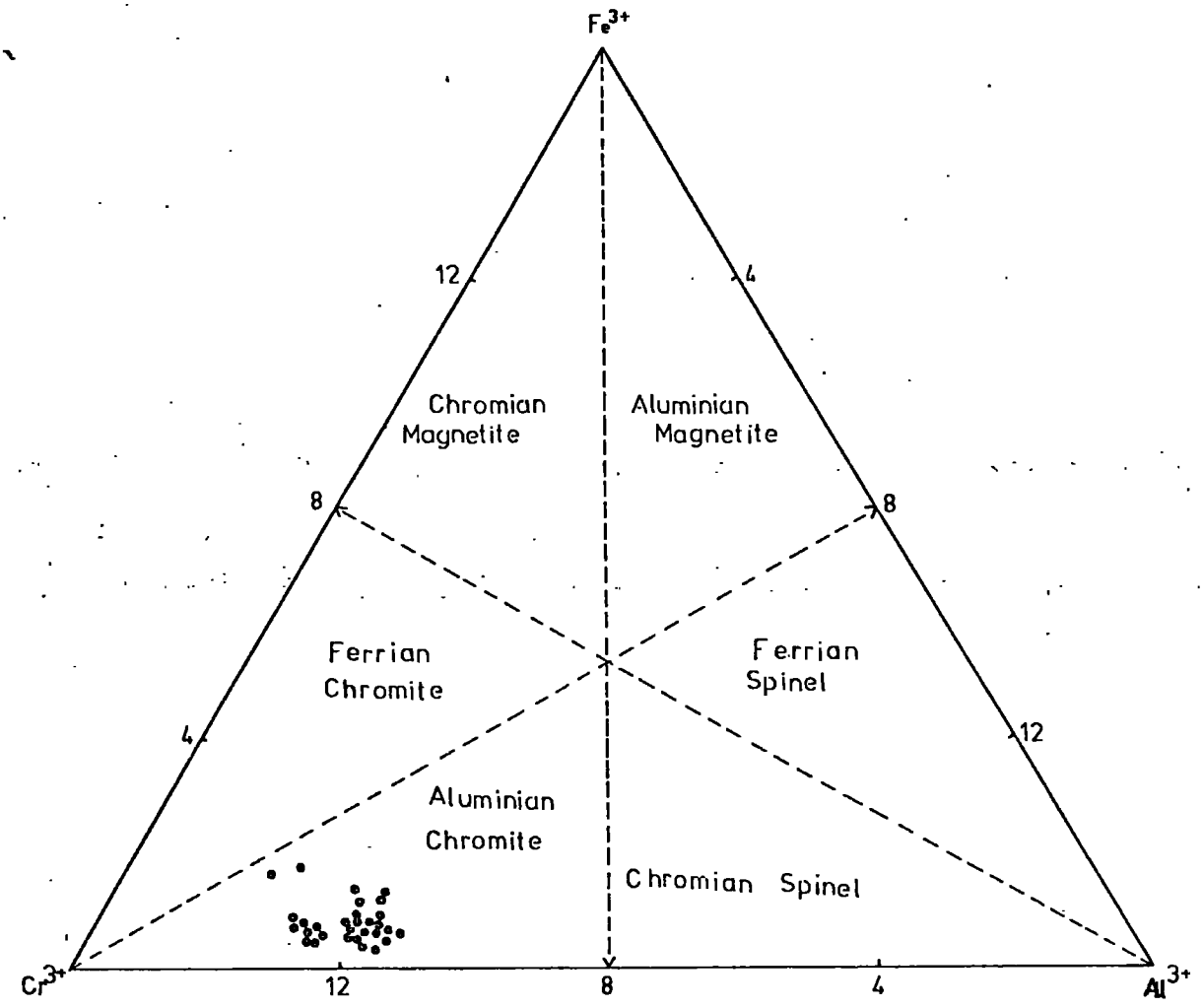

Figure 5.2a

Plot of spinels from Vavdos complex to the triangle of trivalent cations Cr, Al and Fe.

Figure 5.3

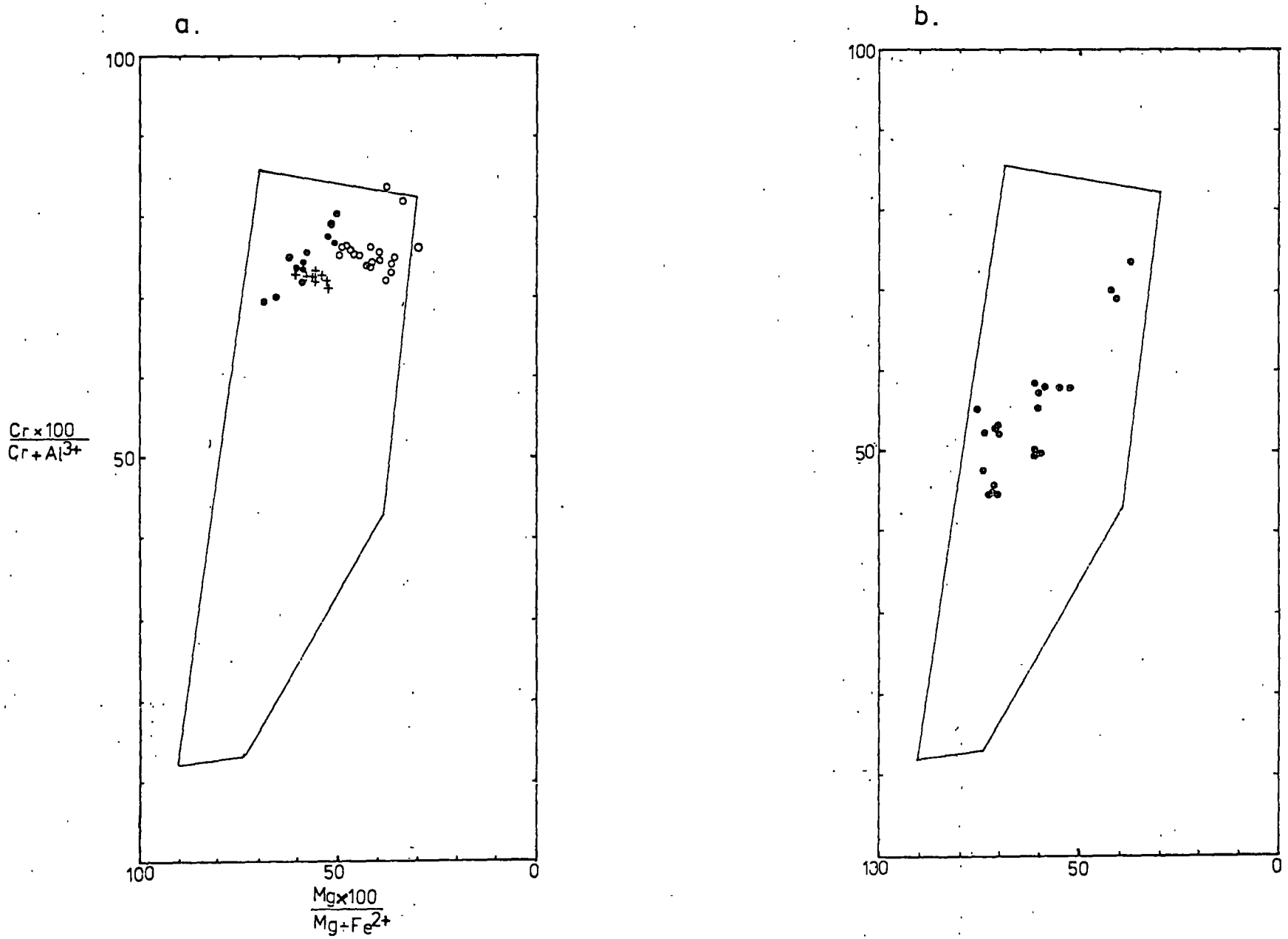

lithology.

The plot of the $Fe^{3+} \times 100 : Cr + Al + Fe^{3+}$ ratio against the $Mg \times 100 : Mg + Fe^{2+}$ ratio for the Cr-spinels from Vavdos is shown in Figure 5.4a. The range of $Mg : Mg + Fe^{2+}$ ratios, is between the values of 0.34 and 0.70. Ratios of $Fe^{3+} : Cr + Al + Fe^{3+}$ are always lower than 0.10, even for accessory spinels showing incipient alteration. This coincides with the general distribution for alpine chromite, which has a low and uniform iron oxidation ratio. Chromite from stratiform intrusions has higher $Fe^{3+}: Cr + Al + Fe^{3+}$ ratios, Irvine (1967). In general, the Cr-spinel from the massive ore and the olivine-chromitite are more Mg-rich than the accessory spinel.

The Cr_2O_3 content of the spinel is always above 52%, even for accessory spinel in dunite. According to Thayer (1969), this is typical for chromite of podiform deposits. The Cr : Fe ratio ranges from 2.06 to 4.06, with the exception of two samples, where the ratio for accessory spinel is below 2, due to alteration. Thayer (1969) gives values above 2 for the Cr : Fe ratio of high chromium ores. The relationship between spinel types and Cr : Fe ratio, is shown by a histogram in Figure 5.7. In general the spinel from massive chromitite has higher Cr : Fe ratios than the spinel from chromitiferous dunite which, in turn, has higher values than the accessory spinels.

The MnO content of the Cr-spinel varies from about 0.40% to 0.80%. In Figure 5.8, the variation of MnO with the other oxides is shown. MnO levels show a tendency to increase with decreasing MgO and Al_2O_3 and increasing FeO. No clear

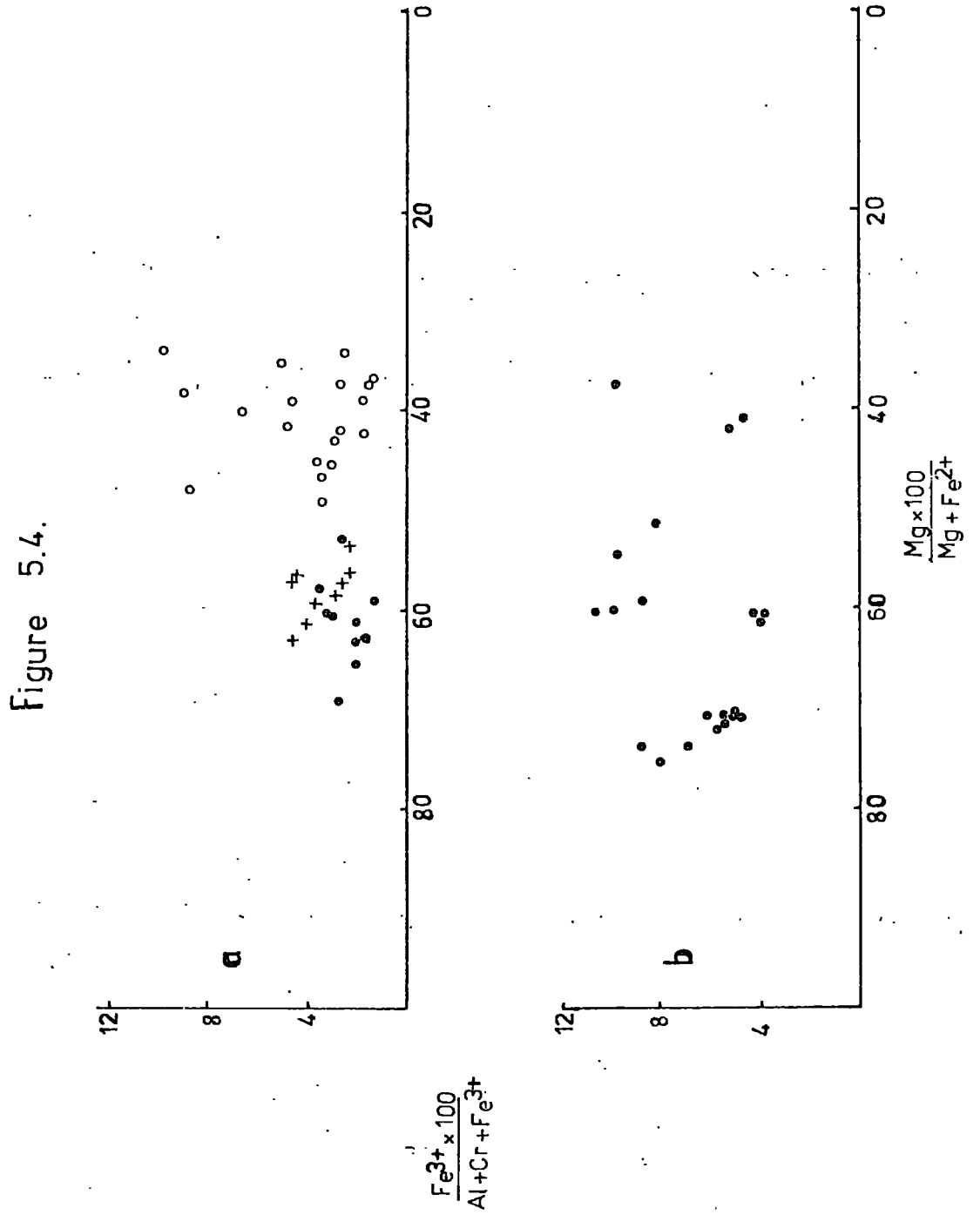

Figure 5.4 Plots of cation ratios for spinels of Vavdos(a) and Gomati(b) complexes. Symbols are as in Figure 5.3.

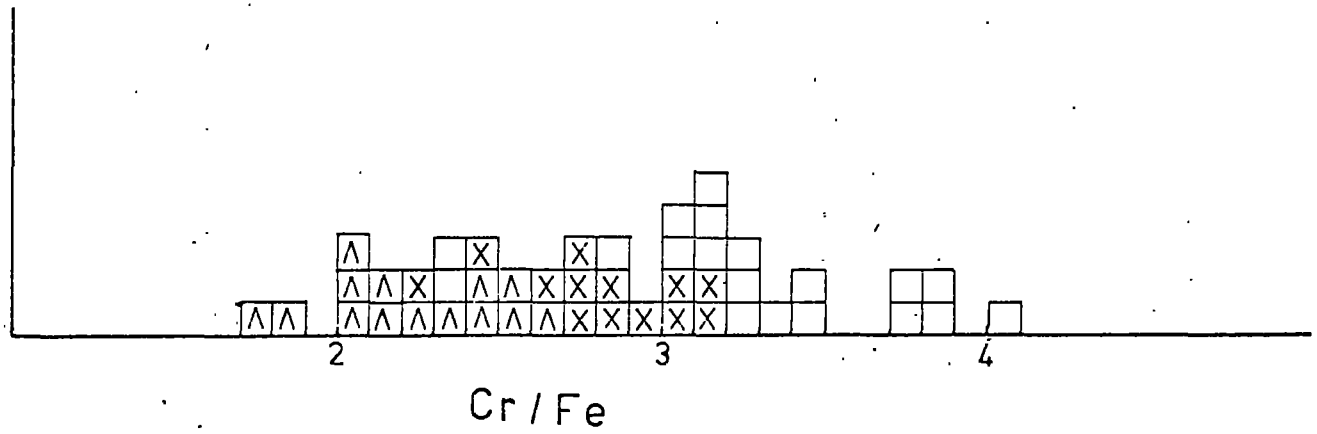

Figure 5.7 Histogram of the distribution of spinels according to their Cr/Fe ratio.

□ Chromite from massive type ore.

Λ Accessory chromite.

X Chromite from disseminated type ore.

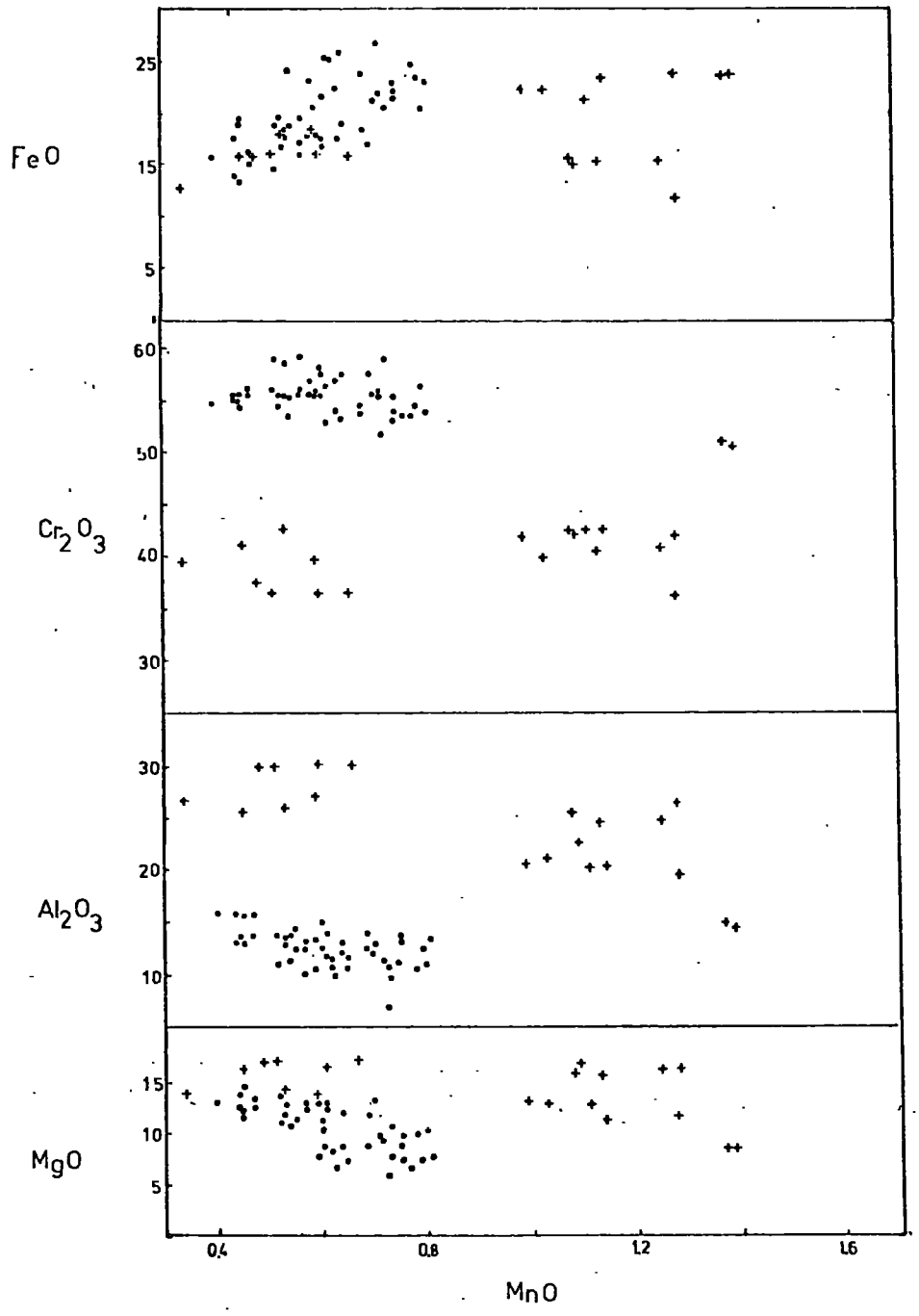

Figure 5.8

Comparative variation of MnO content with the major oxide contents of spinels. Dots are spinels from Vavdos and crosses from Gomati.

trend is shown by the plot of MnO against Cr_2O_3.

5.2.2 Chemical Variations Within Individual Chromite Deposits from Vavdos

The massive concentrations of chromite in pods or irregular shaped bodies grade to disseminated-type ore, and in the close vicinity of the massive ore, dunite lenses appear in the chromite pods forming the olivine-chromitites. Accessory euhedral spinels occur in dunite some distance away from the pods. This relationship for a single deposit is shown in Figure 5.9. There is a distinct decrease in magnesium and increase in iron content from massive pods to accessory chromite. This suggests some process of liquid-crystal fractionation.

Stratiform-like chromites from a chromitiferous dunite have been analysed in sample VA4, from Agitsa. This rock shows repetitive layers of dunite-rich and chromite-rich rock, alternating in a similar manner to the rhythmic layering of stratiform complexes, although the boundaries between different layers interfinger. Plotted analyses in Figure 5.10 reveal a decrease in MgO content with concomitant increase in iron, while nickel and aluminium contents decrease with decreasing magnesium content. Points 2 and 3 are from grains in close proximity to each other. It might be assumed that differentiation proceeds from point 1 to point 4, the sequential increase in total iron content and decrease in nickel content being very characteristic of a differentiation trend produced by a liquid-crystal fractionation process.

5.2.3 Chromite Bands in Dunite

Chromite bands in dunite occur throughout the Vavdos complex. They vary in width and extent from approximately

Figure 5.9

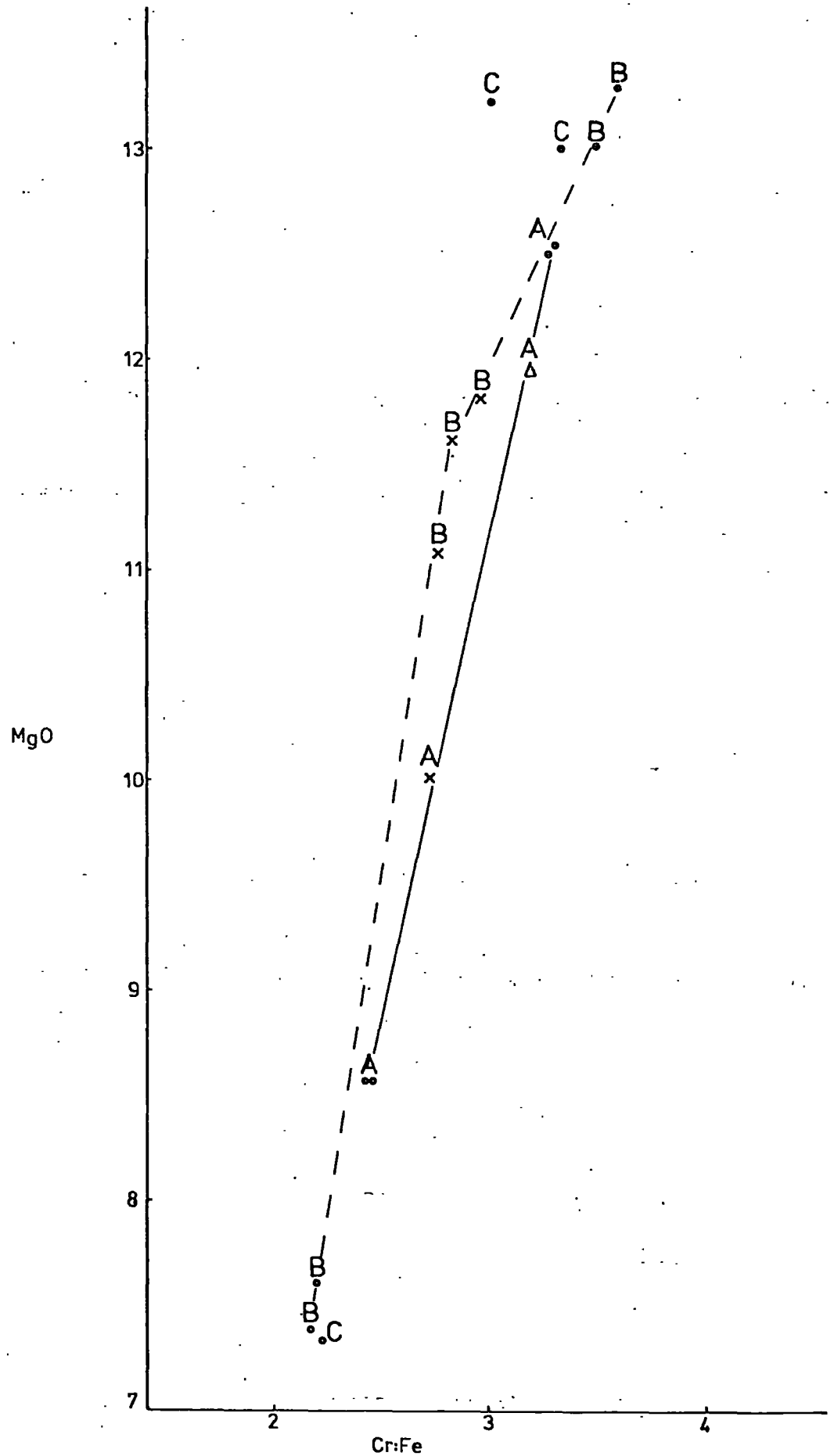

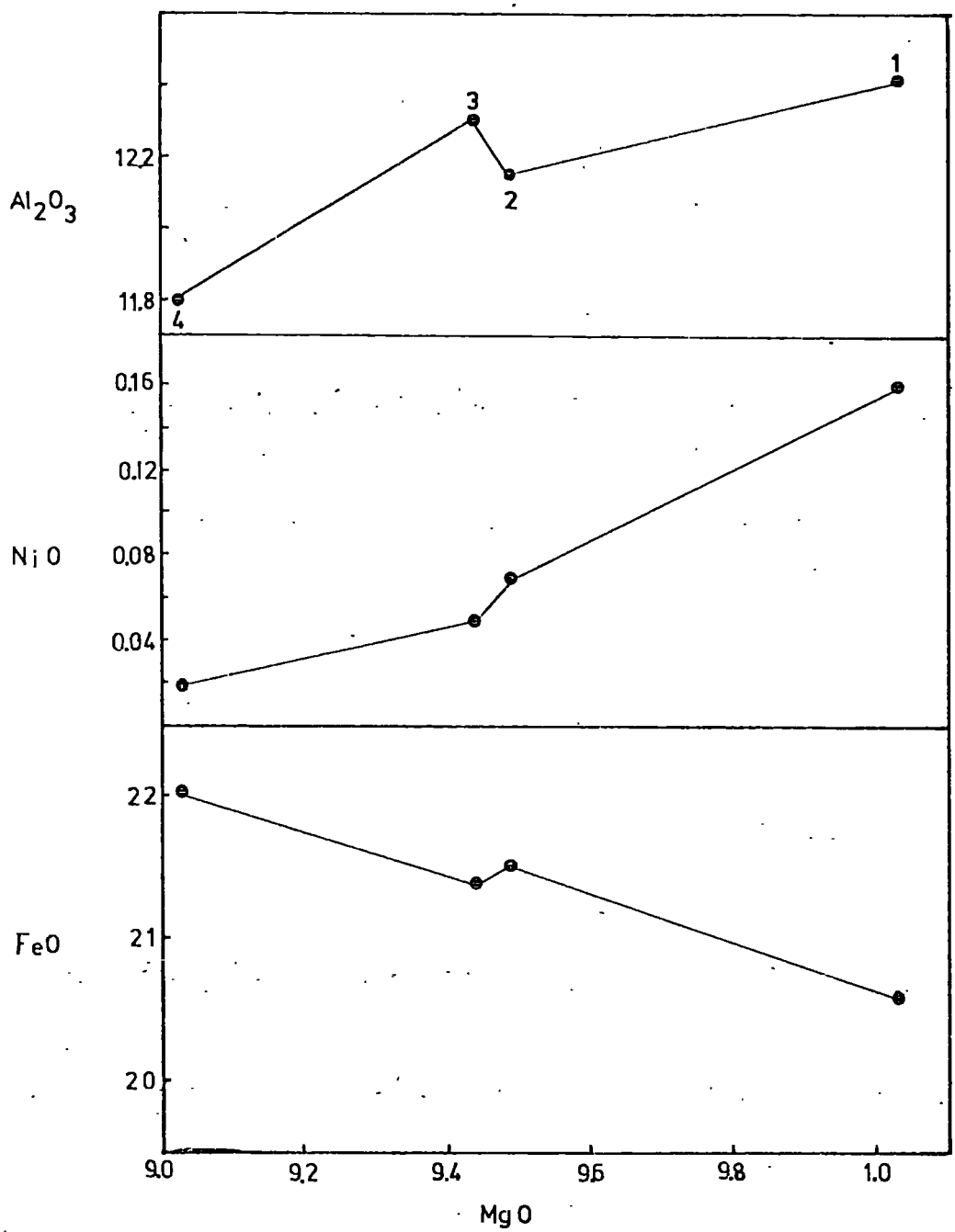

Figure 5.10

Variation of oxides from chromite in alternating chromite-rich and dunite layers of a chromitiferous dunite. Points 1 and 3 represent chromite from chromite rich layers, while points 2 and 4 from dunitic layers.

1 cm to 5-6cm wide and can be traced for up to 2-3 metres. The chromite bands usually commence near to the massive chromite concentrations. The two bands studied are deformed and folded because they occur near the basal thrust zone of the complex, at Climatsida .

The relations between chromites from bands and accessory Cr-spinels in adjacent dunite are shown in Figure 5.11. There is a distinct increase in Al- and Mg-contents from accessory Cr-spinels to chromites in the bands, although the variation is not symmetrical about the band. The total iron content of chromites from bands is much lower than that of accessory Cr-spinels, which in turn show increasing iron content from point (1) to point (3) with concomitant decrease of Al and Mg-contents. This supports a fractionation process proceeding from (1) to (3).

5.3 CHROMITES FROM THE GOMATI COMPLEX

Cr-spinel concentrations associated with bastite-bearing serpentinite are considered to represent chromite within harzburgite, those associated with typical mesh-textured or shattered serpentinite, chromite in dunite, and those associated with banded serpentinite-amphibolite to represent primary layered dunite-werhlite (or clinopyroxenite). It must be remembered,at this point, that all chromite ore concentrations, either disseminated or massive, are highly sheared while the host rock is slightly tectonized; this suggests dismembering of chromite ore bodies. It is thus obvious that the host lithologies now associated with the chromite are not necessarily the primary association. They are only quoted as indicative of the present field relations

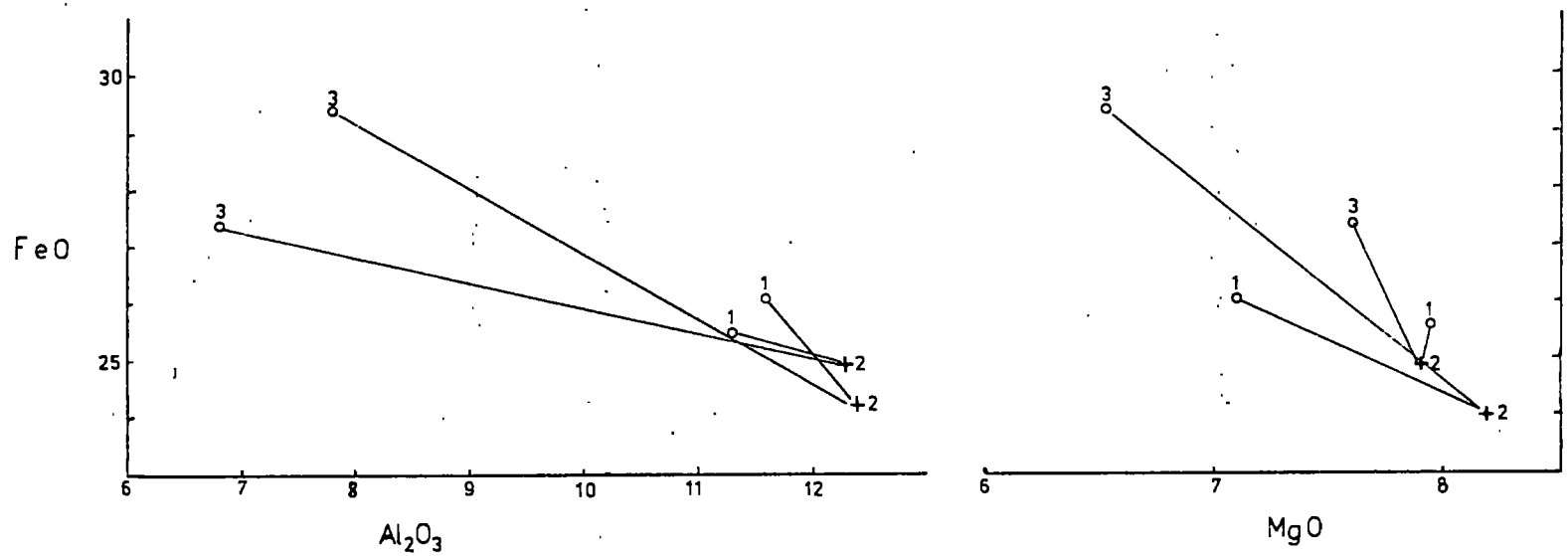

Figure 5.11 Variation of major oxides for Cr-spinels in chromite-bands and adjacent dunite. Crosses represent chromite from the chromite-bands, and open circles chromite from the dunite host at both sides of the chromite-band..

DURHAM UNIVERSITY
16 FEB

of the chromite ores.

The Cr-spinels have been plotted in the trivalent cation compositional triangle Al, Cr and Fe^{3+} in Figure 5.2b. They largely fall in the field of chromian spinel and aluminian chromite. The Cr-spinels from disseminated-type ore are Al-rich falling principally in the chromian spinel field. The spinels from massive chromitite in dunite are Cr-rich and fall in the aluminian chromite field. The spinels from clinopyroxene-bearing chromitite are richer both in chromium and ferric iron than the above spinels, although the spinels from chromitiferous dunite represent the most chromium rich spinels of the complex. There is thus a general bimodality between high chromium- or high aluminium-chromite, a characteristic of podiform chromite, first pointed by Thayer (1970). Spinels falling in the chromian magnetite field of the triangle, result from oxidation during serpentinization. During serpentinization, the Fe^{3+} substitutes more for Al^{3+} than for Cr^{3+} as indicated by Figure 5.2b, and by the following pair of spinels from the same locality.

$Fe^{2+}_{2.3}\ Mg_{5.6}(Fe^{3+}_{0.8}Al_{8.3}Cr_{6.8})O_{32}$, unaltered spinel from massive chromitite, and

$Fe^{2+}_{7.3}\ Mg_{0.7}(Fe^{3+}_{12.6}Al_{0.0}Cr_{2.7})O_{32}$, oxidised spinel from serpentinite.

Date from Arai (1980) shown also in Figure 5.2b, show different spinel distributions according to different host lithologies.

The Cr x 100 : Cr + Al against Mg x 100:Mg + Fe^{2+} ratios of analysed spinels have been plotted in Figure 5.3b. Cr : Cr + Al ratios range from 0.44 to 0.74, with Al_2O_3 contents of 11.7% to 30.4% and Cr_2O_3 contents of 36.4% to 51.1%. The

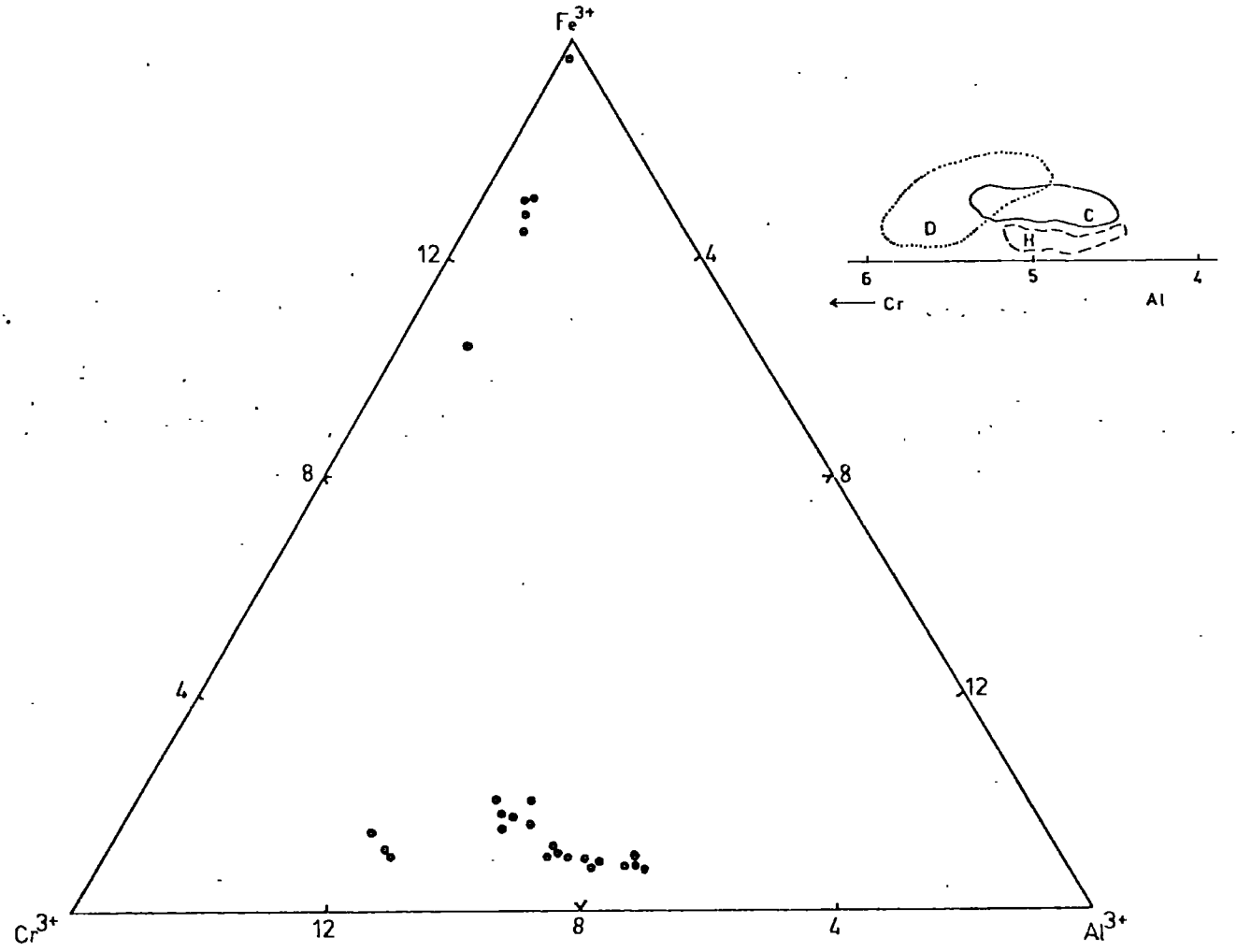

Figure 5.2b

Plot of chromites and magnetites from Gomati complex to the trivalent cations triangle. They occupy the fields of chromian spinel, aluminian chromite and chromian magnetite. Data from Arai (1980) are shown to the right. Chromites associated with dunite host (D), harzburgite host (H) and massive chromitites (C) show little compositional overlapping, with chromites from dunite being more chromium rich relatively to those associated with harzburgite lithologies.

spinels have a wide distribution within the compositional field given by Irvine and Findlay (1972) for alpine chromite. Spinels from clinopyroxene-bearing chromitites have Cr : Al ratios lower than those of the chromitiferous dunite and higher than the disseminated chromites. However, the spinels from massive chromitite associated with a dunite host-rock are very similar to those from the massive ore occurring in banded werhlite (clinopyroxenite) -dunite. There is thus a gradual increase in the Cr : Al ratio of spinels from massive chromitite in dunite, through clinopyroxene-chromitites to chromitiferous dunite. All analysed disseminated chromites have values of Cr x 100 : Cr + Al below the critical value of 58 given by Irvine (1967) as a boundary between alpine-type chromite and chromite from layered intrusions.

The Mg x 100 : Mg + Fe^{2+} ratio of the Cr-spinels is plotted against the Fe^{3+} x 100 : Cr + Al + Fe^{3+} ratio in Figure 5.4b. The Mg : Mg + Fe^{2+} ratio ranges from 0.37 to 0.76 with MgO contents between 7% and 16.5%. The Fe^{3+} : Cr + Al + Fe^{3+} ratios of the spinels always fall below the value of 0.10. The spinels from chromitiferous dunite have the lowest Mg : Mg + Fe^{2+} ratio, this ratio increasing into the spinel from the clinopyroxene-bearing chromitite. There is thus a sequential depletion in Mg-content, and a reciprocal Fe-enrichment from the Cr-spinels of massive chromitite through clinopyroxene-chromitite to chromitiferous dunite. The Cr-spinel populations from Tripes and Paivouni overlap, this being indicative of close genetic relationships. The amount of Fe^{3+} varies and is dependent on the degree of oxidation.

The Al_2O_3 content of the spinel, except for the spinels from chromitiferous dunite, is above 20% which according to Thayer (1969) characterises refractory chromite of alpine-type complexes. The Cr : Fe ratio ranges from 1.76 to 2.74 ; spinel from massive chromitite in banded werhlite-dunite shows the highest values and the chromite from clinopyroxene-chromitite the lowest.

MnO content is plotted against the other major oxides and the reciprocal variations are shown in Figure 5.8. MnO ranges from 0.35% to 1.45%, being lower for spinels from disseminated-type ore, and increasing in spinels from clinopyroxene-chromitite and those associated with dunite. In general MnO increases with increasing total iron content and decreasing Al_2O_3.

5.4 COMPARISON OF CHROMITE FROM THE VAVDOS AND GOMATI COMPLEXES WITH CHROMITE FROM OTHER COMPLEXES

The chromites from Vavdos are compared with chromites from other ophiolite complexes in Figure 5.5. They show overlap with compositional fields for chromite from the Troodos complex (Greenbaum, 1977, and Panayiotou, 1978), from the dunite of the Blue River ultramafic complex (Pinsent, 1974) and from the Twin Sisters dunite (Onyeagocha, 1978). They show no relation, however, with chromite from the Orthris complex of Greece (Hynes, 1972). Figure 5.6 indicates that the chromites from Vavdos have a wider spread of Mg x 100 : Mg + Fe^{2+} ratios than chromites from other complexes. They also include chromites with higher iron contents.

The chromites from Gomati show a wider compositional spread than those of Vavdos. They overlap, in part, with chromite from Troodos complex and the Twin Sisters dunite, as well as

Figure 5.5

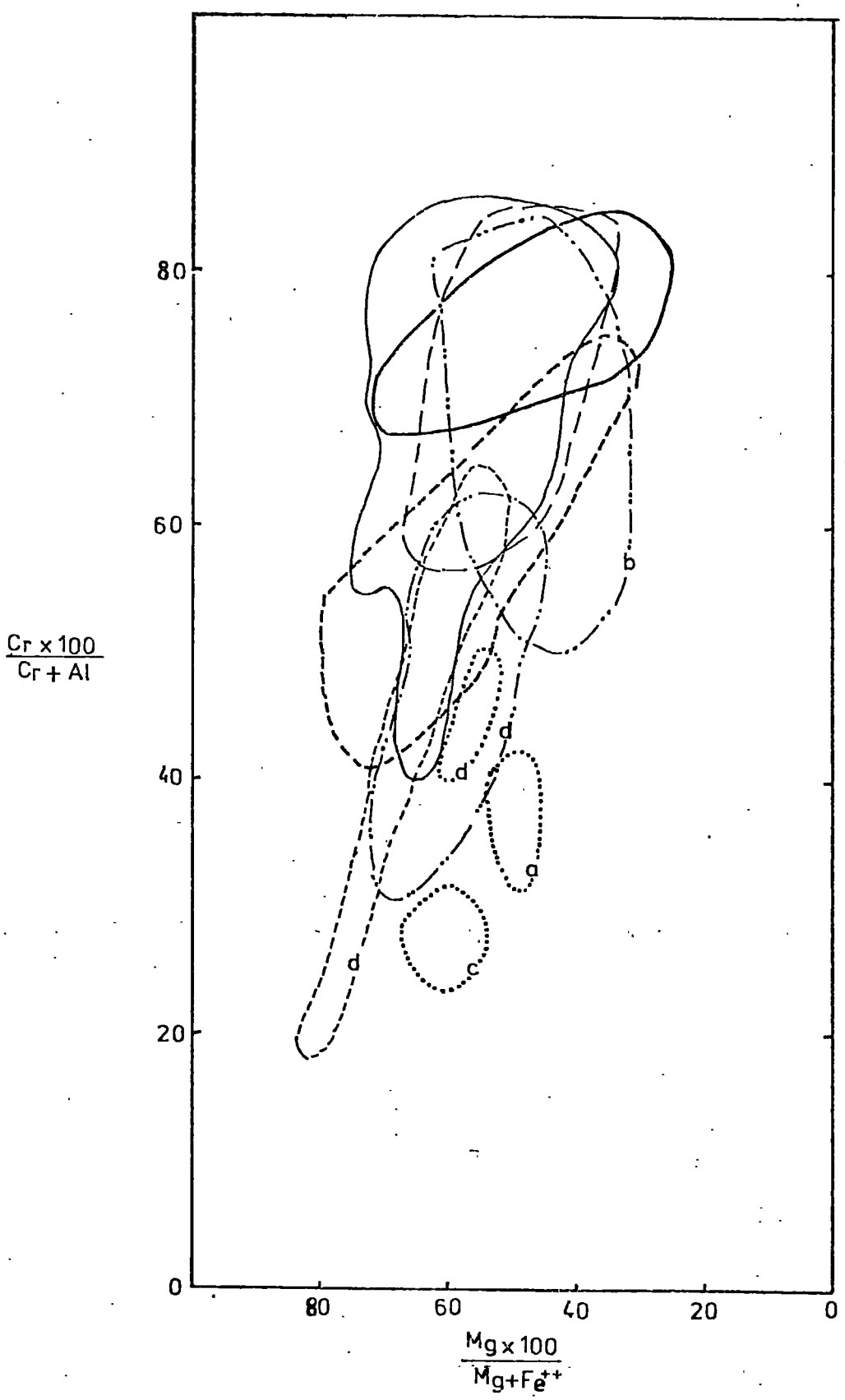

with chromite from the peridotite and dunite of the Blue River ultramafic body. Figure 5.6 indicates that the chromites from Gomati have higher Fe^{3+} contents and cover the entire compositional field with respect to the Mg x 100:Mg+Fe^{2+} ratio.

Massive chromitites in dunite contain high chromium spinels and in general are located at the base of the dunite near the contact with harzburgite. They rarely occur in harzburgite and when so located, the ore bodies are invariably enclosed in a dunitic shell. Engin (1969) described the chromite deposits ofthe Fethiye area in Turkey. Here the massive chromitites occur only in harzburgite. They are characterised by sharp contacts with the surrounding rocks and are enclosed in a dunite envelope. These chromites are also rich in chromium and poor in Al_2O_3, with an increase in Cr_2O_3 content from the disseminated type of ore, through massive to nodular ore. In the ophiolite belt of Oman, the chromite is Cr-rich within the massive ores, according to Peters and Kramers (1974). These authors, however, did not comment on the host lithology, or the nature of the contacts of massive bodies, whether tectonic or gradational. The chromite deposits from the Troodos complex in Cyprus have been carefully described by Greenbaum (1972) and Panayiotou (1978). The massive ores are localised either in dunite or harzburgite, but in the latter case are always immediately enclosed in dunite. The chromites from massive ores are rich in chromium, and although they are always coarse-grained interlocking anhedra, Greenbaum (1972) has concluded that they have a primary magmatic origin through cumulus processes. Conflicting evidence is given by

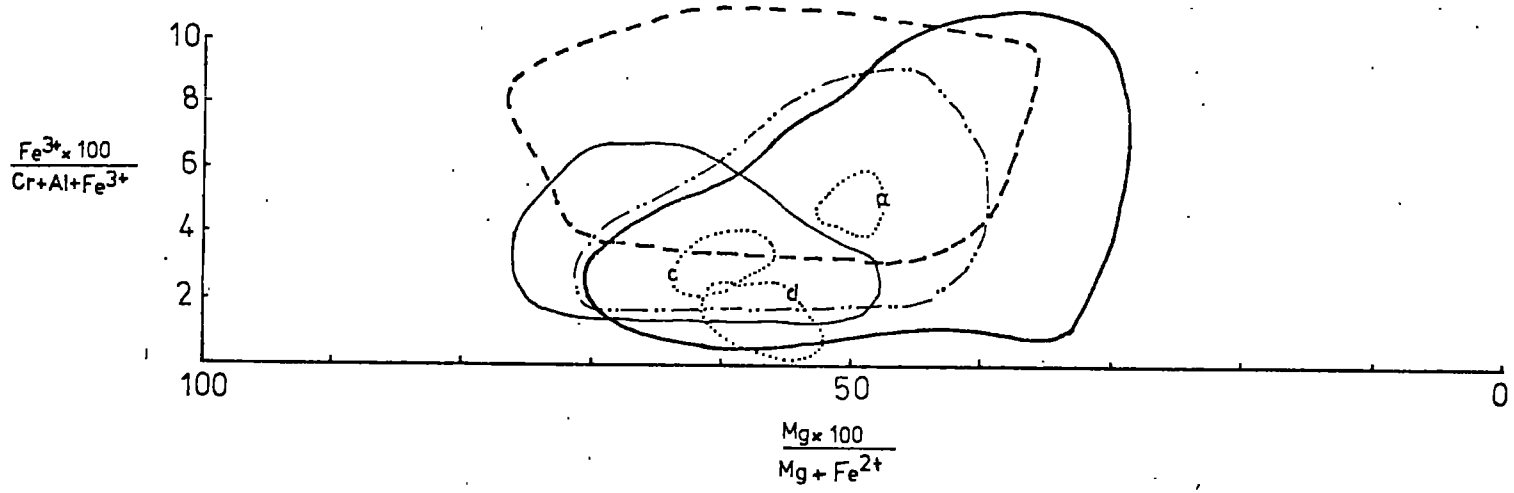

Figure 5.6 A comparative plot of the cation ratios. All symbols are as in Figure 5.5

Malpas and Strong (1975) for chromite occurrences in the Bay of Islands complex, in Newfoundland. They report high chromium chromites as a residual phase in harzburgite and low chromium-high alumina chromites as an intercumulus phase in dunite. These chromites represent disseminations. Sinton (1977) discussed the mineralogy of Red Mountain, New Zealand, alpine peridotite. Here the complex is comprised mainly of harzburgite and minor dunite ; chrome spinel in harzburgite has Cr : Cr + Al + Fe^{3+} ratios between 0.27 and 0.62, while concentrations of chromite are found only in dunite. Accessory Cr-spinel in thedunite is euhedral and contains higher Cr_2O_3 contents than that in harzburgite.

The above mentioned data from different sources, and that displayed in Table 5.1, is comparable with that of Thayer (1969,1970), who states that the wide spread in Cr_2O_3 and Al_2O_3 contents is a unique feature of podiform chromite deposits from ophiolite complexes. Although this extensive variation in Cr_2O_3 and Al_2O_3 contents is shown only by chromites from Gomati, chromites from both complexes have low total iron contents, another characteristic feature of podiform chromite deposits.

The chromites of Vavdos and Gomati are compared with those from typical layered intrusions in Figure 5.12. In this figure, the accessory chrome spinels in dunite show a different compositional trend, towards iron enrichment without much variation in the Cr_2O_3 content, to the trend shown by chromites from layered intrusions. There is little overlap of the two trends. Chromites from massive chromitites, however, plot in the compositional fields ofthe Bushveld and Great Dyke

TABLE 5.1 Accessory Cr-spinels

	Harzburgite		Dunite	
	Cr_2O_3	Al_2O_3	Cr_2O_3	Al_2O_3
Vavdos complex	-	-	51.74-55.45	10.65-14.52
Gomati complex	-	-	-	-
Burro mountain, California, Loney et al (1971)	32.7-39.1	31.5-37.4	50.1-58.0	10.4-20.6
Blue river ultramafic body, Canada, Pinsent (1974)	27.7-37.0	24.5-39.9	53.4-59.5	8.8-24.5
Bay of Islands ophiolite, NWF.,Canada, Malpas and Strong (1975)	33.5-61.3	7.8-33.6	33.7-34.1	29.1-32.1
Troodos complex, Cyprus, Greenbaum (1972) and Panayiotou (1978)	33.5-48.0	21.0-31.8	43.8-56.3	11.5-19.9
Red mountain, New Zealand, Sinton (1977)	26.7-48.9	16.5-39.6	54.5	14.3
Josephine peridotite, U.S.A, Dick (1977)	15.5-50.0	-	22.5-55.0	-
Kempirsai massif, Urals, Pavlov and Grigoreva (1977)	29.8-40.8	27.5-34.7	-	-
Voykar massif, Urals, Savelyev and Savelyeva (1979)	28.1-42.0	20.6-35.0	45.5-48.5	12.8-17.0
Sekinomiya complex, Japan,Arai (1980)	39.6-46.2	23.3-29.5	-	-

TABLE 5.2 Chromite Concentrations

	Cr_2O_3	Al_2O_3	MgO	FeO_{total}
Vavdos complex	53.52-59.16	9.74-15.95	9.15-14.81	13.83-22.32
Gomati complex	36.37-42.71	19.84-30.43	11.0-16.41	16.25-24.24
Andizlik-Zimparalik area, Turkey, Engin (1969)	37.1-58.4	14.2-28.7	10.6-14.5	12.2-18.6
Ophiolite belt, Northern Oman, Peters & Kramers(1974)	38.5-61.3	8.0-22.8	13.0-15.2	13.7-17.0
Troodos complex, Cyprus, Greenbaum (1972) and Panayiotou (1978)	34.6-62.7	8.3-33.5	9.8-17.4	12.5-24.5
Red mountain, New Zealand, Sinton (1977)	62.3	8.23	13.4	14.9
Sekinomiya complex, Japan, Arai (1980)	36.5-43.2	26.6-33.3	-	-

complexes. This may indicate a similar genetic procedure for producing chromite concentrations in layered intrusions, and massive chromitites in the dunites of the Vavdos ophiolite complex. However, at the same time the massive chromites from Vavdos plot atthe low iron end of the trend shown by the accessory spinels. It is apparent from Figure 5.12 that the trend followed by the chromite of layered intrusions involves iron enrichment with contemporaneous chromium depletion, while that followed by the chromite of Vavdos involves iron enrichment with a relatively constant Cr_2O_3 content.

Figure 5.12, also indicates that the chromites from the Gomati complex also have a different trend to that of the stratiform chromite. Disseminated chromites in banded werhlite-dunite have the lowest Cr_2O_3 and total FeO contents, with massive chromite concentrations in both banded werhlite-dunite and dunite being relatively enriched in both components. Chromites from clinopyroxene-bearing chromitites follow the same trend with disseminated chromite in dunite being most enriched in Cr_2O_3 and total FeO. The chromites from Gomati thus follow an entirely different trend to those of layered intrusions, suggesting very different genetic procedures and environment of formation.

The MnO contents of chromites from Vavdos and Gomati range from 0.40 to 0.80% and from 0.34 to 1.40% respectively. Those values are generally higher than those shown by chromite from other ophiolites. Engin (1969) reports a range of 0.21 to 0.59% for ores of Andizlik-Zimparalik area, Turkey, while chromites from the Troodos complex vary between 0.09 and 0.22% according to Greenbaum (1977) or 0.15 and 0.34% according to

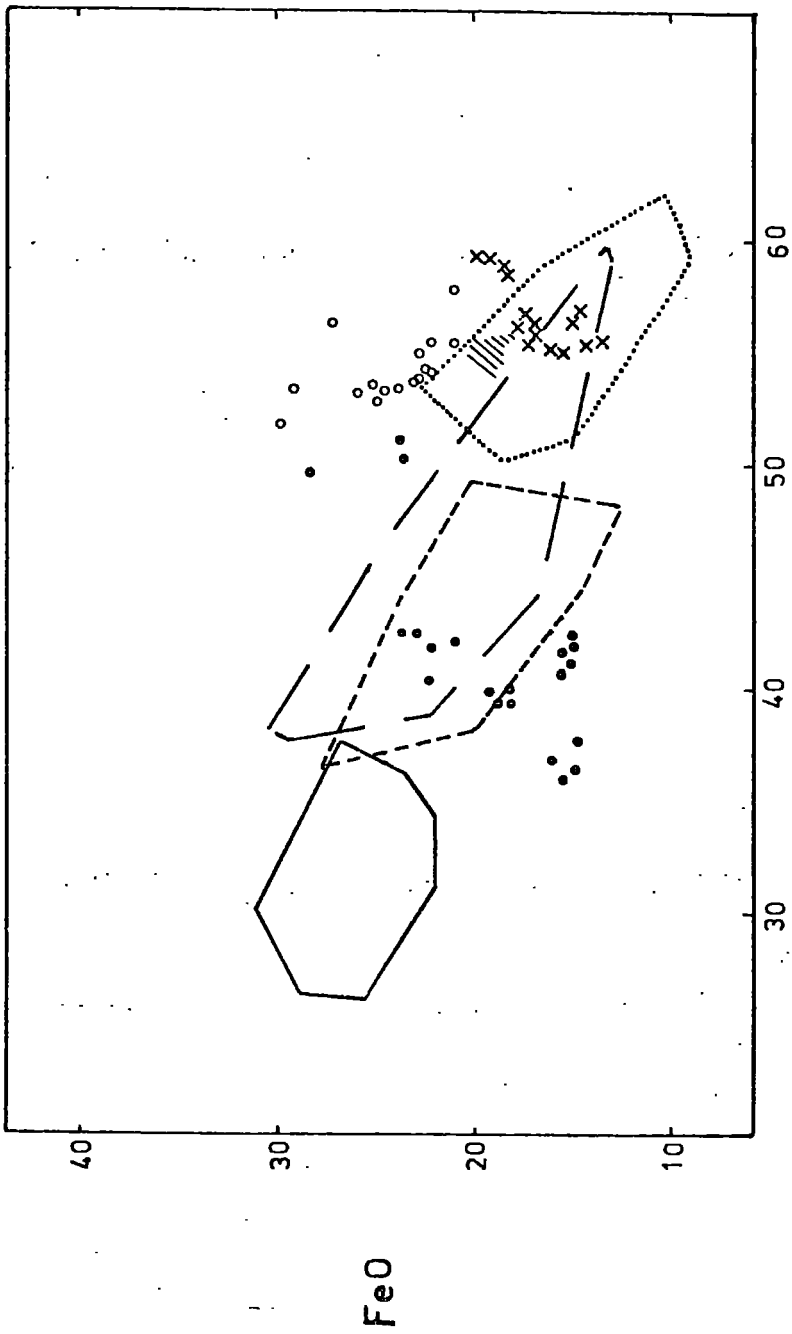

Figure 5.12

Panayiotou (1978), and from Burro Mountain from 0.14 to 0.30%, Loney et al (1971). Chromites from the Triadion complex in N. Greece have Mn-contents between 0.17% and 0.22% (Papadakis, 1977). Chromites from stratiform complexes have much higher values, in general above 1%.

The high MnO contents of chromite from Gomati are attributed to primary enrichment in the residual melt, after the partial fusion of mantle lherzolite.

The TiO_2 contents of chromites from Vavdos and Gomati are generally below 0.65% as shown in Figure 5.13, with chromites from Gomati having higher values than those from Vavdos. Dickey (1975) has pointed out that in general chromites from ophiolite complexes have TiO_2 values below 0.3%. Engin (1969), Pinsent (1974) and Panayiotou (1978) give TiO_2 values between 0.13-0.41%, 0.11-0.31% and 0.07-0.36% respectively, while Malpas and Strong (1975) give values from 0.05 to 0.51% for chromites from Newfoundland ophiolites. The compositional fields of TiO_2 in chromites from the Fiskenaesset (Ghishler, 1976) and Bushveld (Cameron, 1975) layered intrusions are also plotted in Figure 5.13. It is worth noting that chromites from chromite rich dunite from the Bushveld complex have the lowest TiO_2 contents. Cameron (1975) also indicates a low value of 0.43% for a chromite inclusion in olivine. It is apparent that the chromites from the Gomati complex are very rich in TiO_2 in comparison to chromites from other alpine-type complexes. This is also indicated by the presence of exsolved rutile in the chrome-spinels from the banded primary werhlite-dunite rocks.

The V_2O_3 content of chromites from both complexes is low with concentrations below the detection limit of the

Figure 5.13

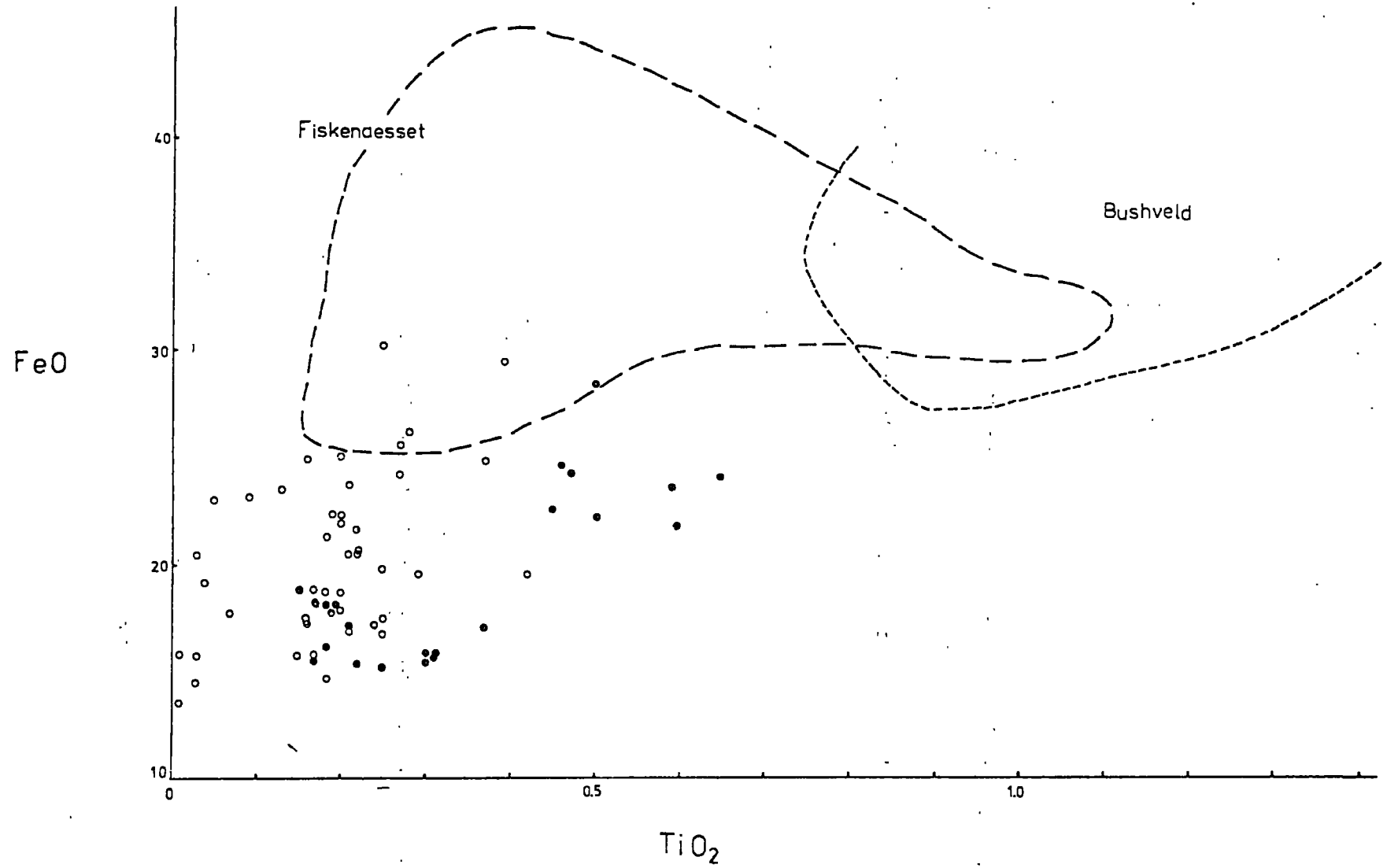

electron microprobe. In contrast chromites from stratiform complexes have much higher values. Cameron (1975) and Ghisler (1976) give values between 0.20-0.61% and 0.20-0.60% for chromites from the Bushveld and Fiskenaesset complexes respectively.

5.5 DISCUSSION

The accessory chrome-spinels of the Vavdos complex have lower chromium and magnesium contents than those from massive chromitites, and have a corresponding enrichment in iron. Chrome spinels in chromitiferous dunite from the Gomati complex show distinct chromium and iron enrichments, and a decrease in Mg-content when compared with massive ores. The results of Fe^{2+} and Mg partitioning between coexisting olivine and spinel indicate that there is continuous equilibrium exchange of Mg and Fe^{2+} between olivine and spinel during slow cooling to relatively low temperatures. It is thus evident that the accessory chrome-spinel compositions represent the final products of igneous fractionation modified by all subsequent metamorphic transformations, probably including serpentinization.

Irvine (1967) indicated that the interstitial spinels in peridotite are aluminous. He supposed that their formation reflects growth from intercumulus basaltic liquid. Greenbaum (1977) has reported the presence of interstitial,"amoeboid", anhedral aluminous spinel in harzburgites from the Troodos complex, while Pinsent (1974) has demonstrated that accessory chromite textures change from small and euhedral in dunites, to large irregular and interstitial in harzburgites. This textural change is accompanied by a chemical change from

Cr-rich in dunite to Al-rich in harzburgite, for these spinels from the Blue River ultramafic body, as shown in Figure 5.5. Pinsent (loc.cit.) showed that the accessory spinels in dunites generally have Cr x 100 : Cr + Al ratios above 57.5 $\pm$ 2.5, whereas accessory spinels in harzburgites generally have ratios below this value. He also stated that the critical Al_2O_3 content is 24.5% and suggested that, on this basis, dunites can be differentiated from peridotites. The average Al_2O_3 content of the Cr-spinels from massive chromitite in the Gomati complex, associated with a dunite host lithology, is 24.9%. This coincidence is important, revealing a relationship between the chromite from massive ores and the first accessory chromite to crystallize from a basaltic melt.

Dick (1977)clearly distinguishes the textures of spinels in dunite and harzburgite. According to his textural interpretation, the spinel in dunite is euhedral to subhedral and represents free growth in a melt, whereas that in harzburgite is highly irregular in shape, interstitial and poikilitic, enclosing brecciated enstatite grains. This spinel reflects formation after partial fusion or results from incongruent melting of pyroxene. Dick (loc.cit.) also states that spinel in harzburgite is Al-rich, giving an upper limit of the ratio Cr x 100 : Cr + Al of around 60, while spinel in dunite is more Cr-rich, and in massive chromite pods shows the highest Cr_2O_3 values.

Table 5.1 lists analyses of accessory chromites from different alpine-type occurrences, and Figure 5.15 shows the distinct trend from Al-rich spinels to Cr-rich spinels. Spinels from the transitional peridotite of Red Mountain,

New Zealand, Sinton (1977), have an Al_2O_3 content of about 20% and could be considered to lie in the boundary zone between spinels from dunite and peridotite respectively.

The only contradicting information comes from the Bay of Islands ophiolite complex in Newfoundland, studied by Malpas and Strong (1975). They indicate the presence of resorbed to euhedral Cr-spinel crystals in harzburgite, and rare euhedral Cr-spinel, enclosing olivine, in dunite. They consider that the chrome spinel in harzburgite is a residual phase, whereas that in dunite has formed from an intercumulus liquid. Chemical analyses of these Cr-spinels from the Bay of Islands complex give conflicting data to that presented in Table 5.1 and Figure 5.15. It is apparent that there is something odd about the field interpretation of these chromites, which represent disseminations. No further comment seems appropriate as neither the rocks nor field area have been examined.

In the harzburgite subtype peridotites (harzburgite-dunite series) of the alpine-type peridotites (Jackson and Thayer, 1972), the spinels show a large compositional range, especially in the Cr : Cr + Al ratio. Lherzolite subtype peridotites are usually accompanied by high temperature metamorphic aureoles, their spinels being aluminium rich. Shervais (1979) reports Al_2O_3 contents for spinels from the lherzolite massif at Balmuccia of 48.5 to 65.9% with an average greater than 55%. Lherzolite subtype peridotites are related genetically to diapirs of possible undepleted mantle. Their spinels must be compositionally different to those from tectonized peridotites (lherzolite-harzburgite) of the ophiolite suite.

Spinels in lherzolite from the ophiolite complex in the Orthris mountains of Greece (Hynes, 1972) show a variation in Cr : Cr + Al ratio from 0.45 to 0.52 and the spinel is interstitial, whereas according to Shervais (1979) the Cr : Cr + Al ratio, for spinels from Balmuccia, ranges only from 0.02 to 0.18. Spinels from lherzolites in the Bay of Islands, Newfoundland, considered by Malpas and Strong (1975) as intrusive mantle diapirs, have Al_2O_3 contents of 53-54% and Cr : Cr + Al ratios of approximately 0.2. The spinels from the Balmuccia lherzolite have Mg : Mg + Fe^{2+} ratios between 0.70 and 0.80, similar to those of the Bay of Islands lherzolite of 0.75-0.81, whereas the spinels from the lherzolite of the Orthris mountains have different Mg : Mg + Fe^{2+} ratios, in the range 0.48-0.52.

It is thus apparent that there is a distinct difference between the spinels in lherzolite from the lherzolite subtype peridotite and those in lherzolites from ophiolite complexes. The latter contain less Al,more Cr and a lower Mg : Mg + Fe^{2+} ratio. This is in agreement with information on spinels from the Orthris ophiolite given by Menzies (1975). He states that interstitial spinel from harzburgite is more Cr-rich than that from depleted lherzolite and that the latter is poorer in Al^{3+} than spinel from plagioclase-lherzolite which, according to Menzies and Allen (1974), represents only slightly modified mantle material.

The lherzolite from lherzolite subtype peridotites may be considered as virtually undepleted mantle, whereas lherzolite and harzburgite from ophiolite complexes represent depleted mantle and refractory residuum respectively. The

accessory spinels in these rocks must have equilibrated with different mineral assemblages at different P, T conditions. They are one of the last formed minerals in all the three types since they occur as interstitial grains. The data described above reflect the high Al_2O_3 and low Cr_2O_3 contents of spinels from lherzolite diapirs. Initial partial fusion of lherzolite subtype peridotite would produce depleted mantle material, the lherzolite of ophiolite complexes. Further extensive partial fusion would lead to a refractory residue, harzburgite, and penecontemporaneously the extraction of a basaltic melt. The sequential compositional change of spinels formed under different equilibration conditions at each stage is demonstrated by Al_2O_3 impoverishment, due to aluminium (Al^{3+}) occurring in both tetrahedral and octahedral coordination because Al^{3+} is an ionic cation with no strongly directed bonds, and by Cr-enrichment, as Cr^{3+} is concentrated into residual phases according to Dickey and Yoder (1972).

It can be assumed, therefore, that sequential change in spinel composition only occurs in response to changes in the bulk composition. The interstitial character of spinel from lherzolite subtype peridotites suggests growth from an interstitial liquid during partial melting. The presence of relatively Al-rich spinel concentrations in harzburgite, compared to dunite, is in agreement with the trend discussed above.

The compositions of accessory chrome-spinels from the Vavdos complex overlap with those of accessory spinels in dunites from other complexes, as shown in Figures 5.14 and 5.15. The chrome-spinels from the Gomati complex shown in Figure 5.14, show sequential chemical changes. The chromites

Figure 5.14

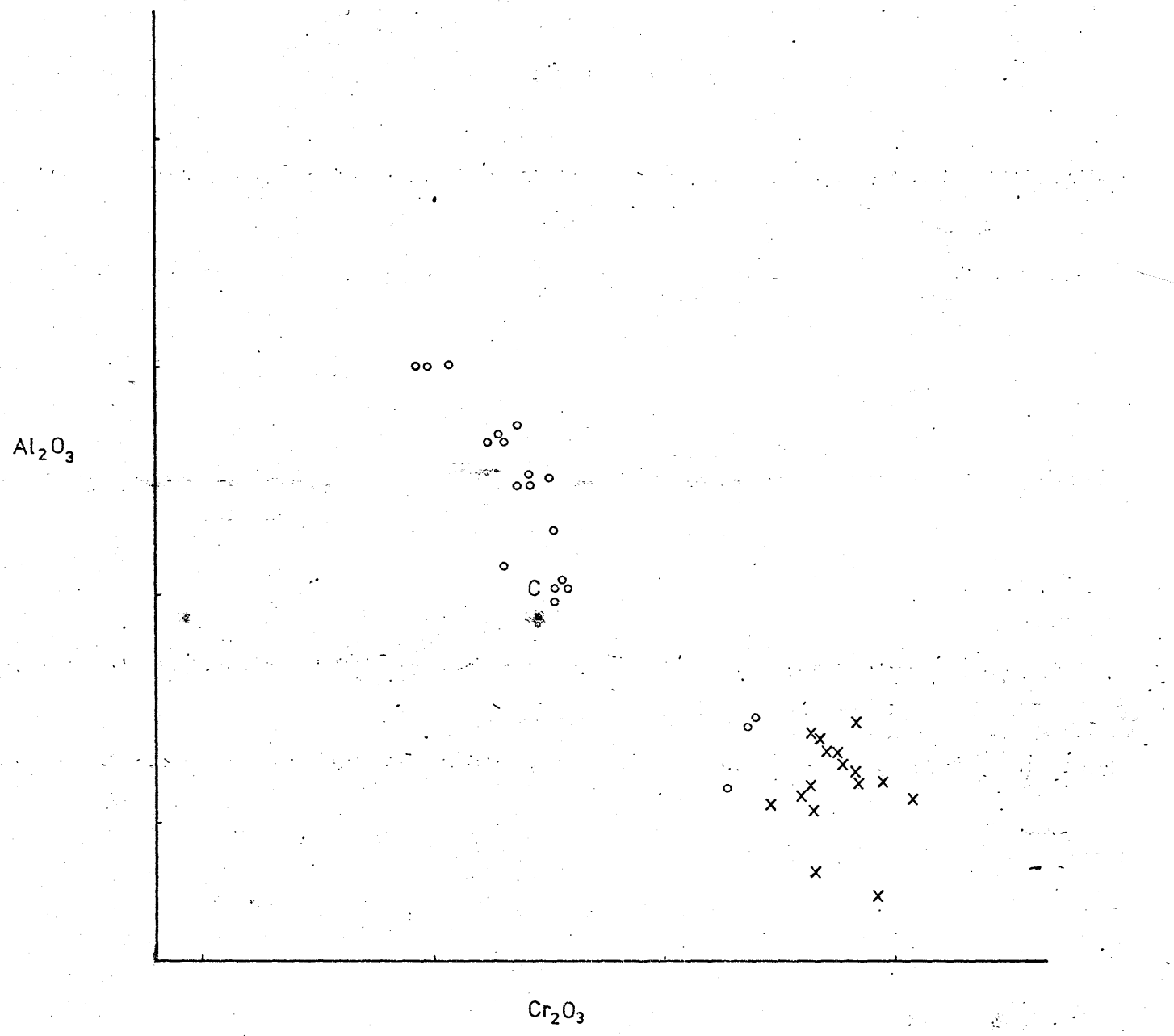

Figure 5.15

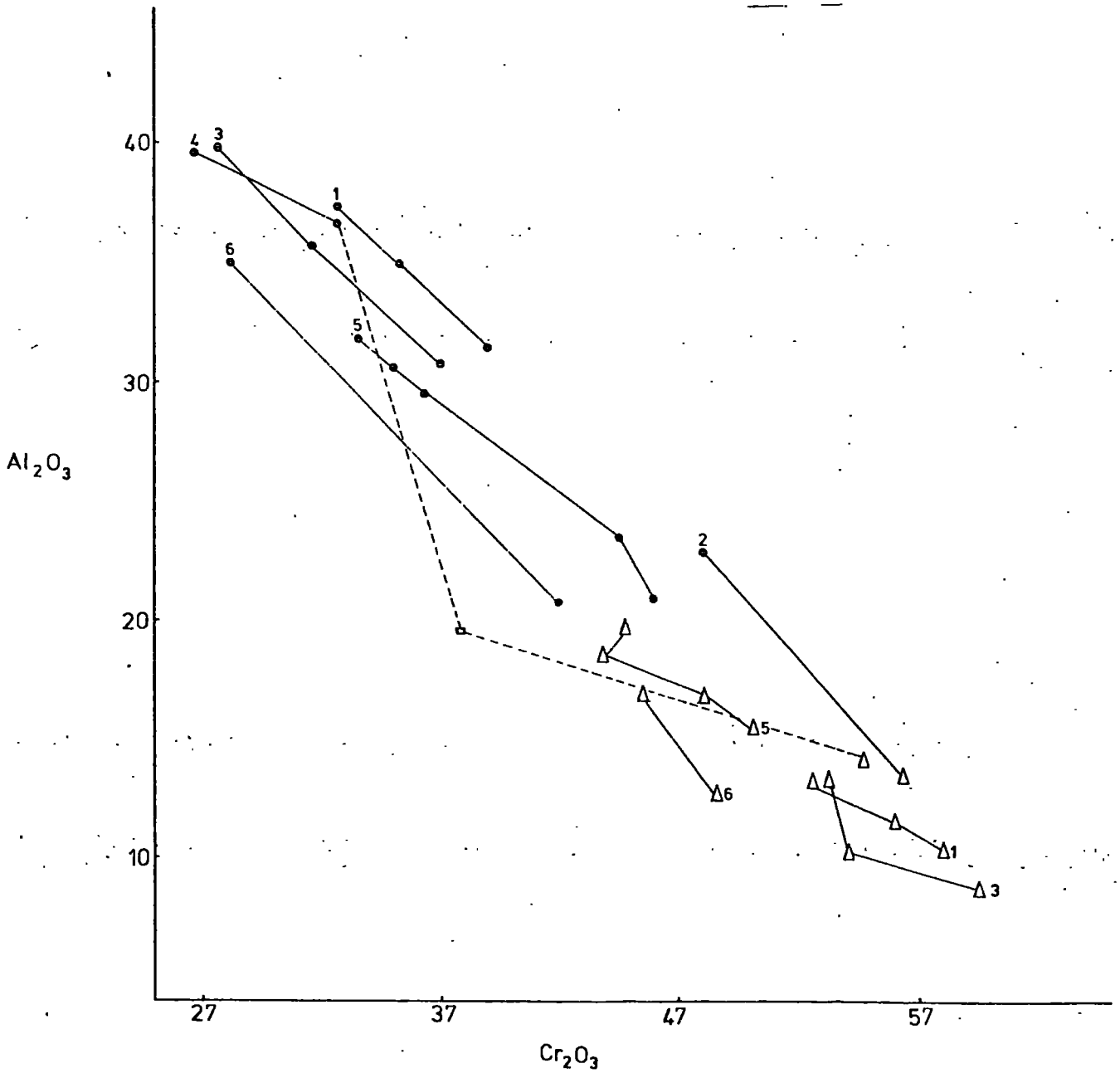

from chromitiferous dunite (around 10% chromite, sample GB4), fall in the compositional field for accessory Cr-spinels in dunites from different complexes, and are very similar in composition to those from Vavdos complex, though somewhat richer in Al_2O_3. Chrome-spinels from the clinopyroxene-bearing chromitites fall near the general boundary between accessory spinels from dunite and harzburgite having more Al_2O_3 and less Cr_2O_3 than those in chromitiferous dunite. Slight decrease in Cr_2O_3 content and increase in Al_2O_3reflects the composition of chromite from massive ores in either a dunite host (sample GB2) or interbanded serpentinite-amphibolite host (sample GT7). The close chemical composition of these two groups of chrome-spinels suggests a close genetic relation. Further decrease in Cr_2O_3 and increase in Al_2O_3 leads to relatively poor massive ore or rich disseminated type with about 50% Cr-spinel (samples GS2, GS4). The presence of exsolved rutile needles in the spinels is a characteristic feature of this group and probably represents a stage during the extraction of titanium in the residual melt. The most aluminous spinels are from a disseminated ore-type containing about 35% Cr-spinel (sample GN15), and occurring in banded serpentinite-amphibolite. These spinels overlap in composition with accessory spinels from harzburgite, as shown in Figure 5.15.

Figure 5.16 is a plot of Cr_2O_3 content against the Al_2O_3 content of spinels and compares data from Greenbaum (1972) with data from the Gomati complex.

Selected analyses from Greenbaum (1972) show a remarkable linearity for chromite from harzburgite. However, it is pertinent to mention that all the chromite concentrations

Figure 5.16

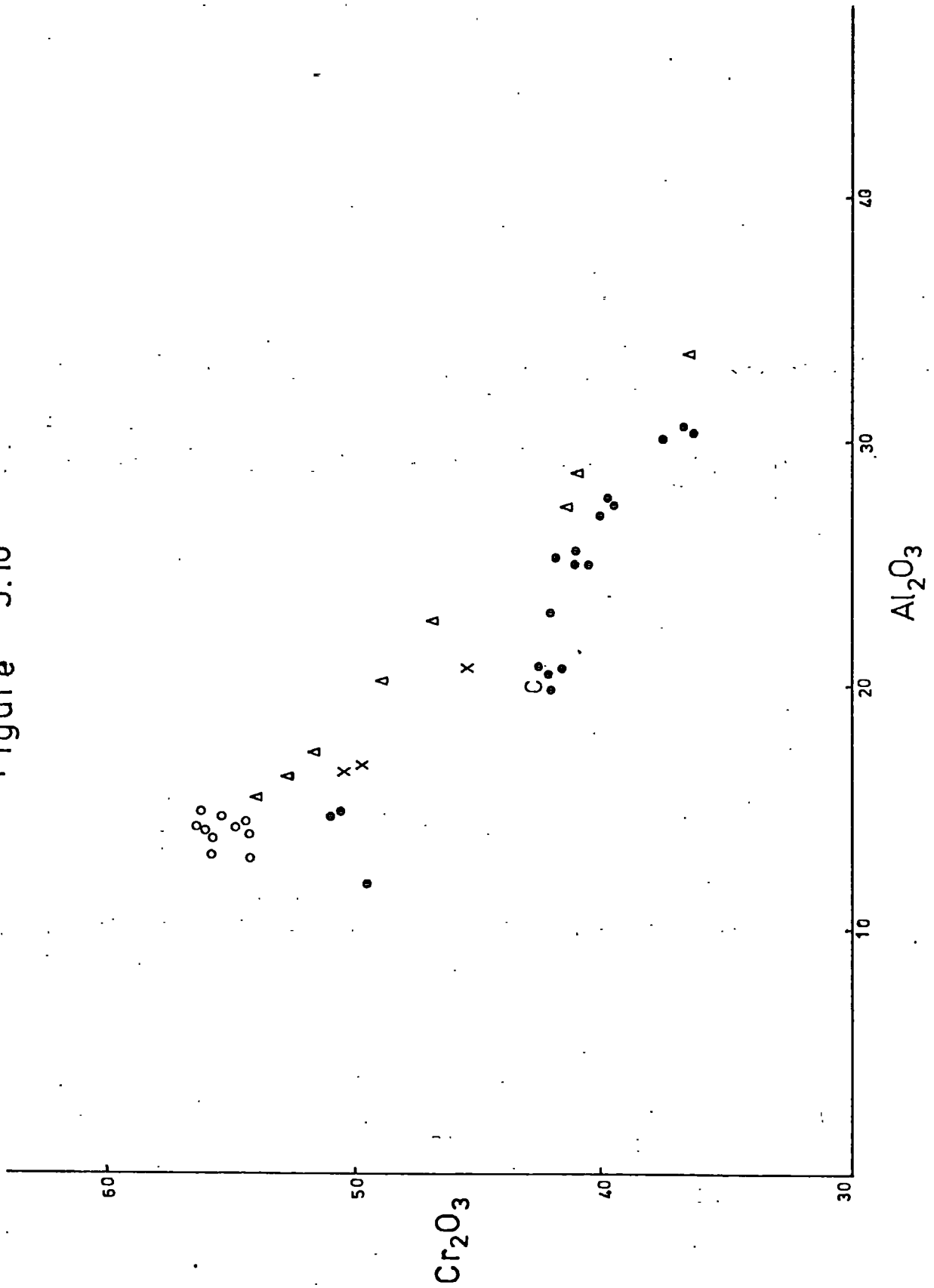

in harzburgite from the Troodos complex, are enveloped by thin dunitic shells. The trend of spinel concentrations in these harzburgites commences at a Cr_2O_3 value of about 36.5%, which is almost identical to that of the most aluminous spinels in ophiolite-associated peridotite. These spinels are from disseminated chromite in a thin dunitic envelope. With increasing chromite proportion relative to silicate matrix the Cr_2O_3 content of spinels increases. From about 46 to 50% Cr_2O_3, there is comparability in composition between spinels from massive ores and accessory spinels from harzburgite. This can be attributed either to very close genetic relationships between the two types of spinel, with the assumption of growth of accessory spinels from interstitial liquid, or to later re-equilibration by reaction with the refractory residue, under slowly changing conditions. The trend of increasing Cr_2O_3 continues towards spinels from massive ores in a dunite host lithology, passing sequentially through chromites of different ore types. Chromite with high chromium contents occurs as disseminations in chromitiferous dunite, those chromites with the highest Cr_2O_3 content belonging to nodular type ore, as found by Engin (1969).

Chromites from the Gomati complex show a closely similar trend, considering the chromite concentrations independent of host lithologies. Disseminated chromites (35% chromite) have the highest Al_2O_3 content, at about 36-37% Cr_2O_3. Chromites from massive ore in dunite and in banded serpentinite-amphibolite show overlapping fields, but concentrations of massive ore, are clearly related to the dunitic part of the complex. Disseminated chromite from a chromitiferous dunite

has a much higher Cr_2O_3 content suggesting sequential chromium enrichment during fractionation of basaltic magma.

The chromites from clinopyroxene-bearing chromitites in Gomati, have lower Cr_2O_3 and Al_2O_3 contents, which displace them from the trend. A similar displacement is shown by chromites from clinopyroxene-dunites in Troodos.

Marakushev (1979, Figure 11) has plotted $Cr:R^{3+}_{total}$ against $Al:R^{3+}_{total}$ for accessory spinels. He showed an increase in the $Al:R^{3+}_{total}$ ratio from spinels in dunites of alpine-type to stratiform dunites to harzburgites to lherzolites with decrease of the $Cr:R^{3+}_{t}$ ratio. He suggests that chromium valency and coordination number fluctuate inversely from harzburgite to dunite. The coordination number rises and so the solubility of Cr decreases with the subsequent result that chromite deposits are segregated and found in association with magnesian dunites.

Irvine (1967) attributed the formation of aluminous spinel to the following reaction,

$(m-2)MgSiO_3.MgAl_2SiO_6 + Mg_2SiO_4 \rightarrow MgAl_2O_4 + m\ MgSiO_3$, which may
aluminous enstatite (fo) (sp) (en)

be considered as the recrystallization of aluminous pyroxene.

Dickey et al (1971) investigated experimentally the system $CaO-MgO-Al_2O_3-Cr_2O_3-SiO_2$ on the join diopside, Ca-Cr-tschermak ($CaMgSi_2O_6$-$CaCr(AlSi)O_6$). They estimated the Cr_2O_3 content in diopsides, over the range diopside-$Di_{90}CrCaTs_{10}$, to be from 0.0 to 3.1%. Dickey et al (1971, Figure 7) indicate that clinopyroxenes containing more than 3% CrCaTs(0.9% Cr_2O_3), melt incongruently to spinel + liquid. The maximum solubility of CrCaTs in diopside is 14% at 1200°C and 1 atm. At 10k.bars P_{H_2O}, diopsides can contain 10% CrCaTs (Dickey, 1975).

Assuming incongruent melting of chromian diopside to chrome spinel + liquid, Dickey et al (loc.cit.), it can be inferred that partial fusion of lherzolite to produce residual harzburgite with accessory spinel and basaltic liquid, is a reasonable process for the formation of harzburgite, but cannot explain the ore concentrations. However, Dickey and Yoder (1972) investigated the distribution of Cr^{3+} and Al^{3+} between spinel and clinopyroxene in the system $CaO-MgO-Al_2O_3-Cr_2O_3-SiO_2$, on an Fe-free basis, and concluded that the accessory chromites in alpine-type peridotites approach the bulk-rock chemistry in Cr:Al ratios due to equilibration with surrounding phases.

Mori (1977), investigating the system $CaO-MgO-Al_2O_3-SiO_2$ at 1200°C and 16k.bars, used a natural starting material with a clinopyroxene containing 1.26% Cr_2O_3. After the run, the analyzed clinopyroxene contained 1.45% Cr_2O_3. Therefore, it is apparent that Cr-diopsides can occur at high pressures (at least above 10k.bars) and that their chromium content decreases with temperature. This reinforces the assumption of Dickey et al (1971), that after incongruent partial fusion of undepleted lherzolite, relatively aluminous chrome-spinel is encountered in the refractory harzburgite. Because the accessory aluminous Cr-spinel has an interstitial nature, it can be regarded as a mineral formed from the interstitial fluid phase at the time that this basaltic liquid is being abstracted. The accumulation of massive concentrations of refractory chromite, is believed to have taken place sequentially from this interstitial fluid phase during separation from the refractory-residue. As physical separation proceeds, the basaltic liquid becomes enriched in Cr^{3+}

due to reaction with the residual minerals and the chromium content of the spinels starts to increase. Thus, the accessory spinels in harzburgites are richer in Al than those from disseminated ore, because they have been formed from a compositionally different and less evolved fluid phase. The increase in Cr_2O_3 content from disseminated to massive ore in the Gomati complex, as shown in Figures 5.14 and 5.16, supports this process. The chromite from concentrations in clinopyroxene-bearing chromitites are more chromium rich, supporting the fact of continuous migration of Cr^{3+} in residual phases. However, even the disseminated chromites in dunite have a lower Cr_2O_3 content in the Gomati complex, than massive, disseminated or accessory chromites from the Vavdos complex. This can be interpreted by a depletion in Cr-content due to the sequential segregation of chromite ores from refractory to chromium-rich at Gomati. This resulted in a considerable early uptake of chromium and a consequent lower availability of Cr_2O_3 for the later accessory chromite of the dunites.

The above process is in agreement with the behaviour of trace transition elements like Ti^{4+} and Mn^{2+}. Ti^{4+} and Mn^{2+} are transition elements without crystal field stabilization energy, having octahedral site preference energy almost zero and so aremainly concentrated into the melt after partial melting ofmantle peridotite (Burns, 1973). The distribution of Ti in the spinels from Gomati is shown in Figure 5.17, together with compositional fields of spinels from the Josephine peridotite (Dick, 1977). In Table 5.3, TiO_2 contents of accessory spinel in harzburgite and dunite from different alpine type complexes are shown. The TiO_2 content is always

Figure 5.17

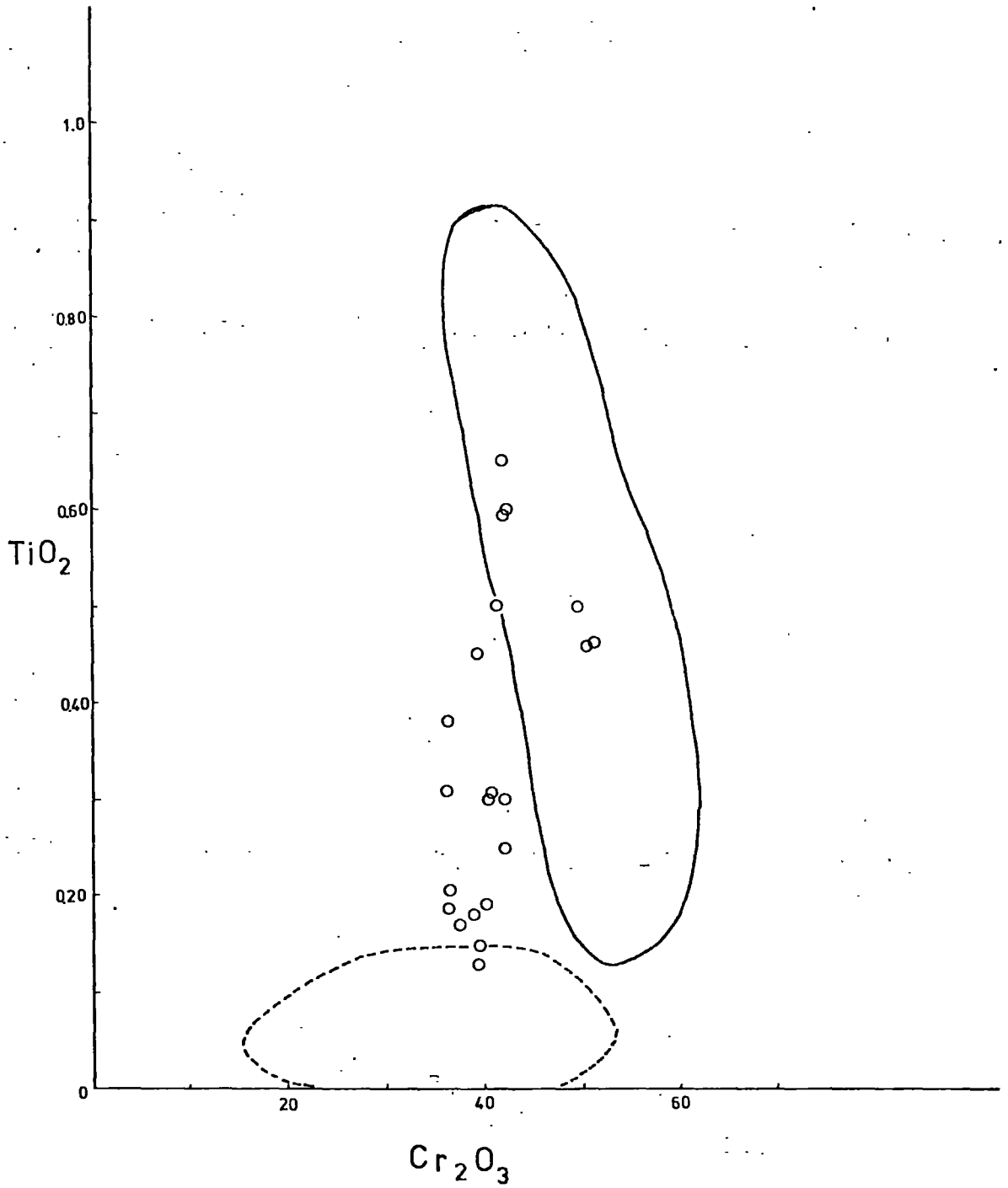

TABLE 5.3 TiO_2 Content of Accessory Spinels, according to Host Rock Type

	Harzburgite	Dunite
Loney et al (1971), Burro mountain, U.S.A.	0.08-0.16	0.16-0.20
Pinsent (1974), Blue river ultramafic body, Canada	0.01-0.06	0.16-0.24
Panayiotou (1978), Troodos complex, Cyprus	0.06-0.07	0.08-0.14
Savelyev & Savelyeva (1979), Voykar Massif, Urals.	0.08-0.19	∿ 0.35
Dick (1977), Josephine Peridotite, U.S.A.	0.02-0.15	0.08-0.30
Arai (1980), Sekinomiya complex, Japan	0.08-0.19	-
Sinton (1977), Red mountain, New Zealand	0.02-0.07	∿ 0.66

lower in spinel from harzburgite than that from dunite. The TiO_2 content of the disseminated chromites from Gomati complex approaches the compositional field of chromites associated with harzburgite according to Figure 5.17, while chromites from disseminations in dunite and clinopyroxene-chromitite overlap with the field of massive chromitites of Josephine peridotite.

There is thus a coincidence of disseminated chromites from Gomati complex with those associated with harzburgite lithologies from other ophiolite complexes.

The high chromium massive ores are always associated with a dunite host lithology, even when they are within harzburgites (Dick, 1977). The high chromium spinels, occurring as disseminations in harzburgite, reported by Malpas and Strong (1975), represent probably a differentiation product of trapped basaltic liquid within pockets in the harzburgite. This is also in agreement with a general characteristic of massive ores which occur in the lowermost parts of the dunite very close to the content with harzburgite. This implies that the massive ores were formed during the very first stages of differentiation of the residual basaltic melt and without reacting with the refractory residue.

The magmatic textures of massive chromite concentrations and associated dunites have been pointed out by Greenbaum (1977) and Dick (1977). The onequivocal magmatic textures of chromite concentrations in the Vavdos complex, together with their high chromium content,are consistent with the assumption of magmatic origin. The trend also towards chromium impoverishment in favour of mutual iron enrichment, as depicted in

Figure 5.9, supports the magmatic genesis of high chromium massive ores.

It is thus necessary to examine the massive chromite concentrations in the light of formation during differentiation processes involving basaltic liquids.

Chromium (+3) has a very limited solubility in basaltic liquid, the maximum being from 200 to 300 ppm at an oxygen fugacity of 10^{-8} atm and 1200°C (Hill and Roeder, 1974). This is mainly because of its high crystal field stabilization energy and subsequent strong octahedral site preference energy. There is thus an early uptake of Cr^{3+} into the spinel crystals resulting in a mutual impoverishment in the liquid and enrichment in the spinel.

Hill and Roeder (1974) have studied the affects of oxygen fugacity on the stability and composition of spinel crystallizing from a basaltic liquid, in a series of experiments in the temperature range of 1100°C-1325°C and oxygen fugacity range of $10^{-6.8}$ to 10^{-14} atm. They have re-confirmed the very low solubility of Cr^{3+} in basaltic liquids and have established a trend for the spinel compositions in response to the increasing or decreasing oxygen content of the system. The Cr_2O_3 content of spinels increases with a concomitant decrease of iron content as the oxygen fugacity decreases. The Cr_2O_3 content of spinels also increases with increasing temperature at a fixed oxygen fugacity. Hill and Roeder (loc.cit.) have also indicated that the addition of more Cr_2O_3 to the system causes precipitation of spinel at higher temperatures and lower oxygen fugacities.

It is thus clear that the basaltic liquid extracted

from the residual harzburgite must be very rich in chromium ; otherwise we must consider an enormous amount of differentiated basaltic liquid, in order to explain the amount of chromite ore. This is not compatible with field evidence. The resultant basaltic liquid will start to evolve as soon as a change in temperature or pressure appears. The differentiation of silicate liquids results in a decrease of octahedral sites in the liquid, due to the shift of the reaction, $2O^{-} \rightleftharpoons O^{o} + O^{2-}$ to the right, where O^{-} is singly bonded, O^{o} doubly bonded and O^{2-} are free oxygen ions. The Cr^{3+}, because of its high octahedral site preference energy (40 kcal.mole^{-1}, Marakushev, 1979), will be the first transition element to occupy octahedral sites in the spinels, which are in-turn, together with the olivine, the first crystallizing minerals from basaltic liquids. The precipitation of Cr-rich spinels will thus take place in the very early stages of evolution of the basaltic liquid and at low oxygen fugacities. The massive chromite concentrations can thus be explained by an abrupt fall in the oxygen content of the basaltic liquid, or by a fall in temperature. These produce a change in the structure of the liquid thus promoting episodic segregation of massive ore. This seems to happen near the dunite-harzburgite contact, some distance within the dunite and the harzburgite. Also implied is a sequential decrease in Cr_2O_3 and an increase of total iron, according to Hill and Roeder (1974). This is in agreement with the trend depicted in Figure 5.9 for chrome spinels from massive chromitites and the main dunite of Vavdos. After the formation of massive chromite ores, the basaltic liquid is depleted in Cr^{3+} and the formation of small single

chromite crystals is expected, due to the high enrichment factor of Cr^{3+} into the chromite relative to the liquid, always at low oxygen fugacity. This is so in the dunites from Vavdos, where the Cr-content of the bulk composition reflects entirely the Cr-content of the chromite. However, lower oxygen fugacities must be expected than those determined by Hill and Roeder (1974), in order to explain the higher Cr-content of chromites from podiform deposits.

CHAPTER 6

THERMODYNAMIC CONSIDERATIONS

6.1 PARTITIONING OF Mg and Fe^{2+} BETWEEN OLIVINE AND CHROME-SPINEL

The reciprocal exchange of Mg and Fe^{2+} between co-existing chrome-spinel and olivine was first considered by Irvine (1965), who described this exchange by the following reactions among the six main end-member spinels and two end-member olivines :

$$\tfrac{1}{2}\,Fe_2SiO_4 + MgCr_2O_4 \rightleftharpoons \tfrac{1}{2}\,Mg_2SiO_4 + FeCr_2O_4 \qquad (a)$$

$$\tfrac{1}{2}\,Fe_2SiO_4 + MgAl_2O_4 \rightleftharpoons \tfrac{1}{2}\,Mg_2SiO_4 + FeAl_2O_4 \qquad (b)$$

$$\tfrac{1}{2}\,Fe_2SiO_4 + MgFe_2O_4 \rightleftharpoons \tfrac{1}{2}\,Mg_2SiO_4 + Fe_3O_4 \qquad (c)$$

Irvine combined the above equations into one expressing solid-solution between the end-member phases. He gave the following general equation :

$$\underset{Fa}{\tfrac{1}{2}\,Fe_2SiO_4} + Y^{sp}_{Cr}\,\underset{Pc}{MgCr_2O_4} + Y^{sp}_{Al}\,\underset{Sp}{MgAl_2O_4} + Y^{sp}_{Fe^{3+}}\,\underset{Mf}{MgFe_2O_4} \rightarrow \underset{Fo}{\tfrac{1}{2}\,Mg_2SiO_4} + Y^{sp}_{Cr}\,\underset{Chr}{FeCr_2O_4} + Y^{sp}_{Al}\,\underset{Hc}{FeAl_2O_4} + Y^{sp}_{Fe^{3+}}\,\underset{Mt}{Fe_3O_4} \qquad (d)$$

where $Y^{sp}_i = \dfrac{i}{Cr+Al+Fe^{3+}}$ and $Y^{sp}_{Cr} + Y^{sp}_{Al} + Y^{sp}_{Fe^{3+}} = 1.$

Considering both the spinel and olivine series to be ideal under equilibrium conditions, he found that the equilibrium

constant for reaction (d) may be written

$$K_d = \left(\frac{\alpha^{ol}_{Fo}}{\alpha^{ol}_{Fa}}\right)^{\frac{1}{2}} \left(\frac{\alpha^{sp}_{chr}}{\alpha^{sp}_{pc}}\right)^{Y^{sp}_{Cr}} \left(\frac{\alpha^{sp}_{hc}}{\alpha^{sp}_{sp}}\right)^{Y^{sp}_{Al}} \left(\frac{\alpha^{sp}_{mt}}{\alpha^{sp}_{mf}}\right)^{Y^{sp}_{Fe^{3+}}},$$

where α^a_i is the activity of component i in phase a. He established the distribution coefficient for Mg and Fe^{2+} as

$$K_D = \frac{X^{ol}_{Mg} \; X^{sp}_{Fe^{2+}}}{X^{ol}_{Fe^{2+}} \; X^{sp}_{Mg}} \quad (1),$$ considering the activity coefficient

quotient $$\frac{\left\{\gamma^{ol}_{Mg_2SiO_4}\right\}^{\frac{1}{2}} \left\{\gamma^{sp}_{FeAl_2O_4}\right\}}{\left\{\gamma^{ol}_{Fe_2SiO_4}\right\}^{\frac{1}{2}} \left\{\gamma^{sp}_{MgAl_2O_4}\right\}}$$ as unity, which presupposes ideal solid solution for both series. X^a_i represents the mole fraction of component i in phase a.

Jackson (1969), utilizing equations (d) and (1), substituted available thermodynamic data for the calibration of his geothermometer. He assumed ideal solid solution between phases, and expressed his geothermometer by the following equation :

$$T(^oK) = \frac{5580Y^{sp}_{Cr} + 1018Y^{sp}_{Al} - 1720Y^{sp}_{Fe^{3+}} + 2400}{0.90Y^{sp}_{Cr} + 2.56Y^{sp}_{Al} - 3.08Y^{sp}_{Fe^{3+}} - 1.47 + 1.987 \ln K_D} \quad (2)$$

Both Irvine (1965) and Jackson (1969) emphasize the uncertainty of the thermodynamic data, especially the Gibbs free energy values, which could affect the temperature values by as much as $\pm$ 300°C. However, unreasonably high values, in the range 2,000-2,300°C have been calculated for coexisting olivine - Cr-spinel pairs from Kilauean volcanic rocks (Evans and Wright,

1972), and equilibrium temperatures in the range 2,042°-3,059°C for mineral pairs from the Josephine Peridotite (Dick, 1977). Hence, many workers have suggested that Jackson's geothermometer must be considered either for relatively rough estimations, or only in conjunction with other geothermometers.

The substitutions $Mg\text{-}Fe^{2+}$ and $Al\text{-}Cr\text{-}Fe^{3+}$ are not independent and hence R_2O_3 influences the Fe^{2+}-Mg exchange. Irvine (1965) has given the following equation, which considers the effects of trivalent cations :

$$\ell n K_D = \ell n \frac{X^{ol}_{Mg} \; X^{sp}_{Fe^{2+}}}{X^{ol}_{Fe^{2+}} \; X^{sp}_{Mg}} = \ell n K_b + Y^{sp}_{Cr} \ell n K_e + Y^{sp}_{Fe^{3+}} \ell n K_f \qquad (3)$$

where K_b, K_e, K_f and K_g are the equilibrium constants of the following four reactions :

$$\tfrac{1}{2} Fe_2SiO_4 + MgAl_2O_4 \rightleftharpoons \tfrac{1}{2} Mg_2SiO_4 + FeAl_2O_4 \qquad (d)$$

$$MgCr_2O_4 + FeAl_2O_4 \rightleftharpoons FeCr_2O_4 + MgAl_2O_4 \qquad (e)$$

$$MgFe_2O_4 + FeAl_2O_4 \rightleftharpoons Fe_3O_4 + MgAl_2O_4 \qquad (f)$$

$$MgFe_2O_4 + FeCr_2O_4 \rightleftharpoons Fe_3O_4 + MgCr_2O_4 \qquad (g)$$

The Fe^{3+} content is very small in general, the $Y^{sp}_{Fe^{3+}}$ mole fraction being always less than 0.05 in spinels from Vavdos, but not necessarily in spinels from Gomati due to incipient alteration and consequent enrichment in Fe^{3+}. This is in accordance with the normal distribution of trivalent cations in spinels with the general formula $R^{2+}_8 \; R^{3+}_{16} \; O_{32}$, because Cr and Al cations show strong preference for the octa-

hedral sites, while Fe^{3+} is the only trivalent cation to show a tendency for concentration in tetrahedral sites. Irvine (1965) has stated that $Y^{sp}_{Fe^{3+}}$ values generally lie between 0.05-0.15 and also suggested a value of 4 for ℓnK_f. Evans and Frost (1975), taking into account the above estimations, normalized the partition coefficient to a ferric-free basis according to the equation $\ell nK^*_D = \ell nK_D - 4.0\ Y^{sp}_{Fe^{3+}}$. However, more recent thermodynamic data give values for ℓnK_f close to 2.0 at 1200°C, Roeder et al (1979).

In Figure 6.1a, isothermal surfaces have been constructed as proposed by Medaris (1975). In Figure 6.1b, these surfaces have been projected to the $\ell nK^*_D - Y^{sp}_{Cr}$ plane assuming that $Y^{sp}_{Fe^{3+}} = 0$ and $\ell nK_f = 4.0$ (data from Medaris, 1975) and $Y^{sp}_{Fe^{3+}} = 0.050$ (data from Evans and Frost, 1975). The positions of coexisting pairs of olivine and spinel from Gomati and Vavdos are also shown in Figure 6.1b. Clearly the data give conflicting temperatures, dependent on whether the $Y^{sp}_{Fe^{3+}}$ value is taken as 0 or 0.050. This mole fraction has values below the value of 0.050 for olivine-spinel pairs from Gomati and Vavdos, as shown in Table 6.1. Estimated temperatures utilizing equation (2) are also given in Table 6.1. There is thus contradiction between these values and values inferred by Figure 6.1b.

Fujii (1978), prepared mixtures of olivine, spinel and orthopyroxene in the ratio 1:1:2, consisting of the components MgO, FeO, SiO_2, Al_2O_3 and Cr_2O_3, holding constant the ratio $Mg:Mg + Fe^{2+}$ at 0.8. He ran the charges at 15k bars and 1 atm, quenching from temperatures of 1200°C, 1250°C, 1300°C and 1350°C. Fujii derived very small subhedral and euhedral crystals after high pressure runs, but only euhedral spinel and olivine crystals

a.

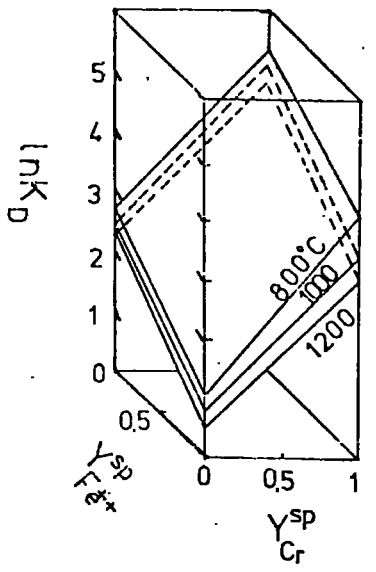
lnK_D
5
4
3
2
1
0
800°C
1000
1200
0.5
0
0.5
1
Y^sp_Fe
Y^sp_Cr

b.

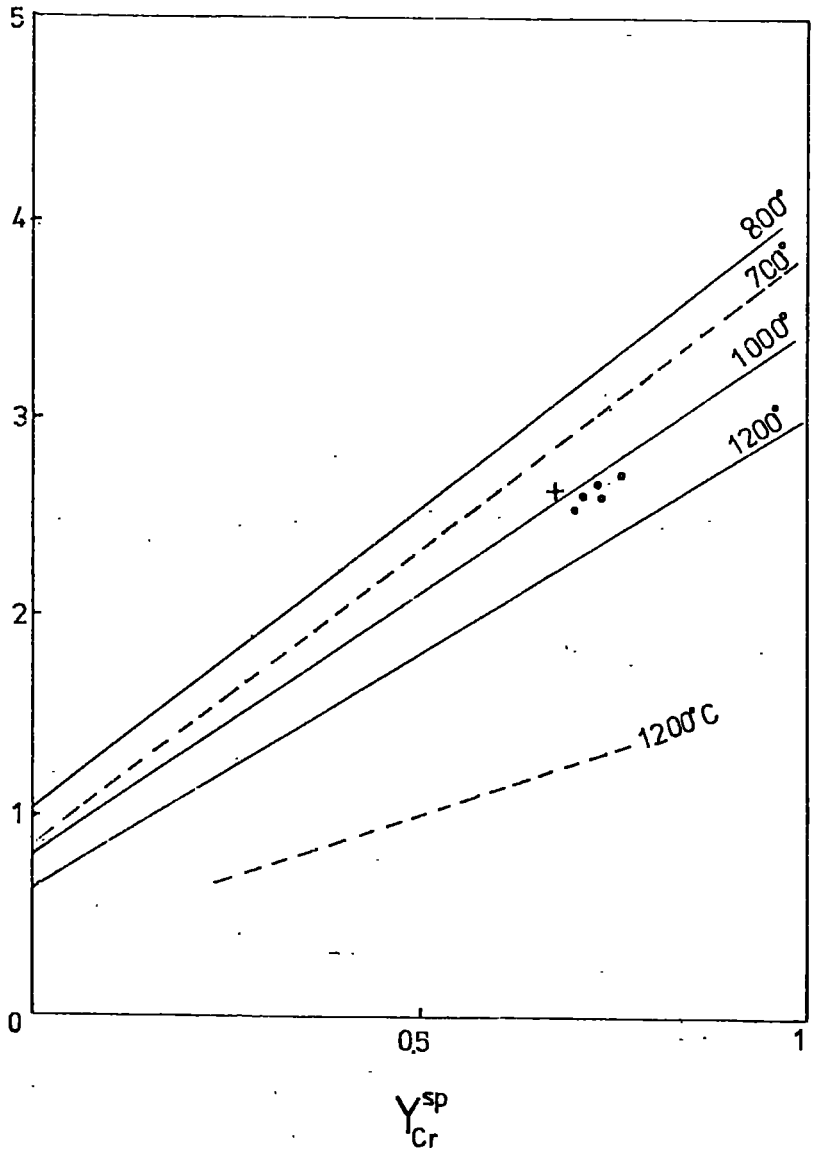
lnK*_D
5
4
3
2
1
0
800°
700°
1000°
1200°
1200°C
0.5
1
Y^sp_Cr

Figure 6.1

from 1 atm runs. After analyzing the derived phases he plotted ℓnK_D^* versus Y_{Cr}^{sp} and found good linearity for results at 15k•bars, whereas at 1 atm the results were very scattered. Fujii then calculated ℓnK_e and ℓnK_f for ΔV values ranging from -0.5 to -0.8 cm^3.

Combining his results the following equation has been produced :

$$T(^oK) = \frac{775 + 2{,}010\ Y_{Cr}^{sp}}{\ell nK_D - 4.0Y_{Fe^{3+}}^{sp} - 0.006 - 0.003\ Y_{Cr}^{sp}} \quad (4).$$

Substituting data from Gomati and Vavdos into equation (4) temperature estimations were derived and they are listed in Table 6.1. The temperature derived using equation (4) are considerably lower than those utilizing Jackson's equation.

Fabries (1979), considered the experimental data of Roeder et al (1979) and estimated two equations for ℓnK_D^*, at 700°C and 1200°C respectively. He calculated the following thermometric equation,

$$T(^oK) = \frac{4250\ Y_{Cr}^{sp} + 1343}{\ell nK_D^* + 1.825\ Y_{Cr}^{sp} + 0.571} \quad (5).$$

Again, substituting data from Gomati and Vavdos into this equation, using the value of 2.0 for the ℓnK_f in the estimation of ℓnK_D^*, the temperature values are remarkably lower than those estimated according to Jackson's equation. Results are given in Table 6.1.

Roeder et al (1979) have re-evaluated the spinel-olivine geothermometer in the light of new thermodynamic and experimental data. They have indicated that discrepancies between the free energy values for particular spinels, and especially for

TABLE 6.1

	X^{ol}_{Mg}	$X^{ol}_{Fe^{2+}}$	X^{sp}_{Mg}	$X^{sp}_{Fe^{2+}}$	Y^{sp}_{Cr}	Y^{sp}_{Al}	$Y^{sp}_{Fe^{3+}}$	K_D	ℓnK_D	ℓnK^*_D	ℓnK^*_D(1)	Cr-Spinel percentage
GB4	0.92	0.08	0.41	0.59	0.67	0.29	0.05	16.54	2.81	2.63	2.72	Around 10%
VC6	0.95	0.05	0.56	0.44	0.70	0.25	0.05	16.26	2.79	2.59	2.69	Less than 40%
VA8	0.96	0.04	0.61	0.39	0.71	0.25	0.03	15.71	2.76	2.64	2.70	Higher than 90%
VA3	0.96	0.04	0.59	0.42	0.73	0.23	0.04	16.17	2.78	2.62	2.70	Around 85%
VA4	0.94	0.06	0.47	0.51	0.73	0.24	0.04	17.89	2.88	2.72	2.80	Less than 5%
VG2	0.95	0.05	0.53	0.47	0.76	0.22	0.03	17.93	2.89	2.77	2.83	Olivine inclusion in chromite. Around 90%

(1) estimated ℓnK^*_D using the value of 2.0 for ℓnK_f

	Estimated equilibrium temperatures after,		
	Jackson(1969)	Fujii(1978)	Fabries(1979), using ℓnK^*_D estimated after Roeder et al (1979)
GB4	926°C	537°C	655°C
VC6	974°C	573°C	679°C
VA8	991°C	565°C	683°C
VA3	1008°C	585°C	692°C
VA4	956°C	553°C	671°C
VG2	984°C	564°C	682°C

$FeCr_2O_4$- $MgCr_2O_4$, strongly influence the estimation of equilibrium conditions. They showed that different free energy values give very different isotherms, if reactions (a), (b) and (c) are considered separately. Data for reactions (a) and (c) are shown in Figure 6.2. The range of ℓnK_D values from data of this study is also indicated. Projections to the horizontal temperature axis from intersections on curves 1, 2 and 3 give very different temperatures. It is thus inferred that no accurate temperature estimations can be achieved. However, Roeder et al (loc cit) also estimated a new value for ℓnK_f, of approximately 2.0 at 1200°C, falling with temperature. Their estimated isotherms have been plotted in Figure 6.3, using corrected values for ℓnK_f of 2 and $Y^{sp}_{Fe^{3+}}$ of 0.05. Spinel-olivine pairs from Vavdos and Gomati have been plotted in this diagram indicating equilibrium temperatures below 600°C. Roeder et al (1979) also indicate that the alumina-rich spinels have the lowest ℓnK_D values and a good correlation of isotherms, whereas the chromium-rich spinels show the widest variation with variation in free energy values. This is in agreement with the results of Pinsent (1974), who found that ℓnK_D decreases for pairs from dunite to harzburgite as shown in Figure 6.4, but is in disagreement with data from Marakushev (1979), who showed that the distribution coefficient (K_D) increases from dunite to lherzolite mineral parageneses. Spinel-olivine pairs from Vavdos indicate that equilibrium is attained at a value of K_D equal to 2.45.

However, it is apparent that continuous exchange of Mg and Fe^{2+} between olivine and spinel exists, and therefore sequential re-equilibration down to low temperatures is believed to occur. It is thus clear that the lowest estimated tempera-

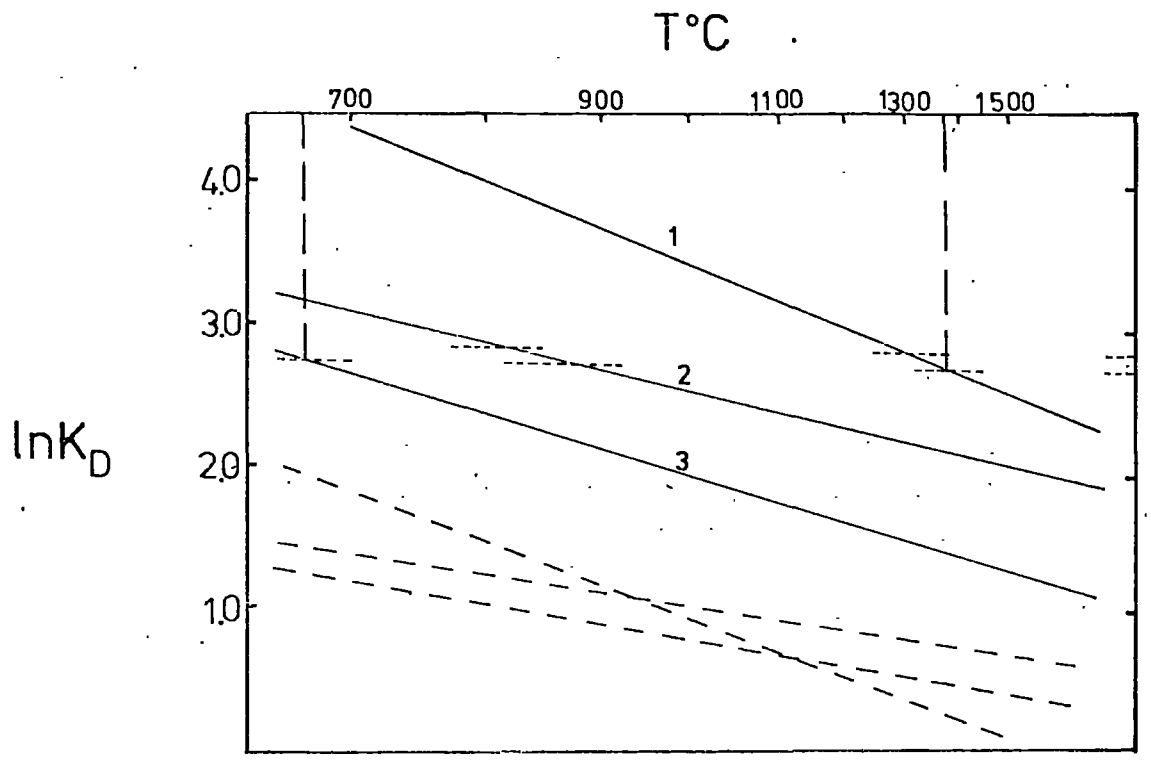

Figure 6.2

Correlation of the distribution coefficient to temperature, with respect to different Gibb's free energy values, after Roeder et al (1979). Solid lines : $\frac{1}{2}\ Fe_2SiO_4 + MgCr_2O_4 \rightleftharpoons \frac{1}{2}\ Mg_2SiO_4 + FeCr_2O_4$. Dashed lines : $\frac{1}{2}\ Fe_2SiO_4 + MgFe_2O_4 \rightleftharpoons \frac{1}{2}\ Mg_2SiO_4 + FeFe_2O_4$. The horizontal dashed lines and the vertical projections represent the space of mineral pairs from Vavdos complex.

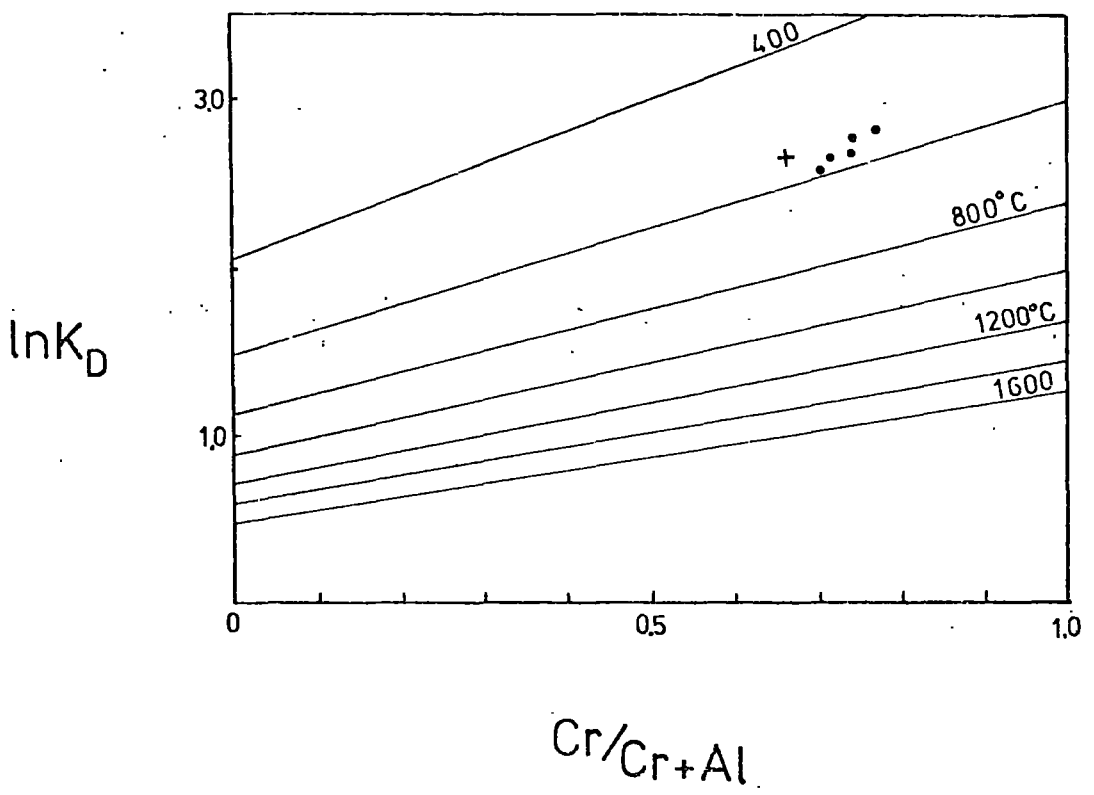

Figure 6.3

Temperature contours after Roeder et al (1979), utilizing $Fe^{3+}/Fe^{3+} + Cr + Al = 0.05$. Dots and the cross are data from the Vavdos and Gomati complexes respectively.

Figure 6.4

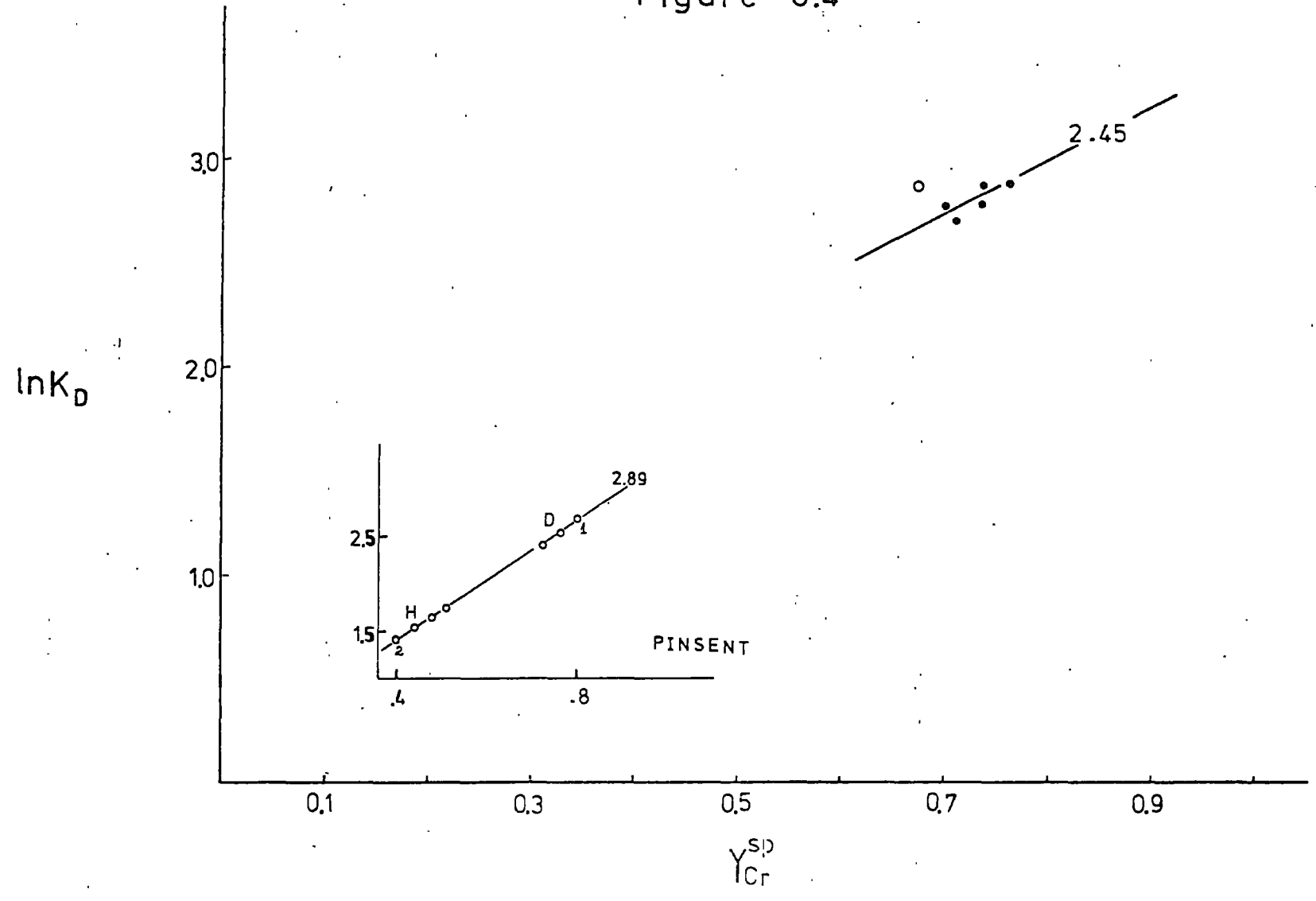

tures could be considered more close to natural systems involving continuous ionic exchange, in this case between Mg and Fe^{2+}.

6.2 Fe^{2+}-Mg PARTITIONING BETWEEN OLIVINE AND MELT

The partitioning of Mg and Fe^{2+} between olivine and liquid is expressed by the following equation : $Mg_{ol} + Fe^{2+}_{liq} \rightleftharpoons Mg_{liq} + Fe^{2+}_{ol}$. The equilibrium constant of this reaction is,

$$K = \frac{\alpha^{ol}_{FeO} \cdot \alpha^{liq}_{MgO}}{\alpha^{liq}_{FeO} \cdot \alpha^{ol}_{MgO}}$$ and the distribution coefficient for

Fe^{2+} - Mg partitioning between olivine and liquid is,

$$K = \frac{X^{ol}_{FeO} \cdot X^{liq}_{MgO}}{X^{liq}_{FeO} \cdot X^{ol}_{MgO}}$$, where X^{ol}_{FeO} is the mole fraction of FeO in olivine and X^{liq}_{MgO} represents the mole fraction of MgO in the liquid.

Roeder and Emslie (1970) have investigated Fe^{2+}-Mg partitioning between olivine and basaltic liquid. Their experiments indicate that olivine is richer in both Mg and ferrous iron than the basaltic liquid. They also concluded that the composition of the olivine is independent of temperature, and depends only on the magnesium and ferrous iron contents of the liquid from which the olivine has crystallized.

Roeder and Emslie (1970) conducted their experiments with basalts at temperatures ranging from 1150°C to 1300°C, at a total pressure of one atmosphere and with oxygen fugacities between $10^{-0.68}$ and 10^{-12} atm. The mineral assemblages present at varying oxygen fugacities and temperatures are shown in

Figure 6.5a. The olivine is richer in Mg at higher temperatures and higher oxygen fugacities, while the ratio Fe^{ol}_{total}: Fe^{liq}_{total} decreases with increasing oxygen fugacity at a constant temperature, Figure 6.5b. Thus, at a temperature of 1200°C, olivine crystallizing at an oxygen fugacity greater than 10^{-6} atm contains less iron than the liquid and is more forsterite rich, Figure 6.5b. This implies that crystallization of olivine at 1200°C and 1 atm total pressure with a change of oxygen fugacity from 10^{-8} atm to 10^{-4} atm, would cause a considerable impoverishment of magnesium in the liquid with an increase in iron. The Fo-contents of olivine in dunites from Vavdos complex are between Fo_{92}-Fo_{96}. Assuming for the moment 1 atm pressure the fO_2 can be estimated, to be from $10^{-0.5}$ to $10^{-4.2}$ atm. These values of fO_2 in turn produce Fe^{ol}:Fe^{liq} ratios between 0.5 and 0.62 with the olivine from the main dunite having the lower Fo-content, and higher Fe^{ol}:Fe^{liq} ratio.

Roeder and Emslie (1970) estimated the K_D to be about 0.30 and experimental results show a good agreement with this value. The FeO:MgO ratio ranges from 0.07 for olivine from chromite pods, to 0.15 for olivine from the main dunite and, according to Figure 6.5c, the FeO:MgO ratio in the liquid varies from 0.2 to 0.5 respectively. This suggests an increase in the FeO:MgO ratio of the liquid, with which olivine is in equilibrium, from chromite concentrations to the main dunite. The K_D is independent of temperature and therefore the composition of the olivine depends entirely on the relative proportions of iron and magnesium in the liquid. Pressure is not an important factor, as results from high pressure runs are in close agreement with the trend in Figure 6.5c (Kushiro, 1973).

Figure 6.5

a.

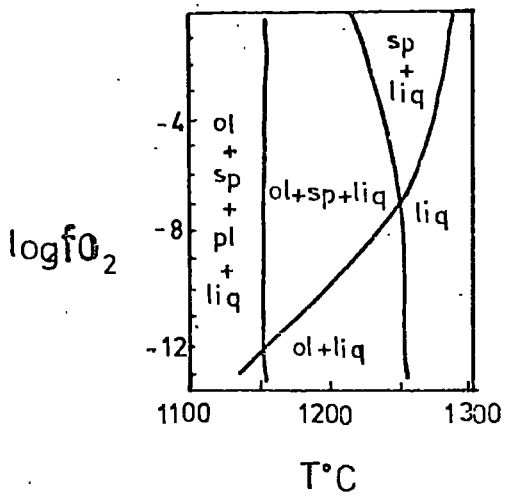

$\log fO_2$

b.

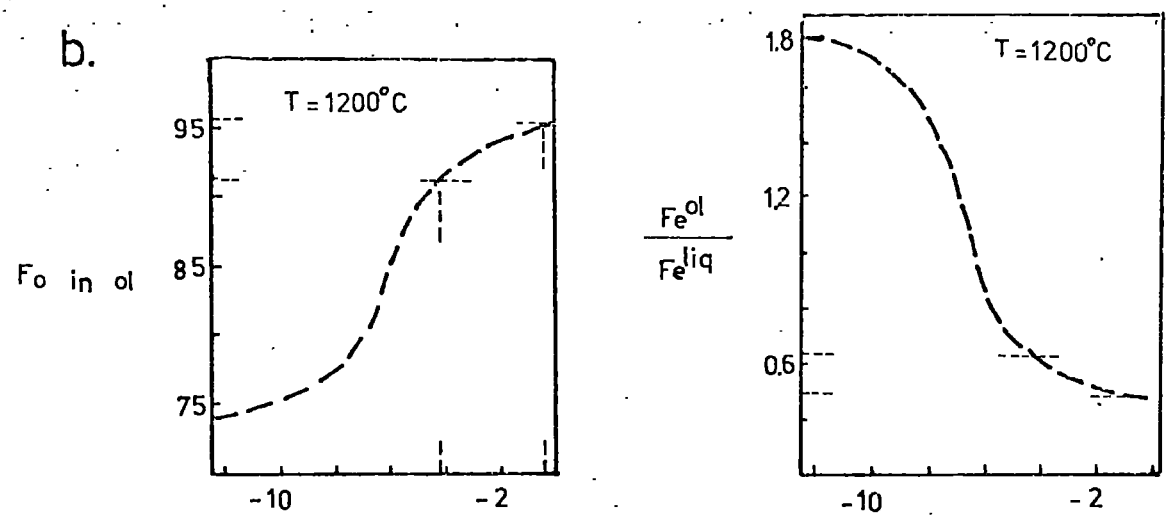

$\log fO_2$

c.

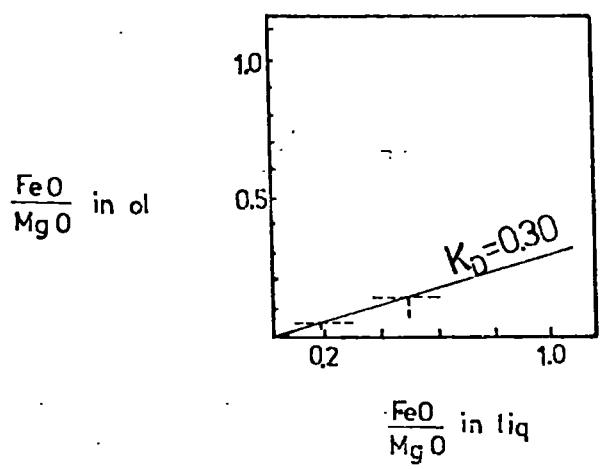

The above considerations lead to the conclusion that the liquid from which olivine crystallizes is poorer in both Mg and Fe^{2+}. If the massive chromite concentrations and disseminated chromite ores are derived by any process of fractional crystallization or equilibrium crystallization of basaltic liquid, then an increase in the ratio $(FeO:MgO)^{liq}$ associated with massive or disseminated chromite concentrations to the main dunite with only accessory chromite would be expected. The oxygen fugacities corresponding to the Fo-content of olivines from Vavdos are extremely high. Values of fO_2, 10^{-7} atm correspond to Fo_{85} which is virtually the Fo-content of olivines crystallizing from basaltic liquid. The crystallization of olivines with Fo-content above the value of 90 seems unlikely from basaltic liquids and it is believed that they crystallized from liquids high in MgO content. This liquid would be progressively depleted in MgO, after giving rise to the main dunite and would then approach a basaltic composition. Olivine from pyroxenites thus must be less forsteritic, this being in agreement with data presented here for olivine from pyroxenites of about Fo_{82}.

6.3 Mn^{2+} PARTITIONING BETWEEN OLIVINE AND LIQUID

The MnO content of olivine is slightly lower in the more forsteritic varieties which occur mainly in association with the massive chromite pods.

The forsterite-liquid partition coefficient for Mn^{2+} is $MnO^{Fo}:MnO^{liq}$ and is equal to $D_{MnO}^{Fo\text{-}liq}$ (mole ratio). Experimental results by Watson (1977) indicate that the partition coefficient increases as the temperature decreases. Therefore, Mn^{2+} is more strongly partitioned into olivine at lower temperatures. Oxygen fugacity effects are considered

negligible by Watson, who tried various oxidation conditions and found that Mn^{2+}, even in highly oxidizing conditions remained divalent. However, the partition coefficient D_{MnO}^{Fo-liq} depends on both the activity of MgO and silica in the melt. There is a curvelinear correlation between D_{MnO}^{Fo-liq} and Si : O in the melt, which is temperature dependent. The Si : O ratio determines the proportion of unbonded oxygens in any silicate melt. The highest value is 0.5, which represents complete polymerization of a pure SiO_2 melt. The entry of another cation, e.g. Mn^{2+} into the pure SiO_2 system causes a decrease in the Si : O ratio, simply because the Mn^{2+} is co-ordinated with oxygen anions. The lowest values of Si : O ratio are encountered in basic melts and thus Mn^{2+} will be more stable in basic melts, because of the availability of unbonded oxygen ions.

Watson (1977, Figure 8) however, showed that the effects of melt composition on the olivine liquid partition coefficient decrease with increasing basicity. For values of Si : O less than 0.28 (believed to reflect ultrabasic magmas) melt composition has no influence on the D_{Mn}^{Fo-liq} which is also very restricted for particular temperatures. This seems to support the very narrow range of MnO contents shown by olivines from the main dunite and massive chromite concentrations of Vavdos complex.

Watson (1977, Figure 8) indicates that, for values of Si : O below 0.29, $\ell n\ D_{Mn}^{Fo-liq}$ will be always less than -0.20. Duke (1976) has produced data for iron-bearing systems with MgO:MgO + FeO between 0.895 and 0.338 in the melt, and with olivines ranging from Fo_{95} to Fo_{61}. His data suggest that

$\ell n\ D_{Mn}^{Fo\text{-}liq} = -0.20$ reflects a temperature of 1242°C. Leeman and Scheidegger (1977) has also produced data for melts with MgO:MgO + FeO between 0.804 - 0.284 and olivines ranging from $Fo_{96.7}$ - $Fo_{50.2}$. Using this data the estimated liquidus temperature for $\ell n\ D_{Mn}^{Fo\text{-}liq} = -0.20$ is 1244° C.

These temperatures are remarkably co-incident and only about 50°C less than those produced by Watson (1977), for iron-free systems. The data suggests that a liquidus temperature for olivine of the order of 1240° - 50°C is likely for the Vavdos dunites and associated chrome-rich segregations.

6.4 Ni PARTITIONING BETWEEN OLIVINE AND MELT

NiO contents of olivine from massive chromite ores show the highest values, contents falling sequentially for olivine from olivine-chromitite to chromitiferous dunite and the main dunite, in Vavdos complex. There is a correlation between magnesium and nickel contents, Figure 4.3b.

The Ni^{2+} cation has a large crystal field stabilization energy (29.2 k cal $mole^{-1}$, Burns, 1970) and thus shows a strong preference for octahedral sites. Ni^{2+} largely occupies M1 sites in the olivine structure. It is not clear, however, whether olivine or melt has more octahedral sites, and whether Ni^{2+} is more strongly fractionated into olivine than Mg during the crystallization of basaltic magmas.

The Ni^{2+} partition coefficient D between olivine and liquid is equal to Ni^{ol}: Ni^{liq}, the partitioning of Ni^{2+} and Mg between olivine and liquid being expressed by the distribution coefficient K_D, $\left\{\frac{Ni}{Mg}\right\}^{ol}$: $\left\{\frac{Ni}{Mg}\right\}^{liq}$. An increase or decrease in these coefficients is affected by iron, silica and alkalies, and might be regarded as a measure of Ni^{2+} and Mg fractionation.

The effect of iron on D and K_D was investigated by Irvine and Kushiro (1976) for the system Mg_2SiO_4-Fe_2SiO_4 at 15 k·bars pressure, in the temperature range of 1550°C-1600°C, and with relatively low oxygen fugacities. At both temperatures D was higher than unity (1.73 and 1.35 respectively) and thus olivine was richer in Ni than the liquid. K_D varied from 0.49 to 0.61 and even when additional FeO was added, values were still within the above range, indicating that the liquid had the higher Ni:Mg ratios. Thus the effect of iron is relative, slightly favouring the entry of Ni^{2+} into olivine with increasing iron content.

Irvine and Kushiro (1976) also showed that there is a large dependence of Ni-Mg partitioning on silica and alkalies. They used the system Mg_2SiO_4-Ni_2SiO_4- K_2O-SiO_2, with NiO contents between 2 and 4%. Their data showed that D was always higher than unity while K_D ranged from 0.8 to 0.60. Both D and K_D increased with increasing silica and alkali contents. The NiO content of olivines in peridotites of probable mantle origin is however only around 0.40% and the NiO content of primary basaltic magmas varies from 0.03% to 0.05% (Sato,1977). Sato also gives values of K_D for basaltic magmas between 2.0 and 2.9. The NiO contents,of olivines from the main dunite in Vavdos complex, are concentrated around the value of 0.40%, and from pyroxenites around 0.17%.

High pressure experiments have revealed that Ni^{2+} enters olivine preferentially to the liquid, Mysen (1976). He gives values of D of 15.5 $\pm$ 0.7 and 12 $\pm$ 0.4 at 20 and 10 k·bars respectively, for the system Fo-Ab_{50}-An_{50}-SiO_2-H_2O, with initial Ni contents above 200 ppm. He concluded that D is slightly dependent on temperature and pressure. During partial

melting of mantle peridotite Ni will not enter into the residual olivine in the same amount that it does into olivine during fractionation processes in shallow magma chambers (Mysen, 1976). Sato (1977) has shown that after 25% partial melting of mantle peridotite the NiO content in olivine increases by 7-9%, while the generated liquid contains 0.03 to 0.05% NiO, which he believes represents the NiO content of primary basaltic magmas. Data for the Ni-content of olivine from lherzolite nodules in kimberlites are shown in Table 6.2; they have an average NiO content approximately 0.43%. This value is slightly higher than the value of 0.40% given by Sato (1977) for olivine from mantle peridotite, and higher than that of olivine from the main dunite in Vavdos. It is distinctly lower, however, than the NiO content of olivine from the massive chromitites of Vavdos.

Data produced by Mysen (1976) is used for high pressures and by Sato (1977) for lower pressures. Irvine and Kushiro (1976) have reported a change in the structure of the melt at 15 k·bars and temperatures between 1575°C and 1600°C.

In general olivine from harzburgites is less forsteritic than that from dunite (Table 3.1) and thus it seems that Ni^{2+} and Mg will prefer themelt in higher amounts than the residue temporarily, during partial melting of mantle peridotite, in agreement with Mysen (1976). With falling temperature and increase of silica content, there is a decrease in octahedral sites in the melt, Ni^{2+} and Mg preferring olivine. At this stage the melt produced by the partial melting process, separates from the harzburgite residue and gives rise during fractionation processes to the highly forsteritic and Ni-rich olivines associated with massive chromite concentrations. The high crystal

TABLE 6.2

	NiO-content of olivine
Spinel harzburgite, xenolith in kimberlite, Kimberley, S.Africa, Basu and MacGregor, 1975.	0.41%
Lherzolite nodules from kimberlites, Lesotho, S.Africa, Nixon and Boyd,1973.	0.39-0.49% (average 0.43%)

field stabilization energy of Ni^{2+} and Cr^{3+} would favour a change in the melt structure, as high chromium spinels of the massive chromites occur principally at the harzburgite-dunite boundary.

The high nickel content of olivine in dunite from the Vavdos complex (about 0.40%) does not seem to be derived from a partial melt basaltic magma, as has been proposed by Sato (1977), due to the very low Ni-content of such magmas. It seems more reasonable to accept the existence of an ultrabasic rather than basaltic magma, to explain the NiO content of dunites ; nickel in dunites exceeds 0.38% (NiO), in pyroxenites 0.03% and in gabbros is not more than 0.01%. The decreasing content of Ni and Mg of olivines from massive chromitites, through dunites to pyroxenites seems to represent a typical fractionation mechanism of a primary magma, irrespective of basaltic or ultrabasic composition.

6.5 DISTRIBUTION OF IRON AND MAGNESIUM BETWEEN CO-EXISTING ENSTATITE AND DIOPSIDE

The exchange of Fe^{2+} and Mg between co-existing pyroxenes is expressed by the following reaction :

$$MgSiO_3 + CaFeSi_2O_6 \rightleftharpoons FeSiO_3 + CaMgSi_2O_6 \qquad (1)$$

Dealing with ideal solid solutions for the reaction (1), the distribution coefficient is,

$$K_{D(Mg-Fe)}^{opx-cpx} = \frac{X_{Mg}^{opx} \cdot X_{Fe^{2+}}^{cpx}}{X_{Fe^{2+}}^{opx} \cdot X_{Mg}^{cpx}}$$, where X_{Mg}^{opx} is the mole fraction of $MgSiO_3$ in orthopyroxene, etc. Values of $K_D^{opx-cpx}$ for co-existing pyroxene pairs from the Vavdos pyroxenite and gabbro are given in Table 6.3.

TABLE 6.3

Co-existing minerals	Fe/Mg	X_{Mg}	$X_{Fe^{2+}}$	$K_{D(Mg-Fe)}^{opx-cpx}$	$\ln K_D$	Rock type
enstatite diopside	0.183 0.133	0.845 0.883	0.1545 0.117	0.725	-0.32	Pyroxenite
enstatite diopside	0.203 0.152	0.831 0.868	0.169 0.132	0.747	-0.29	Pyroxenite
enstatite diopside	0.184 0.135	0.845 0.881	0.155 0.119	0.736	-0.31	Pyroxenite
enstatite diopside	0.240 0.179	0.8065 0.848	0.1935 0.152	0.745	-0.29	Gabbro
enstatite diopside	0.237 0.183	0.808 0.845	0.192 0.155	0.770	-0.26	Gabbro

Figure 6.6 shows that co-existing pyroxene pairs from the pyroxenite of Vavdos fall very close tothe line representing $K_D^{opx-cpx}$ = 0.73, the value given by Kretz (1963) for igneous pyroxenes. Co-existing pyroxenes from the gabbro are also shown, and comparison is made with $K_D^{opx-cpx}$ for Bushveld pyroxenes, according to Atkins (1969), and co-existing pyroxene values from the Thessaloniki gabbros (N.Greece) after Sapountzis (1979).

The values of $\ell nK_D^{opx-cpx}$ for pyroxene pairs, from the Vavdos pyroxenite, indicate a temperature range from 1121°C to 1211°C, according to Figure 3 of Kretz (1963), and a total pressure of the order of 1kb (Kretz, Figure 4).

According to experimental data from Navrotsky (1978), $K_D^{opx-cpx}$ might be variable due to uncertainties of thermodynamic data. Figure 6.7 shows the trend lines which she has produced and data from the Vavdos co-existing pyroxenes. The pyroxene pairs from gabbro indicate a higher temperature of equilibration relative to pyroxenite, but the temperature range in total is rather restricted, from 890°C to 980°C.

Although the $K_D^{opx-cpx}$ gives reasonable crystallization temperatures and is distinct for igneous and metamorphic equilibration reactions, it assumes ideality of solid solutions which is not the true situation. Mg-Fe^{2+} partitioning in co-existing Ca-poor and Ca-rich pyroxenes is also dependent on the accommodation of Mg and Fe^{2+} in the M1 and M2 sites. The different amounts of Mg and Fe^{2+} entering each site influence the $K_D^{opx-cpx}$. Fleet (1974a) has shown that under these circumstances the Fe^{2+}-Mg distributions are non-ideal. There is a distinct preference for Fe^{2+} to enter M2 sites of Ca-rich pyroxene,

Figure 6.6

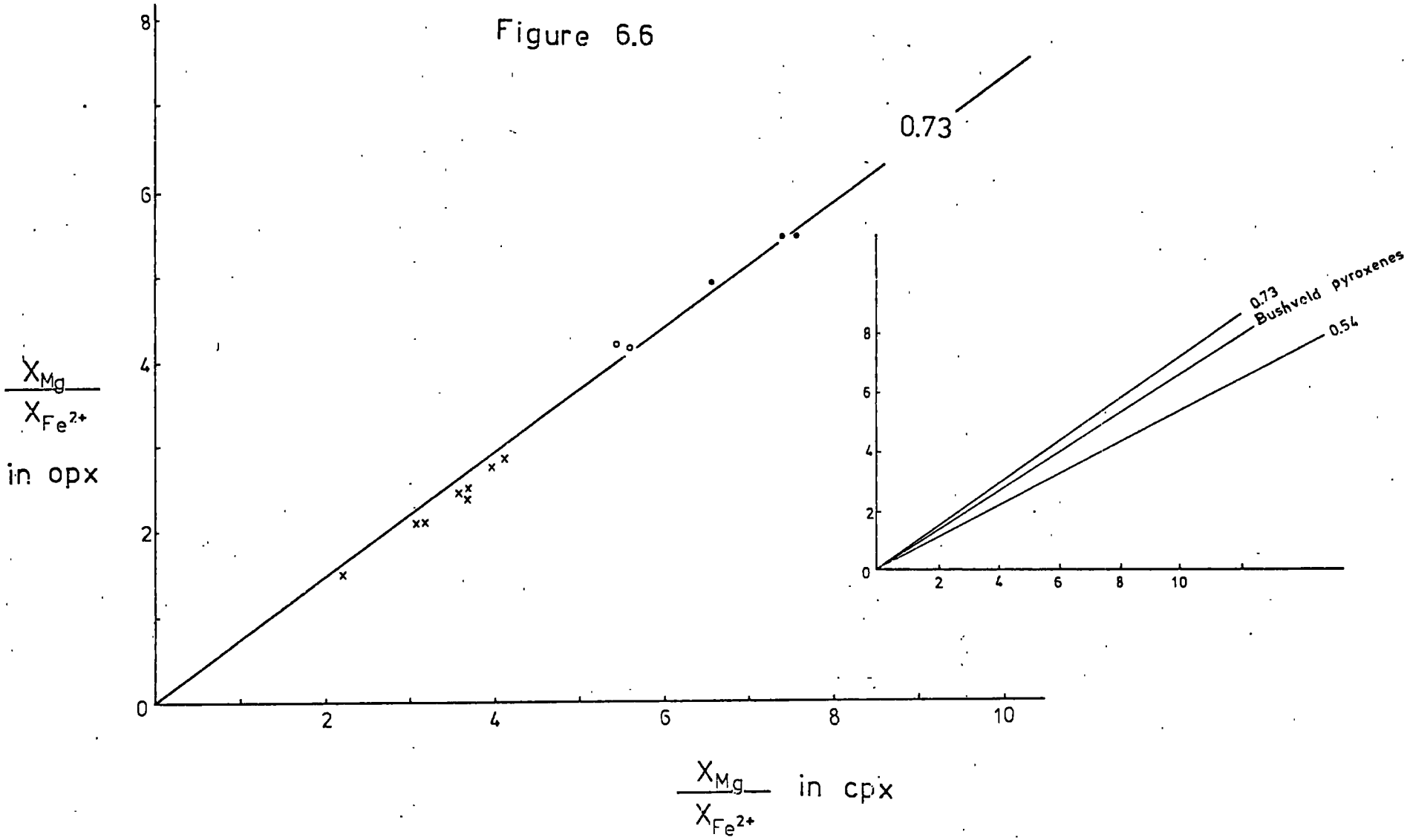
0.73
0.73
Bushveld pyroxenes
0.54
$\frac{X_{Mg}}{X_{Fe^{2+}}}$ in opx
$\frac{X_{Mg}}{X_{Fe^{2+}}}$ in cpx

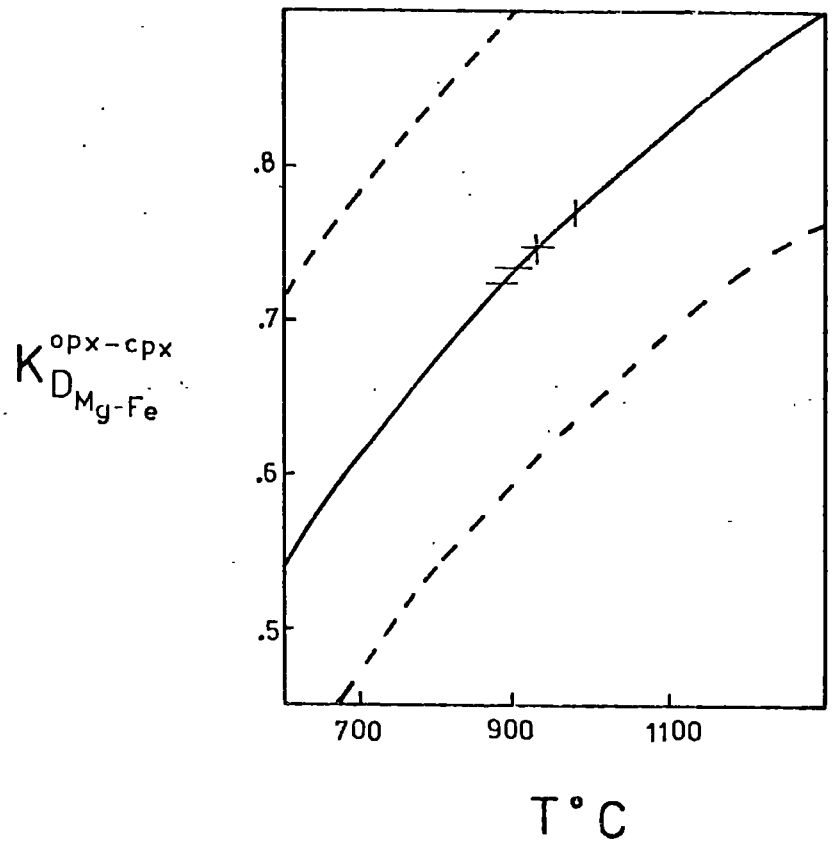

Figure 6.7

Relation of distribution coefficient to temperature. The solid curve represents the estimated K_D in response to the temperature, the dashed curves the range of K_D taking into account an uncertainty of $\pm$ 500 cal for G, and the data are from Navrotsky (1978). Co-existing orthopyroxene and clinopyroxene from pyroxenite (—) and gabbro (|) of Vavdos complex, give temperature values in the range of 890°C to 980°C.

rather than Mg (Blander, 1972) but, while the Fe^{2+} in M2 sites increases with decreasing $MgSiO_3$ content the amount of Mg occupying M2 sites appears to be independent of the $MgSiO_3$ variations (Fleet, 1974b). The situation can be better demonstrated by two separate distribution coefficients, produced by Fleet (1974a). The consequent trends for pyroxenes from the Bushveld and Skaergaard intrusions, together with data from Vavdos, are shown in Figure 6.8. The trends shown have been interpreted by Fleet (1974a) as a consequence of Ca depletion and Fe^{2+} enrichment in the M2 sites of Ca-rich pyroxene. However, the limited data from Vavdos suggest that the very different trends mainly for K_{MgSiO_3}, could be justified if the crystallization trends are also very different. This assumption is favoured here.

6.6 Fe^{2+}-Mg DISTRIBUTION IN CO-EXISTING OLIVINE AND ORTHOPYROXENE

The Fe^{2+}-Mg exchange between co-existing enstatite and olivine can be outlined by the reaction :

$$Fe_2SiO_4 + MgSiO_3 \rightleftharpoons Mg_2SiO_4 + FeSiO_3 \qquad (1)$$

Assuming ideal solid solution the distribution coefficient for the reaction (1) is :

$$K_{D(Fe-Mg)}^{ol-opx} = \frac{X_{Fe^{2+}}^{ol} \cdot X_{Mg}^{opx}}{X_{Mg}^{ol} \cdot X_{Fe^{2+}}^{opx}}$$

, where X_{Mg}^{opx} is the mole fraction of $MgSiO_3$ in the enstatite, etc.

Co-existing olivine-enstatite pairs from the Vavdos websterite give K_D^{ol-opx} values from 1.10 to 1.22, Table 6.4.

Figure 6.8

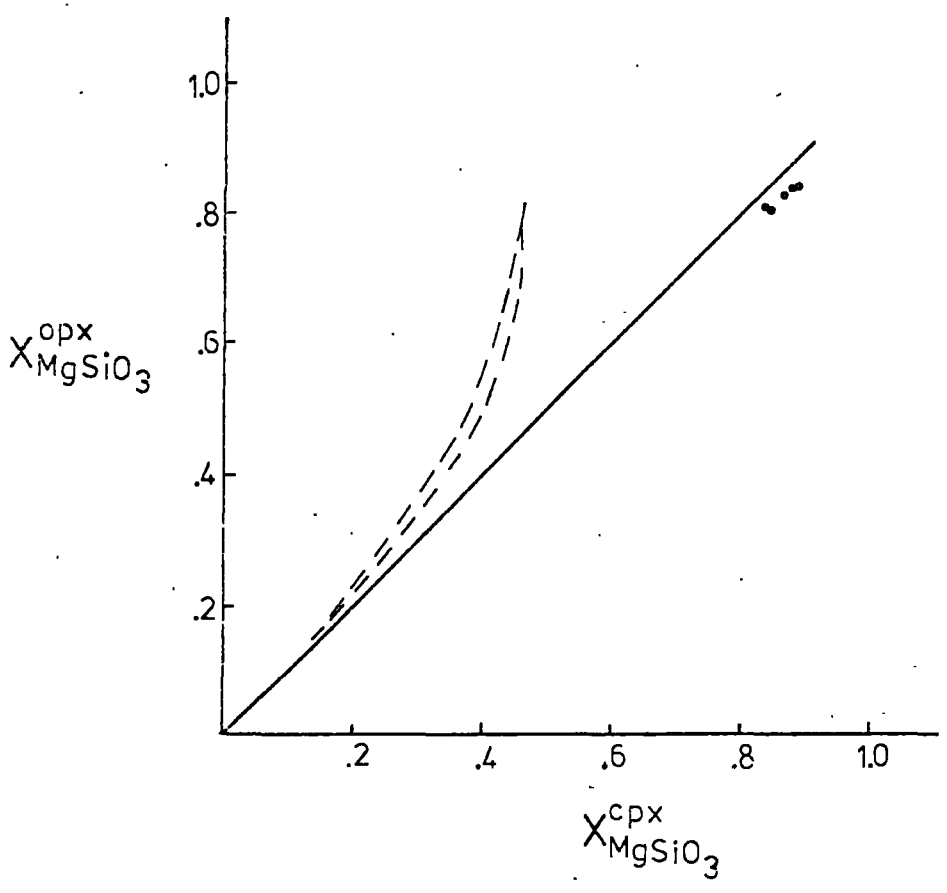
1.0
.8
.6
.4
.2
.2
.4
.6
.8
1.0
$X^{opx}_{MgSiO_3}$
$X^{cpx}_{MgSiO_3}$

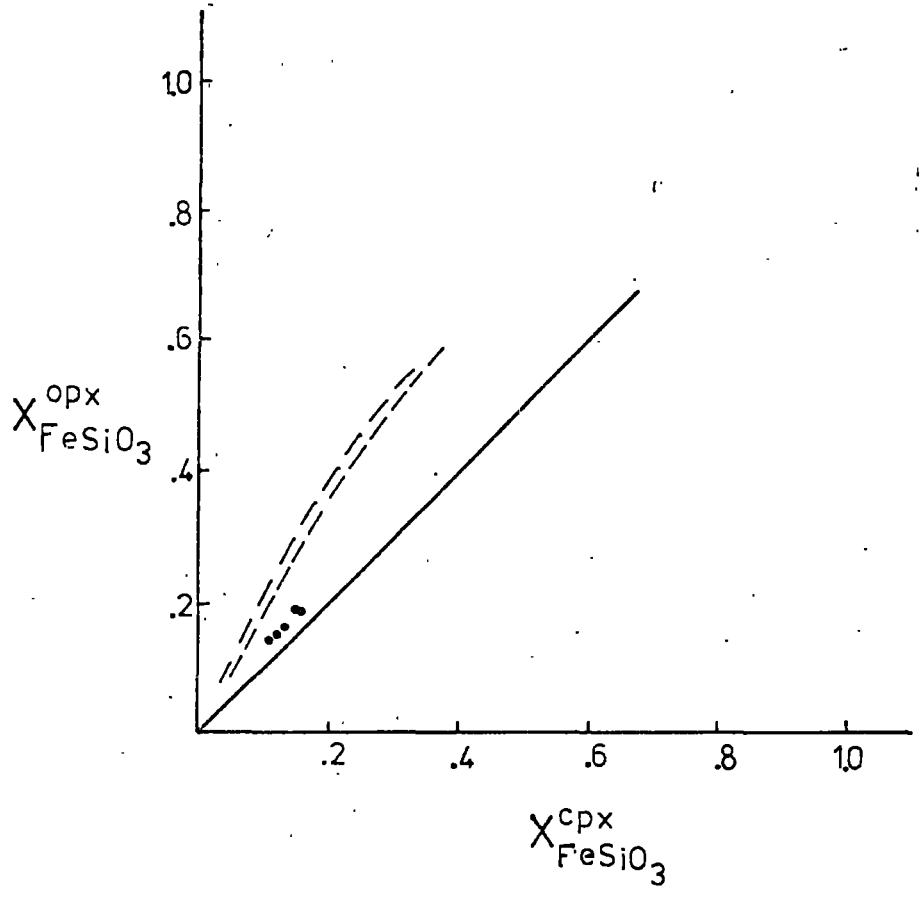
1.0
.8
.6
.4
.2
.2
.4
.6
.8
1.0
$X^{opx}_{FeSiO_3}$
$X^{cpx}_{FeSiO_3}$

TABLE 6.4

Co-existing minerals	$X_{Fe^{2+}}$	X_{Mg}	ol-opx $K_{D(Fe-Mg)}$
orthopyroxene olivine	0.1545 0.1824	0.8455 0.8176	1.22
orthopyroxene olivine	0.1690 0.1817	0.8310 0.8183	1.10
orthopyroxene olivine	0.1553 0.1814	0.8447 0.8186	1.20

Hynes (1972) gives K_D^{ol-opx} values for lherzolites, from the Orthris ultramafic-mafic complex in Greece, between 1.30 and 1.60, while K_D^{ol-opx} ranges from 1.39 to 1.44 for co-existing assemblages in harzburgite. There is thus a decrease in K_D^{ol-opx} from tectonized to cumulate ultramafic rocks in the ophiolite sequence.

Experimental data, under equilibrium conditions, suggest that the mole fraction of $MgSiO_3$ in the orthopyroxene solid solution corresponds to a particular value of $X_{MgSi_{0.5}O_2}$. This relationship is shown in Figure 6.9, with experimental data from different sources. Data from Medaris (1969) represent synthetic mineral assemblages. The co-existing olivine-orthopyroxene pairs from the Vavdos websterite correspond closely with the 1200°C contour of Blander (1972) and show slight deviation from the 900°C contour of Medaris (1969) and the 1200°C contour of Nafziger and Muan (1967). This suggests that equilibration was restricted between 900°C and 1200°C. More recently, Sack (1980) has produced equilibrium trends. If the K_D^{ol-opx} values of olivine-orthopyroxene pairs from the Vavdos websterite are plotted against $X^{ol}_{Fe^{2+}}$, the co-existing pairs indicate an equilibration between 1000°C and 1200°C, according to Figure 6 of Sack (loc.cit).

6.7 OTHER GEOTHERMOMETERS

Temperature estimations have been carried out utilizing the empirical geothermometer of Wood and Banno (1973). Fe^{2+} and Mg have been distributed between M1 and M2 sites in equal proportions, and Fe^{2+} has been considered as total iron, because the analyses are from the microprobe. This last approximation does not affect the actual atomic proportions

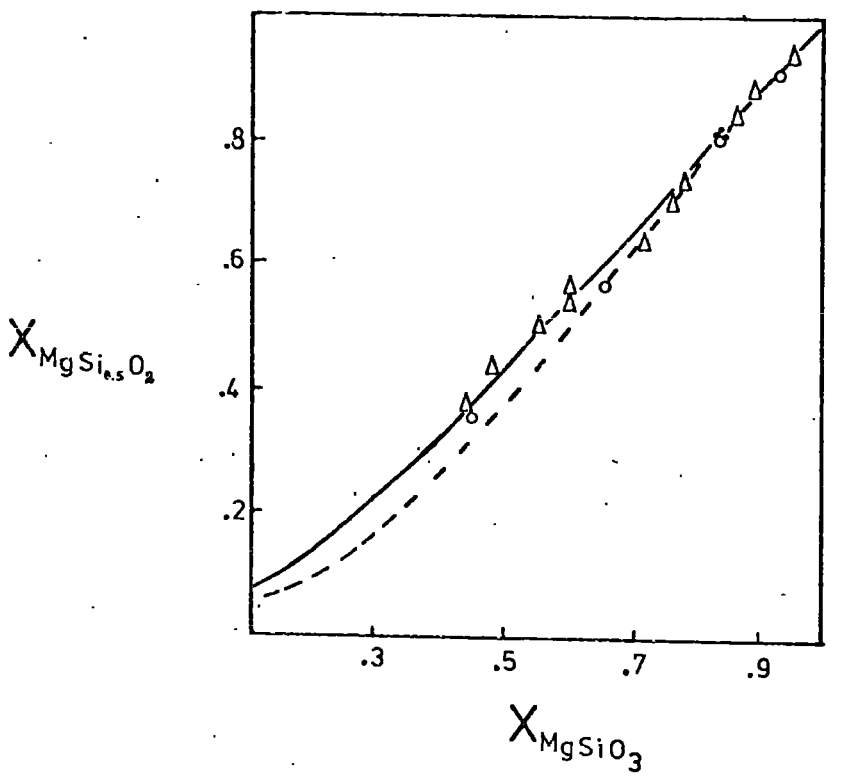

Figure 6.9

The partitioning of Mg-Fe^{2+} between co-existing olivine and orthopyroxene, is shown by the mole fractions of $MgSi_{0.5}O_2$ and $MgSiO_3$. Dots are co-existing mineral pairs from websterite of the Vavdos complex. Triangles represent data for 1200°C from Nafziger and Muan (1967) and circles data for synthetic olivine and enstatite at 900°C after Medaris (1969). Solid curve is the 1200°C contour and dashed curve the 600°C contour of Blander (1972).

due to the low total iron content. Using the equation (1),

$$T = \frac{-10202}{\ln\left(\frac{{}^{\alpha}Mg_2Si_2O_6^{cpx}}{{}^{\alpha}Mg_2Si_2O_6^{opx}}\right) - 7.65\, X_{Fe}^{opx} + 3.88\left(X_{Fe}^{opx}\right)^2 - 4.6} \quad (1),$$

where X_i^a is the mole fraction of i in a, and a_i^a is the activity of i in a, for two orthopyroxene-clinopyroxene pairs from the pyroxenite and the gabbro of the Vavdos complex, the following temperatures have been estimated.

Pyroxenite	Gabbro
$1258^oC \pm 60^oC$	$1215^oC \pm 60^oC$
$1261^oC \pm 60^oC$	$1216^oC \pm 60^oC$

The olivine-clinopyroxene geothermometer of Powell and Powell (1974) has been applied to pairs from the websterite of Vavdos. The equation (2) has been applied to three co-existing pairs.

$$T = \frac{2.X_{Al}^{cpx}\ (920000 + 3.6P) - 0.0435\ (P-1) + 10100}{8 + R\ \ln\left\{\frac{X_{Mg}^{ol}}{X_{Fe}^{ol}}\right\}\left\{\frac{X_{Fe,M1}^{cpx}}{X_{Mg,M1}^{cpx}}\right\} - 714.3\ \ 2\ X_{Al}^{cpx}} \quad (2),$$

where X_i^a is the mole fraction of i in a, P is the pressure in bars and R is the gas constant. The results for three pairs are shown in the table below :

Pressure	5kb	10kb	15kb
Temperature	1037.8°C	1064.4°C	1091.0°C
	1037.7°C	1064.2°C	1090.8°C
	1039.1°C	1065.5°C	1091.9°C

However, the temperature values of a particular pressure are very close, probably due to the large numerical constants and the large pressure values in the numerator.

CHAPTER 7

CONCLUSIONS

7.1 CONCLUSIONS

1. Both complexes have been emplaced tectonically into their present positions. They occur in different regional zones of Northern Greece.

2. The Vavdos complex is comprised of an inverted stack of the following sequential magmatic layers : dunite, websterite and gabbro. The Gomati complex is represented by harzburgite, dunite, banded dunite-wehrlite and basalt. It is highly serpentinized and amphibolitized.

3. The chromite deposits of Vavdos are of "metallurgical" type, while those of Gomati are of the "refractory" type. The high chromium ores are formed by processes related to crystal-liquid fractionation in the lowermost parts of a magma chamber. The refractory ores are allochtonous in their present position. They have been formed during extraction of a basaltic-picritic melt from the harzburgite tectonite, which represents a refractory residuum.

4. The amphibolites of Gomati are of tholeiitic basalt composition. The immobile trace elements suggest formation in an oceanic environment, similar to that of abyssal tholeiites.

5. Thermodynamic data suggest a temperature of about 1200^{o}C for the formation of dunite and chromite concentrations. A temperature of around 1000^{o} C is inferred for the solidification of websterite and a slightly lower temperature for the overlying gabbro, but not below 900^{o}C.

7.2 OPHIOLITE ORIGIN, WITH IMPLICATIONS FOR THE FORMATION OF PODIFORM CHROMITITES

It is generally believed that the ophiolite suite is generated at divergent plate junctions in oceanic ridges or marginal seas. The spreading velocities, at the accreting ridges, are considered to be slow, in order to postulate a steady-state situation in the magma chamber beneath the ridges. Jackson et al (1975) suggest that the presence of cyclic units in the Vourinos ophiolite imply a slowly spreading ridge, in agreement with the above statement.

The ophiolite suite is thus composed of oceanic crust and upper mantle. An ideal section would include the following layers, commencing from the top : sediments (layer 1), pillow basalts (layer 2), sheeted dikes, diorites and gabbros (layer 3) and ultramafic rocks (pyroxenite, dunite and harzburgite). The boundary between the layer 3 and the pyroxenite represents the Mohorovicic discontinuity on geophysical grounds. However, on petrological grounds, it seems unlikely that the crust-upper mantle boundary is there, as pyroxenites and dunites form from cooling magma reservoirs with similar to identical crustal situations.

The model visualised by Greenbaum (1972) considers a steady-state situation in a magma reservoir beneath a slow-spreading ridge. Greenbaum postulates that the crystallizing magma gives rise to the following sequence : lavas, dykes, pyroxene gabbro, olivine gabbro, melagabbro, picrite, poikilitic wehrlite, clinopyroxene dunite, dunite and chromite concentrations at the base of the dunitic layer. The Vavdos complex represents a part of this sequence, while the Gomati complex

extends from the basalts to the dunites and also includes tectonized harzburgites. The petrological units of both complexes show similarities with dredged rocks from the mid-Atlantic ridge (Bonnatti et al, 1971 and Aumento and Loubat, 1971). They represent only parts of the complete sequence discovered in the mid-Atlantic ridge ; however, the processes which give rise to the rocks of the mid-Atlantic ridge and those that gave rise to the Tethyan ophiolites need not have been directly comparable.

The interlayered websterite-gabbro of Vavdos and the banded dunite-wehrlite of Gomati suggest a dynamic situation in the magma chamber, and the prevalence of convection currents.

The genesis of podiform chromite deposits is intimately related to the separation of a basaltic (picritic) liquid from the refractory residue, after the partial melting of primary upper mantle and asthenospheric material (Dickey, 1975). The refractory chromites of Gomati show sequential Cr-enrichment and Al-impoverishment. This is interpreted as a result of segregation of chromite, at various levels, from the upwelling basaltic extract from the harzburgite mush, after liquidus equilibration with the evolving composition of the basaltic magma. The high chromium ores which usually segregate in the lowest and hotest regions of the ultramafic cumulates (dunite-pyroxenite), accumulate, together with olivine, within a zone of turbulence. Stagnation of the magma in hot regions, and continuous influx of new, uprising material from the mantle, suggested by Greenbaum (1972) as being important, are not favoured here. The zone where the velocity of convection currents tends to diminish in the lowermost parts of the magma

chamber. The chromite concentrations occupy this position in the ophiolite sequence, and it is believed that they mainly segregated in such zones, where convection temporarily ceases. The data from Vavdos favour a crystal-liquid fractionation mechanism for the massive chromitites and adjacent dunites. The disseminated ore probably originates in turbulent zones, where the Cr-concentration also diminishes, e.g. after the formation of massive chromites. In general, a dynamic situation is favoured rather than lack of convective stirring. Therefore, it can be postulated that the podiform chromites match the motion of accreting oceanic ridges at a particular level.

REFERENCES

Atkins, F.B. (1969) Pyroxenes of the Bushveld intrusion, South Africa. Journ.Petrol., 10, p 222-249.

Arai, S. (1980) Dunite-harzburgite-chromitite complexes as refractory residue in the Sangun-Yamaguchi zone, Western Japan. Journ. Petrol., 21, p 141-165.

Aumento, F. and Loubat, H. (1971) The mid-Atlantic ridge near 45°N XVI. Serpentinized ultramafic intrusions. Canad.Journ. Earth Sci., 8, p 631-663.

Basu, A.R. and MacGregor, I.D. (1975) Chromite spinels from ultramafic xenoliths. Geochim. Cosmochim. Acta, 39, p 937-945.

Bernoulli, D. and Laubscher, H. (1972) The palinspastic problem of the Hellenides. Eclogue Geol.Helvetiae, 65/1, p 107-118.

Blander, M. (1972) Thermodynamic properties of orthopyroxenes and clinopyroxenes based on the ideal two-site model. Geochim. Cosmoch. Acta, 36, p 787-799.

Boccaletti, M., Manetti, P. and Peccerillo, A. (1974) The Balkanids as an instance of back arc thrust belt : Possible relation to Hellenides. Geol. Soc. Amer. Bull, 85, p 1077-1084.

Bonnatti, E., Honnorez, J. and Ferrara, G. (1971) Peridotite-gabbro-basalt complex from the equatorial mid-Atlantic ridge. Phil. Trans. Royal Soc. London, A, 268, p 385-402.

Bonnatti, E., Honnorez, J. Kirst, P. and Radicati, F. (1975) Metagabbros from the mid-Atlantic ridge at 06°N : contact hydro-thermal-dynamic metamorphism beneath the axial valley. Journ. Geology, 83, p 61-78,

Borci, S., Ferrara, G. and Mercier, J. (1964) Détermination de l'âge des séries métamorphiques du massif Serbo-Macédonien au nord-est de Thessalonique (Grèce) par les mèthods Rb/Sr et K/Ar. Ann. Soc. Gèol.Nord., 84, p 223-225. Lille.

Burns, R.G. (1970) Mineralogical applications of crystal field theory. Cambridge University Press, 210p.

Burns, R.G. (1973) The partitioning of trace transition elements in crystal structures : a provocative review with applications to mantle geochemistry. Geochim. Cosmochim. Acta, 73, p 2395-2405.

Cameron, E.N. (1975) Postcumulus and subsolidus equilibration of chromite and coexisting silicates in the Eastern Bushveld complex. Geochim. Cosmochim. Acta, 39, p 1021-1033.

Church, W.R. and Coish, R.A. (1976) Oceanic versus island arc origin of ophiolites. Earth Planet. Sci. Lett., 31, p 8-14.

Coleman, R.G. (1977) Ophiolites. Springer-Verlag, 220p.

Coleman, R.G. and Peterman, Z.E. (1975) Oceanic plagio-granite. Journ. Geophys. Research, 80, p 1099-1108.

Coombs, D.S. (1963) Trends and affinities of basaltic magmas and pyroxenes as illustrated on the diopside-olivine-silica diagram. Mineral. Soc. Amer. Spec. Paper 1, p 227-250.

Dick, H. (1977) Partial melting in the Josephine peridotite, the effect on mineral composition and its consequence for geobarometry and geothermometry. Amer.Journ.Sci.277, p 801-832.

Dickey, J.S. (1975) A hypothesis of origin for podiform chromite deposits. Geochim.Cosmochim.Acta,39, p 1061-1074.

Dickey, J.S., Jr., Yoder, H.S., Jr. and Schairer, J.F. (1971) Chromium in silicate-oxide systems. Carnegie Inst.Wash. Yearb.70, p 118-122.

Dickey, J.S., Jr., and Yoder, H.S., Jr. (1972) Partitioning of chromium and aluminium between clinopyroxene and spinel. Carnegie Inst. Wash. Yearb. 71, p 384-392.

Duke, J.M. (1976) Distribution of the period four transition elements among olivine, calcic clinopyroxene and mafic silicate liquid : experimental results. Journ.Petrol., 17, p 499-521.

Engin, T. (1969) The geology and geochemistry of ultrabasic rocks and associated chromite deposits of the Audizlik-Zimparalik area, Fethiye, Southwest Turkey. Ph.D. Thesis, University of Durham.

Eğin, D., Hirst, D.M. and Phillips, R. (1979) The petrology and geochemistry of volcanic rocks from the northern Harsit river area, Pontid volcanic province, Northeast Turkey. Journ. Volcanol. & Geotherm. Research, 6, p 105-123.

Evans, B.W. and Wright, T.L. (1972) Composition of liquidus chromite from the 1959 (Kilauea Iki) and 1965 (Makaopuhi) eruptions of Kilauea volcano, Hawaii. Amer. Mineral, 57, p. 217-230.

Evans, B.W. and Frost, B.R. (1975) Chrome-spinel in progressive metamorphism - a preliminary analysis. Geochim. Cosmochim. Acta, 39, p 959-972.

Fabries, J. (1979) Spinel olivine geothermometry in peridotites from ultramafic complexes. Contrib.Mineral. Petrol., 69, p 329-336.

Fleet, M.E. (1974a) Partition of Mg and Fe^{2+} in coexisting pyroxenes. Contrib. Mineral. Petrol., 44, p 251-257.

Fleet, M. E. (1974b) Mg-Fe^{2+} site occupanices in coexisting pyroxenes. Contrib. Mineral. Petrol., 47, p 207-214.

Floyd, P.A. and Winchester, J.A. (1975) Magma type and tectonic setting discrimination using immobile elements. Earth Planet. Sci. Lett., 27, p 211-218.

Fujii, T. (1978) Fe-Mg partitioning between olivine and spinel. Carnegie Inst. Wash. Yearb. 76, p 563-569.

Gass, I.G., Neary, C. R., Plant, J., Robertson, A.H.F., Simonian,K.O., Smewing, J.D., Spooner, E.T.C. and Wilson, R.A.M. (1975) Comments on "the Troodos ophiolitic complex was probably formed in an island arc" by A. Miyashiro and subsequent correspondence by A. Hynes and A. Miyashiro. Earth Planet. Sci. Lett., 25, p 236-238.

Ghisler, M.(1976) The geology, mineralogy and geochemistry of the pre-orogenic archaean stratiform chromite deposits at Fiskenaesset, West Greenland. Monograph Series on mineral deposits No.14 (Dr. Borchert, H., Ed.), Gebruder Borntraeger. p 156.

Green, D.H. and Ringwood, A.E. (1967) An experimental investigation of the gabbro to eclogite transformation and its petrological implications. Geochim. Cosmochim.Acta, 31, p 767-783.

Greenbaum, D. (1972) The geology and evolution of the Troodos plutonic complex and associated chromite deposits, Cyprus. Ph.D. Thesis, University of Leeds, 142p.

Greenbaum, D. (1977) The chromitiferous rocks of the Troodos ophiolite complex, Cyprus. Econ. Geol., 72, p 1175-1194.

Hart, S.R., Erlank, A.J. and Kable, E.J.D. (1974) Sea floor alteration : some chemical and Sr isotopic effects. Contrib. Mineral. Petrol., 44, p 219-230.

Hill, R. and Roeder, P.(1974) The crystallization of spinel from basaltic liquid as a function of oxygen fugacity. Journ. Geology, 82, p 709-729.

Hynes, A.J. (1972) The geology of part of the Western Orthris mountains, Greece. Ph.D. Thesis, Cambridge University.

Hynes, A.J. (1975) Comment on "the Troodos ophiolitic complex was probably formed in an island arc" by A. Miyashiro. Earth Planet. Sci. Lett., 25, p 213-216.

Irvine, T.N. (1965) Chromian spinel as a petrogenetic indicator, part 1. Theory. Canad. Journ. Earth Sci., 2, p 648-672.

Irvine, T.N. (1967) Chromian spinel as a petrogenetic indicator, part 2. Petrologic application. Canad.Journ. Earth Sci., 4, p 71-103.

Irvine, T.N. and Findlay, T.C. (1972) Alpine-type peridotite with particular reference to the Bay of Islands igneous complex. Pub.Earth Physics Branch Dept. Energy, Mines Res.Can., 42, p 97-128.

Irvine, T.N. and Kushiro, I. (1976) Partitioning of Ni and Mg between olivine and silicate liquids. Carnegie Inst.Wash. Yearb. 75, p 668-675.

Jackson, E.D. (1969) Chemical variation in coexisting chromite and olivine in chromitite zone ofthe Stillwater complex. In : Magmatic ore deposits (Wilson H.D.B., ed.), Econ.Geol.Mon.4, p 41-71.

Jackson, E.D. and Thayer, T.P. (1972) Some criteria for distinguishing between stratiform, concentric and alpine peridotite-gabbro complexes. 24th Intern.Geol.Congr.Section 2, p 289-296.

Jackson, E.D. Green, H.W. and Moores, E.M. (1975) The Vourinos ophiolite, Greece : Cyclic units of lineated cumulates overlying harzburgite tectonite. Geol.Soc.Amer.Bull.,86, p 390-398.

Jacobshagen, V., Dürr, St., Kockel, F., Kopp, K.O. and Kowalczyk, G. (1978) In : Alps, Apennines and Hellenides (Closs, H., Roeder, D. and Schmidt, K., ed.) Inter-union commission on Geodynamics, Sci. Report 38, E.Schweizerbart'sche Verlagsbuchhandlung. p 554.

Kockel, F. and Mollat, H. (1970) Geological map of Greece 1:50000, Poliyiros & Ierissos sheets. Instit. of Geol. & Minin. Res. of Greece , Athens.

Kockel, F., Mollat, H. and Walther, H.W. (1971) Geologie des Serbo-Mazedonischen massivs und seines mesozoishen Rahmens (Nordgriechenland) Geol. Jb., 89, p 529-551.

Kretz, R. (1963) Distribution of Mg and iron between orthopyroxene and calcic pyroxene in natural mineral assemblages. Journ. Geology, 71, p 773-785.

Kuno, H. (1968) Differentiation of basaltic magmas. In : Basalts, Vol.II,(Hess, H. H. and Poldervaart, A. ed.), p.623-688, John Wiley & Sons.

Kushiro, I. (1973) Partial melting of garnet lherzolites from kimberlite at high pressures. In: Lesotho Kimberlites, (Nixon, P.H. ed.), Cape and Transvaal Printers Ltd.

Leeman, W.P. and Scheidegger, K.F.S. (1977) Olivine liquid distribution coefficients and a test of crystal-liquid equilibrium. Earth Planet. Sci.Lett., 35, p 247-257.

Loney, R.A., Himmelberg, G.R. and Coleman, R.G. (1971). Structure and Petrology of the Alpine type peridotite at Burro mountain, California. Journ. Petrol., 12, p 245-309.

Malpas,J. and Strong, D.F. (1975) A comparison of chrome-spinels in ophiolites and mantle diapirs of Newfoundland. Geochim. Cosmochim. Acta, 39, p 1045-1060.

Marakushev, A.A. (1979) Some aspects of ore formation in ultramafics. Mineral. Deposita, 14, p 81-101.

Medaris, L.G. Jr. (1969). Partitioning of Fe^{2+} and Mg between coexisting synthetic olivine and opx. Amer.Journ.Sci., 267, p 945-968.

Medaris, L.G., Jr. (1975) Coexisting spinels and silicates in alpine peridotites of the granulite facies. Geochim. Cosmochim. Acta, 39, p 947-958.

Menzies, M. (1973) Mineralogy and partial melt textures within an ultramafic-mafic body, Greece. Contrib. Mineral. Petrol., 42, p 273-285.

Menzies, M. (1974) Petrogenesis of the Makrirrakhi ultramafic complex. Ph.D. Thesis, Cambridge University.

Menzies, M. (1975) Spinel compositional variation in the crustal and mantle lithologies of the Orthris ophiolite. Contrib. Mineral. Petrol., 51, p 303-309.

Menzies, M. and Allen, C. (1974) Plagioclase lherzolite residual mantle relationships within two eastern Mediterranean ophiolites. Contrib. Mineral. Petrol., 45, p 197-213.

Mercier, J. (1973) Contribution à l'etude du métamorphisme et de l'évolution magmatique des zones interness des Hellénides, Vol.II : Annales Géol. Pays Helléniques, 1st ser., tome XX , p 597-792.

Miyashiro, A. (1973) The Troodos ophiolitic complex was probably formed in an island arc. Earth Planet. Sci.Lett.,19, p 218-224.

Miyashiro, A. (1975) Origin of Troodos and other ophiolites : a reply to Hynes. Earth Planet. Sci. Lett., 25, p217-222.

Miyashiro, A. (1975) Origin of Troodos and other ophiolites : a reply to Moores. Earth Planet. Sci.Lett.,25, p 227-235.

Miyashiro, A., Shido, F. and Ewing, M. (1971) Metamorphism in the mid-Atlantic ridge near 24° and 30°N. Phil.Trans. Royal Soc. London, A, 268, p 589-603.

Montigny, R., Bougault, H., Bottinga, Y. and Allegre, C.J. (1973) Trace element geochemistry and genesis of the Pindos ophiolite suite. Geochim. Cosmochim.Acta, 37, p2135-2147.

Moody, J.B. (1976) Serpentinization : a review. Lithos 9, p 125-138.

Moores, E.M. (1969) Petrology and structure of the Vourinos ophiolitic complex of Northern Greece. Geol.Soc.Amer.Spec. Paper 118, p 1-74.

Moores, E.M. (1975) Discussion of "origin of Troodos and other ophiolites : a reply to Hynes" by A. Miyashiro. Earth Planet. Sci. Lett., 25, p 223-226.

Mori, T. (1977) Geothermometry of spinel lherzolites. Contrib. Mineral. Petrol.,59, p 261-279.

Mori, T. (1978) Experimental study of pyroxene equilibria in the system CaO-MgO-FeO-SiO_2. Journ. Petrol., 19, p 45-65.

Myers, J.S. (1976) Channel deposits of peridotite, gabbro and chromitite from turbidity currents in the stratiform Fiskenaesset anorthositic complex, Southwest Greenland. Lithos 9, p 281-291.

Mysen, B.O. (1976) Nickel partitioning between upper mantle crystals and partial melts as a function of pressure, temperature and nickel concentration. Carnegie Inst.Wash.Yearb. 75, p 662-668.

Nafziger, R.H. and Muan, A. (1967) Equilibrium phase compositions and thermodynamic properties of olivines and pyroxenes in the system $MgO-FeO-SiO_2$. Amer.Mineral., 52, p 1364-1384.

Navrotsky, A. (1978) Thermodynamics of element partitioning : (1) Systematics of transition metals in crystalline and molten silicates and (2) Defect chemistry and "the Henry's law problem". Geochim. Cosmochim. Acta, 42, p 887-902.

Nixon, P. and Boyd, F. (1973) Petrogenesis of the granular and sheared ultrabasic nodule suite in kimberlites. In : Lesotho Kimberlites, (Nixon, P.H, ed.), Cape and Transvaal Printers Ltd.

Onyeagocha, A.C. (1978) The twin sisters dunite : petrology and mineral chemistry. Geol. Soc.Amer.Bull.,89, p 1459-1474.

Panayiotou, A. (1978) The mineralogy and chemistry of the podiform chromite deposits in the serpentinites of the Limassol forest, Cyrpus. Mineral. Deposita, 13, p 259-274.

Papadakis, A. (1977) Formation, geology and geochemistry of chromite deposits of Triadion, Thessaloniki, Greece. Sci. Annals, Fac. Phys. & Mathem., Univer. Thessaloniki, 17, p 299-322.

Pav lov, N.V. and Grigoreva, I.I. (1977) Deposits of chromites of the Kempirsai massif. In : Ore deposits of the USSR, Vol.I, (Smirnov, V.I., ed.), Pitman Publishing.

Pearce, J.A. (1979) Geochemical evidence for the genesis and eruptive setting of lavas from Tethyan ophiolites. In : Intern. Ophiolite Symposium, Cyprus.

Pearce, J.A. and Cann, J.R. (1971) Ophiolite origin investigated by discriminant analysis using Ti, Zr and Y. Earth Planet. Sci.Lett., 12, p339-349.

Pearce, J.A. and Cann, J.R. (1973) Tectonic setting of basic volcanic rocks determined using trace element analyses. Earth Planet. Sci. Lett., 19, p 290-300.

Pearce, J.A. and Norry, M.J. (1979) Petrogenetic implications of Ti, Zr, Y and Nb variations in volcanic rocks. Contrib. Mineral. Petrol., 69, p 33-47.

Peters, T.J. and Kramers, J.D. (1974) Chromite deposits in the ophiolite complex of Northern Oman. Mineral. Deposita, 9, p 253-259.

Pinsent, R.H. (1974) The emplacement and metamorphism of the Blue River Ultramafic Body, Cassiar district, British Columbia, Canada. Ph.D.Thesis, University of Durham.

Powell, M. and Powell, R. (1974) An olivine-clinopyroxene geothermometer. Contrib. Mineral. Petrol., 48, p 249-263.

Roeder, P.L. and Emslie, R.F. (1970) Olivine-liquid equilibrium. Contrib. Mineral. Petrol., 29, p 275-289.

Roeder, P.L., Campbell, I.H. and Jamieson, H.E. (1979) A re-evaluation of the olivine-spinel geothermometer. Contrib. Mineral. Petrol., 68, p 325-334.

Raleigh, C.B. (1965) Glide mechanism in experimentally deformed minerals. Science, 150, p 3697.

Sack, R.O. (1980) Some constraints on the thermodynamic mixing properties of Fe-Mg orthopyroxenes and olivines. Contrib.Mineral. Petrol., 71, p 257-270.

Sapountzis, E.S. (1979) The Thessaloniki gabbros. Journ. Petrol., 20, p 37-70.

Sato, H. (1977) Nickel content of basaltic magmas : identification of primary magmas and a measure of the degree of olivine fractionation. Lithos 10, p 113-120.

Savelyev, A.A. and Savelyeva, G.N. (1979) Ophiolites of the Voykar massif (Polar Urals). Contrib. to I.G.C.P. Project 39, Ophiolites (report no.8), p 127-140.

Shervais, J.W. (1979) Thermal emplacement model for the alpine lherzolite massif at Balmuccia, Italy. Journ.Petrol.20, p 795-820.

Sinton, J.M. (1977) Equilibration history of the Basal alpine-type peridotite, Red Mountain, New Zealand. Journ.Petrol., 18, p 216-246.

Stevens, R.E. (1944) Composition of some chromites of the Western Hemisphere. Amer.Mineral.,29, p 1-34.

Thayer, T.P. (1960) Some critical differences between alpine-type and stratiform peridotite-gabbro complexes. Intern. Geol.Congr. 21st Sess. Copenhagen 13, p 247-259.

Thayer, T.P. (1964) Principal features and origin of podiform chromite deposits and some observations on the Guleman-Soridag district, Turkey. Econ. Geol., 59, p 1497-1524.

Thayer, T.P. (1969) Gravity differentiation and magmatic re-emplacement of podiform chromite deposits. In : Magmatic ore deposits (Wilson, H.D.B., ed.) Econ.Geol.Mon.4, p 132-146.

Thayer, T.P. (1970) Chromite segregations as petrogenetic indicators. Geol.Soc.South Africa, Special Publ. 1, p 380-389.

Turner, F.J. and Verhoogen, J. (1960) Igneous and metamorphic petrology. McGraw-Hill (second edition).

Watson, E.B. (1977) Partitioning of manganese between forsterite and silicate liquid. Geochim. Cosmochim.Acta, 41, p 1363-1374.

Whitehead, R. and Goodfellow, W. (1978) Geochemistry of volcanic rocks from the Tetagouche group, Bathurst, New Brunswick, Canada. Canad.Journ.Earth Sci., 15, p 207-219.

Wood, B.J. and Banno, S. (1973) Garnet orthopyroxene and orthopyroxene-clinopyroxene relationships in simple and complex systems. Contrib. Mineral. Petrol, 42, p 109-124.

Zachos, K. (1969) The chromite mineralization of the Vourinos ophiolitic complex, Northern Greece. In : Magmatic ore deposits, (Wilson, H.D.B, ed.), Econ. Geol. Mon. 4, p 147-153.

Zimmerman, J. Jr. and Ross, J.V. (1976) Structural evolution of the Vardar root zone, Northern Greece. Geol.Soc.Amer.Bull. 87, p 1547-1550.

APPENDIX I

SAMPLING DATA

The tables 1 and 2 summarize all analyzed samples. All samples are hand specimens collected during several field trips. The location of certain samples is shown in Figures 3.1 and 3.2 ; in several localities number specification is missing, because certain samples have been collected from a close vicinity. The classification of chromite ores has been done according to that in the text.

TABLE 1 Vavdos Complex

Sample	Rock Type	Sample	Rock Type
VA3	Olivine chromitite	VP1	Dunite
VA4	Chromitiferous dunite	VP2	"
VA8	Massive chromitite	VP3	"
VA15	Dunite	VP5	Massive chromitite
VB1	Chromitiferous dunite	VP10	Gabbro
VB3	Dunite	VP21	Massive chromitite
VB5	Olivine-chromitite	VP24	Granitic rock
VC1	Amphibolite	VP25	Pyroxenite
VC2	"	VP26	Pyroxenite
VC3	"	VX1	Granitic rock
VC4	"	VX4	Pyroxenite
VC6	Chromitiferous dunite	VX5	Pyroxenite
VC8	"	VY3	Olivine-chromitite
VC9	Dunite with chromite bands	VY7	Dunite
VC10	" " "	VY8	Granitic rock
VC11	Dunite	V8-1	Pyroxenite
VD6	Massive chromitite	V8-2	Pyroxenite
VE2	Olivine chromitite	V8-3	Amphibolitized gabbro
VF4	Massive chromitite	V8-8	Amphibolite
VF7	Dunite	V8-9	Sheared amphibolite
VG1	Dunite	V8-10	Amphibolite
VG2	Massive chromitite with small lensoid dunite bodies	V8-11	"
		V8-13	Metamorphosed gabbro
VK2	Serpentinite	V8-15	Underlying country rock
VK8	Sheared chromitite	V8-6	Monomineralic plagioclase rock
VK0	Serpentinite with chromite disseminations	VP16	Sheared amphibolite
VK9	Contact mylonite	VY1	Dunite
VC14	Contact mylonite		

TABLE 2 Gomati Complex

Sample	Rock Type
GB2	Massive chromitite
GB4	Dunite (serpentinized with 10% chromite)
GC1	Serpentinite (mesh-textured)
GC5	Serpentinite
GD1	Garnet-amphibolite
GD2	Serpentinite (mesh-textured)
GK1	Amphibolite
GK2	Garnet-amphibolite
GL1	Serpentinite
GL2	"
GL5	Clinopyroxene-chromitite
GM1	Serpentinized dunite
GM2	Serpentinite
GN10	Banded serpentinite-amphibolite
GN12	Serpentinite
GN15	"
GN17	"
GS2	Chromitite (disseminated type-ore)
GS4	Pyroxene-chromitite
GT1	Banded amphibolite-serpentinite
GT7	Massive chromitite
GT9	Sheared-serpentinite
GN1	Sheared serpentinite
GN2	Serpentinite with strong fabric
GN3	Serpentinite

APPENDIX II

ELECTRON MICROPROBE DATA

All minerals were analyzed using the electron microprobe of Durham University. The instrument is a Geoscan MK-II electron microanalyzer of the Cambridge Instrument Company. The analytical methods used are those of Sweatman and Long (1969).

Polished and polished-thin sections were used for analyzing spinels and silicates respectively. The Geoscan was operated under a high vacuum (0.01 mm Hg), at an accelerating voltage of 15 kV, and a specimen current of 0.04 μA. The electron beam was focussed frequently in order to give a spot of diameter of about 2-5 μm.

Optimum operating conditions for all analyzed elements are given in Table 1. The flow counter was used throughout, and the slits were used for analyzing Co, in order to avoid the interference of Fe K_β. The time of counting was kept constant at 10 seconds, for both peak and background positions. Background values were obtained at $\pm$ 2° about the peak position for both standards and unknown minerals. The measured counts were corrected with the aid of a Varian 620/L-100 computer, using the TIM 3 and the modified TIM 4 programs, written by Dr. A. Peckett.

TABLE 1 Optimum operating conditions and standards for the electron microanalysis.

Atomic Number	Element	Line	Analyzing crystal	2θ (peak position)	Standard
11	Na	$K\alpha_1$	KAP	53°.12'	jadeite (JD-1)
12	Mg	"	KAP	43°.32'	MgO
13	Al	"	KAP	36°.23'	jadeite (JD-1)
14	Si	"	PET	109°.18'	wollastonite (WO-2)
19	K	"	PET	50°.68'	alkali feldspar (AF-15)
20	Ca	"	LIF	113°.03'	wollastonite (WO-2)
22	Ti	"	LIF	86°.04'	TiO_2
24	Cr	"	LIF	69°.17'	Cr_2O_3
25	Mn	"	LIF	62°.55'	rhodonite
26	Fe	"	LIF	57°.28'	Fe
27	Co	"	LIF	52°.44'	Co*
28	Ni	"	LIF	48°.37'	Ni

* The Fe_2O_3 standard was used for obtaining background values.

Table 2 Chromite from Vavdos complex.

	1 VA8	2 VA8	3 VA3	4 VA3	5 VA4	6 VA4	7 VA4	8 VA4	9 VB5	10 VB5
Oxide weight percentage										
TIO2	0.21	0.25	0.22	0.19	0.22	0.21	0.18	0.20	0.15	0.18
AL203	13.77	13.38	11.98	12.25	12.42	12.12	12.32	11.89	13.91	13.90
CR203	55.63	56.02	56.77	57.06	55.91	55.60	55.94	55.49	56.37	56.71
FE203	2.60	2.61	2.80	2.91	2.85	3.03	2.64	3.04	1.62	1.67
FEO	14.56	14.51	18.21	15.22	13.06	18.83	19.05	19.28	13.63	13.27
MNO	0.53	0.57	0.80	0.64	0.60	0.75	0.71	0.72	0.47	0.52
MGO	12.51	12.54	10.01	11.93	10.14	9.49	9.44	9.15	13.04	13.35
NIO	0.16	0.10	0.08	0. 14	0.16	0.07	0.05	0.02	0.11	0.10
Total	99.97	99.98	100.87	100.34	100.41	100.09	100.33	99.79	99.30	99.70
Atomic proportions on the basis of 32 oxygens.										
TI	0.0404	0.0482	0.0431	0.0369	0.0431	0.0415	0.0355	0.0398	0.0289	0.0345
AL	4.1583	4.0459	3.6790	3.7262	3.8190	3.7390	3.8103	3.7098	4.2055	4.1798
CR	11.2606	11.3547	11.6860	11.6343	11.5402	11.5589	11.5969	11.6053	11.4238	11.4307
FE3+	0.5002	0.5030	0.5489	0.5657	0.5546	0.5991	0.5219	0.6053	0.3128	0.3205
FE2+	3.1188	3.1122	3.9654	3.2824	3.9372	4.1404	4.1780	4.2666	2.9223	2.8290
MN	0.1150	0.1238	0.1764	0.1398	0.1325	0.1671	0.1577	0.1613	0.1021	0.1123
MG	4.7738	4.7916	3.8845	4.5856	3.9399	3.7193	3.6883	3.6976	4.9819	5.0728
NI	0.0329	0.0206	0.0167	0.0290	0.0335	0.0148	0.0105	0.0043	0.0227	0.0205

Table 2

	11 VA15	12 VA15	13 VB3	14 VB3	15 VP2	16 VP2	17 VP23	18 VK2	19 VK2	20 VD6
Oxide weight percentage										
SIO2	0.05	0.08	0.20	0.09	0.02	0.17	0.23	0.04	0.29	0.02
TIO2	0.19	0.20	0.09	0.05	0.17	0.13	0.16	0.21	0.20	0.01
AL203	13.23	13.20	13.58	13.93	14.52	12.63	10.65	10.42	9.80	15.95
CR203	54.14	54.14	53.75	53.52	55.45	54.95	53.48	57.32	56.86	55.38
FE203	2.27	2.26	1.18	1.51	1.25	1.49	7.16	2.10	2.11	2.44
FEO	20.37	20.30	22.16	21.64	14.80	22.23	18.53	21.88	23.14	11.39
MNO	0.64	0.75	0.75	0.81	0.47	0.79	0.78	0.59	0.63	0.45
MGO	8.59	8.59	7.39	7.61	12.34	7.33	9.78	7.44	6.69	14.81
NIO	0.09	0.10	0.06	0.08	0.12	0.11	0.10	0.11	0.10	0.35
Total	99.58	99.61	99.17	99.23	99.14	99.82	100.87	100.11	99.82	100.79
Atomic proportions on the basis of 32 oxygens										
SI	0.0143	0.0213	0.0544	0.0229	0.0063	0.0448	0.0599	0.0094	0.0796	0.0045
TI	0.0386	0.0396	0.0179	0.0100	0.0332	0.0268	0.0324	0.0429	0.0405	0.0017
AL	4.1262	4.1143	4.2749	4.3722	4.4035	3.9715	3.2982	3.3005	3.1343	4.6680
CR	11.3164	11.3151	11.3441	11.2595	11.2750	11.5856	11.1017	12.1712	12.1943	10.8646
FE3+	0.4515	0.4488	0.2363	0.3024	0.2424	0.2997	1.4155	0.4235	0.4313	0.4549
FE2+	4.5053	4.4871	4.9479	4.8163	3.1833	4.9580	4.0691	4.9154	5.2497	2.3632
MN	0.1432	0.1675	0.1696	0.1827	0.1030	0.1783	0.1746	0.1338	0.1448	0.0952
MG	3.3855	3.3849	2.9415	3.0165	4.7284	2.9121	3.8270	2.9796	2.7042	5.4789
NI	0.0189	0.0214	0.0134	0.0175	0.0249	0.0232	0.0217	0.0235	0.0214	0.0690

Table 2

	21 VB1	22 VB1	23 VB1	24 VB1	25 VC9	26 VC9	27 VC9	28 VC10	29 VC10	30 VC10
Oxide weight percentage										
TIO2	0.16	0.17	0.16	0.17	0.39	0.27	0.28	0.35	0.37	0.27
AL203	13.92	14.33	14.11	14.08	7.81	12.42	11.73	6.81	12.32	11.34
CR203	55.55	55.48	55.50	54.93	53.68	53.72	53.36	56.40	53.43	52.81
FE203	2.29	1.97	2.57	2.71	7.63	3.94	4.06	7.10	3.68	5.27
FEO	15.66	17.08	15.20	15.90	22.51	20.60	22.43	21.03	21.56	20.94
MNO	0.54	0.55	0.61	0.69	0.77	0.69	0.65	0.73	0.56	0.62
MGO	11.83	11.09	12.19	11.63	6.52	8.44	7.09	7.51	7.88	7.95
NIO	0.11	0.12	0.09	0.10	0.13	0.07	0.10	0.14	0.09	0.08
Total	100.06	100.79	100.43	100.21	99.49	100.14	99.71	100.07	99.89	99.28
Atomic proportions on the basis of 32 oxygens										
TI	0.0309	0.0327	0.0307	0.0328	0.0809	0.0537	0.0566	0.0720	0.0741	0.0546
AL	4.2163	4.3269	4.2471	4.2627	2.5404	3.8748	3.7203	2.1770	3.8683	3.5968
CR	11.2785	11.2209	11.1978	11.1472	11.7041	11.2341	11.3441	12.1966	11.2466	11.2277
FE3+	0.4433	0.3737	0.4936	0.5244	1.5937	0.7836	0.8223	1.4624	0.7365	1.0662
FE2+	3.3627	3.6574	3.2438	3.4129	5.1923	4.5569	5.0454	4.8105	4.8015	4.7096
MN	0.1175	0.1173	0.1319	0.1500	0.1799	0.1546	0.1481	0.1691	0.1263	0.1412
MG	4.5280	4.2514	4.6366	4.4493	2.6799	3.3273	2.8415	3.0616	3.1270	3.1865
NI	0.0227	0.0247	0.0185	0.0206	0.0288	0.0149	0.0216	0.0308	0.0193	0.0173

Table 2

	31 VC1	32 VC6	33 VC6	34 VC6	35 VG2	36 VG2	37 VG2	38 VC11	39 VC8	40 VC8
Oxide weight percentage										
SIO2	-	-	-	-	-	-	-	0.06	-	0.03
TIO2	0.20	0.42	0.29	0.25	0.18	0.22	0.20	0.25	0.25	0.24
AL2O3	13.46	12.98	13.31	13.23	11.15	11.17	11.68	10.88	12.91	12.51
CR2O3	55.40	55.00	54.60	54.46	58.36	57.84	58.43	51.74	55.45	56.07
FE2O3	3.08	3.40	3.77	3.93	2.16	1.56	1.10	6.44	3.11	4.08
FEO	15.22	16.48	16.12	16.20	16.93	20.34	17.87	24.35	14.74	13.59
MNO	0.59	0.45	0.45	0.53	0.52	0.61	0.54	0.73	0.44	0.57
MGO	12.06	11.45	11.66	11.50	10.75	8.56	10.25	5.86	12.29	13.12
NIO	0.12	0.09	0.06	0.06	0.13	0.10	0.02	0.10	0.07	0.10
Total	100.13	100.27	100.25	100.15	100.18	100.40	100.09	100.41	99.26	100.31
Atomic proportions on the basis of 32 oxygens										
SI	-	-	-	-	-	-	-	0.0170	-	0.0065
TI	0.0386	0.0815	0.0562	0.0485	0.0354	0.0438	0.0394	0.0506	0.0487	0.0462
AL	4.0775	3.9521	4.0422	4.0275	3.4391	3.4897	3.6077	3.4748	3.9435	3.7735
CR	11.2495	11.2251	11.1149	11.1128	12.0659	12.1126	12.0974	11.0768	11.3535	11.3362
FE3+	0.5957	0.6598	0.7306	0.7627	0.4248	0.3100	0.2161	1.3132	0.6056	0.7851
FE2+	3.2689	3.5591	3.4709	3.4964	3.7060	4.5063	3.9147	5.5154	3.1937	2.9066
MN	0.1284	0.0984	0.0982	0.1159	0.1152	0.1369	0.1198	0.1680	0.0965	0.1227
MG	4.6166	4.4054	4.4747	4.4238	4.1899	3.3794	4.0007	2.3634	4.7439	5.0025
NI	0.0248	0.0187	0.0124	0.0125	0.0273	0.0213	0.0042	0.0207	0.0146	0.0208

Table 2

	41 VE2	42 VE2	43 VK8	44 VK8	45 VP5	46 VP21	47 VY3	48 VY3	49 VF4
Oxide weight percentage									
SIO2	0.03	0.05	0.03	0.25	-	0.04	0.04	0.02	0.06
TIO2	0.03	0.04	0.01	0.07	0.14	0.14	0.10	0.12	0.11
AL203	9.74	10.01	15.60	15.01	12.77	10.96	11.52	12.37	12.66
CR203	59.12	59.16	54.94	55.81	57.24	57.48	57.71	57.76	58.50
FE203	3.32	2.90	1.72	0.52	2.89	5.19	2.80	3.17	2.09
FEO	17.5	16.58	14.39	17.45	13.67	13.33	14.17	12.92	12.89
MNO	0.73	0.57	0.39	0.60	0.70	0.65	0.61	0.63	0.58
MGO	10.13	10.83	12.89	11.07	13.02	13.22	12.38	13.56	13.67
NIO	0.17	0.07	0.08	0.16	0.02	0.03	0.11	0.02	0.04
Total	100.79	100.21	100.05	100.95	100.45	101.04	99.45	100.57	100.60
Atomic proportions on the basis of 32 oxygens									
SI	0.0090	0.0123	0.0086	0.0645	-	0.0093	0.0110	0.0064	0.0161
TI	0.0066	0.0087	0.0015	0.0143	0.0269	0.0274	0.0205	0.0238	0.0215
AL	3.0217	3.1015	4.6573	4.5080	3.8426	3.3052	3.5312	3.7112	3.7881
CR	12.2893	12.2825	10.9954	11.2355	11.5489	11.6217	11.8579	11.6209	11.7365
FE3+	0.6578	0.5738	0.3271	0.0989	0.5546	0.9996	0.5479	0.6076	0.4000
FE2+	3.8501	3.6422	3.0478	3.7152	2.9173	2.8506	3.0789	2.7494	2.7347
MN	0.1616	0.1266	0.0840	0.1296	0.1514	0.1410	0.1352	0.1354	0.1254
MG	3.9681	4.2384	4.8626	4.2008	4.9541	5.0383	4.7953	5.1414	5.1697
NI	0.0359	0.0139	0.0157	0.0333	0.0042	0.0063	0.0221	0.0039	0.0078

Table 3 Olivine from Vavdos complex

	1 VA8	2 VA3	3 VA3	4 VA4	5 VA4	6 VA4	7 VA4	8 VB5	9 VA15	10 VC1
Oxide weight percentage										
SIO2	42.01	41.08	42.02	41.09	41.70	42.27	41.00	41.99	41.79	42.07
TIO2	0.01	-	-	0.01	-	0.01	0.02	0.01	-	-
AL203	0.05	-	-	0.00	-	0.01	-	-	-	-
FEO	4.34	6.04	4.28	5.02	5.75	5.04	5.74	3.71	6.14	4.43
MNO	0.11	0.13	0.10	0.09	0.11	0.10	0.21	0.06	0.11	0.07
MGO	52.70	52.94	53.57	53.55	52.97	53.03	52.85	53.41	52.33	53.41
CAO	0.03	-	-	0.03	0.02	0.03	0.02	0.02	-	-
NIO	0.77	0.45	0.57	0.45	0.35	0.42	0.50	0.77	0.38	0.46
Total	100.03	100.66	100.55	100.24	100.91	100.91	100.33	99.95	100.80	100.44
Atomic proportions on the basis of 4 oxygens										
SI	1.0060	0.9863	1.0005	0.9861	0.9955	1.0048	0.9867	1.0035	0.9998	1.0025
TI	0.0004	-	-	0.0001	-	0.0001	0.0004	0.0001	-	-
AL	0.0013	-	-	0.0001	-	0.0003	-	-	-	-
FE	0.0870	0.1212	0.0851	0.1007	0.1149	0.1003	0.1156	0.0744	0.1229	0.0883
MN	0.0022	0.0027	0.0020	0.0019	0.0023	0.0021	0.0042	0.0012	0.0023	0.0013
MG	1.8805	1.8943	1.9006	1.9153	1.8646	1.8787	1.8959	1.9024	1.8679	1.8966
CA	0.0007	-	-	0.0008	0.0006	0.0008	0.0004	0.0004	-	-
NI	0.0149	0.0087	0.0109	0.0087	0.0067	0.0080	0.0096	0.0148	0.0074	0.0087
Fo	95.56	93.98	95.71	95.00	94.25	94.93	94.25	96.25	93.83	95.55

Table 3

	11 VB1	12 VB1	13 VB1	14 VC6	15 VC9	16 VC9	17 VC10	18 VC10	19 VG2	20 VG2
Oxide weight percentage										
SIO2	41.25	42.14	41.89	40.67	41.01	41.31	41.27	41.54	41.14	41.05
TIO2	0.08	0.00	-	-	-	-	-	-	-	-
AL203	0.00	0.02	-	-	-	-	-	-	-	-
FEO	4.68	4.80	4.29	4.58	7.34	7.89	6.87	6.33	4.73	7.37
MNO	0.08	0.05	0.07	0.08	0.12	0.13	0.13	0.12	0.11	0.15
MGO	52.47	52.97	52.55	53.20	50.78	50.51	50.65	51.10	53.53	51.20
CAO	0.02	0.02	0.03	-	-	-	-	-	-	-
NIO	0.50	0.56	0.52	0.50	0.44	0.39	0.37	0.43	0.60	0.47
Total	99.09	100.55	99.34	99.03	99.69	100.24	99.29	99.51	100.11	100.24
Atomic proportions on the basis of 4 oxygens										
SI	0.9985	1.0046	1.0082	0.9863	0.9984	1.0020	1.0055	1.0072	0.9878	0.9947
TI	0.0015	0.0000	-	-	-	-	-	-	-	-
AL	0.0001	0.0005	-	-	-	-	-	-	-	-
FE	0.0948	0.0957	0.0864	0.0930	0.1495	0.1601	0.1400	0.1283	0.0951	0.1493
MN	0.0016	0.0010	0.0015	0.0017	0.0024	0.0026	0.0027	0.0025	0.0022	0.0031
MG	1.8931	1.8821	1.8850	1.9230	1.8425	1.8257	1.8390	1.8467	1.9155	1.8491
CA	0.0004	0.0005	0.0007	-	-	-	-	-	-	-
NI	0.0098	0.0107	0.0100	0.0097	0.0087	0.0076	0.0073	0.0083	0.0116	0.0092
Fo	95.23	95.16	95.62	95.39	92.49	91.98	92.93	93.51	95.27	92.53

Table 3

	21 VG2	22 VX5	23 VX5	24 VX5	25 VX5
Oxide weight percentage					
SIO2	40.57	40.06	40.52	40.76	40.90
TIO2	-	0.00	-	-	-
AL203	-	0.01	-	-	0.01
FEO	6.54	16.79	16.90	17.00	16.60
MNO	0.11	0.31	0.27	0.25	0.22
MGO	51.56	42.32	42.69	42.76	42.06
CAO	-	0.03	-	-	0.03
NIO	0.57	0.17	0.18	0.15	0.29
Total	99.35	99.69	100.56	100.92	100.11
Atomic proportions on the basis of 4 oxygens					
SI	0.9895	1.0299	1.0183	1.0203	1.0299
TI	-	0.0000	-	-	-
AL	-	0.0002	-	-	0.0004
FE	0.1333	0.3561	0.3551	0.3558	0.3497
MN	0.0024	0.0067	0.0058	0.0053	0.0046
MG	1.8743	1.6000	1.5989	1.5953	1.5785
CA	-	0.0008	-	-	0.0009
NI	0.0111	0.0034	0.0035	0.0031	0.0059
Fo	93.36	81.79	81.83	81.76	81.86

Table 4a Pyroxene from Vavdos complex, Pyroxenite

	1 VX5	2 VX5	3 VX5	4 VX5	5 VX5	6 VX5	7 VP26	8 VX4
Oxide weight percentage								
SIO2	54.51	56.25	52.31	53.33	56.07	54.42	54.53	54.59
TIO2	0.14	0.09	0.10	0.05	0.05	0.19	0.12	0.05
AL203	1.43	1.54	2.00	1.70	1.80	1.56	1.18	2.00
CR203	0.22	0.23	0.41	0.57	0.23	0.39	0.28	0.64
FEO	10.43	11.21	4.83	4.47	10.08	3.91	4.03	3.45
MNO	0.24	0.22	0.16	0.15	0.20	0.09	0.17	0.12
MGO	32.03	30.93	17.35	18.88	30.76	16.28	16.72	15.93
CAO	1.22	0.62	21.69	22.22	1.27	22.09	23.34	22.94
NA20	0.01	0.00	0.14	0.19	0.00	0.13	0.13	0.12
NIO	0.06	0.04	0.04	0.07	0.03	0.07	0.09	0.10
Total	100.28	101.12	99.52	101.65	100.49	99.14	100.59	99.95
Atomic proportions on the basis of 6 oxygens								
SI	1.9235	1.9625	1.9260	1.9219	1.9617	1.9932	1.9791	1.9843
TI	0.0037	0.0024	0.0027	0.0013	0.0013	0.0052	0.0032	0.0015
AL	0.0595	0.0634	0.0866	0.0724	0.0742	0.0676	0.0505	0.0857
CR	0.0061	0.0063	0.0118	0.0162	0.0064	0.0112	0.0081	0.0185
FE	0.3078	0.3271	0.1488	0.1346	0.2949	0.1198	0.1225	0.1048
MN	0.0071	0.0064	0.0050	0.0047	0.0060	0.0029	0.0052	0.0037
MG	1.6842	1.6080	0.9793	1.0143	1.6039	0.8886	0.9047	0.8629
CA	0.0459	0.0231	0.8556	0.8582	0.0478	0.8671	0.9077	0.8934
NA	0.0009	0.0000	0.0100	0.0135	0.0000	0.0095	0.0095	0.0087
NI	0.0016	0.0010	0.0011	0.0021	0.0008	0.0020	0.0025	0.0030
End member compositions								
Wo	0.86	0.88	43.69	44.35	0.50	45.25	46.08	46.78
En	89.25	82.32	52.67	54.78	83.99	48.24	47.49	47.45
Fs	9.89	16.80	3.64	0.92	15.45	6.51	6.43	5.77

Table 4b Pyroxene from Vavdos complex, Gabbro

	1 VP10	2 VP10	3 VP10	4 VP10
Oxide weight percentage				
SIO2	55.09	53.06	55.56	53.23
TIO2	0.12	0.26	0.14	0.24
AL203	1.21	1.83	1.25	1.89
CR203	0.03	0.07	0.05	0.04
FEO	12.58	5.15	12.38	5.26
MNO	0.24	0.13	0.29	0.14
MGO	29.42	16.16	29.26	16.13
CAO	0.81	22.26	0.91	21.87
NA2O	0.03	0.31	0.02	0.33
NIO	0.00	0.11	0.00	0.00
Total	99.54	99.35	99.83	99.14
Atomic proportions on the basis of 6 oxygens				
SI	1.9673	1.9582	1.9749	1.9651
TI	0.0032	0.0073	0.0038	0.0068
AL	0.0514	0.0798	0.0525	0.0824
CR	0.0010	0.0021	0.0014	0.0011
FE	0.3756	0.1590	0.3680	0.1623
MN	0.0074	0.0042	0.0088	0.0044
MG	1.5656	0.8008	1.5498	0.8873
CA	0.0310	0.8800	0.0346	0.8650
NA	0.0024	0.0219	0.0012	0.0235
NI	0.0000	0.0031	0.0000	0.0001
End member compositions				
Wo	0.00	44.91	0.00	44.17
En	80.65	46.73	80.81	47.19
Fs	19.35	8.36	19.19	8.63

Table 5 Amphibole from clinopyroxenite of Vavdos complex

	1 VX4	2 VX4	3 VP26
Oxide weight percentage			
SIO2	58.43	58.55	57.43
TIO2	0.04	0.01	0.20
AL203	0.34	0.27	0.47
CR203	0.49	0.38	0.76
FEO	4.63	4.29	6.82
MNO	0.10	0.14	0.13
MGO	22.10	21.96	20.95
CAO	12.80	13.74	12.80
NA20	0.12	0.11	0.13
NIO	-	0.05	0.08
Total	99.05	99.49	99.77
Atomic proportions on the basis of 23 oxygens			
SI	7.9561	7.9520	7.8702
TI	0.0041	0.0010	0.0206
AL	0.0546	0.0432	0.0760
CR	0.0527	0.0408	0.0823
FE	0.5273	0.4873	0.7816
MN	0.0115	0.0161	0.0151
MG	4.4848	4.4449	4.2787
CA	1.8675	1.9995	1.8795
NA	0.0317	0.0290	0.0345
NI	-	0.0005	0.0088

Table 6 Chromite from Gomati complex

	1	2	3	4	5	6	7	8	9	10
	GB2	GT7	GT7	GS2	GS2	GS2	GL5	GL5	GL5	GL5
Oxide weight percentage										
SIO2	-	0.01	-	-	-	-	0.02	-	-	-
TIO2	0.38	0.25	0.31	0.15	0.19	0.18	0.59	0.60	0.65	0.50
AL203	26.80	25.09	25.23	27.21	26.82	26.96	20.42	20.63	19.84	20.62
CR203	36.70	42.16	41.22	39.76	40.29	39.39	42.49	42.71	42.28	41.81
FE203	7.86	4.53	4.74	3.76	3.43	3.33	6.68	7.34	8.06	8.29
FEO	10.05	11.29	11.58	15.51	15.08	15.27	17.56	15.25	16.75	14.80
MNO	1.28	1.08	0.45	0.59	0.53	0.34	1.14	1.11	1.28	0.99
MGO	16.16	15.50	15.60	13.31	13.53	13.32	11.00	12.59	11.48	12.82
NIO	0.33	0.13	0.13	0.12	0.12	0.10	0.29	0.32	0.27	0.29
Total	99.56	100.03	99.25	100.41	99.98	98.89	100.19	100.55	100.61	100.12
Atomic proportions on the basis of 32 oxygens										
SI	-	0.0024	-	-	-	-	0.0050	-	-	-
TI	0.0681	0.0451	0.0562	0.0271	0.0345	0.0330	0.1116	0.1119	0.1225	0.0935
AL	7.5363	7.0958	7.1731	7.7121	7.6279	7.7418	6.0560	6.0336	5.8623	6.0456
CR	6.9177	7.9923	7.8554	7.5538	7.6810	7.5819	8.4467	8.3730	8.3741	8.2168
FE3+	1.4098	0.8169	0.8591	0.6798	0.6222	0.6104	1.2641	1.3696	1.5187	1.5506
FE2+	2.0041	2.2635	2.3344	3.1168	3.0403	3.1099	3.6928	3.1620	3.5100	3.0774
MN	0.2585	0.2194	0.0919	0.1201	0.1083	0.0701	0.2428	0.2332	0.2716	0.2085
MG	5.7423	5.5395	5.6047	4.7670	4.8626	4.8334	4.1224	4.6530	4.2864	4.7497
NI	0.0633	0.0251	0.0252	0.0232	0.0233	0.0196	0.0586	0.0638	0.0554	0.0580

Table 6

	11 GN15	12 GN15	13 GL5	14 GB2	15 GB2	16 GB2	17 GB4	18 GB4	19 GB4
Oxide weight percentage									
SIO2	0.01	-	-	-	0.02	0.11	0.22	0.08	0.02
TIO2	0.21	0.31	0.45	0.30	0.30	0.22	0.50	0.46	0.47
AL203	30.12	30.14	21.38	22.96	24.96	24.93	11.70	14.47	14.74
CR203	36.87	36.37	39.99	42.22	40.79	41.12	49.77	50.75	51.08
FE203	4.94	5.16	8.86	7.05	5.53	6.07	7.55	4.18	3.72
FEO	11.61	11.28	14.72	9.25	10.80	10.03	21.69	20.31	20.86
MNO	0.51	0.66	1.03	1.09	1.13	1.25	1.44	1.39	1.37
MGO	16.24	16.33	12.76	16.41	15.51	16.15	7.27	8.39	8.15
CAO	0.01	0.02	0.02	0.02	0.03	0.03	0.16	0.10	0.05
NIO	0.22	0.26	0.26	0.24	0.34	0.30	0.30	0.30	0.28
Total	100.73	100.53	99.47	99.55	99.41	100.21	100.60	100.43	100.74
Atomic proportions on the basis of 32 oxygens									
SI	0.0023	-	-	-	0.0048	0.0263	0.0586	0.0209	0.0052
TI	0.0368	0.0543	0.0844	0.0545	0.0544	0.0395	0.1002	0.0905	0.0922
AL	8.2705	8.2849	6.2866	6.5433	7.1001	7.0186	3.6786	4.4630	4.5364
CR	6.7861	6.7013	7.8819	8.0652	7.7777	7.7598	10.4892	10.4922	10.5375
FE3+	0.8652	0.9051	1.6628	1.2825	1.0037	1.0901	1.5144	0.8220	0.7312
FE2+	2.2600	2.1981	3.0683	1.8701	2.1793	2.0023	4.8353	4.4424	4.5524
MN	0.1006	0.1303	0.2175	0.2231	0.2309	0.2527	0.3252	0.3079	0.3028
MG	5.6349	5.6722	4.7411	5.9096	5.5754	5.7454	2.8884	3.2700	3.1695
CA	0.0025	0.0050	0.0053	0.0052	0.0078	0.0077	0.0457	0.0280	0.0140
NI	0.0412	0.0487	0.0521	0.0466	0.0659	0.0576	0.0643	0.0631	0.0587

Table 6

	20 GN15	21 GN15	22 GS4
Oxide weight percentage			
SI02	0.01	0.02	0.02
TI02	0.18	0.18	0.13
AL203	30.43	30.02	27.48
CR203	36.66	37.75	39.79
FE203	4.70	4.37	3.74
FEO	12.05	11.82	15.51
MNO	0.60	0.48	0.28
MGO	15.91	16.20	13.57
NIO	0.25	0.16	0.18
Total	100.79	100.99	100.70
Atomic proportions on the basis of 32 oxygens			
SI	0.0023	0.0046	0.0048
TI	0.0315	0.0297	0.0234
AL	8.3582	8.2300	7.7493
CR	6.7496	6.9371	7.5213
FE3+	0.8245	0.7641	0.6730
FE2+	2.3464	2.2978	3.1015
MN	0.1184	0.0945	0.0567
MG	5.5223	5.6122	4.8356
NI	0.0468	0.0299	0.0346

Table 7 Altered Cr-spinel and secondary magnetite from Gomati complex

	1 GM2	2 GM2	3 GM1	4 GN17	5 GN17	6 GN10	7 GT1
Oxide weight percentage							
SI02	0.04	0.02	0.05	0.08	0.04	0.01	0.03
TI02	1.87	1.21	0.49	1.15	1.39	1.30	0.32
AL203	0.11	0.03	-	0.03	0.04	-	0.01
CR203	19.67	9.10	0.02	9.13	11.19	10.46	1.83
FE203	45.74	57.34	68.14	57.54	55.92	55.38	65.44
FE0	30.30	30.18	29.82	30.25	29.17	30.83	29.99
MN0	1.36	0.80	0.15	0.54	0.79	0.53	0.15
MG0	0.76	0.55	0.69	0.77	1.49	0.30	0.28
CA0	0.06	0.03	0.07	0.03	0.04	0.03	0.02
C00	0.48	0.34	0.17	0.23	0.36	0.12	0.81
NI0	0.31	0.35	0.39	0.29	0.41	0.29	0.31
Total	100.70	99.94	100.00	100.03	100.84	99.26	99.19
Atomic proportions on the basis of 32 oxygens							
SI	0.0120	0.0061	0.0153	0.0244	0.0120	0.0031	0.0093
TI	0.4231	0.2780	0.1129	0.2634	0.3139	0.3010	0.0747
AL	0.0390	0.0108	-	0.0108	0.0142	-	0.0037
CR	4.6781	2.1977	0.0048	2.1982	2.6560	2.5458	0.4489
FE3+	10.3547	13.1816	15.7177	13.1874	12.6348	12.8313	15.2788
FE2+	7.6245	7.7101	7.6446	7.7041	7.3248	7.9391	7.7807
MN	0.3466	0.2070	0.0389	0.1393	0.2009	0.1382	0.0394
MG	0.3407	0.2504	0.3152	0.3495	0.6667	0.1376	0.1295
CA	0.0193	0.0098	0.0230	0.0098	0.0129	0.0099	0.0066
CO	0.1158	0.0833	0.0418	0.0562	0.0867	0.0296	0.2015
NI	0.0750	0.0860	0.0961	0.0710	0.0990	0.0718	0.0773

Table 8 Olivine from Gomati complex

	1 GB4.	2 GB4	3 GB4	4 GB4	5 GM1	6 GM1	7 GM1
Oxide weight percentage							
SIO2	42.68	42.15	42.12	42.01	42.02	41.86	41.81
TIO2	0.02	0.03	-	-	-	-	-
AL2O3	0.05	0.02	-	-	-	-	-
CR2O3	0.04	0.05	-	-	-	-	-
FEO	7.59	7.43	7.50	7.02	10.50	9.97	10.89
MNO	0.12	0.10	0.09	0.09	0.14	0.15	0.17
MGO	49.74	48.81	50.41	49.59	47.43	47.56	47.16
CAO	0.03	0.03	-	-	-	-	-
NIO	0.32	0.30	0.35	0.42	0.40	0.40	0.43
Total	100.86	99.17	100.47	99.13	100.49	99.95	100.46
Atomic proportions on the basis of 4 oxygens							
SI	1.0260	1.0296	1.0149	1.0233	1.0251	1.0248	1.0228
TI	0.0004	0.0006	-	-	-	-	-
AL	0.0014	0.0006	-	-	-	-	-
CR	0.0008	0.0010	-	-	-	-	-
FE	0.1525	0.1518	0.1511	0.1431	0.2142	0.2041	0.2229
MN	0.0024	0.0021	0.0019	0.0020	0.0030	0.0032	0.0035
MG	1.7820	1.7769	1.8104	1.8002	1.7247	1.7351	1.7196
CA	0.0008	0.0008	-	-	-	-	-
NI	0.0062	0.0059	0.0068	0.0083	0.0079	0.0079	0.0085
Fo	92.1	92.1	92.3	92.6	88.9	89.5	88.5

Table 9 Pyroxene from Gomati complex

	1 GL5	2 GL5	3 GL5	4 GS4	5 GS4
Oxide weight percentage					
SIO2	54.70	54.17	54.02	52.21	52.65
TIO2	0.22	0.34	0.32	0.51	0.54
AL203	1.43	2.15	2.40	2.13	2.56
CR203	0.72	1.02	1.16	1.96	2.19
FEO	1.39	1.72	1.82	1.92	2.06
MNO	0.08	0.08	0.34	0.07	0.06
MGO	16.55	16.76	16.29	16.31	16.12
CAO	24.30	22.90	23.89	22.94	23.65
NA2O	0.40	0.58	0.58	0.85	0.80
NIC	0.00	0.04	0.08	0.03	0.09
Total	99.87	99.76	100.91	98.94	100.73
Atomic proportions on the basis of 6 oxygens					
SI	1.9830	1.9640	1.9471	1.9254	1.9120
TI	0.0059	0.0093	0.0087	0.0142	0.0148
AL	0.0612	0.0918	0.1021	0.0927	0.1096
CR	0.0207	0.0293	0.0331	0.0572	0.0628
FE	0.0421	0.0521	0.0548	0.0591	0.0627
MN	0.0024	0.0024	0.0104	0.0021	0.0019
MG	0.8939	0.9059	0.8748	0.8967	0.8721
CA	0.9439	0.8896	0.9228	0.9065	0.9203
NA	0.0339	0.0410	0.0406	0.0610	0.0565
NI	0.0000	0.0011	0.0023	0.0010	0.0026
End member compositions					
Wo	50.2	48.2	48.5	48.6	49.1
En	47.5	49.0	48.5	48.2	47.5
Fs	2.2	2.8	3.0	3.2	3.4

Table 10 Chlorite from Gomati complex

	1 GB2	2 GB2	3 GB2	4 GN10	5 GN17	6 GN15	7 GN15	8 GT1
Oxide weight percentage								
SIO2	27.50	30.54	28.28	34.42	34.95	30.00	30.79	33.78
TIO2	0.01	0.04	0.02	-	-	-	-	-
AL2O3	21.40	18.93	20.76	9.90	8.83	20.39	19.82	13.04
CR2O3	2.44	1.70	2.25	1.26	0.74	0.94	0.39	0.45
FEO	1.58	1.30	1.48	6.20	6.78	1.21	1.19	4.42
MNO	0.01	0.27	0.26	0.00	0.00	0.00	0.00	-
MGO	32.73	33.21	32.52	33.17	33.90	34.04	33.32	33.60
CAO	0.01	0.01	-	-	-	0.01	-	-
NIO	0.15	0.20	0.21	-	-	0.00	0.01	-
Total	85.82	86.22	85.78	84.94	85.19	86.60	85.51	85.30
Atomic proportions on the basis of 28 oxygens								
SI	5.2733	5.7922	5.4207	6.7651	6.8639	5.6395	5.8348	6.5259
TI	0.0010	0.0052	0.0026	-	-	-	-	-
AL	4.8415	4.2347	4.6930	2.2948	2.0442	4.5211	4.4292	2.9712
CR	0.3703	0.2556	0.3406	0.1960	0.1146	0.1399	0.0578	0.0692
FE	0.2537	0.2069	0.2375	1.0189	1.1129	0.1898	0.1880	0.7148
MN	0.0009	0.0430	0.0425	0.0000	0.0000	0.0000	0.0000	-
MG	9.3539	9.3870	9.2904	9.7159	9.9212	9.5373	9.4100	9.6740
CA	0.0014	0.0023	-	-	-	0.0025	-	-
NI	0.0237	0.0307	0.0329	-	-	0.0000	0.0020	-

Table 11 Amphibole from contact amphibolite of Gomati complex

	1 GD1	2 GK1	3 GK2
Oxide weight percentage			
SIO2	44.62	43.44	51.89
TIO2	0.58	0.61	0.18
AL203	11.83	12.73	5.12
CR203	0.09	-	-
FEO	15.02	17.28	13.43
MNO	0.14	0.03	0.03
MGO	11.20	9.48	15.16
CAO	11.91	11.31	11.89
NA20	1.02	1.49	0.57
K20	0.58	0.98	0.13
Total	97.00	97.35	98.35
Atomic proportions on the basis of 23 oxygens			
SI	6.6363	6.5249	7.4466
TI	0.0653	0.0694	0.0198
AL	2.0745	2.2549	0.8660
CR	0.0110	-	-
FE	1.8684	2.1703	1.6118
MN	0.0171	0.0039	0.0031
MG	2.4825	2.1229	3.2351
CA	1.8986	1.8211	1.8279
NA	0.2937	0.4331	0.1579
K	0.1104	0.1880	0.0230

Table 12 Sphene from amphibolites of Gomati complex

	1 GK1	2 GK2	3 GD1
Oxide	weight percentage		
SIO2	29.67	30.14	29.19
TIO2	37.68	37.50	37.54
AL203	2.03	1.40	1.83
CR203	0.00	0.00	0.01
FEO	1.51	0.33	0.26
MNO	0.04	0.02	0.02
MGO	0.05	0.06	0.00
CAO	27.27	27.94	28.30
K20	0.03	0.01	0.02
Total	98.29	97.41	97.18
Atomic proportions on the basis of 20 oxygens			
SI	3.9501	4.0322	3.9263
TI	3.7726	3.7731	3.7984
AL	0.3191	0.2211	0.2903
CR	0.0004	0.0000	0.0008
FE	0.1682	0.0372	0.0294
MN	0.0045	0.0024	0.0024
MG	0.0102	0.0116	0.0000
CA	3.8894	4.0058	4.0800
K	0.0057	0.0018	0.0042

APPENDIX III

X-RAY FLUORESCENCE ANALYSIS

The procedure for the preparation of samples for X-Ray Fluorescence Analysis is as follows ; all samples were cleaned from weathering products, and then split using a hydraulic splitter. The resultant coarse pieces were passed through a jaw crusher, and the derived aggregate was ground in a tungsten-carbide mill. The fine powder obtained was admixed with 5-8 drops (according to a particular sample, usually in serpentinites more than 6 drops) of Mowiol, and then pressed in a hydraulic press at 5.5 tons/sq.in.

XRF analyses were carried out using a Philips PW 1400 X-Ray Spectrometer, incorporating a 3 kW generator allowing a maximum kV of 100 kV, and utilizing a rhodium tube so that both major and trace elements were analyzed at the same time. The conditions used are summarized in Table 1. Background positions were measured as + and - offset to the peaks.

Abbreviations of Table 1 are as follows :

Collimator : C = coarse, F = fine

Detector : F = flow, S = seint

Crystal : 5 = Germanium

4 = TLAP (Thallium AP)

3 = PE (penta erythritol)

2 = LIF 200

1 = LIF 220

TABLE 1

Element	Na	Mg	Al	Si	P	S	K	Ca	Ti	Cr	Mn	Fe	Ni	Cu	Zn	Rb	Sr	Y	Zr	Nb	Ba	La	Ce
Radiation	$K\alpha_1$	$K\alpha_1$	$K\alpha_1$	$K\alpha_1$	$K\alpha_1$	$K\alpha_1$	$K\alpha_1$	$K\alpha_1$	$K\alpha_1$	$K\alpha_1$	$K\alpha_1$	$K\alpha_1$	$K\alpha_1$	$K\alpha_1$	$K\alpha_1$	$K\alpha_1$	$K\alpha_1$	$K\alpha_1$	$K\alpha_1$	$K\alpha_1$	$K\alpha_1$	$K\alpha_1$	$K\alpha_1$
Collimator	C	C	C	C	C	C	C	C	C	C	C	F	C	C	C	C	C	C	C	C	F	C	C
Detector	F	F	F	F	F	F	F	F	F	F	F	F	S	S	S	S	S	S	S	S	S	F	F
Crystal	4	4	3	3	5	3	2	2	2	1	1	2	1	1	1	1	1	1	1	1	1	1	1
KV	35	35	35	35	70	60	35	35	35	40	50	35	80	80	80	90	90	90	90	90	90	35	35
M amps	80	80	80	80	40	50	80	80	80	80	70	60	35	35	35	30	30	30	30	30	30	80	80
Angle	55.165	45.220	145.225	109.230	141.100	75.890	136.820	113.28	86.275	107.305	95.32	57.635	71.280	65.575	60.615	37.990	35.845	33.905	32.095	30.450	15.575	139.095	11.84

Trace Elements

Cr, Ni, Cu, Zn, Rb, Sr, Y, Zr, Nb, Ba and Ce were determined as trace elements and their concentrations are given in ppm. Standards used include the International Standards DTS-1, GSP-1, PCC-1, G-1, T-1, BOB-1, BR, BCR-1, W-1, G-2, GR, GA and GH. The correction program used is the TRATIO program written by R.C.O.Gill which includes contamination and interference corrections.

The lower and upper limit of detection of each element is given below :

Element	Lower limit (ppm)	Upper limit (ppm)
Cu	0	10,000
Ni	0	"
Cr	0	"
Ba	0	50,000
Nb	0	5,000
Zr	0	"
Y	0	"
Sr	0	"
Rb	0	"
Zn	0	"

Major Elements

The following major elements (as oxides) were determined : SiO_2, Al_2O_3, Fe_2O_3, MgO, CaO, Na_2O, K_2O, TiO_2, MnO, S, P_2O_5 and H_2O, CO_2 and FeO in certain samples. The International Standards used, were limited to mafic-ultramafic standards ; they include the DTS-1, PCC-1, W-1, BOB-1, BR and BCR-1. The computer program used, is the XRF PL1 which

incorporates a mass absorption correction procedure described by Holland and Brindle (1966).

Table 2 VAVDOS COMPLEX (FE203 as total iron)

	1 VG1	2 VA15	3 VF7	4 VB3	5 VP3	6 VP1	7 VY7	8 V8-1	9 V8-2	10 VP25
PERCENT										
SI02	39.75	41.69	39.41	40.23	39.16	40.70	40.08	45.98	46.69	51.43
AL203	0.43	0.34	0.32	0.43	0.38	0.40	0.39	1.49	2.62	1.62
FE203	10.46	9.94	11.00	10.82	10.14	10.71	10.92	9.61	10.21	9.16
MGO	49.07	47.65	48.92	48.26	49.89	47.73	48.12	30.64	25.77	23.94
CAO	0.03	0.20	0.05	0.00	0.18	0.21	0.22	11.91	14.27	13.39
NA20	0.04	0.00	0.03	0.04	0.04	0.03	0.04	0.00	0.04	0.02
K20	0.00	0.00	0.00	0.00	0.00	0.00	0.00	0.00	0.00	0.00
TI02	0.04	0.04	0.03	0.03	0.04	0.04	0.04	0.10	0.15	0.13
MNO	0.14	0.10	0.17	0.14	0.14	0.13	0.15	0.18	0.18	0.20
S	0.01	0.05	0.02	0.03	0.00	0.02	0.01	0.09	0.06	0.09
P205	0.03	0.01	0.03	0.03	0.03	0.03	0.02	0.01	0.01	0.01
TOTAL	100.00	100.00	100.00	100.00	100.00	100.00	100.00	100.00	100.00	100.00
PPM										
BA	15	21	23	17	21	21	22	19	17	18
NB	2	1	1	2	2	2	2	2	2	1
ZR	2	1	1	1	2	1	1	2	3	2
Y	3	3	4	3	4	4	3	5	7	6
SR	2	1	3	3	2	5	3	4	4	4
RB	1	1	1	1	0	1	1	1	1	2
ZN	4	16	24	15	11	15	21	24	22	20
CU	0	2	0	0	0	34	12	104	13	268
NI	2614	2782	2332	2693	2695	2107	2273	592	370	382
CR	3190	3006	2096	1711	1899	2134	2134	2167	1941	1514

Table 2 VAVDOS COMPLEX (FE203 as total iron)

	11 VP26	12 VX4
PERCENT		
SI02	53.73	51.25
AL203	1.95	1.81
FE203	7.01	7.64
MGO	24.24	23.42
CAO	12.59	15.37
NA20	0.01	0.02
K20	0.00	0.00
TI02	0.12	0.10
MNO	0.14	0.16
S	0.01	0.00
P205	0.02	0.02
TOTAL	100.00	100.00
PPM		
BA	20	23
NB	2	2
ZR	3	2
Y	6	6
SR	4	3
RB	2	1
ZN	19	7
CU	382	1
NI	347	265
CR	2556	3016

Table 3 VAVDOS COMPLEX (FE203 as total iron)

	13 V8-3	14 VP10	15 V8-13	16 VC2	17 VC3	18 VC4	19 V8-8	20 V8-9	21 V8-11	22 V8-10
PERCENT										
SI02	51.85	48.81	52.95	46.32	49.06	50.19	50.13	50.68	48.19	45.67
AL203	12.26	16.72	11.94	13.20	11.09	8.92	8.04	12.12	11.28	13.02
FE203	3.93	5.93	6.55	12.35	6.97	6.53	8.04	6.01	7.28	12.69
MG0	14.61	13.05	3.53	11.75	17.76	18.41	18.24	14.69	18.18	11.82
CA0	16.92	14.46	21.04	13.83	14.15	15.07	14.62	15.18	14.21	14.33
NA20	0.19	0.73	1.94	1.77	0.47	0.47	0.49	0.84	0.45	1.67
K20	0.00	0.00	0.96	0.12	0.07	0.15	0.13	0.22	0.06	0.10
TI02	0.13	0.13	0.79	0.44	0.12	0.11	0.12	0.11	0.13	0.46
MN0	0.08	0.12	0.10	0.19	0.12	0.14	0.17	0.14	0.13	0.19
S	0.00	0.04	0.02	0.00	0.17	0.00	0.00	0.00	0.06	0.00
P205	0.02	0.02	0.19	0.03	0.02	0.02	0.02	0.02	0.02	0.03
TOTAL	100.00	100.00	100.00	100.00	100.00	100.00	100.00	100.00	100.00	100.00
PPM										
BA	21	19	201	33	32	23	36	40	23	27
NB	2	2	19	2	2	3	3	3	2	2
ZR	3	2	160	3	3	3	2	12	2	4
Y	7	5	30	9	5	6	5	5	6	9
SR	63	102	750	79	32	36	43	90	32	76
RB	1	3	21	4	5	7	6	9	5	3
ZN	0	6	73	16	11	14	12	8	9	18
CU	40	105	20	13	60	22	70	47	42	32
NI	101	66	39	75	79	165	120	100	93	75
CR	614	211	76	240	565	1184	312	330	572	188

Table 4 VAVDOS COMPLEX (FE203 as total iron)

	23 V8-15	24 VX1	25 VY8	26 VP24
PERCENT				
SI02	71.40	75.29	75.45	74.12
AL203	14.40	13.83	14.72	14.89
FE203	3.32	0.90	0.48	0.64
MG0	0.51	0.61	0.57	0.60
CA0	1.54	0.47	0.47	0.42
NA20	3.39	3.75	5.20	4.32
K20	4.70	4.31	2.87	4.12
TI02	0.51	0.10	0.03	0.04
MN0	0.05	0.02	0.03	0.07
S	0.00	0.00	0.00	0.00
P205	0.17	0.07	0.06	0.04
TOTAL	100.00	99.36	99.88	99.26
PPM				
BA	815	103	20	21
NB	14	2	49	35
ZR	185	44	14	32
Y	31	28	11	37
SR	119	28	2	3
RB	167	180	283	358
NI	10	14	9	27
CR	21	188	10	10

Table 5 GOMATI COMPLEX (FE203 as total iron)

	1 GM1	2 GM2	3 GL1	4 GL2	5 GN10	6 GN12	7 GN17	8 GT1	9 GT9	10 GC5
PERCENT										
SI02	40.30	42.12	38.84	41.45	41.86	42.47	47.48	45.37	45.14	38.30
AL203	2.13	1.36	1.80	1.78	3.53	1.66	2.56	4.23	3.03	0.33
FE203	8.05	7.07	6.42	8.85	7.11	7.55	9.95	5.28	9.42	7.35
MGO	42.24	39.04	39.88	37.45	35.36	37.65	39.53	32.49	40.65	40.08
CAO	0.00	0.61	1.21	0.06	1.40	0.00	0.16	5.37	0.00	3.16
NA20	0.00	0.00	0.00	0.00	0.09	0.00	0.00	0.33	0.00	0.00
K20	0.00	0.00	0.00	0.00	0.00	0.00	0.00	0.01	0.00	0.00
TI02	0.10	0.06	0.17	0.18	0.15	0.06	0.08	0.10	0.12	0.03
MNO	0.12	0.10	0.10	0.15	0.10	0.11	0.13	0.06	0.11	0.21
S	0.07	0.04	0.05	0.02	0.01	0.01	0.02	0.02	0.03	0.03
P205	0.02	0.02	0.02	0.02	0.03	0.02	0.02	0.02	0.02	0.02
H20	6.98	9.58	10.38	10.05	10.38	10.46	0.07	6.72	1.49	7.57
C02	-	-	1.17	-	-	-	-	-	-	2.91
TOTAL	100.00	100.00	100.00	100.00	100.00	100.00	100.00	100.00	100.00	100.00
PPM										
BA	19	67	13	12	12	9	13	46	163	18
NB	2	2	2	2	3	2	2	2	2	2
ZR	5	3	4	7	45	7	3	5	5	2
Y	5	4	5	5	6	5	4	7	6	3
SR	5	19	19	3	28	2	7	115	11	40
RB	1	-	1	1	1	1	-	1	2	1
ZN	40	36	19	60	42	43	53	26	56	9
CU	2	38	4	27	8	14	15	36	27	47
NI	1893	1969	1975	1906	1757	1706	1929	1491	1842	2187
CR	4753	2782	2642	2061	2800	3280	3888	2087	2607	2087

Table 5 GOMATI COMPLEX (FE203 as total iron)

	11 GC1	12 GD2	13 GB4
PERCENT			
SI02	40.48	42.03	44.75
AL203	0.28	1.34	0.95
FE203	9.09	7.85	4.58
MGO	39.83	39.51	45.86
CAO	2.54	0.18	0.87
NA20	0.00	0.00	0.00
K20	0.00	0.00	0.00
TI02	0.04	0.06	0.06
MNO	0.10	0.10	0.05
S	0.02	0.07	0.07
P205	0.02	0.02	0.02
H20	7.60	8.84	2.65
C02	-	-	0.14
TOTAL	100.00	100.00	100.00
PPM			
BA	20	62	16
NB	2	2	2
ZR	1	2	1
Y	4	4	4
SR	9	13	8
RB	1	1	1
ZN	39	60	0
CU	0	27	3
NI	2544	1946	2640
CR	2853	3377	*

Table 6 GOMATI COMPLEX

	14 GD1	15 GK1	16 GK2
PERCENT			
SIO2	42.30	40.84	45.08
AL203	10.55	10.54	11.81
FE203	6.57	7.72	5.13
FEO	12.84	8.22	11.41
MGO	9.68	7.80	9.82
CAO	13.40	18.44	10.78
NA20	0.99	2.12	1.67
K20	0.45	0.77	0.50
TIO2	2.26	1.64	1.61
MNO	0.36	0.25	0.28
S	0.09	0.05	0.02
P205	0.37	0.20	0.21
H20	0.14	1.41	1.67
TOTAL	100.00	100.00	100.00
PPM			
BA	59	68	39
NB	11	5	6
ZR	50	97	97
Y	62	34	40
SR	42	132	56
RB	6	18	11
ZN	129	72	101
CU	69	32	8
NI	78	72	65
CR	547	292	222
C E	24	8	8

APPENDIX IV

X-RAY DIFFRACTION ANALYSES

A Philips PW1130 3 Kilowatt X-Ray generator/diffractometer utilizing Cu and Cr X-Ray tubes used for powder photography and X-Ray diffractometry techniques.

Chromites

X-ray powder photographs of five chromite samples were taken, with a Debye-Scherrer camera of 114.6 mm diameter ; fine collimators and CrK_{α} radiation were used. Exposure time varied from 30-48 hours. The minute, necessary amount of chromite was obtained by scratching the surface of larger chromite crystals, which had been analysed by the microprobe analyser before. Then the unit cell edges of chromites have been calculated and plotted in relation to major oxides as shown in Figure 1. There is a positive increase of the cell edge with the Cr_2O_3 and a negative with the Al_2O_3 . This agrees with data from Greenbaum (1972) and Peters and Kramers (1974), for chromites of the Troodos complex and the Northern Oman ophiolites respectively. The variation of other oxides is not distinct.

Figure 1

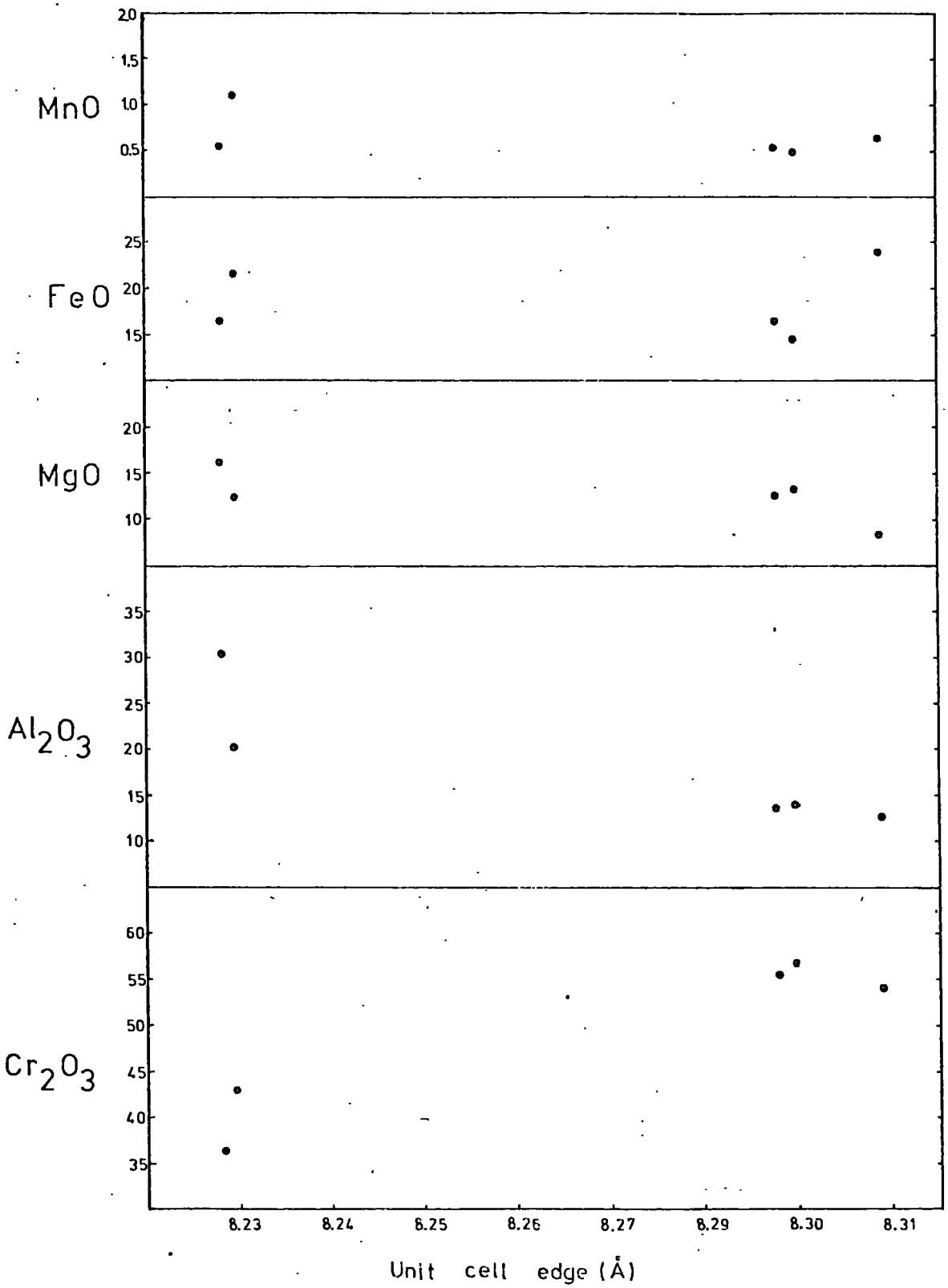
MnO
FeO
MgO
Al2O3
Cr2O3
8.23
8.24
8.25
8.26
8.27
8.29
8.30
8.31
Unit cell edge (Å)

Other Minerals

The other minerals were analysed by X-ray diffractometry. The powder sample was smeared onto a glass slide and exposed to CuK_{α} radiation in the diffractometer. Charts were produced using a scan speed of 1^{o} of 2θ per minute, and a chart speed of 10mm per minute. The minerals were identified by comparison with the standard mineral patterns contained in the J.C.P.D.S. File.

Several charts of the black tourmaline crystals occurring in the granitic rocks of Vavdos, indicate that the tourmaline is dravite. The matrix in the breccia of the Vavdos basal thrust, has been identified as dolomite. Kämmererite has been found in elongate and relatively large crystals near disruption zones. Magnesite veins have been identified crosscutting chromitiferous dunite in the Vavdos complex, near the Cremasmata locality. Feldspar (orthoclase-oligoclase) veins, not more than 1.5 cm in width have been determined and they crosscut dunite and chromitiferous rocks in the Vavdos complex.

Serpentine minerals have not been studied in detail, but charts of rock powder were run ; they suggest that the mesh textured serpentinites are usually comprised of lizardite, while the sheared and bladed mat serpentinites are basically antigorite. This stands in agreement with data produced by Maltman (1978), for serpentinite textures and XRD patterns from North Wales, U.K.

REFERENCES

Flanagan, F.J., 1973. 1972 values for international geochemical reference standards. Geochim. Cosmochim. Acta, 37, p 1189-1200.

Greenbaum, D., 1972. The geology and evolution of the Troodos Plutonic complex and associated chromite deposits. Ph.D. thesis, University of Leeds.

Holland, J.G. and Brindle, D.W., 1966. A self-consistent mass absorption correction for silicate analysis by X-ray fluorescence analysis. Spectrochim. Acta, 22, p 2083-2093.

Peters, T.J. and Kramers, J.D, 1974. Chromite deposits in the ophiolite complex of Northern Oman. Mineral.Deposita 9, p 253-259.

Maltman, A.J., 1978. Serpentinite textures in Anglesey, North Wales, U.K. Geol. Soc. Am. Bull., 89, p 972-980.

Sweatman, T.R. and Long, J.V.R., 1969. Quantitative electron probe microanalysis of rock-forming minerals. J.Petrology, 10, p 332-379.

DURHAM UNIVERSITY
16 FEB
SCIENCE LIBRARY

Figure 2.1

GEOLOGICAL MAP OF THE VAVDOS COMPLEX

SCALE 1:10000

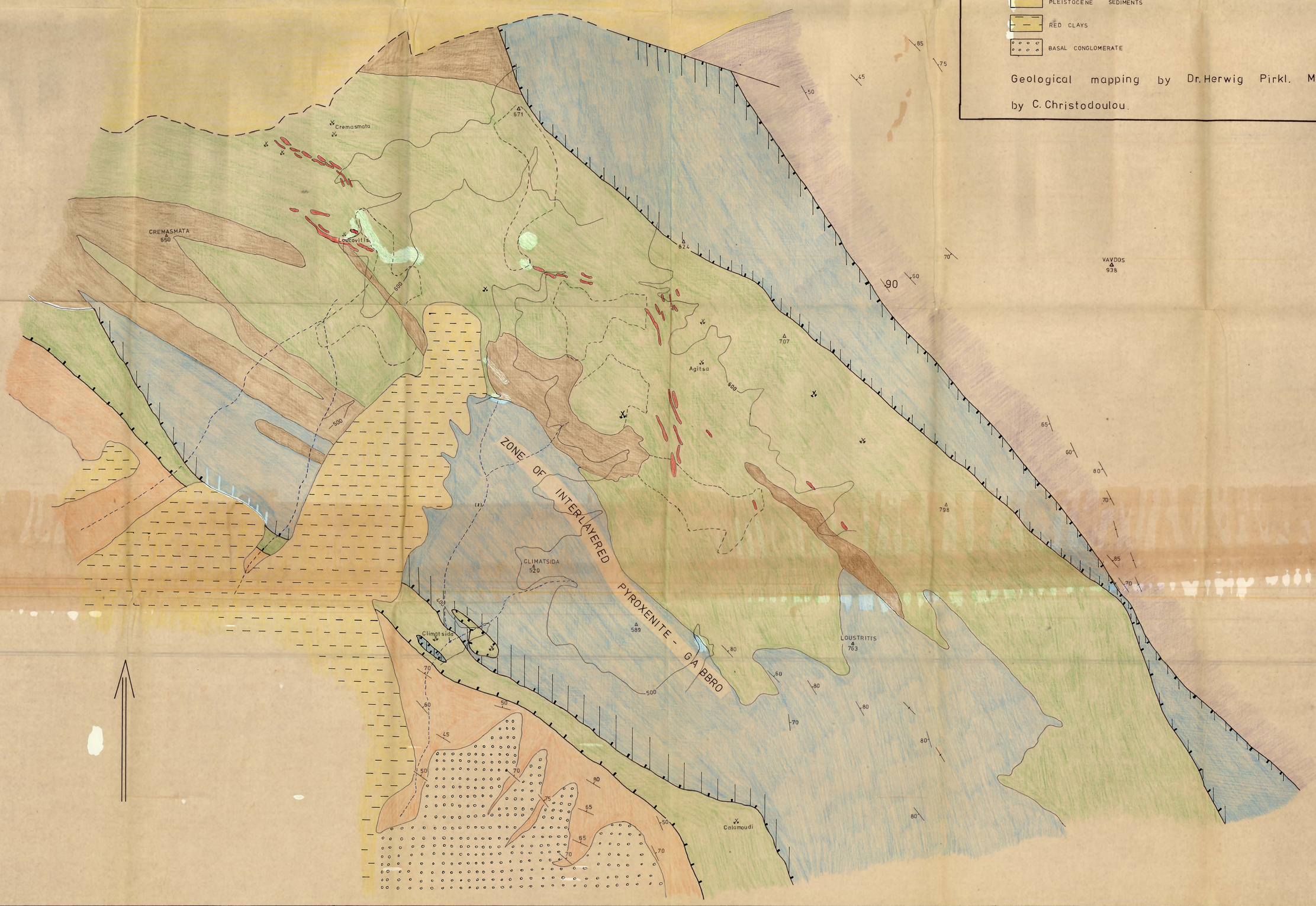

GEOLOGICAL EXPLANATION.

- DUNITE - SERPENTINITE
- PYROXENITE
- GABBRO
- AMPHIBOLITE
- GREEN SCHIST
- TWO MICA GNEISS
- GRANITIC ROCKS
- PLEISTOCENE SEDIMENTS
- RED CLAYS
- BASAL CONGLOMERATE

- OBSERVED THRUST FAULT
- SUPPOSED OR COVERED FAULT
- MAGNESITE EXCAVATIONS
- CHROMITE OCCURENCES

Geological mapping by Dr. Herwig Pirkl. Modified by C. Christodoulou.

FIGURE 2.3

GEOLOGICAL MAP OF THE GOMATI COMPLEX

SCALE 1:25000

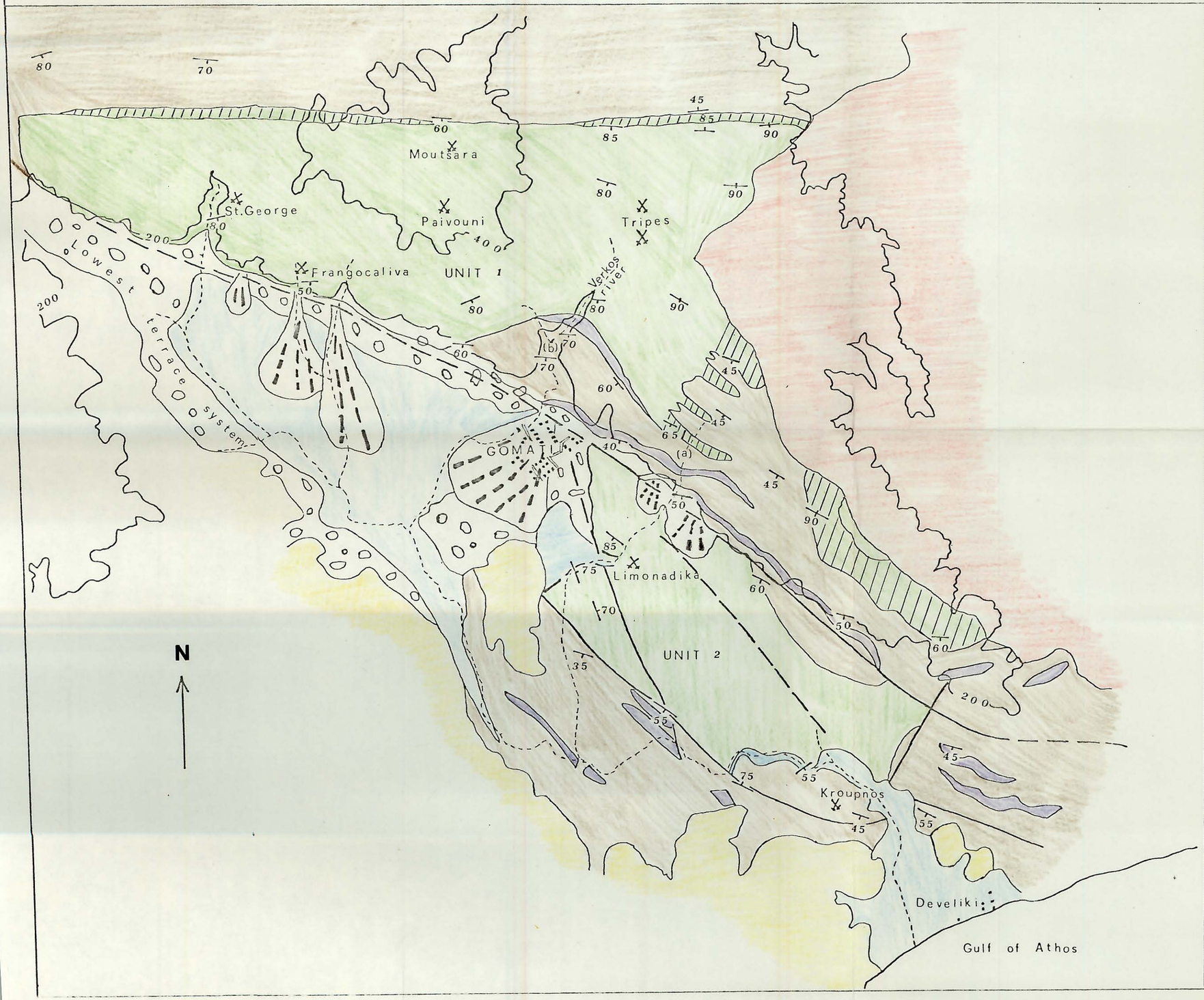

LEGEND

- Serpentinized Ultramafic rocks
- Amphibolite
- Two-mica Gneiss
- Marble
- Granite of Ierissos
- Tertiary red clays
- Alluvial fans
- Alluvial deposits
- Thrust fault
- Supposed fault
- Chromite ore occurences
- Streams